Mechanistic and Metabolic Insights into Bioengineering the Bone Marrow Niche *In Vitro*

Hannah Donnelly

BSc Hons

Submitted in fulfilment of requirements for the degree of Doctor of Philosophy (PhD)

Centre for the Cellular Microenvironment
Institute of Molecular, Cell and Systems Biology
College of Medical, Veterinary and Life Sciences
University of Glasgow
Glasgow
G12 8QQ

February 2020

Abstract

Stem cell balance of proliferation, differentiation and self-renewal, is regulated by the microenvironment in which they reside, termed the *stem cell niche* (Schofield, 1978). Niche microenvironments provide physical and functional regulatory cues that control fundamental cell intrinsic and extrinsic mechanisms. In adults, the process of haematopoiesis is sustained by a population of haematopoietic stem cells (HSCs) that are found primarily in the bone marrow (BM) (Jagannathan-Bogdan and Zon, 2013). The BM niche also houses populations of mesenchymal stromal and perivascular cells (MSPCs), that are themselves regulated by the niche, and are fundamental cellular constituents in HSC regulation (Pinho and Frenette, 2019).

Both HSCs and MSPCs hold enormous clinical potential. HSCs have the ability to reconstitute the entire blood and immune system (Jagannathan-Bogdan and Zon, 2013), whereas MSPCs contain immunosuppression capacity and have the ability to regenerate damaged and diseased tissue (Caplan, 1991; Uccelli et al., 2008). However, there are still important hurdles that must be overcome before the potential of these cells are fully realised. The regenerative capacity of these stem cells is quickly lost upon *ex vivo* culture, meaning achieving clinically relevant numbers of cells is challenging (Dalby et al., 2018; Zon, 2008).

Although BM MSPCs (such as nestin+ MSPCs) contain HSC support activity, their ability to maintain HSCs *ex vivo* is only modest due to loss of expression of these niche factors in culture (Kunisaki et al., 2013; Nakahara et al., 2019). The absence of sustained self-renewal or maintenance of the stem cell phenotype could be related to the lack of integration of biophysical and biochemical cues required for stem cell regulation, provided by the native BM niche microenvironment *in vivo*. This has led to a focus on biomaterial and engineering strategies that aim to recapitulate BM niche properties *in vitro* (Müller et al., 2014). It is envisaged that bioengineered artificial niches will offer protocols for *ex vivo* expansion and maintenance of HSCs without the need for high risk protocols (e.g. genetic manipulations (Nakahara et al., 2019)), but also platforms on which to study the fundamental mechanisms that control self-renewal in both HSCs and MSPCs in the niche.

In this thesis, biomaterial strategies were employed to mimic aspects of the BM niche microenvironment. First retention of HSC support activity in a population of MSPCs was investigated and the metabolic mechanisms that may support this phenotype were probed. The ability of the system to support HSC maintenance *in vitro* was then assessed. Poly(ethyl acrylate) (PEA) is a polymer that causes spontaneous unfolding of the extracellular matrix protein (ECM) fibronectin (FN). These physiological-like networks expose key binding sites on the FN molecule, which can be harnessed for cell adhesion and growth factor tethering (Cheng et al., 2018; Llopis-hernández et al., 2016). Noting that low-stiffness matrices support nestin expression in MSPCs (Engler et al., 2006), a key niche marker (Kunisaki et al., 2013; Pinho et al., 2013), low-stiffness collagen hydrogels were introduced into the system. We were able to use this system to promote a population of nestin+ MSPCs that express key HSC support factors and were able to maintain a population of HSCs *in vitro*. The nestin+ MSPCs utilise hypoxic-like metabolic mechanisms in response to low-stiffness, that may be important in retaining this BM niche-like phenotype in long term *in vitro* culture.

Table of Contents

Abstract ..... *ii*

List of Tables ..... *vii*

List of Figures ..... *viii*

Publications ..... *x*

Conference Proceedings ..... *x*

Awards ..... *xi*

Acknowledgements ..... *xii*

Author's Declaration ..... *xiii*

Abbreviations ..... *xiv*

Chapter 1 Introduction *1*

1.1 Stem Cell Niches **1**

1.2 Bone Marrow Architecture **4**

1.3 Bone Marrow Resident Stem Cells **6**

1.3.1 Mesenchymal stromal cells 6

1.3.2 Pericytes 9

1.3.3 Haematopoietic stem cells 14

1.4 The Bone Marrow Niche **17**

1.4.1 Bone marrow niche cellular constituents 18

1.4.2 Secreted niche factors 22

1.4.3 Bone marrow ECM 23

1.4.4 The hypoxic niche 25

1.5 Engineering Stem Cell Niches for Differentiation and Self-Renewal **27**

1.5.1 Mechanotransduction 28

1.5.2 Topography 31

1.5.3 Stiffness and mechanics 36

1.5.4 Chemistry 42

1.5.5 Modelling the bone marrow niche 46

1.6 Conclusion **51**

1.7 Aims and Objectives **51**

Chapter 2 General Materials and Methods *53*

2.1 Materials and Reagents **53**

2.1.1 Cell culture reagents 53

2.1.2 Immunostaining Reagents 54

2.2 Preparation of Cell Culture Solutions **54**

2.3 General Methods **55**

2.3.1 Substrate preparation 55

2.3.2 Pericyte isolation and culture 56

2.3.3 Flow cytometry 58

2.3.4 Immunocytochemistry 58

2.3.5 Microscopy 59

2.3.6 In cell western (ICW) 60

2.3.7 RNAseq 60

Chapter 3 Characterisation of Materials *62*

3.1 Introduction **62**

3.1.1 Fibronectin 62
3.1.2 BMP-2 65
3.1.3 Collagen 67
3.1.4 Objectives/aims 68

3.2 Materials and Methods 68
3.2.1 BCA protein assay 68
3.2.2 BMP-2 ELISA 69
3.2.3 Atomic Force Microscopy 69
3.2.4 Rheology 69
3.2.5 Coomassie staining 70

3.3 Results 70
3.3.1 Fibronectin conformation and availability of domains 70
3.3.2 Cell adherence 74
3.3.3 Gel stiffness 75

3.4 Discussion 76
3.4.1 PEA drives fibronectin fibrillogenesis 76
3.4.2 Low stiffness collagen gels in the range of bone marrow 81
3.4.3 Summary 84

Chapter 4 Characterising a Bone Marrow Niche MSPC Phenotype 85

4.1 Introduction 85
4.1.1 Nestin 85
4.1.2 HSC maintenance cytokines 86
4.1.3 Aims and objectives 87

4.2 Materials and Methods 88
4.2.1 Phenotyping of pericytes by flow cytometry 88
4.2.2 Brefeldin A treatment 90

4.3 Results 90
4.3.1 Support of a niche phenotype in MSPCs 90
4.3.2 Intermediate filament expression 96
4.3.3 HSC maintenance factor expression 98

4.4 Discussion 101
4.4.1 Low-stiffness gels support expression of phenotypic niche markers 101
4.4.2 Low-stiffness gels promote nestin expression 103
4.4.3 Fibronectin +gel driven nestin expression correlates with HSC maintenance cytokine production 106

4.5 Summary 108

Chapter 5 Hypoxia and Metabolism 109

5.1 Introduction 109
5.1.1 HIF1α 111
5.1.2 MSPCs and hypoxia 114
5.1.3 HSCs and hypoxia 116
5.1.4 Investigating cellular metabolism with metabolomics 118
5.1.5 Objectives and aims 119

5.2 Materials and Methods 120
5.2.1 HIF1α co-localisation analysis 120
5.2.2 Hypoxyprobe™ 120
5.2.3 Metabolomics analysis 121
5.2.4 $^{13}C_6$-Glucose metabolomic tracing 121

5.3 Results 122
5.3.1 Analysis of HIF1α levels and its downstream targets 122
5.3.2 Hypoxia gradient analysis 125
5.3.3 Analysis of the cell metabolome in response to material mechanics and hypoxia 127

5.3.4 Flux of heavy glucose in glycolysis 130

5.4 Discussion 131

5.4.1 HIF1α increases with gel addition 132
5.4.2 Gel addition down regulates TCA cycle 134
5.4.3 Summary 136

Chapter 6 HSC Co-Culture and Characterisation 138

6.1 Introduction 138

6.1.1 The HSC phenotype 138
6.1.2 HSC *ex vivo* culture 140
6.1.3 Aims and objectives 141

6.2 Materials and Methods 142

6.2.1 HSC culture 142
6.2.2 HSC phenotyping by flow cytometry 143
6.2.3 LTC-IC 144
6.2.4 CFU assay 146

6.3 Results 147

6.3.1 Low-stiffness gels reduce HSC/HSPC proliferation 147
6.3.2 Low-stiffness gels support LT-HSCs 151

6.4 Discussion 154

6.4.1 PEA FN BMP-2 systems support proliferation (-gel) or maintenance (+gel) of the CD34+ CD38- population 155
6.4.2 Low-stiffness gels and fibronectin networks support maintenance of LT-HSCs in the absence of supplemented cytokines 156
6.4.3 Summary 161

Chapter 7 Discussion 163

7.1 Project Summary 163

7.2 Recommendations for Future Work 164

7.3 Prospective Applications of Bone Marrow Niche Models 168

7.3.1 Probing haematopoiesis and niche dynamics 169
7.3.2 Modelling disease 170
7.3.3 NAT pharmaceutical screening 170
7.3.4 Cell source for clinical applications and research 171
7.3.5 Gene editing platform 172

7.4 Conclusion 172

Appendices 173

List of References 174

List of Tables

Table 1-1 Markers associated with mesenchymal stem cell phenotype subsets. ..8
Table 1-2 Markers associated with pericyte phenotype. 12
Table 1-3 Cellular contributions to the bone marrow niche. 20
Table 1-4 Cytokines and secreted factors associated with HSC regulation in the BM niche..... 22
Table 1-5 Current material strategies to engineer the bone marrow niche..... 49
Table 2-1 Antibodies for fluorescent activated cell-sorting of pericytes from adipose tissue. 57
Table 2-2 Primary antibodies used for immunocytochemistry..... 59
Table 2-3 Primary antibodies used for in cell western..... 60
Table 3-1 Integrin and growth factor receptor synergistic signalling and biological effects. 80
Table 4-1 Antibodies used for flow cytometry assessment of pericyte phenotype. 88
Table 4-2 Summary of changes in expression of surface markers assessed by flow cytometry at day 14. 95
Table 6-1 HSC media formulations. 143
Table 6-2 Antibodies used for flow cytometry assessment of HSC phenotype .. 143
Table 6-3 Antibodies used for cell sorting to LTC-IC. 145
Table 6-4 Colony types counted in colony-forming unit assay..... 153
Table 6-5 Summary of current small molecules used for ex vivo HSC expansion. 160
Table 7-1 GFs and cytokines to be considered for future model development. 166

List of Figures

Figure 1-1 Parameters of the stem cell niche. 3
Figure 1-2 Bone marrow structure. 5
Figure 1-3 Model of the organization of MSCs. 7
Figure 1-4 Therapeutic potential of MSCs. 9
Figure 1-5 Pericytes and MSCs share surface markers and differentiation capacity. 10
Figure 1-6 Haematopoietic development including identifying surface markers for HSCs and progenitor cells. 14
Figure 1-7 The estimated annual numbers of haematopoietic stem cells transplant (HSCT) recipients in the USA. 16
Figure 1-8 HSC niche locations. 18
Figure 1-9 Proposed biophysical ECM contributions to niche-mediated HSC regulation. 24
Figure 1-10 Model of focal adhesion molecular architecture. 29
Figure 1-11 Mechanical coupling of ECM-nucleus translocates YAP to the nucleus. 30
Figure 1-12 Scale of cellular components. 32
Figure 1-13 Topography to control mesenchymal stem cell (MSC) adhesion for self-renewal and osteogenesis. 33
Figure 1-14 Stiffness of various tissues. 37
Figure 1-15 MSCs have mechanical memory. 39
Figure 1-16 Cells ‘sense’ matrix stiffness through receptor-adhesion presentations. 41
Figure 1-17 Soluble and matrix bound growth factor delivery. 44
Figure 1-18 FN nanonetwork formation and GF presentation. 45
Figure 1-19 Schematic of *in vitro* niche models. 52
Figure 3-1 Fibronectin (FN) subunit. 62
Figure 3-2 BMP-2 signalling. 66
Figure 3-3 FN forms networks on PEA surfaces. 71
Figure 3-4 FN adsorption and domain availability on PEA and PMA. 72
Figure 3-5 Surface density of BMP-2 on PEA FN and PMA FN. 73
Figure 3-6 Cell adherence to PEA and PMA substrates. 74
Figure 3-7 The Young’s modulus of collagen type I gels. 75
Figure 3-8 Integrin-GF receptor crosstalk. 80
Figure 4-1 Timeline of model culture. 88
Figure 4-2 Gating strategy and representative histograms for analysis of pericyte phenotype. 89
Figure 4-3 RNA-seq profiling of niche-related and differentiation markers at day 7. 92
Figure 4-4 Assessment of pericyte phenotype after 14 day culture in niche models. 94
Figure 4-5 Nestin expression at 7 and 14 days. 97
Figure 4-6 Vimentin expression on PEA FN BMP-2 at 7 days. 98
Figure 4-7 CXCL12 and SCF production in niche models. 100
Figure 4-8 MSPC phenotypes in the BM niche. 106
Figure 5-1 Stem cells reside in and adapt to hypoxic niches. 110
Figure 5-2 Oxygen gradient in the bone marrow niche. 111
Figure 5-3 HIF1α regulation by oxygen tension. 112
Figure 5-4 HIF1α analysis using CellProfiler script. 120

Figure 5-5 RNA-Seq profiling of pericyte transcripts relating to hypoxic adaption after 7 days. 123
Figure 5-6 Nuclear HIF1α levels increase with low-stiffness gels. 124
Figure 5-7 Analysis of HIF1α downstream targets LDH and VEGF. 125
Figure 5-8 Hypoxia gradient analysis. 126
Figure 5-9 Principle component analysis (PCA) of entire metabolome in all niche systems. 128
Figure 5-10 PCA of PEA FN BMP-2 conditions. 129
Figure 5-11 Glycolytic and TCA cycle metabolite profile in PEA FN BMP-2 - gel/+gel/hypoxia. 130
Figure 5-12 $^{13}C_6$-Glucose metabolomic tracing. 131
Figure 6-1 Surface markers associated with human haematopoietic stem cell (HSC) differentiation into lineage progenitors. 139
Figure 6-2 Schematic of HSC co-culture in niche systems. 142
Figure 6-3 Gating strategy for analysis of HSC identification. 144
Figure 6-4 Gating strategy used for cell sorting for LTC-IC. 145
Figure 6-5 Fold increase of CD34+CD38- cells at day 5 in 3 media types. 148
Figure 6-6 Fold increase of CD34+CD38+ and CD34-CD38+ cells at day 5 in 3 media types. 150
Figure 6-7 Total number of colonies maintained from niche systems. 152
Figure 6-8 Representative colony types in CFU assay after 7 days. 153
Figure 6-9 Lineage specification state of CD34+ cells cultured in niche systems. 154
Figure 7-1 Potential applications of an *in vitro* BM niche model. 168
Figure 7-2 Nuclear HIF1α levels increase with low-stiffness gels in Stro1+ MSCs. 173
Figure 7-3 TPO in cell media. 173

Publications

Publications authored by the candidate on research relating to this thesis.

Donnelly H, Salmeron-Sanchez M, Dalby M.J. Designing stem cell niches for differentiation and self-renewal. *Journal of the Royal Society Interface*, 2018, 15(145).

Cheng Z.A, Alba-Perez A, Gonzalez-Garcia C, **Donnelly H**, Llopis-Hernandez V, Jayawarna V, Childs P, Shields D.W, Cantini M, Ruiz-Cantu L, Reid A, Windmill J.F.C, Addison E.S, Corr S, Marshall W.G, Dalby M.J, Salmeron-Sanchez M. Nanoscale coatings for ultralow dose BMP-2-driven regeneration of critical-sized bone defects. *Advanced Science*, 2018, 6(2).

Donnelly H, Dalby M.J, Salmeron-Sanchez M, Sweeten P. Current approaches for modulation of the nanoscale interface in the regulation of cell behaviour. *Nanomedicine: Nanotechnology, Biology, and Medicine*, 2017, 14(7).

Conference Proceedings

2019 Gordon Research Conference Biomaterials and Tissue Engineering: Metabolic and mechanistic insights into bioengineering the bone marrow niche *in vitro*. Barcelona, Spain (poster presentation).

2019 4th Nanoengineering for Mechanobiology: Synergistic integrin-GF receptor microenvironments to bioengineer the bone marrow niche *in vitro*. Genova, Italy (oral presentation).

2019 Royal Society of Chemistry Biomaterials Annual Conference: Synergistic integrin-GF receptor microenvironments to bioengineer the bone marrow niche *in vitro*. Liverpool, UK (oral presentation).

2018 Biointerfaces International: Integrin-growth factor synergistic microenvironments to investigate metabolic mechanisms for a bone marrow niche-like phenotype. Zurich, Switzerland (flash oral presentation and poster presentation).

2018 European Society for Biomaterials: Material driven fibronectin assembly and growth factor presentation to investigate metabolic mechanisms for a bone marrow niche-like pericyte phenotype. Maastricht, Netherlands (oral presentation).

2018 UK Tissue and Cell Engineering Society: Integrin-growth factor synergistic microenvironments to investigate metabolic mechanisms for a bone marrow niche-like phenotype. Keele, UK (poster presentation).

2018 Glasgow Orthopaedic Research Initiative: Metabolic and mechanistic insights into bioengineering the bone marrow niche *in vitro*. Glasgow, UK (oral presentation).

2017 FEBS Workshop Biological Surfaces and Interfaces: Bioengineering the bone marrow niche *in vitro*. St Feliu, Spain (poster presentation).

2016 British Orthopaedic Research Society: Material-driven fibronectin assembly and growth factor presentation for bone regeneration in 3D. Glasgow, UK (poster presentation).

Awards

Gibson Research Scholarship, Institute of Molecular, Cell and Systems Biology, University of Glasgow, 2019.

Best Poster Prize, Biointerfaces International, Zurich, 2018.

Conference Support Award, Institute of Molecular, Cell and Systems Biology, University of Glasgow, 2018.

Group Prize Winner, Impact in 60 seconds competition, University of Glasgow, 2016.

Young Researcher of the Month, Institute of Molecular, Cell and Systems Biology, University of Glasgow, 2016.

Acknowledgements

I would like to thank my supervisors Professors Matt Dalby and Manuel Salmeron-Sanchez. Thank you to Matt for the ongoing support, encouragement and wealth of opportunities given to me over the years; for advising and guiding me closely as an undergraduate, and now at RA level. Thank you to Manuel for the continual encouragement, support and advice throughout my PhD. For supplying the great conference locations that I have been lucky enough to have had the opportunity to attend, as well as for providing the litres of PEA that it has taken to complete this project. To both Matt and Manuel, I will be eternally grateful.

I would also like to thank Dr Ewan Ross, without whom a large portion of this thesis would not have been possible. I am endlessly grateful for the knowledge, advice and skills he has imparted on me, along with the time he has taken to do so. I will forever be indebted to him for putting fat through a cheese grater with me, so that I could complete this work.

I thank everyone in the Centre for the Cellular Microenvironment, both past and present, who have given their valuable time and expertise to support me throughout this project. Particularly I extend thanks to Carol-Anne Smith, Monica Tsimbouri, Paula Sweeten, Annie Cheng, Andres Alba-Perez and Tom Hodgkinson for technical and practical support throughout my research. Thank you to Dr Mathis Riehle for always fixing the microscope for me.

Finally, I would like to express my utmost gratitude for my family and friends. Thank you to my family - Mum, Dad and Joe - for believing and always encouraging me to believe, that anything is possible. Thanks to Eva Lindsay, for years of living the daily ups and downs of this PhD with me, and remaining endlessly supportive. Thanks to all the amazing friends made at the University of Glasgow: Eleanor Gall, Rachel Mackie, Mhairi McGowan, Isy Reed and Hannah Kirkbride - who have all been there daily, for almost a decade now, with love and support no matter the distance.

Author's Declaration

I hereby declare that the research reported within this thesis is my own work, unless otherwise stated, and at the time of submission is not being considered for any other academic qualification.

Hannah Donnelly

31st August 2019

Abbreviations

α-SMA	Alpha smooth muscle actin
AFM	Atomic force microscopy
AGPT1	Angiopoietin 1
AhR	Aryl hydrocarbon receptor
ALCAM	Activated leukocyte cell adhesion molecule
ASC	Adult stem cell
ATP	Adenosine triphosphate
BICD1	Bicaudal D homolog 1
BIT	Bovine insulin transferrin
BM	Bone marrow
BMP	Bone morphogenetic protein
BMPR	Bone morphogenetic protein receptor
BSA	Bovine serum albumin
CAR	CXCL12-abundant reticular cells
CD	Cluster of differentiation
Cdk5	Cyclin-dependent kinase 5
CFU	Colony forming units
CFU-F	Colony forming units-fibroblast
CLP	Common lymphoid progenitor
CMP	Common myeloid progenitor
CNS	Central nervous system
CXCL12	C-X-C motif chemokine 12
CXCR4	C-X-C motif chemokine receptor type 4
DMEM	Dulbecco's modified eagle's medium
DNA	Deoxyribose nucleic acid
EA	Ethyl acrylate
ECM	Extracellular matrix
EGF	Epidermal growth factor
EGFR	Epidermal growth factor receptor
EGM	Endothelial growth medium
ELISA	Enzyme-linked immunosorbent assay
ESC	Embryonic stem cell
ETC	Electron transport chain
FACS	Fluorescent activated cell sorting
FDA	Food and drug administration
FGF	Fibroblast growth factor
Flt3	Fms-like tyrosine kinase 3 ligand
FSC-A	Forward scatter area
FSC-W	Forward scatter width
G-CSF	Granulocyte colony-stimulating factor
GAG	Glycosaminoglycan
GF	Growth factor
GFP	Green fluorescent protein
GFR	Growth factor receptor
Glut	Glucose transporters
HA	Hyaluronic acid
HBSS	Hank's balanced salt solution
HC	Hydrocortisone
HIF	Hypoxia induced factor
HLA	Human leukocyte antigen

HLA-DR	Human leukocyte antigen-DR isotype
HLTM	Human long-term culture medium
HRE	Hypoxia response elements
HRP	Horseradish peroxidase
HS	Human serum
HSC	Haematopoietic stem cell
HSCT	Haematopoietic stem cell transplant
HSPC	Haematopoietic stem and progenitor cell
ICW	In-cell western
IF	Intermediate filament
IL	Interleukin
IMDM	Iscove's modified Dulbecco's medium
iPSC	Induced pluripotent stem cell
LC/MS	Liquid chromatography-mass spectrometry
LDH	Lactate dehydrogenase
LepR	Leptin receptor
LIF	Leukaemia inhibitory factor
LSC	leukemic stem cell
LT-HSC	Long term - haematopoietic stem cell
MA	Methyl acrylate
MCAM	Melanoma cell adhesion molecule
MEP	Megakaryocyte-erythroid progenitor
MFI	Median fluorescent intensity
MIIA	Myosin-IIA
MIIB	Myosin-IIB
MPP	Multipotent progenitor
MRTF-A	Myocardin-related transcription factor A
MS	Mass spectrometry
MSC	Mesenchymal stromal cell
MSPC	Mesenchymal stromal and perivascular cell
NAT	Non-animal technology
NCAM	Neural cell adhesion molecule
NG2	Chondroitin sulphate proteoglycan
NMR	Nuclear magnetic resonance
OCN	Osteocalcin
ODDD	Oxygen-dependent degradation domains
ON	Osteonectin
OOC	Organ-on-a-chip
OPN	Osteopontin
OSX	Osterix
OXPHOS	Oxidative phosphorylation
PBS	Phosphate-buffered saline
PCA	Principle component analysis
PDGF	Platelet derived growth factor
PDGFR	Platelet derived growth factor receptor
PDH	Pyruvate dehydrogenase
PDK	Pyruvate dehydrogenase kinase
PEA	Poly (ethyl acrylate)
PECAM-1	Platelet and endothelial adhesion molecule-1
PEG	Poly(ethylene glycol)
PEO	Poly(ethylene oxide)
PGE2	Prostaglandin E2
PHD	Prolyl hydroxylases

PI3K	Phosphoinositide 3- kinase
PLA	Proximity ligation assay
PlGF2	Placental growth factor-2
PMA	Poly (methyl acrylate)
pO_2	Partial pressure of O_2
RGB	Red green blue
RGD	Arginine, glycine and aspartic acid
RNA	Ribonucleic acid
ROS	Reactive oxygen species
RT	Room temperature
SAM	Self-assembled monolayer
SCF	Stem cell factor
SDF1	Stromal cell-derived factor 1
SLAM	Signalling lymphocyte activation molecule
Smad	Small mothers against decapentaplegic
SNS	Sympathetic nerve signals
SR1	StemReginin1
SSC-A	Side scatter area
ST-HSC	Short term - haematopoietic stem cell
SVF	Stromal vascular fraction
TCA	The citric acid
TGF	Transforming growth factor
TPO	Thrombopoietin
UCB	Umbilical cord blood
VCAM1	Vascular cell adhesion molecule 1
VEGF	Vascular endothelial growth factor
VHL	von Hippel-Lindau

Chapter 1 Introduction

Stem cells are defined by their ability to self-renew and produce specialised progeny (Lane et al., 2014). Consequently, they hold great clinical potential as the cell source for the regeneration of aged, injured and diseased tissues. However, despite the remarkable potential their use is currently hindered as functionality is lost when they are removed from their *in vivo* regulatory microenvironment – termed the *stem cell niche* (Schofield, 1978). It is therefore a significant goal to engineer new culture environments that recapitulate strategies used by stem cell niches *in vivo*, that promote differentiation of stem cells into specialised cell types and maintain adult stem cells throughout life, without a loss of 'stemness' (Lutolf et al., 2009).

The bone marrow (BM) stem cell niche has a key role in regulating haematopoiesis and is home to two major clinically relevant sources of adult stem cells (ASCs); mesenchymal stromal and perivascular cells (MSPCs) and haematopoietic stem cells (HSCs) (Pinho and Frenette, 2019). This specialised microenvironment is comprised of heterogenous populations of cells types, alongside physical and chemical characteristics that are fundamental to its function (Mendelson and Frenette, 2014; Morrison and Scadden, 2014; Pinho and Frenette, 2019). This chapter will give an overview of stem cell niches, with focus on the BM niche. It will then explore how biomaterial strategies can be employed to direct stem cell behaviour by closely mimicking niche properties, and how these approaches have provided insight into fundamental stem cell mechanisms. Finally, it will describe the aims and objectives of this thesis.

1.1 Stem Cell Niches

Stem cells are the focus of many applications in regenerative medicine because of their ability to self-renew and to generate differentiated progeny (Lane et al., 2014). There are three main categories of stem cells; embryonic stem cells (ESCs) that are derived in culture from pre-implantation embryos, they are pluripotent as they have the ability to differentiate into all cell types in the body, generating diverse tissues (Martello and Smith, 2014). Most adult tissues retain resident stem cells (ASCs), these are multipotent, specialised and essential for tissue maintenance and repair throughout life (Wagers and Weissman, 2004). Finally,

pluripotent stem cells can be generated by reprogramming adult cells through the induction of a small number of specific genes, these are known as induced pluripotent stem cells (iPSCs) (Yu et al., 2007).

In adulthood, tissue homeostasis and regeneration are critically dependent on both the self-renewal and the differentiation capacity of ASCs. These unique properties mean the potential clinical applications of ASCs are vast, for example in the treatment of injury due to trauma and to treat various genetic diseases and cancers.

A central strategy in regenerative medicine is to transplant stem cells or their differentiated derivatives into patients. Perhaps of greatest success are HSC transplants (HSCT), which for over 50 years have been extracting HSCs from the BM to restore the haematopoietic system of cancer patients after chemotherapy, for the treatment of genetic blood disorders such as thalassemia (Gaziev et al., 2005), and more recently in the treatment of autoimmune diseases such as multiple sclerosis (Radaelli et al., 2014).

Other validated adult cell therapies include transplantation of cultured sheets of autologous epidermal cells to repair burn injuries (Wood et al., 2006), *ex vivo*-expanded autologous chondrocytes to repair cartilage defects (Oldershaw, 2012), and co-transplantation of immunomodulatory mesenchymal stromal cells (MSCs) to augment graft-versus-host disease in procedures such as islet transplant (Ito et al., 2010). These examples involve cells from adult tissues, but there have also been recent advancements in the application of pluripotent stem cells towards the clinic; human ESCs differentiated into retinal pigment epithelium to treat age-related blindness is currently in clinical trials (Da Cruz et al., 2018), and neuronal precursors generated from iPSCs were recently shown to restore function when implanted into a primate model of Parkinson's disease (Kikuchi et al., 2017).

The future of the use of stem cells for regenerative medicine is promising, however inherent hurdles still need to be overcome to harness their full therapeutic potential. The clinical application of ASCs which are easily harvested from adult tissues such as BM or fat, is currently limited, as in contrast to their embryonic counterparts ASCs will spontaneously differentiate in culture, only retaining their unique functions if they are in contact with an instructive

microenvironment (Donnelly et al., 2018; Lane et al., 2014; Lutolf et al., 2009). This specialised local microenvironment, the *stem cell niche*, was first described four decades ago by Schofield and refers to the extrinsic physical and functional factors of the localised microenvironment, which stem cells integrate in concert with induced cell-intrinsic regulatory networks to mediate cellular behaviour – balancing self-renewal and differentiation in response to physiological demands (Schofield, 1978) (Figure 1-1).

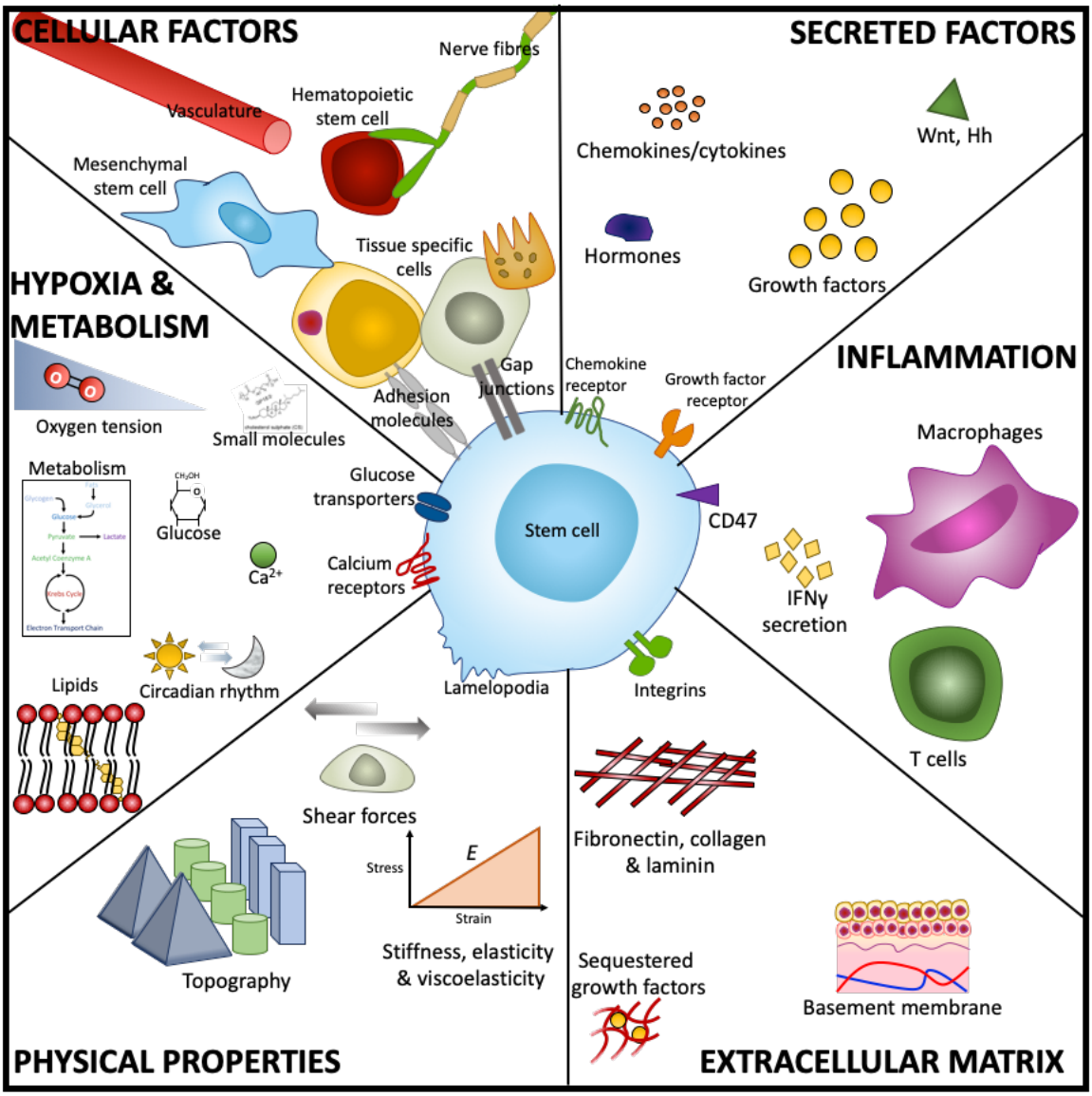

Figure 1-1 Parameters of the stem cell niche. Niches are multi-faceted and complex microenvironments that are specific to function. However principle parameters of these environments are shared throughout multiple tissue types. Generally, they are comprised of physical and dynamic factors such as heterologous cellular components and cell-cell interactions, secreted and membrane-bound factors, immunological activation and response, extracellular matrix (ECM) protein components and structure, physical and architectural parameters, oxygen tension and metabolic regulation. Adapted from (Donnelly et al., 2018) with permissions.

Schofield's original article hypothesized that retention of transplanted HSCs ability to self-renew depends upon the environment provided by neighbouring non-HSC cells, and that progeny of these stem cells will differentiate unless they occupy a similar 'niche' (Schofield, 1978). Since this description of the BM niche for HSCs, stem cell niches have been described in several adult tissues, including intestine (Yen and Wright, 2006), skin (Tumbar et al., 2004) and the nervous system (Fuentealba et al., 2012). With this, Schofield's original concept of the niche has been extended to include many aspects of the stem cell microenvironment. Key components include direct interactions between stem cells and neighbouring heterologous cell types, secreted and membrane-bound factors, extracellular matrix (ECM) protein composition and architecture, physical parameters such as stiffness and shear stress, inflammation and scarring and environmental factors such as local oxygen tensions (Figure 1-1)(Lane et al., 2014).

To better harness the therapeutic potential of ASCs, fundamental questions regarding the cell-intrinsic and cell-extrinsic regulation of stem cell functions still need to be addressed. Understanding how and what factors in niches result in the balance between differentiation and self-renewal of the stem cell pool would allow us to better exploit these cells for clinical use, and for the development of more humanised *in vitro* models that recreate tissue complexity. The development of such *de-novo* niches would reduce costly animal testing and also present simplified experimental systems in which to investigate processes fundamental to stem cell regulation.

1.2 Bone Marrow Architecture

The BM is the primary site of haematopoiesis, a continuous process of blood-cell production throughout the life-span of mammals (Jagannathan-Bogdan and Zon, 2013). Haematopoiesis orchestrates the balance between self-renewal, differentiation and proliferation of HSCs in the BM, followed by egress of mature progeny with specialised functions into the circulating blood (Mendelson and Frenette, 2014). An adult human is estimated to generate ~4-5 x 10^{11} haematopoietic cells per day (Kaushansky, 2006), and as such, the production of blood requires a highly regulated and responsive system to ensure haematopoietic homeostasis throughout life. Dysregulation of haematopoiesis can lead to

myeloproliferative diseases or leukaemia if self-renewal is unrestrained, or depletion of the stem cell pool if self-renewal is insufficient (Bonnet, 2005).

The BM microenvironment is integral in HSC homeostasis, it maintains and directs self-renewal and differentiation of both HSCs and MSCs (Pinho and Frenette, 2019). Located in the cancellous portions of long bones, BM is a complex and dynamic organ, containing a central marrow cavity that is surrounded by vascularised and innervated bone. Minute projections of bone (trabeculae) are found throughout the metaphysis providing a large surface area so that many cells are in close proximity to the bone surface (Figure 1-2) (Morrison and Scadden, 2014). The endosteum is at the interface of the bone surface and the marrow, it is covered by bone-lining osteoblasts and bone-resorbing osteoclasts. There is a rich supply of arterioles and sinusoids near the endosteum. Arterioles carrying oxygen, nutrients and growth factors (GFs) into the BM feed into sinusoidal vessels, which coalesce as a central sinus to form the venous circulation (Figure 1-2). Sinusoids are specialised vessels that allow cells to pass in and out of circulation, the connection between arterioles and the sinusoidal network preferentially occurs adjacent to the endosteal surface (Ehninger and Trumpp, 2011; Mendelson and Frenette, 2014; Morrison and Scadden, 2014; Pinho and Frenette, 2019).

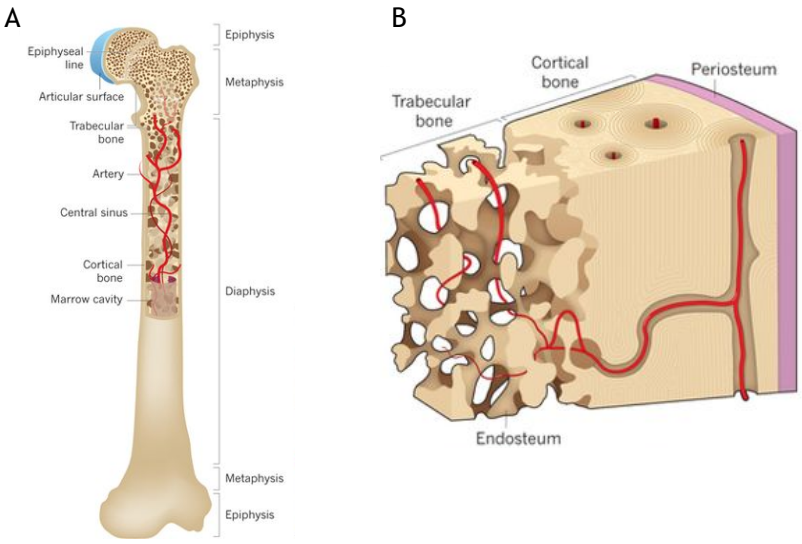

Figure 1-2 Bone marrow structure. Bone marrow is a complex organ that regulates haematopoiesis. A. Minute projections of bone (trabeculae) are found throughout the metaphysis, this creates a large surface area and means many cells are in close proximity to the bone surface. B. The endosteum is the interface between the bone and bone marrow. The bone marrow is well vascularised, containing nutrient/oxygen carrying arteries, which feed into sinusoids that form the central venous circulation. Sinusoids are specialised vessels that allow cells to pass in and out of circulation. Adapted with permissions from (Morrison and Scadden, 2014).

Local cues from the BM microenvironment, termed the BM or HSC niche, alongside long-range humoral and neural signals integrate to regulate HSC activity. Since Schofield's seminal 1978 article, referring to the niche as the regulatory unit balancing HSC self-renewal and differentiation, the field has grown rapidly; considerably so in the last ten years as imaging, computational techniques and functional genetic tools have advanced, providing a better understanding of the *in situ* BM microenvironment (Pinho and Frenette, 2019).

The BM niche is now regarded as a complex and dynamic tissue, comprised of a heterogenous cellular, molecular and physical environment (Morrison and Scadden, 2014). Imaging techniques combined with conditional deletion of crucial regulatory factors from candidate niche cell types in mouse models have identified distinct BM niche constituents, including both HSC-progeny and non-haematopoietic cell types (Pinho and Frenette, 2019). Although, as the literature currently stands, there is a paradoxical situation where almost all cellular constituents of the BM have been proposed to contribute to HSC regulation and niche homeostasis. The situation is further complicated by both the HSC and stromal stem cell populations of the BM being functionally and molecularly heterogenous. This has led to the proposition that distinct niches exist for distinct subpopulations of HSCs (Boulais and Frenette, 2015; Mendelson and Frenette, 2014; Morrison and Scadden, 2014).

1.3 Bone Marrow Resident Stem Cells

The BM comprises several key cell types, including several types of stem cell, that are themselves regulated by the niche microenvironment and, in turn, are integral in the regulation of haematopoiesis.

1.3.1 Mesenchymal stromal cells

MSCs, first discovered in 1974, are ASCs that reside in many organs and tissues of the body, including the BM, adipose tissue and umbilical cord (Friedenstein, 1976). MSCs are multipotent and produce cells of mesenchymal lineage, including osteoblasts, chondrocytes, adipocytes and myoblasts (Figure 1-3)(Caplan, 1991). They are important in healing and tissue regeneration, have immunomodulatory capacity and are crucial in the support of HSCs in the bone marrow niche.

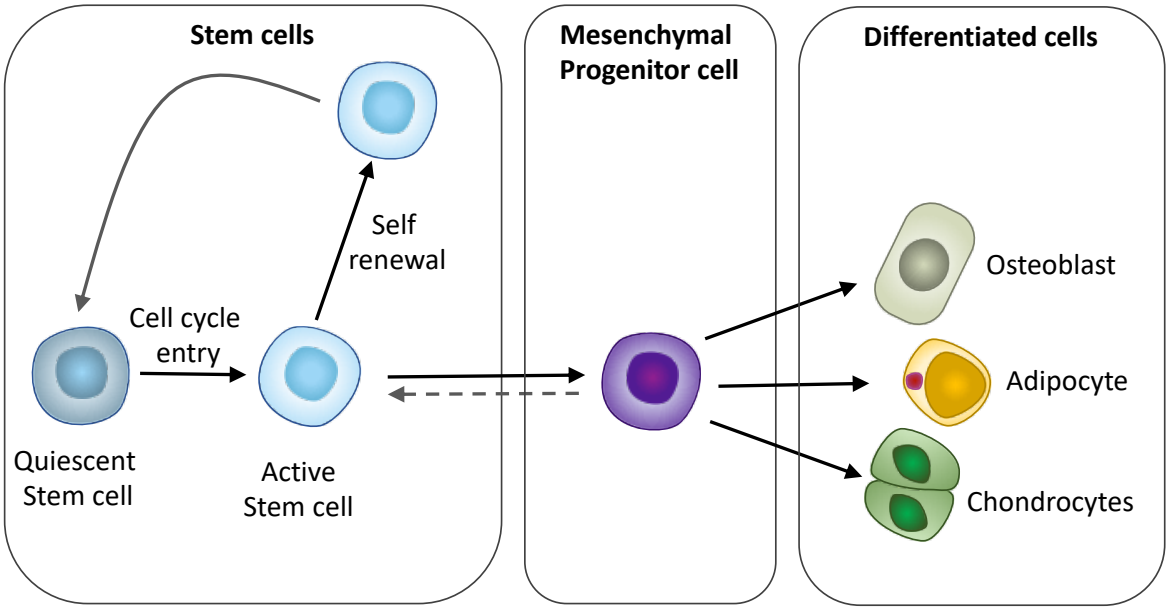

Figure 1-3 Model of the organization of MSCs. Multipotent stem cells exist in homeostasis between quiescence and an activated state. Activation, and entry to the cell cycle, occurs upon tissue damage or other physiological stimuli. Upon activation (regenerative demand), multipotent progenitor cells with transit amplification capacity arise. These progenitors are the precursors to the tissue-specific mature cells, for example osteoblasts, adipocytes and chondrocytes in the MSC compartment. The activated stem cell and its daughter cells differentiate or can return to a quiescent state once the tissue repair or other physiological process is complete. This homeostasis between quiescence and self-renewal is tightly regulated to avoid transformations and to retain a viable stem cell pool throughout the life of the organism. Adapted from (Donnelly et al., 2018) with permissions.

MSCs are most commonly isolated from the BM, despite only comprising 0.001 – 0.01 % of the total BM cell number (Banfi et al., 2000). Although these cells can be expanded *ex vivo,* a loss of differentiation capacity is associated with long-term culture (Zaim et al., 2012). Adipose tissue offers a viable alternative MSC source, as it is easily obtained in larger quantities and avoids donor site morbidity or pain associated with BM extraction (Schneider et al., 2017). However, identification of MSCs is complex in part due to this ability to be obtained from multiple tissues, and several subsets exist even within the same tissues that exhibit subtle, yet significant, biological differences. A position statement from the International Society for Cellular Therapy (ISCT) has defined the minimal criteria for MSCs as: (i) MSCs must be plastic-adherent when maintained in standard culture; (ii) MSCs must express CD105, CD73, and CD90, and lack expression of CD45, CD34, CD14 or CD11b, CD79α or CD19 and HLA-DR surface molecules (cluster of differentiation; CD. Human leukocyte antigen-DR isotype; HLA-DR); (iii) MSCs must be able to differentiate into osteoblasts, adipocytes and chondrocytes under standard *in vitro* differentiating conditions (Dominici et al., 2006) (Figure 1-3). No single marker associated with MSC 'stemness' has been agreed, instead many 'proxy' identifiers for subsets of MSCs with differing

functions are utilised. The markers most commonly used as identifiers or for isolation of MSC subsets and are shown in Table 1-1.

Table 1-1 Markers associated with mesenchymal stem cell phenotype subsets.

Marker	Protein	Biological properties	Reference
CD90+	Thy-1, glycosylated membrane protein	Cell-cell and cell-matrix interactions.	(Dominici et al., 2006)
CD44+	Cell-surface glycoprotein	Cell-cell interactions, adhesion, migration.	(Herrera et al., 2007)
CD140a+	Platelet derived growth factor receptor-α (PDGFRα)	HSC supportive. Express nestin.	(Pinho et al., 2013)
CD51+	Integrin α_v	HSC supportive. Express nestin.	(Pinho et al., 2013)
CD271+	Low-affinity nerve growth factor receptor (NGFR)	Isolates immunosuppressive MSCs from BM but not adipose tissue.	(Álvarez-Viejo et al., 2015; Lv et al., 2014; Mo et al., 2016)
CD73+	5'-nucleotidase (5'-NT)	Enzyme, conversion of AMP to adenosine.	(Dominici et al., 2006)
CD105+	Endoglin	Cell adhesion.	(Dominici et al., 2006)
CD106+	Vascular cell adhesion molecule (VCAM)	Cell adhesion.	(Yang et al., 2013)
CD166+	Activated leukocyte cell adhesion molecule (ALCAM)	Cell adhesion.	(Rojewski et al., 2008)
STRO1+	Cell surface receptor	Promote angiogenesis. May not support HSC engraftment.	(Lv et al., 2014; Mo et al., 2016)

1.3.1.1 MSCs in the clinic

MSCs are easily harvested from autologous tissues such as the BM and are amenable to *in vitro* cell culture, therefore allowing growth of significant cell numbers in the lab - provided the correct cues are employed. These two factors, alongside their multilineage potential and immunomodulatory properties have made MSCs an attractive target for regenerative medicine and therapeutic applications (Figure 1-4). However, since their discovery in 1974 there have been less clinical success stories than first imagined, owing to limitations such as batch-to-batch variability and poor definition. Highlighting that further understanding of fundamental and basic mechanisms need to be understood to harvest the full potential of these cells (Dalby et al., 2018; Donnelly et al., 2018).

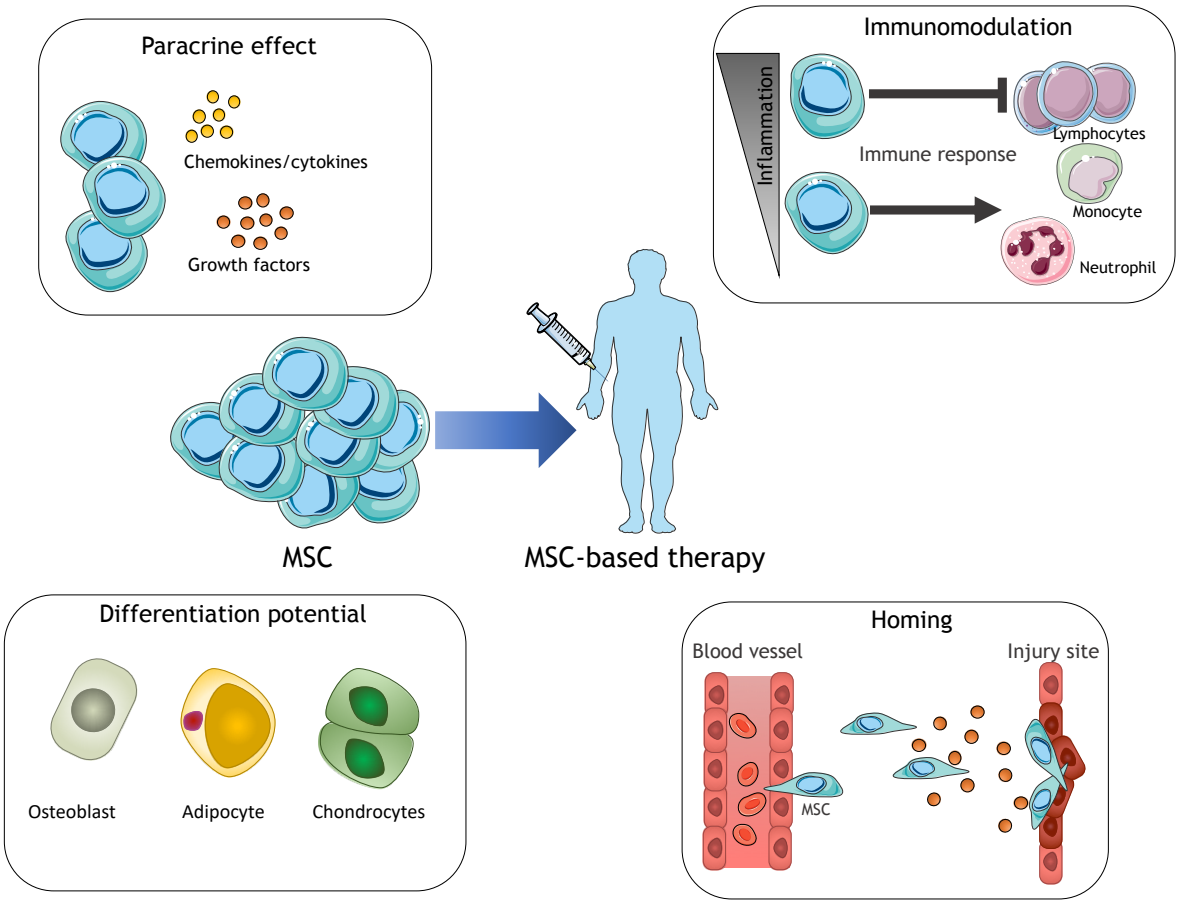

Figure 1-4 Therapeutic potential of MSCs. Unique biological properties of MSCs supporting their clinical application include: the ability to secrete soluble factors that regulate surrounding cells, ability to modulate the immune response, multi-lineage differentiation capacity and the ability to migrate to sites of injury. Adapted from (Squillaro et al., 2016). This figure was created using Servier Medical Art, licensed under a Creative Commons Attribution 3.0 Generic License.

Currently, a search on www.clinicaltrials.gov for 'mesenchymal stem cells' returns 955 studies (accessed 16/05/2019). These trials range from the use of both allogenic or autologous MSCs for orthopaedic applications (bone regeneration), to the treatment of chronic conditions (e.g. liver failure, diabetes), tumour homing and to offset graft-versus-host disease. One example of an autologous MSC-based product currently in advanced clinical trials is 'Bonofill', which harvests adipose-derived MSCs and combines with a 3D mineralised scaffold to engineer 'custom' bone grafts for use in maxillofacial bone augmentations and regeneration (ClinicalTrials.gov identifier: NCT02153268, reviewed in (Paduano et al., 2017)).

1.3.2 Pericytes

Pericytes, originally defined by their anatomical location, are perivascular stellate cells that encircle the endothelium of small vessels and have been identified in nearly all vascularised tissues (Crisan et al., 2008). Originally thought to play a

major role in vascular support, pericytes gained renewed interest when over a decade ago they were identified as the *in vivo* origin of the MSC (Crisan et al., 2008). Using a defined set of markers, the landmark paper by Crisan et al, identified perivascular cells from diverse human tissues, such as BM, adipose, brain, pancreas and placenta. They then validated that these pericytes display hallmark characteristics of *in vitro* MSCs; such as adherence to plastic, MSC marker expression and multilineage differentiation capacity for osteogenic, chondrogenic, adipogenic and myogenic lineages (Figure 1-5)(Crisan et al., 2008).

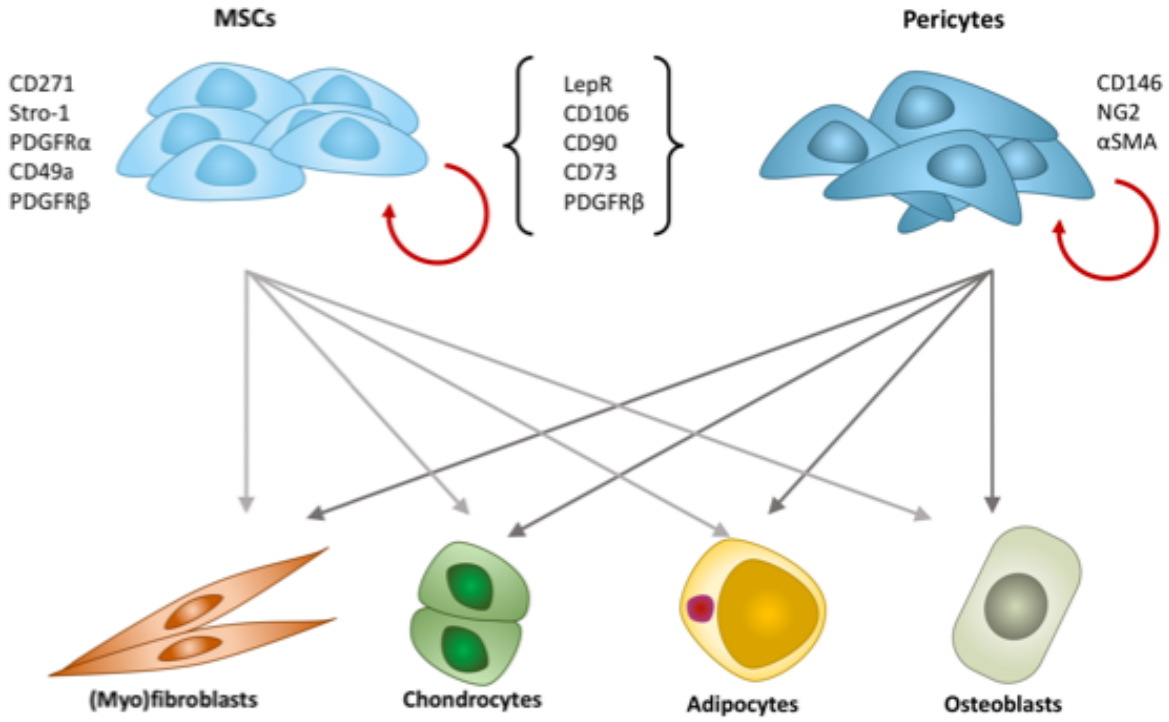

Figure 1-5 Pericytes and MSCs share surface markers and differentiation capacity. Both unique and shared markers (in brackets) are shown.

The markers used to identify pericytes are all present on other cell types, hence there is no single 'pericyte-marker', however there are well-defined combinations of surface antigens that are now routinely used for their identification (Sá da Bandeira et al., 2016). CD146, or melanoma cell adhesion molecule (MCAM), is highly expressed on pericytes and is an adhesion molecule involved in the interaction between endothelial cells and pericytes (Ishikawa et al., 2014). CD146 expression is also found on smooth muscle cells, endothelial cells and some T and B lymphocytes, and so negative expression of the markers CD31, CD34 (endothelial/haematopoietic), CD56 (myogenic) and CD45 (haematopoietic) are commonly used to isolate pericytes from various tissues (i.e. CD146+CD31-CD34-CD45-CD56-). Several other markers are associated with pericytes, such as α-SMA

(α-smooth muscle actin) and NG2 (chondroitin sulphate proteoglycan 4), these are summarised in Table 1-2. However, it should be noted that varying expression of these markers have been observed in pericytes from different tissues, at different time points in development and discrepancies exist even within pericytes isolated from the same tissue (Crisan et al., 2008; Kunisaki et al., 2013; Sá da Bandeira et al., 2016). It has been suggested α-SMA and NG2 expression can be used to discriminate between pericytes associated with arterioles (NG2+ α-SMA+), capillaries (NG2+ α-SMA-) and venules (NG2- α-SMA+) (Crisan et al., 2008; Nehls and Drenckhahn, 1991).

Since the study by Crisan et al, it has been contentiously thought that pericytes are the *in situ* equivalent of the MSC. Many studies have supported this model, showing that transplanted purified perivascular cells and genetically traced pericytes contribute to tissue-specific lineages *in vivo* (Chen et al., 2014; Dellavalle et al., 2007; Feng et al., 2011; Gortiz et al., 2011). Pericytes with heterogeneous sets of markers have also been implicated as key components supporting HSCs in the BM. CD146 expressing perivascular cells from the BM were initially shown by Sacchetti et al, to regenerate bone and stroma, establishing a functional haematopoietic microenvironment upon transplantation *in vivo* (Sacchetti et al., 2007). Then, more recently, nestin+ pericytes have been shown to regulate HSC quiescence, and LepR+ pericytes shown to regulate HSC activation (discussed in detail in Table 1-3) (Kunisaki et al., 2013). In much of the literature related to the BM niche, the terms perivascular cell/pericyte/mesenchymal stem/stromal cell are often used indiscriminately and interchangeably, adding further uncertainties and complexity to the area.

Table 1-2 Markers associated with pericyte phenotype.

Marker	Protein	Biological properties	Reference
CD146+	melanoma cell adhesion molecule (MCAM)	Pericyte-endothelial cell interaction.	(Crisan et al., 2008; Pinho et al., 2013; Sacchetti et al., 2007)
NG2+	Chondroitin sulphate proteoglycan 4	Expressed during vascular morphogenesis.	(Crisan et al., 2008; Kunisaki et al., 2013; Ozerdem et al., 2001)
Nes+	Nestin	Intermediate filament protein type IV. Expressed in arteriolar-associated pericytes.	(Kunisaki et al., 2013; Pinho et al., 2013)
PDGFR-α+	Platelet derived growth factor receptor α	Interacts with PDGFA, PDGFB, integrin β3, caveolin-1 and nexin.	(Crisan et al., 2008; Sá da Bandeira et al., 2016)
PDGFR-β+	Platelet derived growth factor receptor β	Interacts with PDGFA and PDGFB. Expression restricted to pericytes and smooth muscle in adults. Not a suitable marker during embryogenesis. Role during capillary sprouting.	(Crisan et al., 2008; Guimaraes-Camboa et al., 2017)
CD51+	Integrin α_v	HSC supportive.	(Pinho et al., 2013)
LepR+	Leptin receptor	Expressed in sinusoidal-associated pericytes.	(Ding et al., 2012; Kunisaki et al., 2013)
α-SMA+	α-smooth muscle actin	Expressed in pericytes, smooth muscle cells and myofibroblasts.	(Crisan et al., 2008; Sá da Bandeira et al., 2016)
CD45-	Protein tyrosine phosphatase receptor type C	Transmembrane protein expressed on all haematopoietic cells	(Crisan et al., 2008)
CD34-	Transmembrane glycoprotein	Expressed in haematopoietic and endothelial cells. Involved in cell-cell adhesion	(Crisan et al., 2008)
CD56-	Neural cell adhesion molecule (NCAM)	Myogenic and neural marker	(Crisan et al., 2008)

However, it should be noted that in a study in 2017 Guimaraes-Camboa et al, challenged the idea of pericytes as MSC equivalents. Here they identified *Tbx18* as a gene specifically expressed in pericytes in many adult organs, including brain, heart, skeletal muscle and adipose tissue. By generating a transgenic mouse line expressing an inducible Cre recombinase in *Tbx18*-expressing cells they performed lineage tracing of this marker in pericyte progeny during aging and tissue repair over the course of 2 years. Surprisingly, they found that *Tbx18* lineage-derived cells maintain their perivascular identity, suggesting pericytes do not give rise to other tissue specific cell types in these organs, in the context of both aging and tissue repair. Implying strongly, that these cells do not behave as MSCs in the organs studied (Guimaraes-Camboa et al., 2017).

The Guimaraes-Camboa et al, study raises important questions. By demonstrating that cells possessing all the hallmarks of MSCs *in vitro* can lack any MSC potential *in vivo*, this challenges the established idea of pericytes as the origin of MSCs, and also of the existence of MSCs in many adult organs that have been identified through transplantation studies, as such further work will be needed to fully understand and define the MSC both in their native environment and as therapeutic tools (Cano et al., 2017).

Due to the contention in definition and identity of MSCs/pericytes, this thesis will use the term mesenchymal stromal and perivascular cells (MSPCs) to refer to the heterogenous BM perivascular and stromal cell populations. Where appropriate, the populations will be specifically defined as MSCs or pericytes.

1.3.2.1 Pericytes in the clinic

Pericytes hold similar properties for tissue regeneration and immunosuppression as that identified for other MSC subsets. They have been highlighted as candidates for orthopaedic applications and adipose-derived pericytes are currently in clinical trials for osteoarthritic treatments (Pak et al., 2017). However due to their vascular origin, many pre-clinical applications for pericytes have focussed on their potential for therapeutic vasculogenesis (Riu et al., 2017), or in the treatment of heart disease (Avolio et al., 2015).

1.3.3 Haematopoietic stem cells

Of all the known stem cell types, HSCs are the best characterised and studies of haematopoiesis have provided critical information into other areas of stem cell biology in development, homeostasis and reprogramming (Orkin and Zon, 2008). HSCs can self-renew and differentiate, forming the mature progeny that make up the haematopoietic system; mature blood cells are predominantly short lived, meaning stem cells are required throughout the lifetime of the organism to replenish multilineage progenitors and the precursors committed to individual haematopoietic lineages (Figure 1-6) (Orkin and Zon, 2008). HSCs are tightly controlled by cues from the BM niche microenvironment in order to maintain homeostasis, during which most HSCs are quiescent (Passegué et al., 2005). They sit at the top of a hierarchy of progenitors that become progressively restricted to produce precursors of uni-lineage differentiation potential and of mature blood cells, including red blood cells, megakaryocytes, myeloid cells (monocyte/macrophage and neutrophil) and lymphocytes (Figure 1-6).

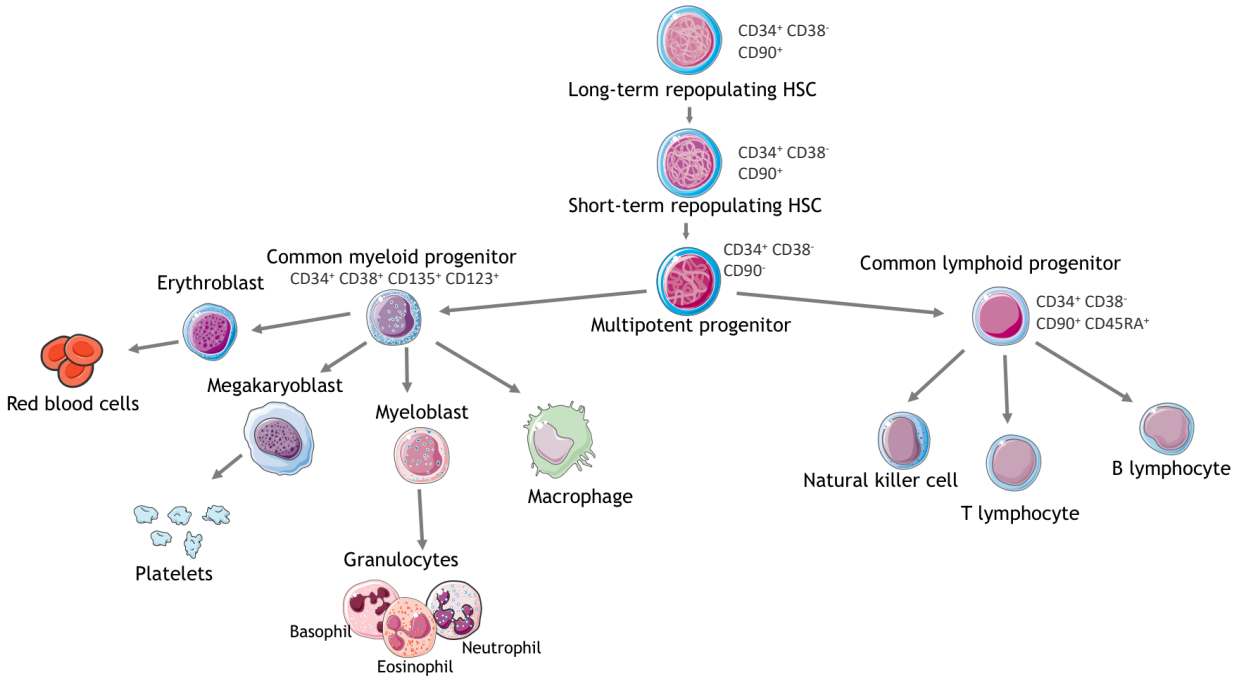

Figure 1-6 Haematopoietic development including identifying surface markers for HSCs and progenitor cells. Long-term repopulating HSCs progressively lose self-renewal capacity, progressively restricting differentiation potential, until they retain the ability to differentiate down one lineage, either lymphoid or myeloid. This progressive restriction eventually leads to the formation of mature blood cells that contribute to the haematopoietic system. HSC; haematopoietic stem cell. This figure was created using Servier Medical Art, licensed under a Creative Commons Attribution 3.0 Generic License.

HSCs either self-renew or generate multipotent progenitors (MPPs), which retain short-term multilineage repopulation potential (Yamamoto et al., 2013). MPPs

give rise to lineage committed progenitors of common lymphoid (CLP) and common myeloid progenitors (CMP). CMP give rise to granulocyte/monocyte and megakaryocyte/erythrocyte progenitors (MEP), which differentiate ultimately to platelets and red blood cells (Hao et al., 2001; Manz et al., 2002) (Figure 1-6).

First identified in 1961 through transplantation studies HSCs have since been widely researched, providing a solid foundation in which to study the cells. HSCs are characterised by their capacity to reconstitute the entire blood system of a recipient (Eaves, 2015). Isolation and lineage tracing of HSCs is routinely carried out by flow cytometry where a series of cell surface markers have been well-defined for each development stage of haematopoiesis, highlighted in Figure 1-6 (Chao et al., 2008). HSCT experiments have led to classification of two-distinct HSC populations: short-term engrafting (ST-HSC) and long-term engrafting (LT-HSC). LT-HSCs contribute to peripheral blood for up to 6 months, and can be transferred to new hosts by secondary transplantation; whereas, ST-HSCs can produce blood cells for up to 3 months post-HSCT (Zon, 2008).

1.3.3.1 Clinical demand for HSCs

Autologous HSCT is the current standard treatment for many haematological conditions; such as Hodgkin's lymphoma, non-Hodgkin's lymphoma, multiple myeloma, sickle cell anaemia and autoimmune diseases such as multiple sclerosis (Mendelson and Frenette, 2014; Radaelli et al., 2014). Transplantable HSCs can be obtained from BM, peripheral blood and umbilical cord blood (UCB). BM and BM transplants have been the standard source for many years (Figure 1-7), however it is now becoming increasingly common to pharmacologically mobilize HSCs out of the marrow, then isolate from peripheral blood (Mendelson and Frenette, 2014).

Autologous transplants are the gold standard method as they avoid immune rejection, which ultimately leads to delayed engraftment, graft-versus-host disease and graft rejection. Although this is often not possible as it requires HSCs to be obtained before the clinical need, i.e. pre-malignancy. Therefore, the use of donor HSCs, known as allogenic transplants, are routinely employed and have high success rates providing a human leukocyte antigens- (HLA) matched donor is available (Park and Seo, 2012).

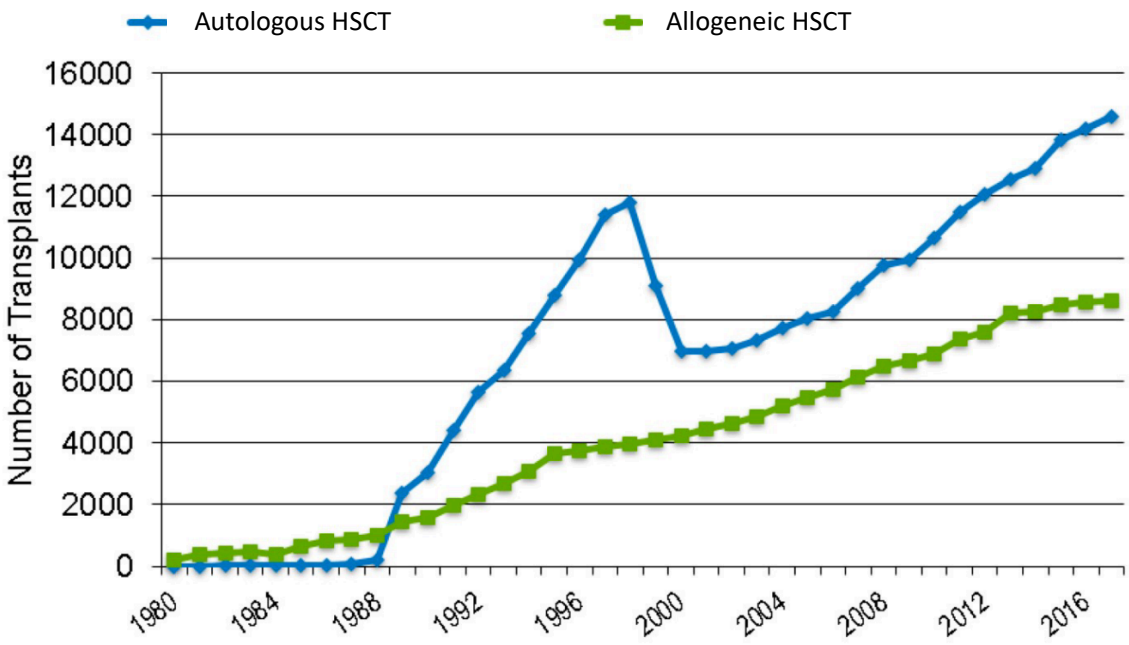

Figure 1-7 The estimated annual numbers of haematopoietic stem cells transplant (HSCT) recipients in the USA. Graph shows increasing incidence and therefore need for HSCT. Reproduced with permissions from (D'Souza and Fretham, 2018).

However, difficulties in finding suitable adult allogenic donors alongside low cell yields from cord blood has focussed investigations into methods of stem cell expansion (Hofmeister et al., 2007). *Ex vivo* HSC expansion is itself difficult due to an inability to retain these cells in synthetic culture environments for significant time periods. Once HSCs are removed from the niche microenvironment their self-renewal capacity is lost quickly, cells robustly proliferate and spontaneously differentiate in a matter of days rendering them clinically ineffective (Boitano et al., 2010). Further to this, although HSCT are successfully used to treat cancers and are seeing great success in clinical trials for treatment of other diseases, there remains an unmet demand for matched donors (Figure 1-7). There is focus on strategies to counteract poor HSC survival in culture and to increase HSC yield, these include complex and expensive media formulations (Murray et al., 1999), the use of small molecules that promote *ex vivo* HSC and progenitor expansion (Boitano et al., 2010; Goessling et al., 2009) and material and engineering strategies that aim to recapitulate aspects of the *in vivo* niche (Müller et al., 2014), several of which are summarised in Table 1-5.

1.4 The Bone Marrow Niche

The exact location and composition of the BM niche remains a major topic of debate in the field. Direct visualisation of the BM would be essential to fully understand HSC activity and define bona fide niches *in situ*. However, this is a major challenge owing to a lack of exclusive markers for identifying and tracking HSCs and other stromal niche cells, and due to the calcified nature of bone. However, the distribution of HSCs within the BM is not random, it has been demonstrated that there are specific cellular components in each environment that are indispensable regulators of HSC activity (Pinho and Frenette, 2019).

Initial reports traced homing of transplanted green fluorescent protein (GFP)-marked HSCs and haematopoietic stem and progenitor cells (HSPCs) in the mouse BM, and suggested that quiescent LT-HSCs preferentially localised near the endosteal surface, whereas mature lineage-committed cells were redistributed throughout the central marrow region; suggesting an endosteal niche for HSCs (Lo Celso et al., 2009; Nilsson et al., 2001; Xie et al., 2009; Zhang et al., 2003). However, the endosteum is highly vascularised with arterioles that are proximal to the endosteal surface, and sinusoids that are distributed throughout the cavity, it has therefore been suggested that HSCs may be interacting with both endosteal and vascular niche components simultaneously (Nombela-Arrieta et al., 2013).

As such, as imaging techniques have advanced, it has been demonstrated that the endosteal model was perhaps over simplified, and that in the trabecular bone the endosteum is enriched with arterioles that are in tight association with adrenergic nerves fibres and are ensheathed with nestin+ MSPCs, to which subsets of dormant LT-HSCs have been shown to localise (Kunisaki et al., 2013). This is referred to as the arteriolar niche. Putative HSCs have also been identified to be located close to sinusoids (Kiel et al., 2005). Leptin receptor(LepR)+ MSPCs are localised close to sinusoidal vessels and these are thought to support more active HSCs, referred to as the sinusoidal niche (Boulais and Frenette, 2015).

These observations give rise to the current model of the niche, in which the endosteum/arteriolar niche houses quiescent HSCs, with more active cycling HSCs located around the sinusoid, and is illustrated in Figure 1-8 (Ehninger and Trumpp, 2011; Pinho and Frenette, 2019).

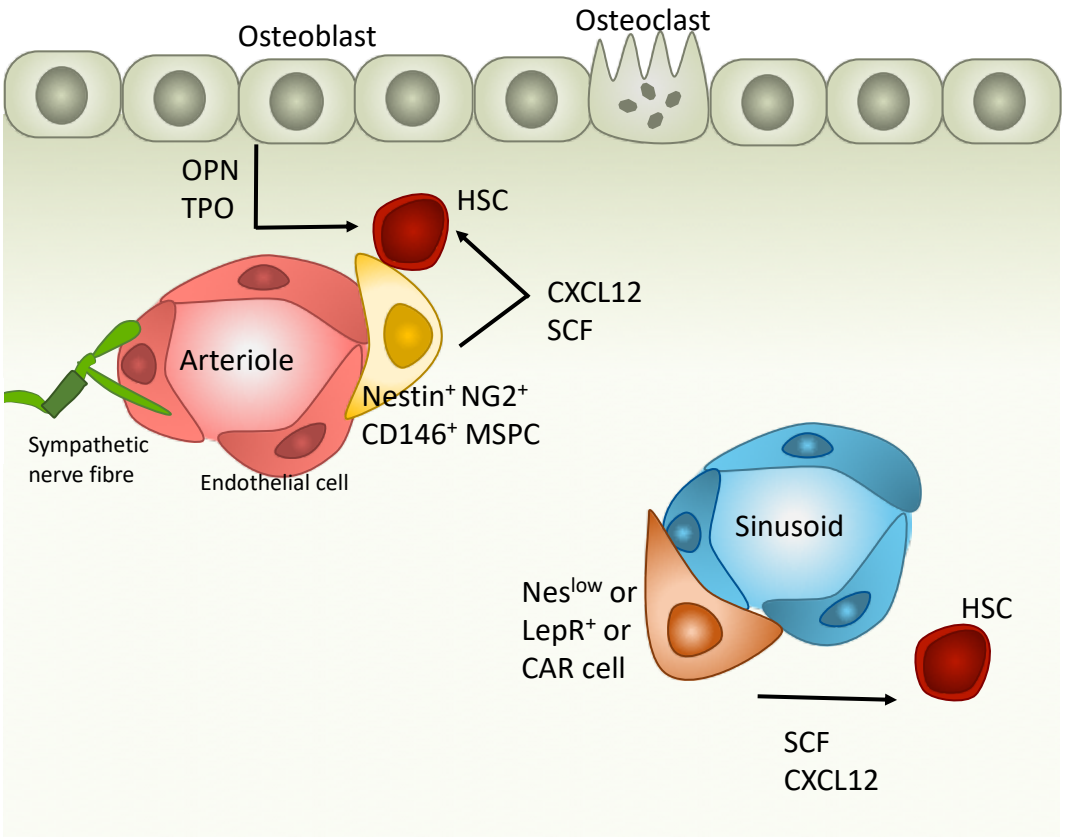

Figure 1-8 HSC niche locations. Osteoblasts secrete HSC maintenance factors TPO and OPN, and HSCs located near the endosteum are also in close proximity to arterioles that are lined with endothelial cells and MSPCs that are Nes^{high} or NG2+ which secrete CXCL12 and SCF. This niche zone is thought to regulate quiescent HSCs. Sympathetic nerves regulate HSC mobilization. The sinusoidal zone is where more active HSCs reside, close to Nes^{low} or LepR+ or CXCL12-abundant reticular cells (CAR cells), that also secrete SCF and CXCL12.

The subtle differences in localisation reported support the notion that functional quiescent and active niches may exist in close proximity. But elucidating the precise location of HSCs and the signals responsible for maintaining haematopoietic homeostasis remains challenging, due to current limitations of *in situ* imaging approaches (Kokkaliaris et al., 2012), and the rarity of bona fide HSCs within the marrow (<1:50,000 marrow cells) (Morrison and Scadden, 2014).

1.4.1 Bone marrow niche cellular constituents

The bone marrow is comprised of a heterogeneous population of cell types, various haematopoietic and non-haematopoietic cells have a proposed role in HSC regulation; MSPC subsets, endothelial cells, osteoblasts and sympathetic nerve fibres.

MSPCs resident in the BM have been identified as major niche components; both the niche microenvironment is required for MSPC maintenance and MSPCs are

required as niche constituents for the maintenance of HSCs. Many subsets of BM resident cells with MSPC-like properties have been identified at various locations within the niche. A landmark study by Méndez-Ferrer *et al.*, 2010 identified a stromal nestin-expressing cell population that are perivascular, enriched for MSC activity and express high levels of factors required for HSC maintenance (Méndez-Ferrer et al., 2010). Similarly, a population of sinusoidal adipo-osteogenic progenitor cells expressing high amounts of HSC maintenance factor CXCL12 (C-X-C motif chemokine 12), CAR cells (CXCL12-abundant reticular cells) (Omatsu et al., 2010; Sugiyama et al., 2006), and of perivascular (sinusoidal) LepR+ MSPCs have been implicated to have a major role in regulation of haematopoiesis in the niche (Ding et al., 2012; Zhou et al., 2015). These cell types all show overlapping properties and functions within MSCs, pericytes and other stromal stem cell compartments.

There is currently evidence for virtually all BM cell types playing major roles in HSC maintenance, and the situation is further complicated by the fact that the HSC pool is itself heterogenous. The current evidence and roles of the major BM constituent cells are described in detail in Table 1-3.

Table 1-3 Cellular contributions to the bone marrow niche. OPN; osteopontin, TPO, thrombopoietin, SCF; stem cell factor, ANGPT1; angiopoietin 1, VCAM1: vascular cell adhesions molecules 1, G-CSF; granulocyte colony-stimulating factor, SNS; sympathetic nerve signals, TGFβ; transforming growth factor β, SMAD; small mothers against decapentaplegic.

Cell type	Role in the bone marrow niche	References
Osteolineage cells	• Early studies suggested HSCs are enriched in the endosteal regions of bone and locate preferentially at bone surface. (First cell population linking BM to HSC regulation). • Could support HSPC expansion *in vitro*. • Increase in BM osteoblastic cells leads to HSC expansion via Notch ligand Jagged1 *in vivo*. • Primitive HSCs adhere to OPN via integrin β1 *in vitro* and OPN negatively regulates HSC pool size. • HSCs interact directly with N-cadherin positive osteoblasts which regulate niche size, although this has been disputed. • Osteoblasts produce HSC maintenance factor TPO. Whether they are the major functional source of this has been disputed. TPO found to act systemically from hepatocytes.	(Calvi et al., 2003; Decker et al., 2018; Gong, 1978; Kiel et al., 2009; Nilsson et al., 2005; Qian et al., 2007; Taichman et al., 1996; Yoshihara et al., 2007; Zhang et al., 2003)
Nestin+ stromal cells	• Perivascular *Nes*-GFP+ cells associate tightly with nerves and HSCs, are enriched for MSC activity. • Express high levels of HSC maintenance factors CXCL12, SCF, ANGPT1, OPN and VCAM1. • Perivascular Nestin+ cells express high levels of HSC niche associated genes. • Rare nestin+ perivascular cells expressing pericyte marker NG2 are associated with arterioles and a subset of quiescent HSCs *in vivo*.	(Asada et al., 2017; Kunisaki et al., 2013; Méndez-Ferrer et al., 2010; Pinho et al., 2013)
LepR+ stromal cells	• Main source of AGPT1 in BM. • Perivascular LepR+ cells produce SCF and CXCL12 in the BM. • Approximately 90% of *Lepr*-Cre+ cells overlap with CAR cells. • *Lepr*-Cre+ cells also represent a large subset of *Nes*-GFP+ cells. • Deletion of SCF from LepR+ cells reduces HSC numbers.	(Asada et al., 2017; Ding et al., 2012; Kunisaki et al., 2013; Yue et al., 2016; Zhou et al., 2015, 2014)

CAR cells	• Sinusoidal stromal cells expressing high amounts of CXCL12. • Adipo-osteogenic progenitors have elevated levels of early commitment markers such as RUNX2, OSX and PPARγ. • CAR cell ablation reduces number of LT-HSCs *in vivo*. • Major producers of SCF.	(Omatsu et al., 2010; Sugiyama et al., 2006)
Endothelial cells	• Express low levels of CXCL12 in BM. • *cxcl12* deletion from endothelial cells depletes HSCs but has no effect on early progenitors. • Express Notch ligands that regulate LT-HSCs. • Arterial, but not sinusoidal, BM endothelial cells secrete SCF.	(Butler et al., 2010; Ding and Morrison, 2013; Greenbaum et al., 2013; Xu et al., 2018)
Adipocytes	• Negatively regulate HSC function. • Inhibition of adipogenesis with a PPARγ antagonist after BM transplantation leads to faster recovery. • Adiponectin, an adipocyte secreted protein, impairs proliferation of HSPCs *in vitro*. • BM adipocytes increase with aging and impair niche function.	(Naveiras et al., 2009; Saraiva et al., 2017; Yokota et al., 2000)
Sympathetic nerve cells	• Sympathetic nerves innervate the BM. • G-CSF stimulated HSC egression from the BM requires SNS. • SNS regulate bone CXCL12 G-CSF stimulated production. • SNS target nestin+ BM cells through β3-adrenergic receptor (which nestin+ cells express) to mediate circadian oscillations of CXCL12 and HSC egression. • Nonmyelinating Schwann cells (glial cells insulating sympathetic nerves along arteries) promote HSC quiescence through activation of TGFβ and SMAD signalling.	(Katayama et al., 2006; Lucas et al., 2008; Méndez-Ferrer et al., 2010, 2008; Yamazaki et al., 2011)

1.4.2 Secreted niche factors

Secreted factors, such as GFs and cytokines, contribute to HSC maintenance within the BM niche (Mendelson and Frenette, 2014). Cytokines are small proteins that are active in cell signalling, they are produced by many cell types and are recognised by cells through cell surface receptors (Bazan, 1990). Cytokine recognition triggers intracellular signalling cascades that ultimately influence cell behaviour, they are fundamental in the immune response and during development as well as in the BM microenvironment (Mendelson and Frenette, 2014). There are several cytokines important for attracting, activating and maintaining HSCs in the niche, and these are discussed in detail in Table 1-4.

Table 1-4 Cytokines and secreted factors associated with HSC regulation in the BM niche. MPL, myeloproliferative leukaemia protein; VLA-4, Very Late Antigen-4.

Niche factor	HSC receptor	Producing cell type	Effect on HSCs	References
CXCL12	CXCR4	CAR cells Nestin+ perivascular cells LepR+ stromal cells Endothelial cells	Maintenance and retention	(Greenbaum et al., 2013; Matsuzaki et al., 2014; Méndez-Ferrer et al., 2010; Omatsu et al., 2010; Pinho et al., 2013; Sugiyama et al., 2006)
SCF	KIT	CAR cells Nestin + perivascular cells LepR+ stromal cells Endothelial cells	Maintenance	(Ding et al., 2012; Kunisaki et al., 2013; Omatsu et al., 2010; Xu et al., 2018; Zhou et al., 2014)
TPO	MPL	Osteoblasts	Maintenance	(Qian et al., 2007; Yoshihara et al., 2007)
OPN	CD44, multiple integrins	Osteoblasts Nestin+ perivascular cells	Quiescence	(Nilsson et al., 2005; Pinho et al., 2013; Stier et al., 2005)
VCAM1	VLA-4 Integrin $\alpha_4\beta_1$	Endothelial cells Nestin+ perivascular cells	Retention	(Frenette et al., 1998; Pinho et al., 2013)
ANGPT-1	Tie2	Osteoblasts LepR+ stromal cells	Quiescence	(Arai et al., 2004; Zhou et al., 2015)

However, two of the best studied cytokines that are known to be non-cell-autonomously required for HSC maintenance are CXCL12 (Nagasawa et al., 1996)

and SCF (stem cell factor) (Ogawa et al., 1991), which bind to their receptors CXCR4 (C-X-C chemokine receptor type 4) and KIT on HSCs, respectively. CXCL12 and SCF are expressed by different cells types in the BM (Table 1-3 and Table 1-4), and several studies have attempted to find the most abundant source/s, primarily using conditional deletion of *Cxcl12* (Asada et al., 2017; Ding and Morrison, 2013; Greenbaum et al., 2013) and *Scf* (Asada et al., 2017; Ding et al., 2012) by Cre-mediated recombination in candidate niche cells. Effects observed on HSC frequency and function in multiple studies are varied, and together suggest no one cell type is responsible for major cytokine production. More likely HSCs reside in a niche in which multiple cell types collectively contribute to maintenance factor expression to support and regulate BM HSCs (Pinho and Frenette, 2019).

1.4.3 Bone marrow ECM

In the BM, the ECM is secreted primarily by stromal cells and is composed mainly of collagens type I-XI, other non-collagenous ECM proteins such as fibronectin (FN), laminin, tenascin and elastin make up 10 -15 % of total bone protein (Clarke, 2008). The endosteal region is particularly enriched for collagen I and FN, whereas the distribution changes to become more laminin dense towards the BM vasculature (Figure 1-9) (Nilsson et al., 1998). Proteoglycans, with their large glycosaminoglycan (GAG) sidechains, such as hyaluronic acid (HA), perlecan and heparin, are also important for BM ECM integrity (Klamer and Voermans, 2014). The ECM provides a dynamic network to sequester secreted GFs and cytokines, establishing functional GF/cytokine gradients, and important domains that control cell properties such as adherence, migration and proliferation.

Gradients of cellular and ECM protein composition across the niche impact the biophysical environment to which MSPCs and HSCs are exposed (Choi and Harley, 2017; Clarke, 2008; Nilsson et al., 1998). These differences in composition ultimately produce gradients in matrix stiffness, although the *in situ* stiffness of BM has proved difficult to measure. Efforts to characterise stiffness by rheology fall short due to techniques often requiring destructive sample preparation, meaning the intact cavity cannot be analysed. Recently, one study used three different but complementary techniques and found the cavity possessed a large amount of heterogeneity, but produced an effective Young's modulus ranging

from 0.25 – 24.7 kPa (Jansen et al., 2015). This has led to the proposed biophysical model of the BM niche demonstrated in Figure 1-9.

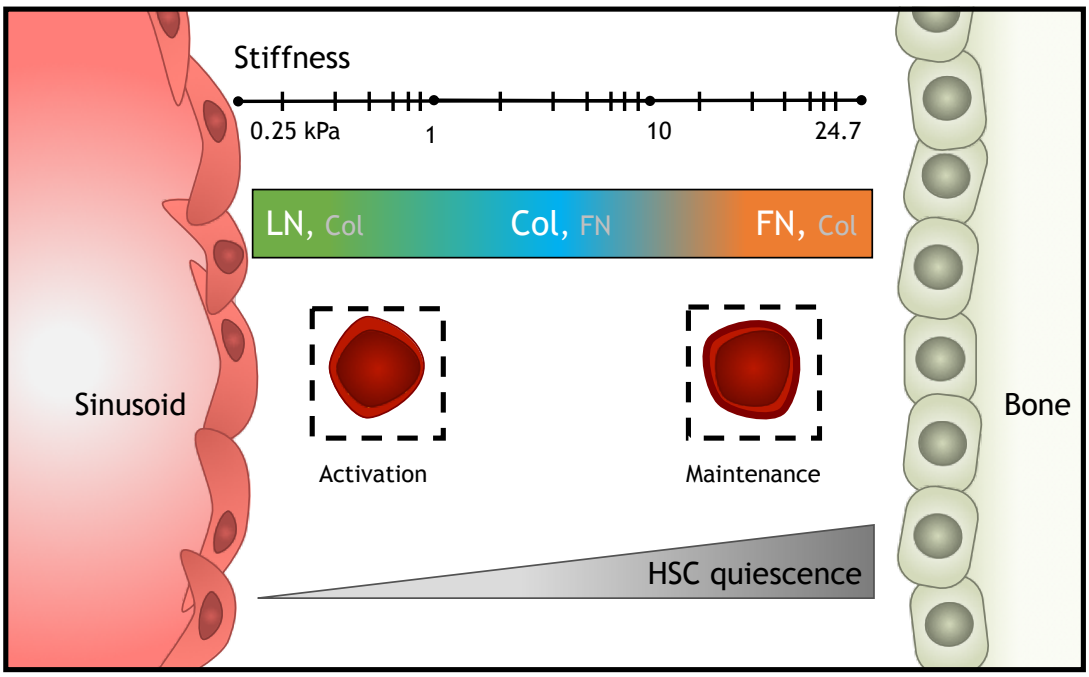

Figure 1-9 Proposed biophysical ECM contributions to niche-mediated HSC regulation. Collagens are distributed throughout the BM, whereas the endosteal region has a high FN content with increased stiffness, and the vascular region has a high laminin content with low stiffness. This is thought to correlate to distinct environments within the BM niche that regulate HSC function, where quiescent HSCs are maintained in the endosteal zones, and active HSCs in the sinusoidal zones. Adapted from (Choi and Harley, 2017).

Due to the non-adherent nature of HSCs, their interactions with the ECM was largely neglected in the literature until recently. Some studies observed haematopoietic perturbation using mutation studies of BM niche ECM components, indicating the ECM as a key regulatory factor both directly and indirectly. For example, mutations in collagen X indirectly attenuate haematopoiesis via disruption of the endochondral ossification process (Sweeney et al., 2011). However, HSCs have been shown to interact with other cells and matrix components via transmembrane protein receptors, such as integrins (Choi and Harley, 2017). In fact, laminin-binding integrin-α_6 (*ITGA6*/CD49f) is now routinely used to isolate populations of very rare LT-HSCs (Klamer and Voermans, 2014).

A recent study showed direct influence of different ECM ligands on HSC phenotype, by culturing HSCs in either collagen I, FN or laminin rich environments they were able to map changes in HSC functional capacity through lineage specification. Specific integrin activation was shown to impact early fate specification of HSCs in this system, with activation of the integrin $\alpha_v\beta_1$ selectively maintaining early

myeloid progenitors, whereas activation of integrin $\alpha_v\beta_3$ pointed to erythroid specification (Choi and Harley, 2017). Other studies have also highlighted that expression of multiple integrins are found to be differentially regulated during the development and regeneration of the BM, this suggests that HSC cell-matrix interactions during discrete stages of haematopoiesis may be crucial in orchestrating HSC homeostasis (Choi and Harley, 2017; Klamer and Voermans, 2014).

These studies highlight that modulating the ECM to represent the *in vivo* composition is an important factor for stem cell regulation. Many studies have focused on controlling ECM characteristics, and therefore microenvironmental mechanics, in order to control stem cell behaviour *in vitro* and determine its role *in vivo*. This will be discussed in detail in section 1.5.

1.4.4 The hypoxic niche

Low oxygen tension (hypoxia) is a hallmark shared by different niches that is thought to be important for maintaining stem cell quiescence (Mohyeldin et al., 2010). Adult tissues experience a wide range of oxygen tensions that are vastly different from inhaled oxygen tensions of 21% (160 mmHg), the partial pressure of O_2 (pO_2) progressively decreases after it enters the lungs and travels throughout the body in the blood. By the time it reaches organs and tissues pO_2 levels are around 2 - 9% (1 - 65 mmHg), extremely different to those considered 'normoxic' (Brahimi-Horn and Pouysségur, 2007; Mohyeldin et al., 2010). Such normoxic conditions (21% O_2) are conventionally used in standard cell-culture, although some argue that 2 -9% oxygen concentrations should become standard practice to represent physiological normoxia (Mohyeldin et al., 2010). However, the precise levels of oxygen a given cell may experience *in vivo* is challenging to assay, not only due to difficulties in direct measurements, but also due to subtle heterogeneities in oxygen tensions within tissues, so physiological normoxia for cells within the same tissue, and during pathological conditions, may differ.

The BM is a highly vascularised organ, although despite this it exhibits relatively low oxygen tension. Initially, support for the 'hypoxic niche' largely came from indirect measurements such as expression of hypoxia inducible factor 1-α (HIF1α) and related genes and proteins, or from detection of surrogate markers that bind

at low pO_2 (such as pimonidazole) (Mohyeldin et al., 2010); further support came from an *in silico* model that proposed the existence of very steep oxygen gradients forming hypoxic zones at short distances from the blood vessels (Chow et al., 2009, 2001). It was initially assumed that the endosteal zones of the BM would be the most hypoxic, evidenced through location of quiescent LT-HSCs that displayed hypoxic phenotypes, and that the central vascularised cavity was less hypoxic and housed activated HSCs (Parmar et al., 2007). However, no direct measurement of local oxygen tension within the BM had been reported until 2014, and this study contradicted this previous model (Spencer et al., 2014).

To measure absolute pO_2 Spencer et al, developed two-photon phosphorescence lifetime microscopy specifically for non-invasive live animal imaging. Using this method, they confirmed that although densely perfused, the overall pO_2 in the BM cavity was low (ranging from 1.5 – 4.2% oxygen). Measurements at distinct BM sites revealed heterogeneities and a steep internal gradient of local oxygen tension. Unexpectedly, based on the previously proposed models, the deep sinusoidal regions (>40 um from bone) had the lowest pO_2 (~1.3-2.4%), compared to the endosteal zone which exhibits a slightly increased oxygen gradient (1.8-2.9%) (Spencer et al., 2014). The endosteal zone is perfused with small vessels (Kunisaki et al., 2013; Méndez-Ferrer et al., 2010), and these vessels are always upstream of and drain into sinusoidal vessels, suggesting arterial characteristics (Spencer et al., 2014).

The local hypoxia within the BM microenvironment has been shown to be integral to augment niche functionality in HSCs themselves and in influencing other niche constituents. HSCs retain quiescence and balance differentiation through adaptation and utilisation of the low pO_2 of the BM; through tight regulation of HIF1α quiescent HSCs drive a strict metabolic profile that relies heavily on anaerobic glycolysis rather than mitochondrial oxidative phosphorylation (OXPHOS) (Simsek et al., 2010; Takubo et al., 2010). The initial hypothesis that the endosteal zone of the BM housed the lowest pO_2 and most quiescent HSCs, was demonstrated to be incorrect by the Spencer et al, study. Slight increase in pO_2 was measured for arterioles that were nestin+ and close to the endosteum, and nestin+ vessels have been documented to harbour quiescent HSCs (Kunisaki et al., 2013; Spencer et al., 2014), although it could be possible that the oxygen tension

is lower just outside of the relatively thick arterioles (Boulais and Frenette, 2015). The role of hypoxia on stem cell metabolism is discussed in more detail and investigated in Chapter 5.

1.5 Engineering Stem Cell Niches for Differentiation and Self-Renewal

Many challenges remain about what niche components are fundamental for retaining stem cell properties – how, when and what is being controlled, and for what purpose? Aims to address these challenges rely on advances in technologies that will allow the recapitulation of niches outside the body. These technologies will offer greater insight into components, and cell-intrinsic and -extrinsic interactions that regulate stem cells in specific microenvironments. This will allow a further understanding of what challenges must be first overcome to exploit these cells using biotechnological expansion approaches for therapeutic potential. Advances in biomaterial strategies are providing an interesting platform on which to answer such questions, with the ability to construct and manipulate '*de novo*' niches and harness the differentiation potential of stem cells *ex vivo,* fundamental mechanisms and robust and reproducible clinical applications are being elucidated (Donnelly et al., 2018).

Biomaterial (surfaces, tissue engineering scaffolds), biofabrication (microfluidics, 3D bioprinting) and bioreactor (physiological environment) techniques hold the potential to allow construction, deconstruction and investigation into the important components of cellular microenvironments. Such approaches could evolve the development of both reductionist stem cell interfaces allowing high throughput analysis and discovery and non-animal technologies (NATs) that recreate tissue complexity and reduce costly/inefficient animal experimentation. Niche microenvironments, such as the BM, are however highly complex and multifactorial, as illustrated in Figure 1-1.

By recapitulating aspects of stem cell niches, biomaterials have developed our understanding of cell-substrate interactions and of fundamental mechanisms and signalling pathways utilised by stem cells during differentiation and self-renewal. This allows us to consider important factors when harnessing stem cells for use in regenerative medicine and in targeting *in vivo* niches.

1.5.1 Mechanotransduction

To understand how properties of the biomaterial interface, such as stiffness, topography and chemistry can regulate cell behaviour, we must first consider how cells sense and adapt to forces and physical constraints imposed by the ECM and other microenvironmental cues. Cell membrane receptors are a vital part of how cells interact with their environment and perceive changes in the physio-chemical milieu - the binding of receptors to ligands is highly specific, but other factors can influence both the binding and the downstream effects of receptor binding. Receptor activation may be required for ligand binding, for example, clustering or phosphorylation. The ligand may need to be released from the surrounding ECM by degrading or distorting the matrix, or the downstream signalling effects from several receptor types can interact in a synergistic or inhibitory manner (Monteiro A. et al., 2018). This process in which cells convert the mechanical stimuli they sense, into biochemical signals that lead to cell response is termed *mechanotransduction*.

Cell adherence to substrates is typically through integrins, transmembrane receptors that tether to the ECM, thus connecting the extracellular environment to the cytoskeleton (Kasemo and Lausmaa, 1988). Integrins are heterodimeric proteins (containing α and β subunits) that specifically ligate to peptide motifs on ECM proteins, for example the integrin $\alpha_v\beta_3$ binds the well-known arginine, glycine and aspartic acid (RGD) tripeptide present on many ECM proteins (Pierschbacher and Ruoslahti, 1984). There are many different combinations of integrin α and β subunits, and these are specific to different types of ECM proteins and adhesion domains (Hynes, 2002). Different cell types will produce different types of integrins, contributing to differing cellular responses to the environment (Monteiro A. et al., 2018).

After integrins bind to the ECM there is a process of integrin clustering into supramolecular complexes called focal adhesions. Focal adhesions contain a number of structural and signalling molecules that link the ECM to the actin cytoskeleton (Jansen et al., 2017; Vicente-Manzanares and Horwitz, 2011). Super-resolution microscopy has determined the molecular architecture of focal adhesions – in which integrins and actin are separated by a ~40 nm core region that consists of partially overlapping protein specific layers. Talin tethers span

these layers to regulate the ultra-structures, and to form integrin-talin-actin complexes that work as mechanical linkages, demonstrated in Figure 1-10 (Kanchanawong et al., 2010; Liu et al., 2015).

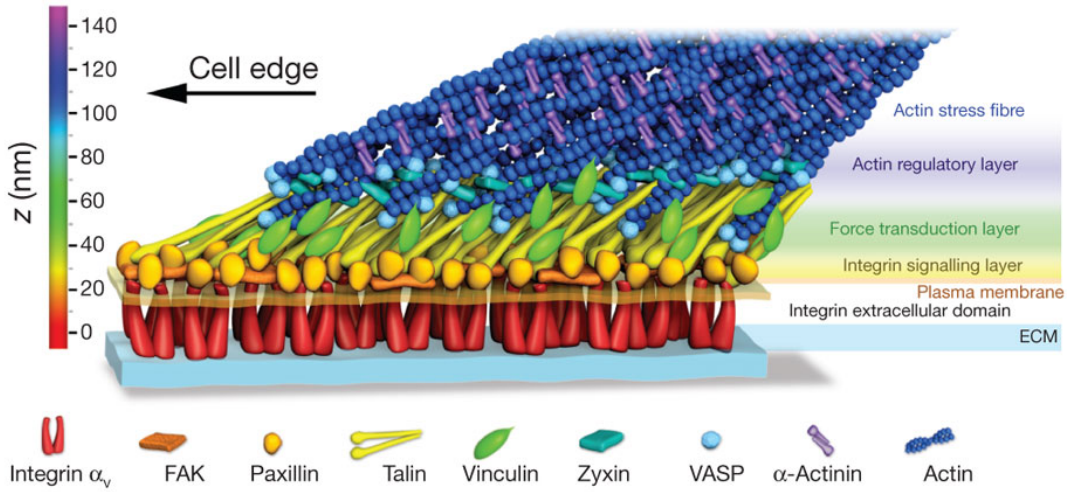

Figure 1-10 Model of focal adhesion molecular architecture. Schematic shows integrins bound to the ECM and the three overlapping layers of the focal adhesion core linking the ECM to the actin cytoskeleton: integrin signalling layer, force transduction layer and the actin regulatory layer. Adapted with permission from (Kanchanawong et al., 2010).

Integrins have no enzymatic activity, but the β subunit connects to the signal-transducing kinase, focal adhesion kinase (FAK), directly or indirectly through vinculin or paxillin (Figure 1-10) (Hayashi et al., 2002; Thomas et al., 1999). FAK mediates activity of several downstream signalling cascades; including Src (nonreceptor tyrosine kinase family), ERK (extracellular signal-regulated kinase) and Rho (small GTPase). Rho signalling is a critical regulator of cytoskeletal dynamics, contractility and motility – G-protein activation leads to phosphorylation of the myosin light chain kinase (MLCK) through Rho-associated protein kinase (ROCK), increasing actin-myosin contractility causing integrin clustering and cell adhesion formation (Kilian et al., 2010; McBeath et al., 2004).

Cell mechanosensing responses also occur at the transcriptional level. Both YAP (Yes-associated protein) and TAZ (transcriptional coactivator with PDZ-binding motif) are mechanosensitive transcriptional activators with critical roles in development (Porazinski et al., 2015), cancer (Moroishi et al., 2015) and organ size control (Zhao, Li, Lei and Guan, 2010). YAP/TAZ activity in a cell is controlled directly by cell shape and polarity, which is in turn dictated by the cytoskeletal structure – *in situ* the structure and tensional state of the cytoskeleton reflect the position of the cell within a tissue – and physical cues such as these are converted

by YAP/TAZ into gene expression signatures and coherent, context dependent biological responses (Dupont et al., 2011; Totaro et al., 2018). YAP mechanical regulation requires the cytoskeleton tension induced by ECM stiffness and cell spreading, and recently it was demonstrated that these forces result in nuclear flattening, leading to increased nuclear import of YAP due to decreased mechanical restriction to molecular transport in nuclear pores (Figure 1-11) (Dupont et al., 2011; Elosegui-Artola et al., 2017). These studies highlight how the ECM mechanically couples to the nucleus to lead directly to transcription level control of cell behaviour.

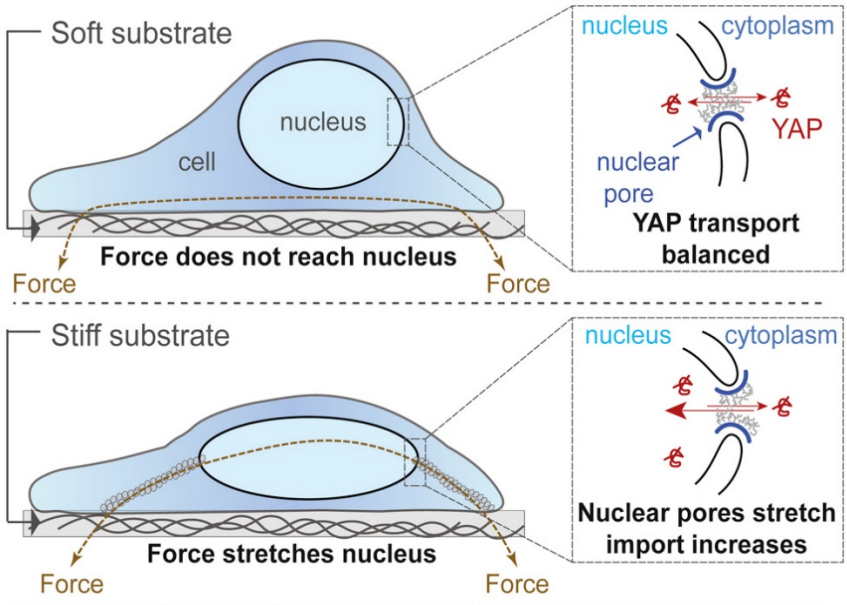

Figure 1-11 Mechanical coupling of ECM-nucleus translocates YAP to the nucleus. Force increases YAP nuclear import by reducing mechanical restriction in nuclear pores. Demonstrating molecular mechanical stability as a general regulator of nuclear transport and resulting transcriptional activity. From (Elosegui-Artola et al., 2017) with permissions.

The mechanism of how interactions at the integrin-ligand interface modulate cellular response to stiffness has recently emerged. The 'molecular clutch theory' has long been proposed to explain actin cytoskeleton and cell migration dynamics (Mitchison and Kirschner, 1988), but has now been used, somewhat counter-intuitively, to explain cell adhesion dynamics (Elosegui-Artola et al., 2018). Controlled substrate stiffness and ECM ligand (RGD) density were used to show that at low stiffness, close to that of softer tissues (>5 kPa), when RGD spacing was increased, focal adhesion growth also increased. Remarkably, at higher stiffnesses in ranges typical of many body tissues, increased ligand spacing leads to focal adhesion collapse. At 30 kPa the rigidity threshold was around 100 nm RGD spacing, whereas at 150 kPa focal adhesion collapse was observed at 50 nm

spacing. Above this stiffness range, that of tissue culture plastic (TCP), conventional rules apply – increased ligand density is required for adhesion formation. Whereas for stiffness in the range of physiological interfaces, the molecular clutch can be applied, i.e. ligand spacing is not via direct sensing, but instead individual integrin-ECM ligands (or cell adhesion molecule-neighbouring cell ligand) act as 'molecular clutches' and as force load increases more clutches are recruited, up to a threshold value. The recruitment of more clutches redistributes the force load among them, thus reducing the total force each individual clutch is exposed to. When the threshold recruitment is reached at high stiffness and increased spacing, no further distribution can occur and the adhesion collapses (Donnelly et al., 2018; Elosegui-Artola et al., 2018; Oria et al., 2017).

As such, mechanotransduction pathways are engaged by the cells' external mechanical environment, enabling the cell to adapt and respond by activating internal biochemical signalling pathways in a constant feedback loop. There are many signalling pathways implicated in mechanosensitivity, and biomaterial strategies have been integral in elucidating these mechanisms by permitting nanoscale control of cell receptors at the material interface (Dalby et al., 2018; Donnelly et al., 2016).

1.5.2 Topography

The architecture (topography) of a cell's microenvironment contains stimuli ranging from the micro to the nanoscale; microscale features are in the range of the size of the cell itself and result in whole-cell responses such as alignment of cells with topographical features, known as contact guidance (Curtis and Varde, 1964). However, nanoscale features present a multitude of cues that are several orders of magnitude below that of the cell (Figure 1-12) (Dalby et al., 2014).

Adhesion formation is dynamic, cells use unbundled, actin-driven membrane projections, filopodia, to probe the external environment. It has been shown that filopodia can follow contact guidance cues down to 10 nm in height (Dalby et al., 2004). At the sub- 10 nm height nanoscale projections have been detected, evidencing the great sensitivity of cellular sensing. Though, it is noteworthy that at this sub-10 nm scale, contact guidance was not observed, just feature interactions (McNamara et al., 2014).

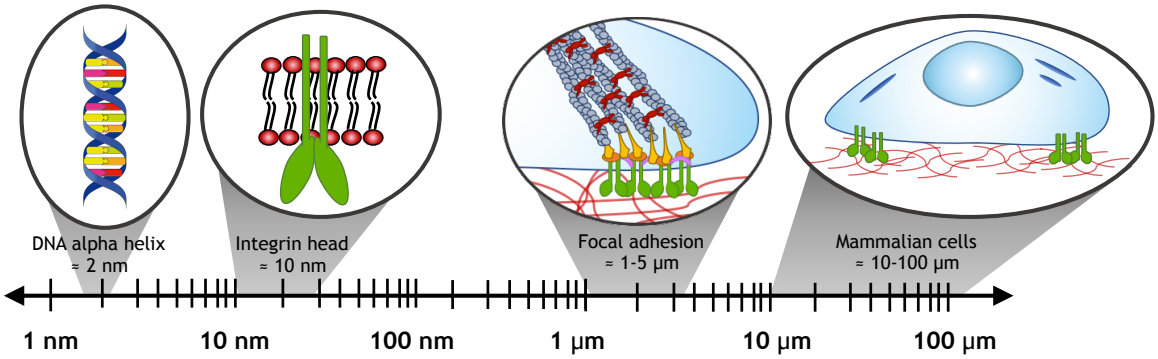

Figure 1-12 Scale of cellular components. Starting from nanometre scale of genetic material and single integrin heads, to the micrometre range of focal adhesion complexes and mammalian cells. Adapted from (Monteiro A. et al., 2018). This figure was created using Servier Medical Art, licensed under a Creative Commons Attribution 3.0 Generic License.

Material engineering strategies have been employed to gain control over adhesion size. Nanopatterned substrates with controlled size, shape, spacing and symmetry have been created using lithography in a variety of materials; patterns have included nanopits (Dalby et al., 2007b; McMurray et al., 2011) nanopillars (Bucaro et al., 2012) and nanogrooves (Watari et al., 2012). Control of these nano-features allows control over adhesion size, number and spacing. Large super-mature adhesions (>5 µm long) are required for osteogenesis of MSCs (Biggs et al., 2009), and on substrates created to promote increased adhesion size, intracellular tension is also increased. This conformational change is linked to mechanical changes in the cytoskeleton, which can transfer tensile (contractile forces) to the nucleus (Elosegui-Artola et al., 2017; Ingber, 2003a, 2003b; Wang et al., 2009), and increased intracellular tension is linked to osteogenesis (Biggs et al., 2009). These changes in nucleus shape can consequently affect chromosomal arrangements; repositioning of chromosomes from euchromatic to heterochromatic sites via the nuclear lamina occurs and leads to transcript level changes in components of the chromatin remodelling machinery and to lineage specific genes. Ultimately leading to impact upon stem cell phenotype (Dalby et al., 2007a; McNamara et al., 2012; Tsimbouri et al., 2013).

Such responses have been well characterised using topographical control over MSC fate by our group. Electron beam lithography was used to create well-defined, yet remarkably similar, nanopatterns able to direct MSCs to commit to osteogenic differentiation or to maintain self-renewal (Figure 1-13). The pattern that permits out-of-niche self-renewal is comprised of pits with a diameter of 120 nm, depth of 100 nm and centre-centre spacing of 300 nm in a square lattice (SQ) (McMurray

et al., 2011). Adding just ± 50 nm offset from the centre position, changing the surface to near-square (NSQ) directs MSC fate to osteogenesis (Dalby et al., 2007b). It was found that this subtle 50 nm offset led to significant differences in cell adhesion: MSCs on NSQ form larger, more mature adhesions, increasing intracellular tension compared to SQ (Dalby et al., 2007b; McMurray et al., 2011).

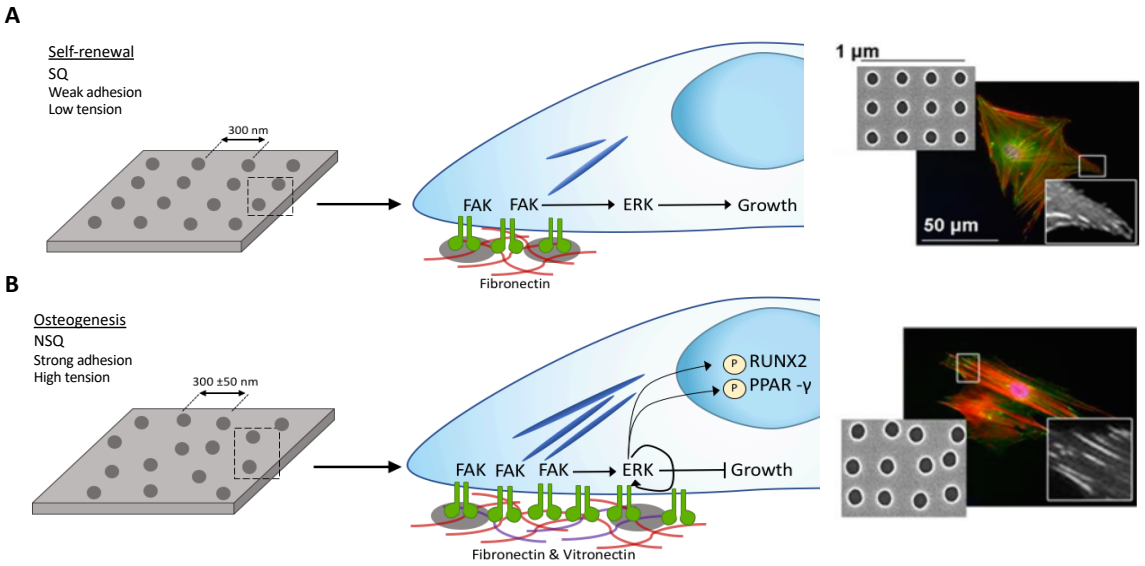

Figure 1-13 Topography to control mesenchymal stem cell (MSC) adhesion for self-renewal and osteogenesis. Self-renewing MSCs adhere more-weakly than osteo-committed cells, leading to lower levels of integrin-mediated signalling through focal adhesion kinase (FAK), retaining levels of extracellular signal-regulated kinase (ERK1/2) to support growth but not differentiation. B. MSCs undergoing osteogenesis require larger adhesions, increased FAK activation elevates ERK1/2 activation to levels required for lineage commitment, increasing intracellular tension, activating Runt-related transcription factor 2 (RUNX2), a key regulator of osteogenesis, whilst simultaneously inactivating adipogenic regulator peroxisome proliferator-activated receptor gamma (PPAR-γ). Fluorescent images show a marked increase in adhesion size on near square (NSQ) compared with square (SQ) surfaces. From (Donnelly et al., 2018) with permissions.

Directed differentiation of MSCs has been well investigated by many of these material systems; as stated, osteogenesis requires large adhesions that support high intracellular tension (Dalby et al., 2007b; Tsimbouri et al., 2012), while adipogenesis occurs when adhesion is weak and tension low (Kilian et al., 2010; McBeath et al., 2004). Strategies exploiting these requirements have been integral in dissecting biochemical mechanisms fundamental to these processes, however, less well understood are the mechanisms required for long term self-renewal of MSCs. For MSCs, self-renewal requires an intermediate adhesion state that suppresses differentiation and allows for long term growth *in vitro*. As such, conditions favouring self-renewal sit mid-way between the adhesion requirements for osteo- and adipo- commitment. However, these conditions will also favour

fibroblast formation, rendering this difficult to harness in culture (Dalby et al., 2018; Kilian et al., 2010; McBeath et al., 2004).

Due to the well-defined osteogenic phenotype and commitment profile, many studies focus on the generation of osteogenic nanotopographies with orthopaedic implants in mind, where incorporation of such nanopatterns to already existing implants could help improve implant success. Orthopaedic implants are typically made from titanium or titanium alloys, for example, hip replacements that are stabilised by titanium stems into the BM of the femoral canal (McCutchen et al., 1990). When the BM microenvironment is disrupted it loses niche functions and resident stem cells differentiate in response to the implant, mainly into soft tissue forming fibroblasts or adipocytes. Encapsulation of the implant within soft tissue leads to micromotion and ultimately implant failure. As such, nanotopographical patterns such as the NSQ developed by our group, have been featured on titania (the oxide of titanium) with aims to promote osteogenesis around the implant (Sjöström et al., 2013).

To decouple adhesion requirements for cell spreading topographical substrates have been engineered coupled with RGD adhesive sites. As integrins ligate, they are coupled to actin cytoskeleton. Actin-myosin contraction through activation of G-proteins leads to integrin clustering and the formation of mature adhesions. Nanocolloidal particles, with one covalently linked RGD motif per colloid, were used to demonstrate that at an RGD spacing of <70 nm integrin clustering occurs, forming mature adhesions. Above this density integrins cannot gather (Cavalcanti-Adam et al., 2008, 2007). Then, using electron beam lithography approaches to create groups (dimers to heptamers) of RGD within 70 nm of each other, it was demonstrated that smaller clusters were separated beyond gathering distance, whereas tetramers of gathered integrins were required for complete cell spreading – i.e. functional adhesions (Schvartzman et al., 2011).

By altering cell adhesion, cytoskeletal organisation and mechanotransduction fate changes are likely driven by the topography-protein interface (Donnelly et al., 2018). When FN, a cell-adhesive protein and major component of the ECM, is adsorbed onto nanopit patterned surfaces it is adsorbed within the pit structures, and cells have been shown to probe these pits with filopodia. This leads to ‘nanoimprinting’ of the pits on the cell membrane, an effect that is absent when

the nanopattern is not coated with FN (Ngandu Mpoyi et al., 2016). Indicating that nanoimprinting is cell-adhesion mediated, with adhesion to topographical features leading to mimics of the topography in the basal cell cytoskeleton (Wood et al., 2008). If the integrins are blocked then nanoimprinting cannot occur (Wood et al., 2008), indirectly demonstrating the importance of the ECM on cell response to shape. This suggests that the topography-driven changes in cell cytoskeleton organisation and adhesion are mediated by the protein-adhesive interface and cells interact with topography dependant on this interface (Ngandu Mpoyi et al., 2016).

Cell adhesion and subsequent spreading governing size and shape influence physiological processes such as cell survival, differentiation and growth (Chen et al., 1997). Using microcontact printed ECM islands of decreasing size, it was shown that cell confinement governs control over growth and death, with small areas that restrict spreading leading to apoptosis (Chen et al., 1997). Since then, this technique has been employed to confine MSCs in specific morphologies, controlling adhesion and intracellular tension (Kilian et al., 2010; McBeath et al., 2004). On ECM islands/shapes where the MSCs remained rounded, they were unable to form mature adhesions, leading to adipogenic lineage commitment. Whereas, ECM islands/shapes and sizes that allowed spreading, promoted actin-myosin contractility and mature adhesion formation support MSC osteogenesis (Kilian et al., 2010; McBeath et al., 2004). The actomyosin tension of the cytoskeleton contributes to this geometric control, which is biophysically linked through adhesion formation governed at the nanoscale by changes in plasma membrane. It was also recently demonstrated that modulation of the plasma membrane lipid assembly, using similar contact printed shapes, can regulate intracellular signalling and thus stem cell fate (von Erlach et al., 2018).

A similar approach was also used to show how mechanotransductive responses play important roles in other cell types, such as macrophages, which regulate distinct pathways associated with inflammation. Macrophages are understood to be majorly responsive to chemical cues and stimulation such as chemokine signals from injury sites, though recent work has suggested that the physical environment may also be a critical mediator in macrophage behaviour (McWhorter et al., 2013). Like many adherent cell types, surface receptors are likely to be involved in this process, however in 2018 Jain and Vogel demonstrated that the cytoskeleton is a

critical mediator in macrophage response to the physical environment. By spatially confining macrophages on cell adhesive islands they found that changes in actin polymerisation leads to modulation of a G-actin bound transcription factor, myocardin-related transcription factor A (MRTF-A). When macrophages are unconfined and well-spread, actin polymerisation leads to MRTF-A release, upon which it translocates to the nucleus, enhancing expression of 'late' inflammatory response genes. Whereas, preventing actin polymerisation via macrophage confinement reduces MRTF-A-mediated transcription and nuclear volume, thereby compacting chromatin and leading to changes in epigenetic signatures. Notably the same effects are observed if cells are confined in both 3D structures and by local cell crowding (Jain and Vogel, 2018).

1.5.3 Stiffness and mechanics

The ECM and surrounding cell junctions have major physical influence in transmitting forces between cells, ultimately regulating cellular processes and behaviours (Vining and Mooney, 2017). Cells can intrinsically generate mechanical forces within their environment, for example actin-myosin contractility leading to matrix remodelling (Daley et al., 2011, 2009). Equally, mechanical force can come from microenvironmental niche factors, extrinsic sources include tensile, compressive forces or shear stresses (Vining and Mooney, 2017). Whether individually or collectively, these mechanical forces impact and regulate cellular behaviour (Donnelly et al., 2018).

Intrinsic and extrinsic mechanical forces guide embryonic development from as early as the blastocyst stage (Vining and Mooney, 2017). Remodelling of cell-cell junctions is driven by intrinsic cell forces to relieve tension as the embryo transitions through germ-band elongation, where myosin II-dependent spatial reorganisation leads to local forces at cell boundaries (Bertet et al., 2004). Later in development, organ morphogenesis is regulated by mechanical properties of the ECM, where cell layers are organised into defined structures by traction forces on the ECM providing the template for organ growth (Vining and Mooney, 2017). Such tissue remodelling and development continues into adulthood as tissues maintain structure and function. For example, epidermal stem cells use biomechanical signalling to regulate and balance stem cell proliferation, differentiation rates and coordination of cell fate with position. Local crowding

from dividing stem cells deforms cell shape and stress distribution, altering cell-intrinsic processes and triggering differentiation of the neighbouring cell (Miroshnikova et al., 2017). Owing to the complexity of this communication between cells and the environmental mechanical milieu, biomaterial strategies have played a key role in elucidating how these cues affect stem cell behaviour. By deconstructing complex environments and by taking early reductionist approaches we are beginning to understand how mechanical force regulates cell behaviour (Donnelly et al., 2018).

Much research on MSCs is carried out on TCP, or on other stiff and planar substrates. Many tissues and stem cell niches however, often have low or gradients of stiffness and are 3-dimensional (3D) *in situ*, implicating key mechanical properties important for cell behaviour (Figure 1-14). Hydrogel systems are now routinely employed, and due to their unique properties, they provide optimal systems for understanding cell response on or in substrates with controlled stiffness that are more physiological-like. Natural or synthetic polymers can be physically or chemically cross-linked in a controlled manner to produce hydrogel systems with tuned degradability, hydrophilicity and stiffness. The water that fills the space between the macromolecules leads to a degree of flexibility similar to that of natural tissues, making them both biocompatible and biomimetic (Ahmed, 2015; Donnelly et al., 2018).

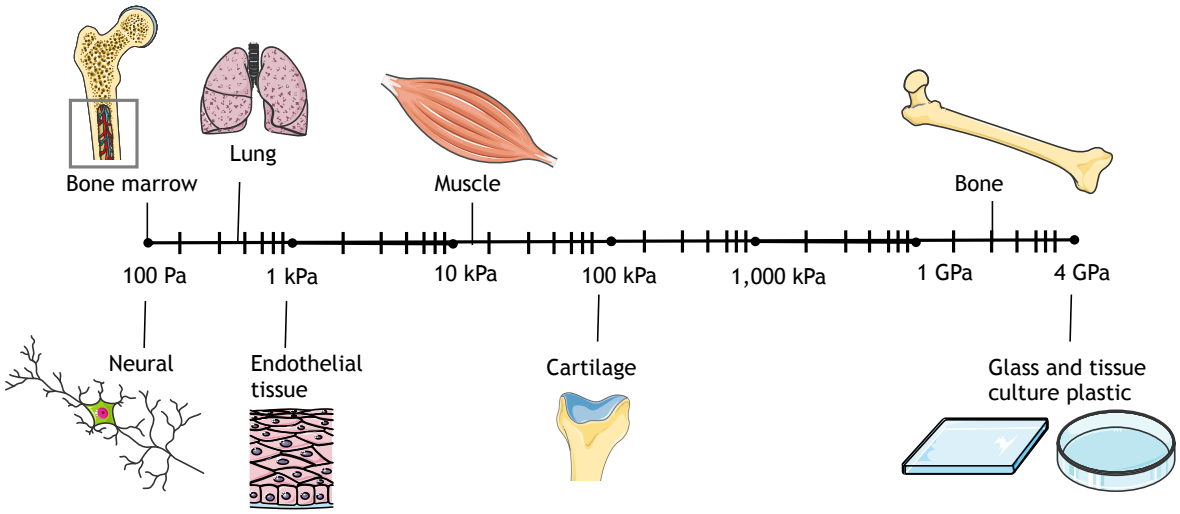

Figure 1-14 Stiffness of various tissues. Biomechanical properties of various tissues in terms of stiffness (elastic modulus) in kilopascals (kPa). Stiffness varies between tissues and relates to functions. Mechanically static tissues such as neural exhibit low stiffness, whereas tissues exposed to high mechanical loading, such as bone exhibit high elastic moduli with a stiffness that is several orders of magnitude greater. This figure was created using Servier Medical Art, licensed under a Creative Commons Attribution 3.0 Generic License.

Original work from Engler et al, used polyacrylamide (PAM) gels of tuneable matrix stiffness to guide stem cell fate through distinct tissue lineages; neural at 0.1-1 kPa, muscle at 12 kPa and bone at 30 kPa. This simple tuneable system has set the pace over the last decade for the unravelling and exploiting of the biological mechanisms linked to mechanoregulation of MSCs (Engler et al., 2006).

Gradients of stiffness are exhibited *in vivo* at physiological interfaces, such as those at tissue junctions or at pathological boundaries, e.g. neuromuscular junctions and the tumour boundary (Hadden et al., 2017). Isolated cells are known to migrate to regions of different stiffness, 'durotaxis', the axis of migration depends upon the cell type; with stem cells known to migrate to regions of increasing stiffness (Tse and Engler, 2011; Vincent et al., 2013). Cancer cell lines, meanwhile, have been shown to have a variable relationship with substrate stiffness (Cavo et al., 2016; Reid et al., 2017). Multicellular clusters exhibit collective durotaxis, groups of epithelial cells were found to migrate towards stiffer regions - cells atop stiffer substrates are able to gain better traction than on softer regions through integrin binding, intercellular junctions and the action of myosin motors are then able to contract neighbouring cells resulting in collective movement to firmer ground (Sunyer et al., 2016).

These observations highlight a need to think about inherent substrate stiffness and the underlying gradient of stiffness. Some polymerisation methods have now been developed to allow user control over stiffness gradients in PAM hydrogels. One study designed a system ranging from 0.5-8.2 kPa/mm, permitting an *in vitro* model spanning the *in vivo* physiological and pathological range therefore facilitating investigation of a range of mechanical signals on one surface and cell population (Hadden et al., 2017). Previous work by our group combined two biomaterial strategies with modulated mechanical and topographical properties in order to achieve tissue interface-like differentiation of MSCs. An HA hydrogel at the stiffness boundary of cartilage, but lower than that of bone, was combined with the stiff, topographically patterned substrate, known to promote osteogenesis (NSQ). This led to anisotropic commitment of MSCs from a single source down chondrogenic and osteogenic lineages, similar to the interface of articular cartilage and bone found at the end of long bones (Donnelly et al., 2018, 2017).

Polymeric hydrogels have been used to elucidate fundamental processes involved in mechanosensing and how this effects osteogenesis of MSCs. To uncover the role of YAP/TAZ in mechanosensing PAM hydrogels of modulated stiffness were used. By varying substrate stiffness, it was found that if forces from adhesion and/or the cytoskeleton are high enough (above 5k Pa) the cytoskeleton is reinforced by stress fibres, mechanically coupling it to the nucleus. Thus, providing a direct link from focal adhesion to the nucleus, leading to nuclear flattening, stretching of nuclear pores and thereby increasing YAP nuclear import (Figure 1-11) (Elosegui-Artola et al., 2017). Osteogenesis of MSCs occurs on stiff substrates (above 5 kPa), here YAP translocates to the nucleus via this mechanosensitive mechanism and consequently activates the master regulator of osteogenesis, transcription factor runt-related transcription factor 2 (RUNX2) (Yang et al., 2014). Nuclear compartmentalisation of YAP/TAZ is preserved when MSCs are cultured on stiff substrates for long culture periods (~10 days), and consequently, the ability to respond to softer substrates is lost. These MSCs remain committed to an osteogenic differentiation profile, suggesting they possess mechanical memory, illustrated in Figure 1-15 (Yang et al., 2014).

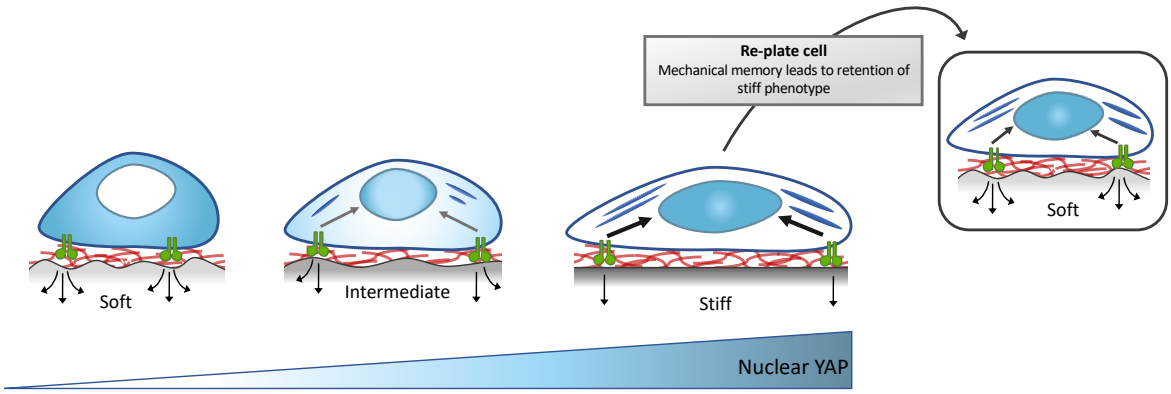

Figure 1-15 MSCs have mechanical memory. Cell mechanosensing through integrin-ECM (e.g. fibronectin RGD domain) detect changes in matrix stiffness, as stiffness increases so does nuclear important of Yes-associated protein (YAP) and its transcriptional co-activator TAZ. The YAP/TAZ complex is a master regulator of many downstream effectors, including differentiation of MSCs. MSCs will preferentially differentiate into osteoblasts on stiff matrices, and soft tissue types (such as adipose tissue) on soft matrices, hence increased nuclear import of YAP/TAZ on stiff substrates attenuates osteogenic differentiation of MSCs. In MSCs that are preconditioned on a stiff substrate, and then re-plated to a softer substrate, YAP/TAZ signalling remains active, and the cells remain committed to an osteogenic differentiation profile. Adapted with permissions from (Donnelly et al., 2018).

Substrate stiffness is perceived by cells through the localisation of receptor-ligand interactions. Therefore, stiffness correlates to the expression and localisation of integrins (cell-matrix) and cadherins, transmembrane receptors important in cell junctions (cell-cell). This mechanosensitive mechanism can

thus be exploited to modulate cellular signalling (Aragona et al., 2013; Driscoll et al., 2015; Dupont et al., 2011). Materials modified to present adhesive peptide motifs have been used to modulate fate commitment in MSCs. HA hydrogels of tuned stiffness were integrated with peptide motifs mimicking cell-cell and cell-matrix interactions through co-presentation of the N-cadherin adhesive sequence HAVDI (histidine, alanine, valine, aspartic acid, isoleucine), and the FN RGD sequence. Co-presentation on stiff 2-dimensional (2D) gels led to YAP/TAZ remaining cytosolic, thereby preventing osteogenic commitment. However, when the HAVDI motif was removed, exposing MSCs to an environment with more ECM-like interactions YAP/TAZ translocated to the nucleus and MSCs underwent osteogenic differentiation (Cosgrove et al., 2016). Interestingly, differences were observed when the system was transferred to 3D. Incorporation of the HAV sequence (the conserved part of the HAVDI sequence) with MSCs encapsulated within the gels led to chondrogenic commitment, illustrated in Figure 1-16. The MSCs perceived this interface as an increase in cell-cell like adhesions, a crucial component for chondrocytes that typically live in pairs (Bian et al., 2013).

Due to studies such as these, the focus on the effects of 3D matrices on stem cell differentiation go beyond controlling the bulk mechanical properties, i.e. the traditional model proposed by Engler, where bulk stiffness leads to differentiation down lineages of similar native stiffness (Engler et al., 2006). For example, MSCs encapsulated in alginate gels of varied stiffness (2.5 – 110 kPa) presenting RGD motifs at various clustering densities, demonstrated stiff substrates that hindered cell spreading but permitted RGD clustering – in a process similar to traction-mediated unfolding of FN - were still able to permit osteogenic commitment i.e. cell fate was not correlated to cell morphology but to integrin-adhesion-ligand bonds (Huebsch et al., 2010).

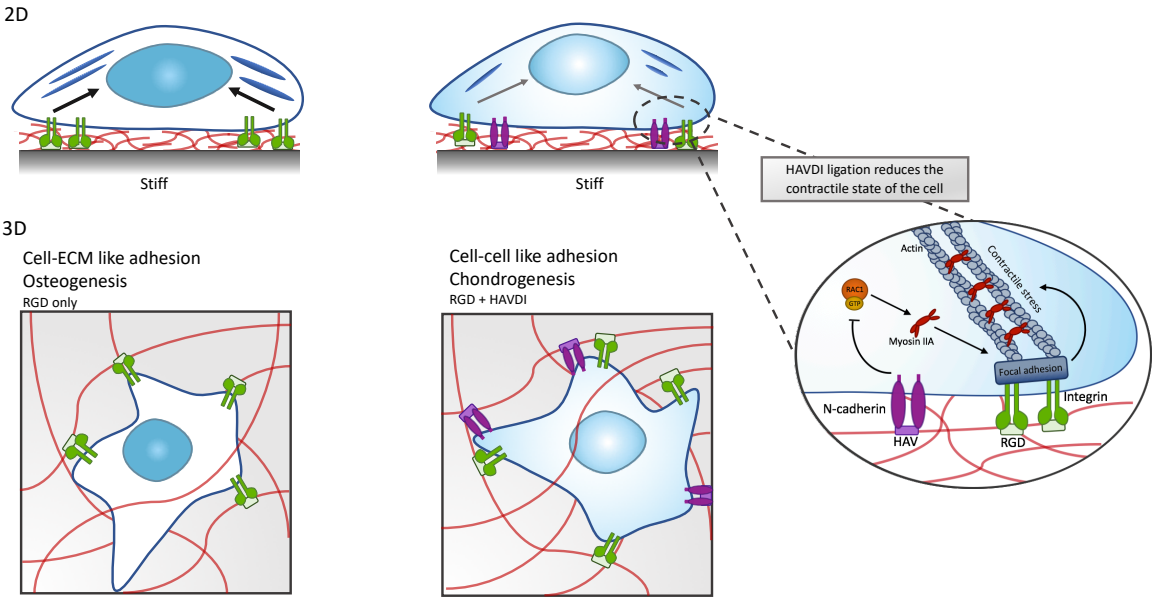

Figure 1-16 Cells 'sense' matrix stiffness through receptor-adhesion presentations. Materials modified to contain specific peptide sequences can modulate mechanosensitive pathways. Interactions mimicking cell-cell adhesions (N-cadherin-based interactions) through the HAV motif, pathways triggered by soft substrates are activated, reducing the contractile state of the cell. Whereas interactions mimicking cell-ECM adhesion (integrin-based interactions) through the RGD motif lead to focal adhesion formation, increasing intracellular tension, enabling osteogenesis of MSCs. HAV-N-cadherin interactions inhibit Rac-GTP levels, decreasing myosin IIA-actin interactions, reducing focal adhesion-related protein recruitment to integrins. This reduces the contractile force generation on the cytoskeleton and cells behave as though on a softer substrate. In 3D, peptide motif incorporation can tune control over osteogenic and chondrogenic differentiation. Chondrocytes typically live in pairs, as such, cell-cell interactions are preferable to cell-matrix for chondrogenic commitment – i.e. the presence of the HAV motif promotes chondrogenesis. Taken from (Donnelly et al., 2018) with permissions.

A further example incorporated matrix degradable sites into tuneable 3D HA hydrogels, presenting a system that either permits or prevents cell-mediated degradation (Khetan et al., 2013). This study also demonstrated cell fate was morphology-independent when the matrix is nondegradable, but is instead directed by cell-mediated traction forces (Khetan et al., 2013). However, by incorporating matrix metalloproteinase (MMP)-degradable peptides, encapsulated cells were able to reach otherwise unavailable adhesive ligands, rearranging their cytoskeletal structure to generate traction forces that potentially led to osteogenic commitment, this was irrespective of morphology or bulk matrix stiffness (Khetan et al., 2013). These studies support the premise, in 3D, that 'sensing' of matrix stiffness by integrin-adhesion-ligand bonds can act as sensors of matrix elasticity and dimensionality, in a morphology-independent manner (Huebsch et al., 2010).

1.5.4 Chemistry

Manipulation of chemical properties of substrates has also been investigated. Changes in cell adhesion to substrates can be controlled by manipulation of material properties such as surface wettability (Celiz et al., 2014; Mei et al., 2010), control of protein adsorption, such as ECM proteins or GFs (Keselowsky et al., 2005, 2004, 2002) and incorporation of different chemical groups has also been shown to be sufficient to influence MSC fate (Benoit et al., 2008). The key study by Benoit et al, employed poly(ethylene glycol) (PEG) hydrogels functionalised with small-molecule functional groups to direct adipogenesis with hydrophobic *t*-butyl groups, and osteogenesis with charged phosphate groups (Benoit et al., 2008). Since original studies that alter surface charges and functional group presentation such as these, advances in organic chemistry are beginning to offer new strategies for biomaterial synthesis and control, for example click-chemistry (Deforest et al., 2009; DeForest and Anseth, 2012; Jiang et al., 2014) and GF tethering techniques (Alberti et al., 2008; Llopis-hernández et al., 2016). With added both spatial and temporal control through *in situ* degradability and delivery, such advances offer a diverse toolbox for precise functionalisation of substrates (Donnelly et al., 2018).

PEG hydrogels are commonly used and can be easily modified to contain photodegradable cross linkers, this permits the user post-gelation control over substrate properties, such as gel conformation and biochemical composition - with stem cells *in situ*. Degradation of the hydrogel network changes the physical 3D environment of encapsulated cells and can lead to migration or lineage commitment (Kloxin et al., 2009). Cell adhesive moieties, such as RGD, are often incorporated into PEG hydrogels, and one example used pendular RGD motifs that could be dynamically cleaved by a light-stimuli, decreasing RGD availability and therefore adhesion formation. On-demand temporal control of pendant release created spatial changes that could be controlled to direct MSC fate towards chondrogenesis (Kloxin et al., 2009). Other click-chemistry strategies incorporate a combination of integrin-binding domains, protease-degradable sites and locally sequestered GFs into PEG hydrogels; upon cell infiltration cell-secreted MMPs degrade networks leading to GF release (Lutolf et al., 2003). This strategy was used to deliver recombinant human bone morphogenetic protein-2 (BMP-2) to a critical sized defect in rat cranium, where they found bone regeneration was

dependent on the ability of cells to infiltrate the matrices through the proteolytic sensitive sites (Lutolf et al., 2003).

GFs are potent biomolecules that have strong influence on cells, such as stimulation of proliferation, differentiation and migration. They are instrumental during development and play key roles in physiological and pathological processes, including tissue homeostasis (e.g. in the BM niche) and tissue repair (e.g. wound healing). GFs also have essential roles in directing stem cell phenotype, such as BMP-2 to promote osteogenesis, vascular endothelial growth factor (VEGF) to promote vascularisation and TGFβ to promote chondrogenesis (Salmerón-Sánchez and Dalby, 2016).

Due to this regenerative potential the roles and potential of GFs for tissue engineering/regenerative purposes has been widely explored. Typically, GFs used in clinic or *in vivo* are used at supraphysiological doses to enable delivery of effective local concentrations, as there will be initial rapid break down and propagation from the implant site. The current gold standard for *in vivo* bone repair is a collagen I-based sponge which delivers BMP-2 at a concentration of 1.5 mg/mL (INFUSE®), however, due to the serious off-target side effects experienced in patients the Food and Drug Administration (FDA) released a public health notification of life threatening complications associated with this device (Woo, 2012). Such high GF doses are not only harmful but also extremely costly. Systems that bind GFs to surfaces in a solid-phase state, more similar to how the native ECM binds and presents GFs in stem cell niches, have been developed - controlled-release (Lutolf et al., 2003; Mooney et al., 2000) and protein engineered (Martino et al., 2011) strategies have aimed to provide a solution for better translation of GFs to the clinic by creating matrices that retain GFs, with the hope of decreasing off-target effects and cost (Figure 1-17).

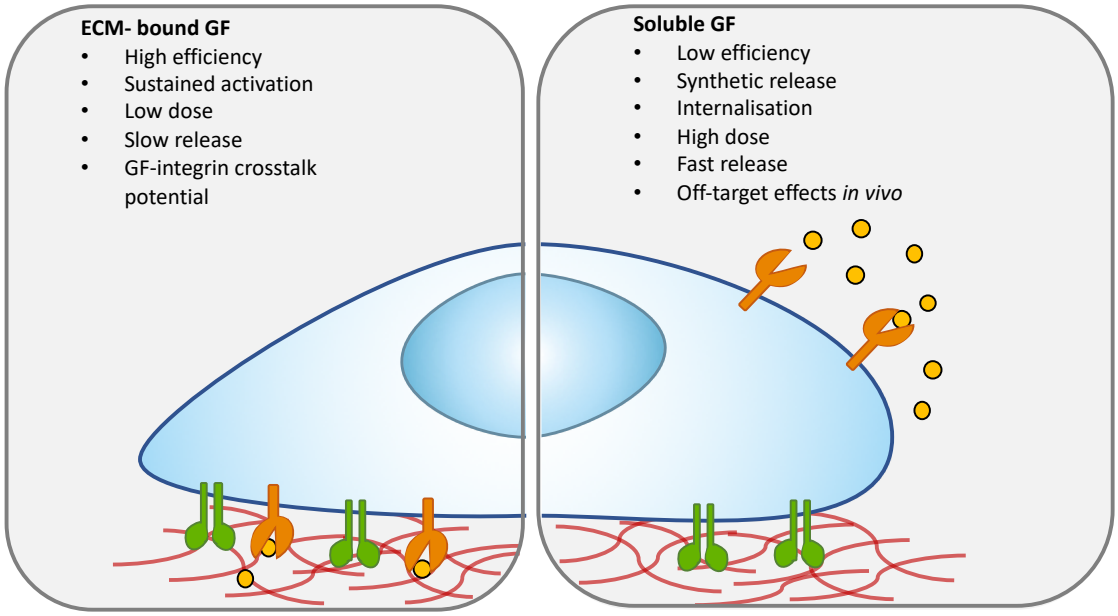

Figure 1-17 Soluble and matrix bound growth factor delivery. Conventional soluble delivery of GFs (right) typically requires high concentrations, which rapidly propagate away from the site when applied *in vivo*. Solid-phase GF delivery, for example by tethering to the ECM (left), allows the use of significantly lower concentrations of GFs and more targeted and effective delivery. ECM-bound presentation facilitates integrin-GF receptor cross talk due to the close proximity of the receptors. From (Donnelly et al., 2018) with permissions.

Controlled binding of GFs to synthetic materials ('solid-phase' delivery) has proved difficult. Non-specific crosslinking may compromise bioactivity of the molecule, with further concerns over stability, amount and cellular accessibility to the ligands. With this in mind, one study developed a poly(ethylene oxide) (PEO) based co-polymer to covalently tether epidermal growth factor (EGF) to the substrate, a GF associated with tissue repair. By specifically tethering at the N-terminus, bioactivity was retained but restricted it to the surface. Tethered EGF led to signalling through its receptor EGFR (epidermal growth factor receptor), in a manner akin to physiological-like matrix-embedded EGF – where EGF is stimulated but not internalised (Fan et al., 2007). Using a similar copolymer system, immobilised leukaemia inhibitory factor (LIF) was presented, to ESCs. LIF is essential for self-renewal in ESCs, and is typically added in ESC feeder-free culture conditions. ESCs cultured in this system showed retention of pluripotency for up to 2 weeks, in the absence of soluble LIF in the culture media (Alberti et al., 2008).

More recently, substrates were coated with evenly spaced and tuneable arrays of gold nanoparticles functionalised with BMP-2. Using block copolymer micellar nanolithography, the system permits precise control over the nanoscale distribution of BMP-2. One BMP-2 molecule is tethered per nanoparticle, meaning

local density and distance between BMP-2 anchor points can be modulated. Here it was found that when compared to soluble GF administration, immobilised BMP-2 increased intracellular Smad-signalling. Even at concentrations as low as 0.2 ng/cm^2 Smad-dependent signalling was observed (Schwab et al., 2015). Tethering of BMP-2 in this manner permits sustained local delivery of BMP-2 (or other GFs) and allows the user precise ligand control on a platform to investigate effects of GF density and spacing on intracellular signalling.

Other approaches to immobilise GFs exploit the natural affinity of ECM molecules for GF binding. FN is a major component of native ECM, it contains the RGD integrin-binding domain in its 9th type III repeat, which has been incorporated into many materials. FN also contains a highly promiscuous GF binding domain in its 12th to 14th type III repeats, and is known to sequester GFs from different families with high affinity (Martino and Hubbell, 2010). Seminal work by Martino et al, exploited this affinity for GF binding by developing recombinant FN fragments that incorporate the GF binding region of FN (FNIII$_{12\text{-}14}$) as an approach for GF delivery. A fibrin matrix was functionalised with two FN fragments, one containing FNIII$_{9\text{-}10}$, the RGD cell adhesion site, another containing the FNIII$_{12\text{-}14}$, the GF binding region. Upon functionalisation with platelet-derived growth factor (PDGF)/VEGF or BMP-2, they demonstrated the system could promote wound repair and bone growth, respectively (Martino et al., 2011).

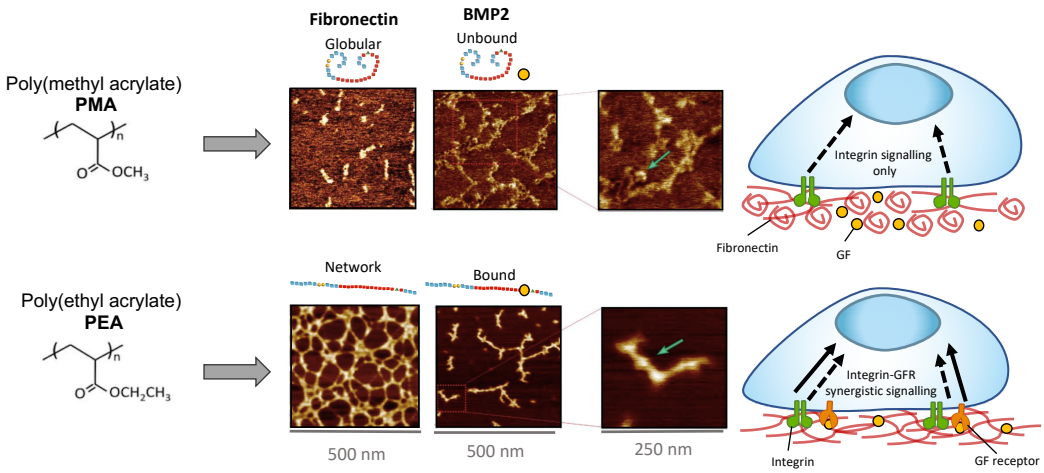

Figure 1-18 FN nanonetwork formation and GF presentation. Atomic force microscopy (AFM) images after FN adsorption shows spontaneous formation of FN nanonetworks on PEA, but not PMA which results in globular FN aggregates. Sequential adsorption of growth factor (here BMP-2, at 25 ng/mL) shows interactions of BMP-2 with FN fibrils on PEA, but not PMA, due to an open molecular conformation exposing the key GF binding domain. The proximity of the GF binding and integrin binding domain on FN molecules in networks leads to synergistic integrin and GF receptor signalling. Adapted from (Donnelly et al., 2018) with permissions.

This technique illustrated delivery of significantly lower dosages of GFs could be effectively used in a clinical setting. The approach, however, relies on complex recombinant protein technology. This is due to delivery of whole FN molecules to substrates leading to FN adopting a globular conformation, thus concealing these key binding domains. However, work by our group has developed a novel strategy to drive physiological-like FN network formation. The polymer poly(ethyl acrylate) (PEA) causes spontaneous unfolding of FN molecules, leading to assembly into nanonetworks, exposing the cell and GF binding domains. Then, by incorporation of BMP-2, we demonstrated that due to the close proximity of the integrin- and GF-binding domains on open FN molecules, this system drives synergistic signalling between integrins and growth factor receptors (GFRs), which attenuates intracellular signalling (Figure 1-18). This led to robust osteogenesis of MSCs *in vitro* and bone fracture repair *in vivo* (Cheng et al., 2018; Llopis-hernández et al., 2016). This strategy has been incorporated into implanted biomaterials - orthopaedic titanium was coated with PEA/FN and BMP-7 tethered to improve osteointegration (Al-jarsha et al., 2018), whereas tethering of VEGF has shown improved vascularisation of biomaterial scaffolds *in vivo* (Moulisová et al., 2017). This PEA system developed by the Centre for the Cellular Microenvironment is used in this thesis, and will be discussed in further detail in Chapter 3.

1.5.5 Modelling the bone marrow niche

As *in vivo* stem cell niches are complex, combinatorial bioengineering techniques such as those discussed above, are moving towards allowing deconstruction and reconstruction of these multifaceted systems. The use of overly simplified cell culture models could be replaced by engineering *de novo* niche models, these models could be built using biomimetic materials with human stem cells to replicate tissue complexity (Lee-Thedieck and Spatz, 2012; Müller et al., 2014). Such systems could be used to promote *in vitro* expansion for regenerative medicine purposes, e.g. HSCs for HSCT, or to more reliably predict drug mechanism, toxicity and efficacy.

Previous efforts to expand HSCs have mainly focused on identifying cytokines or small molecules that target cell signalling to regulate HSC function (Boitano et al., 2010; Guo et al., 2018; Hagedorn et al., 2015). Some of these strategies have demonstrated extensive cell expansion, but a concomitant loss of long-term *in*

vivo function has also been observed (Nakauchi et al., 2006). The absence of sustained self-renewal is thought to be a result of complete removal of physical and biochemical cues of the native niche when HSCs are placed into standard tissue cultureware. As such, HSC expansion or long-term maintenance in culture has been notoriously difficult to harness, and approaches such as delivery of small molecules - e.g. StemReginin1 (SR1) (Boitano et al., 2010) - that target just one parameter of HSC regulation are proving insufficient and completely lack the ability to study HSC niche-like behaviour and interactions.

With this regard, microarray platforms have been developed as multifactorial approaches toward deconstructing, and thus elucidating, key stem cell niche properties. By modulating and combining biochemical and biophysical niche properties to allow screening of key microenvironmental perturbations, microarray platforms offer the ability to study single cells in high throughput. Using robotic spotting technologies mixtures of protein cues, such as ECM components, niche interaction ligands and other signalling proteins can be presented and analysed at the single-cell level (Flaim et al., 2005; Gobaa et al., 2011).

Recently, one such platform was engineered to systematically analyse early HSC fate choices during *in vitro* culture. First, gene expression signatures and cell-cycle hallmarks of single HSCs and MPPs were defined. Then, two niche interaction ligands were identified that were specifically expressed on the most naïve HSCs, and these corresponded to expression of cell-cell adhesion ligands detected in populations of stromal niche support cells (such as LepR+ MSPCs). Then, using chemically modified hydrogel microwells, these putative ligands were incorporated into artificial niches to mimic cell-cell interactions with HSCs. Remarkably, single HSCs presented with these ligands demonstrated long term maintenance *in vitro* and the ability to reconstitute the blood system *in vivo* (Roch et al., 2017).

The above approach is reductionist in nature, however in the endeavour towards BM niche recapitulation *ex vivo*, multiple biomaterial strategies have become a central focus in recent years. Many approaches to deconstruct/reconstruct niche parameters incorporate one or several niche factors; such as specific cell types,

matrix stiffness, fluid flow, or ECM components, and several of these are discussed in detail in Table 1-5.

It should be noted that despite the relative success of some of these systems, the complexity of the BM niche must not be underestimated. The BM microenvironment itself is multifactorial, with many processes known to regulate HSCs directly or indirectly (Pinho and Frenette, 2019). In addition, hormonal and neural inputs likely play a fundamental role. The studies that investigate combinations of niche factors will ultimately prove significant in elucidating the physical and functional properties important in regulating HSC behaviour *ex vivo* and providing insight into fundamental niche behaviours *in vivo*.

Table 1-5 Current material strategies to engineer the bone marrow niche

System	Materials	Cell types	Remarks	Reference
Co-culture of non-adherent cells with a feeder layer	None	PDGFRα+ CD51+ nestin+ MSCs, HSCs	• Identify PDGFRα+ CD51+ MSCs as nestin expressing. • Capable of forming HSC supportive mesenspheres *in vitro* and *in vivo*.	(Pinho et al., 2013)
		Pericytes, HSCs	• Pericytes support HSCs *ex vivo* through cell-cell contact and activation of Notch signalling.	(Corselli et al., 2013)
		BM MSCs, HSCs	• Enhanced HSC proliferation, especially primitive CD34+ CD38- fraction and maintained for several population doublings. • Knock-down of NCAM and VCAM-1 increased the number of slow dividing HSCs. • Knock-down of integrin B1 and CD44 impaired differentiation.	(Diehlmann et al., 2010)
Co-culture in collagen hydrogel	3D collagen I/III gel	BM-MSCs, UCB-MSCs, CD34+ HSCs	• UCB-MSCs are unsuitable for HSC maintenance long term. • Collagen promotes HSC migration and MSCs promote CD34+CD38- phenotype. • MSC-derived FN may contribute to increased HSC migration compared to cell free collagen.	(Leisten et al., 2012)
3D microcavity array	GAG-PEG hybrid hydrogel, functionalised with RGD, Flt3, TPO and SCF.	HSPCs	• Defined cavity sizes for single (15 μm) or multiple cells (40 μm). Allowing modulation over cell-cell and cell-matrix interactions. • Large cavities (cell-cell contact) led to increased expansion rates of HSPCs, single cells more quiescent.	(Müller et al., 2017)
Perfusion co-culture	3D PEG hydrogel functionalized with RGD and flow	HSCs, MSCs	• Perfusion was as effective as static culture at maintaining CD34+ cells. • Perfusion increased the number of progenitors and enhanced erythroid differentiation.	(Rödling et al., 2017)

Decellularized marrow	Decellularized bovine bone marrow (DeBM)	HSCs, BM stromal cell line	• Stromal cells secreted CXCL12 and SCF on DeBM. • Supported CD34+ expansion	(Bianco et al., 2019)
3D scaffold with perfusion	Porous HA scaffold	MSCs, HSCs	• MSCs deposit matrix, display osteogenic differentiation, some maintenance of niche markers e.g. nestin • HSPC expansion compared to control plain scaffold. • Progenitor expansion compared to control plain scaffold. • HSPCs localise and adhere to MSCs on scaffolds, committed cells found in the supernatant.	(Bourgine et al., 2018)
Endosteal and vascular spheroid co-culture	Collagen I hydrogel, magnetic nanoparticles	MSC, HSC, osteoblasts, fibroblasts, HUVECs	• MSCs maintain niche/MSC phenotypic markers, such as stro-1 and nestin. • Endosteal model supported HSC quiescence. • Increased HSC activity in vascular model. • HSC differentiation and migration were supported by both models.	(Lewis et al., 2016, 2017; Lewis, 2018)
3D hydrogel	Puramatrix gel	MSCs, HSCs	• Retained HSCs in the hydrogel. • Maintained primitive HSCs and increased number of progenitors. • LT-HSCs had enhanced engraftment potential that 2D cultured controls.	(Sharma et al., 2012)
Bone marrow-on-a-chip	PDMS device, central cavity containing collagen I, demineralized bone powder, BMP-2 and -4	Populated with host cells following implantation, then extracted bone with central marrow compartment	• Reconstitute complex *in vivo* niche architecture and physiology. • HSC culture with perfusion maintained LT-HSCs more efficiently than static stromal feeder layers.	(Torisawa et al., 2014)

1.6 Conclusion

Stem cell niches are complex and dynamic systems that are fundamental during homeostasis, aging and tissue repair. Understanding the stem cell niche is evidently important and will help us generate strategies to better harness the full clinical potential of stem cells. The BM niche is of significant interest as it harbours two sources of clinically relevant stem cells, yet how this microenvironment regulates these cells remains to be fully understood. Biomaterial and engineering strategies have great potential to recapitulate some of the varied facets described in this chapter; such as the supportive cells, 3D architecture, oxygen tension, ECM proteins and secreted factors which all contribute to BM niche functionality. Development of *in vitro* platforms such as these will allow better understanding of both MSPC and HSC biology within the niche, which ultimately will lead to development of better drug screening methods and therapeutic application of these cells.

1.7 Aims and Objectives

The aim of this thesis is to engineer a biomimetic BM niche model. The model will incorporate and compare several important niche factors, including variations in ECM proteins and mechanics, GF presentation and local oxygen tensions. First, by investigating the response of these factors on a population of MSPCs, pericytes, to enable investigation of fundamental mechanisms important in response to niche properties. Then investigation into the functional output by co-culturing HSCs within the model.

The model is based on the PEA FN BMP-2 system developed by our group (Cheng et al., 2018; Llopis-hernández et al., 2016). Where the addition of FN onto PEA causes spontaneous unfolding, allowing the tethering of ultralow GF concentrations. Then the addition of a low-stiffness matrix is incorporated using a collagen type I hydrogel, and the effects of hypoxia are investigated. The collagen type I hydrogel is based on a model previously developed in our group (Sweeten, 2019), where a gel of ~1 cm thickness was added on top of cells seeded onto PEA substrates, creating a biphasic cell-material interface. This low-stiffness component was shown to support a niche-like phenotype of MSCs. Figure 1-19 represents a schematic of the three niche models used.

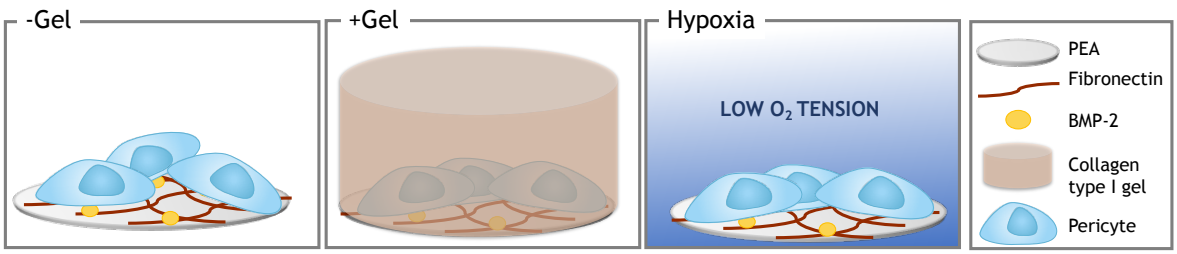

Figure 1-19 Schematic of *in vitro* niche models. To investigate the contribution of niche components to niche-phenotypes in a population of stromal stem cells (pericytes), a collagen type I gel was used to add a low stiffness matrix, and low oxygen tension to investigate hypoxic mechanisms.

With this regard, the aims of this thesis are as follows:

- Characterisation of the material components of the model. This will include verification of FN network formation on PEA, subsequent GF adsorption and assessment of elastic properties of the collagen type I gel.

- Assessment of pericyte phenotype when cultured in the model. This includes investigation into the effects of different niche properties in supporting a niche-like population of MSPCs, evaluated by expression of niche-related markers.

- Investigation into the effects of hypoxia and matrix mechanics on cellular metabolism. A metabolomics approach is used to assess the influence of low-stiffness matrices on metabolic mechanisms that may be important in niche regulation.

- Assessment of HSC support in the model. Introduction of HSCs to the model and analysis of HSC phenotype after co-culture is evaluated to determine if the model can support long-term HSCs in culture.

Chapter 2 General Materials and Methods

This chapter describes the general materials and methods that were used to carry out the experiments in this work. Specific methods, or methods that were developed will be detailed in the relevant chapter.

2.1 Materials and Reagents

2.1.1 Cell culture reagents

Reagent	Supplier
10X Modified Eagle's Medium	Sigma-Aldrich, UK
4- (2-hydroxyethyl)-1-piperazine-ethanesulphonic acid (HEPES)	Thermo Fischer Scientific, UK
Accutase™	Thermo Fischer Scientific, UK
Alpha Minimum Essential Medium Eagle (a-MEM)	Sigma-Aldrich, UK
Bone Morphogenic Protein-2 (BMP-2)	Sigma-Aldrich, UK
Bovine Insulin Transferrin (BIT)	Stem Cell Technologies, UK
Bovine Serum Albumin (BSA)	Sigma-Aldrich, UK
Brefeldin A	Thermo Fischer Scientific, UK
Collagenase D	Sigma-Aldrich, UK
Dulbecco's Modified Eagle's Medium (DMEM)	Sigma-Aldrich, UK
Endothelial Cell Growth Medium 2 (EGM)	Lonza, UK
Ethylenediaminetetraacetic acid (EDTA)	Sigma-Aldrich, UK
Fibronectin	Sigma-Aldrich, UK
Flt3 Ligand	Peprotech, UK
Foetal Bovine Serum (FBS)	Sigma-Aldrich, UK
Fungizone® Amphotericin B (250 μg/mL)	Gibco by Life Technologies, UK
Gelatin solution, type B	Sigma-Aldrich, UK
Hank's balanced salt solution (HBSS)	Stem Cell Technologies, UK
Human AB Serum (HS)	Sigma-Aldrich, UK
Hydrocortisone	Stem Cell Technologies, UK
Iscove's Modified Dulbecco's Medium (IMDM)	Thermo Fischer Scientific, UK
L-Glutamine (200 nM)	Invitrogen, UK
Methocult™	Stem Cell Technologies, UK
Minimum Essential Medium Non-Essential Amino Acids (MEM-NEAA)	Sigma-Aldrich, UK
MyeloCult™	Stem Cell Technologies, UK
Penicillin-Streptomycin (10 mg/mL stock)	Sigma-Aldrich, UK

Phosphate-Buffered Saline (PBS)	Sigma-Aldrich, UK
Rat tail collagen type I, > 2 mg/mL	First Link Ltd., UK
Sodium hydroxide (0.1 M)	Sigma-Aldrich, UK
Sodium Pyruvate (100 mM)	Sigma-Aldrich, UK
Stem Cell Factor (SCF)	Peprotech, UK
Thrombopoietin (THPO)	Peprotech, UK
TrypLE	Thermo Fischer Scientific, UK
Trypsin (10X solution)	Sigma-Aldrich, UK
Type II-S collagenase 1	Sigma-Aldrich, UK

2.1.2 Immunostaining Reagents

Reagent	**Supplier**
Biotinylated anti-mouse IgG produced in horse	Vector Laboratories, UK
Biotinylated anti-rabbit IgG produced in horse	Vector Laboratories, UK
Fluorescein Streptavidin	Vector Laboratories, UK
Formaldehyde	Thermo Fischer Scientific, UK
Magnesium Chloride Hexahydrate ($MgCl_2.6H_2O$)	Sigma-Aldrich, UK
Rhodamine Phalloidin	Molecular Probes, Life Technologies
Sodium Chloride	VWR Chemicals
Sucrose	Thermo Fischer Scientific, UK
Triton X-100	Thermo Fischer Scientific, UK
Tween 20	Sigma-Aldrich, UK
Vectashield mounting medium with DAPI	Vector Laboratories, UK

2.2 Preparation of Cell Culture Solutions

Reagent	**Component**	**Amount**
Trypsin/Versene solution	NaCl	150 nM
	KCl	5 mM
	glucose	5 mM
	HEPES	10 mM
	Phenol red solution	0.5 % (v/v)
	Trypsin	5 % (v/v)
HEPES saline solution	NaCl	150 nM
	KCl	5 mM
	glucose	5 mM
	HEPES	10 mM
	Phenol red solution	0.5 % (v/v)
20 % DMEM	DMEM	500 mL
	FBS	100 mL
	Penicillin-streptomycin	10 mL
	MEM-NEAA	5 mL
	Sodium pyruvate	5 mL
2 % DMEM	DMEM	500 mL

	HS	10 mL
	Penicillin-streptomycin	10 mL
	MEM-NEAA	5 mL
	Sodium pyruvate	5 mL
Fixative solution	PBS	90 mL
	Formaldehyde	10 mL
	Sucrose	2 g
Permeabilisation buffer	Sucrose	0.1 % (w/v)
	NaCl	50 mM
	$MgCl_2.6H_2O$	3 mM
	HEPES	20 mM
	Triton X-100	0.5 % (v/v)
Blocking buffer	PBS	100 mL
	BSA	1% (w/v)
ICW blocking buffer	PBS	100 mL
	Milk powder	1% (w/v)
FACS buffer	PBS	100 mL
	BSA	0.5 % (w/v)
	EDTA	2 mM
Human long-term culture medium (HLTM)	MyeloCult™	100 mL
	Hydrocortisone in αMEM	1×10^{-4} M

2.3 General Methods

2.3.1 Substrate preparation

2.3.1.1 Spin coating

Sheets of polymer were obtained by radical polymerization of a solution of either MA (methyl acrylate) or EA (ethyl acrylate) (Sigma-Aldrich, UK), using 1 and 0.35 weight percent benzoin (98% pure; Scharlau) as the photoinitiator. Polymerization carried out up to limiting conversion. After polymerization, low molecular mass substances extracted by drying under vacuum to constant weight. PMA and PEA were dissolved in toluene at a concentration of 6% or 9% and 2.5% or 12% dependent on batch. Thin films were then created on glass coverslips using a spin coater (Brewer science, USA), 100 μL of polymer was pipetted onto glass coverslips that were spun at 2000 rpm for 30 s. Samples dried under vacuum at 60°C for 2 h, and sterilised under UV light for 30 min before use.

2.3.1.2 Fibronectin and growth factor adsorption

Polymer coated coverslips were placed on parafilm and FN from human plasma was adsorbed in solution (20 μg/mL) and incubated at room temperature (RT) for 1 h. For GF adsorption, substrates were washed twice with PBS, then BMP-2 in PBS

(50 ng/mL) was added and incubated at RT for 2 h. After two washes with PBS substrates were transferred into 24-well plates in PBS until ready for use.

2.3.1.3 Collagen gel

For the relevant conditions (+gel) 1 mL of collagen type-I gel solution was added to culture after either 24h (for short term culture) or 72h (for long term culture), in 24-well plates. On ice, approximately 6 mL of collagen gel solution was generated by addition of 2.5 mL type-I 2.05 mg/mL rat tail collagen in 0.6% acetic acid to 0.5 mL human serum (HS), 0.5 mL 10x DMEM, 0.5 mL 2% DMEM, adjusted to pH 8.2 using 0.1 M NaOH. Plates were then placed into the incubator for gelation to occur for 12-24h, then topped up with 1 mL 2% DMEM. The resulting collagen gel is ~1 cm in thickness.

2.3.2 Pericyte isolation and culture

2.3.2.1 Pericyte isolation from adipose tissue

Pericytes were isolated from the adipose tissue of healthy adult donors undergoing cosmetic lipectomy procedures with prior written consent, or from patients undergoing breast reconstruction procedure, using deep inferior epigastric perforators (DIEP), from adult donors. Ethical approval for the collection of tissue and subsequent research was granted by the South-East Scotland Research Ethics Committee 3 (SESREC03, reference no. 10/S1103/ 45). Incisions were made in the adipose tissue using a scalpel to divide the Scarpa's fascial layer, then tissue was mechanically minced using a cheese grater and 150 mL of the resulting tissue combined with 100 mL PBS. After 30 s of manual shaking, tissue was centrifuged at 445 g for 10 mins at RT, causing phase separation. The 3 phases include the top phase (liquid fat/oil), central phase containing the tissue of interest (adipose tissue), and the bottom phase (blood/fluid). 25 mL of the middle layer was removed and mixed with 25 mL PBS/2% (v/v) FBS and centrifuged at 445 g for 10 mins. Supernatant was removed leaving the Stromal Vascular Fraction (SVF) pellet, which was then enzymatically digested with 25 mL digestion solution (type II-S collagenase 1 mg/mL in DMEM/0.5% (v/v) BSA) for 45 mins in a water bath at 37^{o}C with shaking. After incubation, samples were centrifuged at 445 g for 10 mins to obtain the digested SVF. Supernatant was aspirated (containing oil and adipocytes) and pellets resuspended in 25 mL PBS/2% (v/v) FBS, manually

disrupting or removing large clumps. The tissue solution was then sequentially strained through 400 μm, 100 μm and 70 μm cell pluristrainers to remove undigested material. Filtered solution centrifuged at 445 g for 10 mins, supernatant discarded, and pellets resuspended in 10 mL red blood cell lysis buffer and incubated RT for 10 mins. 20 mL PBS/2% (v/v) FBS added and samples centrifuged at 400 g for 10 mins. Supernatant aspirated and SVF pellet resuspended in Fluorescent Activated Cell Sorting (FACS) buffer and cells counted ready for FACS staining.

2.3.2.2 Fluorescent activated cell sorting of pericytes

The SVF isolated from adipose tissue was stained with the antibodies in Table 2-1. Pericytes were sorted to homogeneity using FACS cell sorter (BD Bioscience) based on the following phenotype: CD146+ CD45- CD34- CD31-.

Table 2-1 Antibodies for fluorescent activated cell-sorting of pericytes from adipose tissue.

Target	Fluorochrome	Dilution	Manufacturer
CD146-Alexa647	Ch5	1:100	BC Biosciences
CD45	APC-cy7	1:200	BD Biosciences
CD34	FITC	1:100	BD Biosciences
CD31	PE	1:100	BD Biosciences

2.3.2.3 Primary cell culture

Immediately after FACS, pericytes were seeded onto 0.1% gelatin-coated wells at a density of 2 x 10^4 cells/cm^2 in EGM-2 endothelial growth medium (Lonza) in a humidified incubator with 5% CO_2 at 37°C. When confluent, cells were detached using trypsin/v and split into uncoated wells and cultured in 20% DMEM for all subsequent passages. Media changed twice per week and cultured until ready for use or until passage 10.

2.3.2.4 Primary cell culture on polymer substrates

For cell culture on materials, non-coated glass and polymer coated coverslips were transferred to 24 well plates, and cells seeded at 1.5 x10^3 cells/cm^2 in 500 μL 2% DMEM. Culture plates were incubated under a humidified atmosphere of 5% CO_2 at 37°C, and 500 μL 2% DMEM added after 24 h. After 3 days for long term experiments, or 24h for short term, all culture media was removed and replaced, or for the +gel conditions 1 mL collagen gel was added. Hypoxia conditions were

moved to hypoxic workstation (Ruskinn) at an oxygen tension of 1%, CO_2 5% and 37ºC. Cultures were thereafter fed every 3 days for the remainder of experiment time period. Cells were cultured for times indicated in each experiment.

2.3.3 Flow cytometry

BD FACS Canto II analyser was used for flow cytometry analysis. Cells were prepared from culture models as indicated in Section 2.3.3.1. Unstained control cells were used to set the voltage for each of the 6 channels used, and unstained cells or isotype controls for each channel were also included with cells as negative controls. Allowing for the non-specific background signal to be differentiated from the antibody signal.

2.3.3.1 Preparation of cells from culture models

For the culture models, the collagen gel was first digested by adding equal volume of collagenase D solution (2.5 mg/mL in PBS) into the media and/or gel in each well, and incubated at 37ºC for 90 min. The solution in each well, containing digested collagen gel and media, was then passed through a 70 μm filter. The polymer or glass substrates were then washed once with hepes saline and incubated with TrpLE for 5-10 min at 37ºC. If required, multiple wells for each condition were pooled, then centrifuged at 400 g for 4 mins.

2.3.3.2 Flow cytometer and compensation

To correct spectral overlap UltraComp eBeads™ were used to perform fluorescence compensation. 1 drop of beads were added to 8 FACS tubes and 2 μL of an antibody corresponding to each of the 8 channels was added. The tubes were then stored in the dark at 4ºC for 30 mins. 2 mL of flow buffer was then added and tubes centrifuged for 4 mins at 600 g. Supernatant was removed and pellets resuspended in 200 μL of FACS buffer. Each sample was then run as instructed by machine software, and compensation automatically calculated.

2.3.4 Immunocytochemistry

After removal of media, samples were washed once with PBS and 10% formaldehyde fixation solution (Chapter 2.2) added at 37ºC for 15 mins. Fixation

solution was then removed, and collagen gels discarded. Cell membranes were then permeabilised with 0.5% Triton-X permeabilisation buffer (Chapter 2.2) for 5 mins at 4ºC, and subsequently blocked in 1% BSA blocking buffer (Chapter 2.2) for 15 min at 37ºC. Cells were then incubated overnight at 4ºC with the required primary antibody diluted in PBS/1% BSA (Table 2-2).Then cells were washed three times for 5 min with 0.5% Tween20 in PBS and incubated for one hour at 37ºC with the corresponding secondary antibody (1:50 in PBS/1% BSA). Cells were then washed as before and, if required, incubated 4ºC for 30 min with streptavidin conjugated FITC, and washed 3 times in PBS/0.5% Tween20 after this incubation. Samples were mounted onto glass microscope slides with a drop of vectasheild-DAPI (a glycerol based mounting medium containing nucleic acid staining). All samples were then stored at 4ºC in the dark to preserve from photobleaching, until ready for microscopic analysis. Secondary antibodies used throughout this thesis are well validated in our group and have been demonstrated for specificity in many publications (Alakpa et al., 2017b, 2017a; Roberts et al., 2016; Tsimbouri et al., 2017, 2012; J. Yang et al., 2014).

Table 2-2 Primary antibodies used for immunocytochemistry.

Primary antibody	Supplier	Dilution	Source
CXCL12	Abcam, UK	1:200	monoclonal mouse
HIF1α	Abcam, UK	1:300	monoclonal rabbit
Hypoxyprobe™	Hypoxyprobe™	1:200	monoclonal mouse
Nestin	Abcam, UK	1:200	monoclonal mouse
SCF	Abcam, UK	1:200	polyclonal rabbit
Vimentin	Sigma-Aldrich, UK	1:300	monoclonal mouse

2.3.5 Microscopy

Immunostained samples were viewed in 3 channels using an Axiophot microscope (FITC, TRITC and DAPI), linked to a camera. Images were obtained using ImagePro software and were converted to red green blue (RGB) format using ImageJ software (National Institute of Health, USA), subsequent quantification using either ImageJ or CellProfiler software will be detailed in later chapters. To indicate scale, an image of a 1 mm graticule was taken under the associated magnification lens and converted to pixels using ImageJ.

2.3.6 In cell western (ICW)

Following cell culture, cells were fixed and permeabilised as outlined in Chapter 2.3.4. Samples were then blocked in 1% milk ICW blocking buffer (Chapter 2.2) for 1.5 hours. Cells were then incubated overnight at 4ºC with the required primary antibody (Table 2-3) diluted in ICW blocking buffer (1:100). Then cells were washed five times for 5 min with 0.5% Tween20 in PBS and incubated for one hour at 37ºC with the corresponding IRDye 800CW/700CW secondary anti-rabbit/mouse antibody (1:800), CellTag 700 stain (1:500) and 0.2% Tween20. Secondary antibodies and CellTag 700 stain acquired from Li-Cor. CellTag700 is a non-specific cell stain used for normalisation to cell number. After 1h, cells were washed five x 5 min with 0.5% Tween20 in PBS. Following the final wash, coverslips were transferred to a new 24-well plate and left to air dry before imaging.

Table 2-3 Primary antibodies used for in cell western.

Primary antibody	Supplier	Dilution	Source
Lactate dehydrogenase	Abcam, UK	1:100	Monoclonal rabbit
P5F3	Sant Cruz Biotechnology, UK	1:100	Monoclonal mouse
HFN7.1	Developmental Studies Hybridoma Bank, USA	1:100	Monoclonal mouse
Fibronectin	Sigma Aldrich, UK	1:100	Polyclonal rabbit

Samples were then scanned using the Li-Cor Odyssey Sa scanner in the 800 nm and 700 nm channels. A grid was then drawn, and measurements of fluorescent units taken. Where appropriate the signal of the protein of interest was divided by the control (CellTag700)

2.3.7 RNAseq

Cells were cultured on substrates as described in 2.3.2.4 for 7 days. They were then trypsinised, centrifuged to pellet and lysed using Qiagen RLT lysis buffer.

Sequencing libraries were then prepared from total RNA using the Illumina TruSeq Stranded mRNA Sample Preparation Kit. Libraries were sequenced in 75 base, paired end mode on the Illumina NextSeq 500 platform. Raw sequence reads were trimmed for contaminating sequence adapters and poor quality bases using the

program Cutadapt (Martin, 2011). Bases with an average Phred score lower than 15 were trimmed. Reads that were trimmed to less than 54 bases were discarded. The quality of the reads were checked using the Fastqc program (http://www.bioinformatics.babraham.ac.uk/projects/fastqc/) before and after trimming. The reads were "pseudo aligned" to the transcriptome using the program Kallisto (Bray et al., 2016). The differential expression for the analysis groups were assessed using the Bioconductor package DESeq2 (Love et al., 2014). This was provided as a service by Glasgow Polyomics Facility. Heatmaps were subsequently generated using Cluster 3.0 and Java Treeview 3.0 software, with average linkage clustering method.

Chapter 3 Characterisation of Materials

3.1 Introduction

To engineer increasingly biomimetic materials, current strategies focus on control of integrin adhesion receptor-related signalling to direct stem cell behaviour (Dalby et al., 2018). These approaches aim recapitulate structures topographically, mechanically or chemically similar to native ECM, as discussed in Chapter 1. Techniques that present cell adhesive motifs or protease degradable cross-links however often fail to reconstitute the network structure and bioactivity of native ECM molecules such as FN, this is due to the absence of domains that contain complementary or modulatory sequences involved in cellular processes (Petrie et al., 2006).

3.1.1 Fibronectin

Fibronectin is a ubiquitous ECM glycoprotein that is assembled into fibrillar matrices in all tissues. FN forms dimers consisting of two subunits (~220 kDa) linked by a disulphide bond near the carboxyl termini (Figure 3-1). Each subunit contains domains for mediating interactions with other FN molecules, ECM components, and cell surface receptors, contained in three types of repeating modules (types I, II and III). FN dimers then multimerise to form fibrillar networks, in a process that is normally cell-mediated via an integrin-dependent contractile process (Singh et al., 2010).

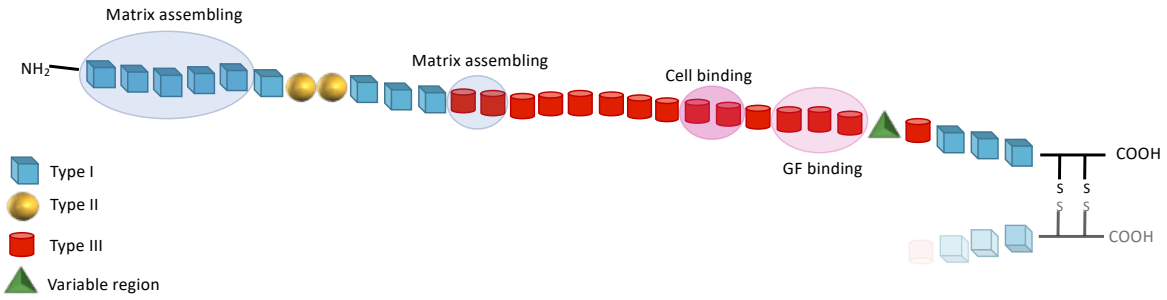

Figure 3-1 Fibronectin (FN) subunit. FN has three types of repeat, types I (blue), II (yellow) and III (red). Domains required to initiate assembly include the cell binding site (RGD in III_{10} and synergy in III_9), the N-terminal assembly domain ($_{I1\text{-}5}$), and the intramolecular cysteine dimers at the C-terminal. The $III_{1\text{-}2}$ domain contains two FN-binding sites involved in conformational changes that promote assembly. The $III_{12\text{-}14}$ domain contains the GF binding site (Singh et al., 2010). Image adapted from (Donnelly et al., 2018).

Cells primarily interact with FN through integrins, and most cells will assemble FN-dense matrices, incorporating FN either synthesised by cells or reorganised from their surroundings (Singh et al., 2010). Cells mediate FN matrix assembly through integrin binding to the RGD cell-binding domain in the type III_{10} domain, the primary receptor for which is integrin $\alpha_5\beta_1$ (Obara et al., 1988). However, a synergy sequence is also required to initiate fibril formation, the PSHRN site in the type III_9 domain enhances the affinity of integrin binding over forty-fold (Aota et al., 1994) (Figure 3-1). Further to these cell adhesion sites, FN contains the GF binding site in $III_{12\text{-}14}$ previously discussed in Chapter 1.5.4, which has been shown to be highly promiscuous in its GF binding. This site, also known as the heparin-binding domain, binds GFs in several families, including PDGF/VEGF, FGF (fibroblast growth factor) and TGFß (Martino and Hubbell, 2010), through their affinity to heparin and heparin sulfate (Kirkpatrick and Selleck, 2007; Pankov and Yamada, 2002).

FN presents a strategy to increase adhesive properties and GF delivery of engineered materials. However, upon adsorption to biomaterials FN typically adopts a globular conformation, concealing these binding domains and physically disrupting the affinity of GF binding to the heparin-binding domain. Only when cells adhere are they able to reorganise the FN molecules and mediate fibrillogenesis (Singh et al., 2010).

3.1.1.1 Engineered fibronectin fragments for cell adhesion and growth factor delivery

In approaches to exploit the cell adhesive properties of FN, recombinant fragments have been engineered to contain both the RGD and PHSRN synergy site. A fragment containing $FNIII_{7\text{-}10}$ was produced that retains the native spacing between the adhesive domains, presenting the binding sites in correct structural context (Cutler and Garcia, 2003). Surfaces presenting RGD-only, or an oligopeptide that failed to control site distances, showed a decrease in cell adhesion primarily through integrin $\alpha_5\beta_1$ binding, and reduced FAK activation (Petrie et al., 2006). This control over integrin binding using FN fragments was found to promote osteoblast differentiation *in vitro*, and improve osteointegration of titanium implants *in vivo* (Agarwal et al., 2015; Cutler and Garcia, 2003; Petrie et al., 2006).

The work by Martino et al, discussed in Chapter 1 built on this to further exploit FNs integrin- and GF-binding abilities. A recombinant fragment was engineered to contain the major cell binding domain (FN III_{9-10}) and the GF binding domain (FN III_{12-14}) (Martino et al., 2011). By incorporating PDGF and 2 BMP-2, they found the system could promote both wound repair and bone growth (Martino et al., 2011). Presentation of the FN III_{9-10} and FN III_{12-14} repeats proximally in the same polypeptide chain led to potent synergistic signalling through recruitment of integrins and GF receptors to adhesion domains.

These strategies, however, rely on complex recombinant protein technology - the FN fragment engineered by Martino et al, relies on addition of extra sequence to bind to a fibrin matrix – and intricate engineering that increase cost and complexity. Other strategies to deliver GFs, as discussed in detail in Chapter 1, typically involve high doses, low efficiency, and lack potential for GFR-integrin cross talk.

3.1.1.2 Material-driven fibronectin assembly

In efforts to exploit FN molecules for GF delivery without the use of complex recombinant technologies, other approaches focus on methods to drive self-organisation of FN fibrils at the material interface. Material properties are known to alter protein adsorption, and seminal work has demonstrated that by carefully tuning interface chemistry, FN conformation and subsequent cell adhesion can be altered. In these studies, self-assembled monolayers (SAMs) were used to present terminal functionalities of differing chemistries (CH_3, OH, COOH, NH_2), without altering other surfaces properties, such as roughness. The effects on adsorbed FN conformation were observed through changes in affinity of integrin binding (Keselowsky et al., 2002), focal adhesion composition (Keselowsky et al., 2004) and cell differentiation (Keselowsky et al., 2005).

Screening of polymers of different chemistries, with the hypothesis that particular surface chemistries would induce exposure of self-assembly domains of FN, identified PEA as a potential chemistry to generate FN fibrils (Rico et al., 2009; Salmerón-Sánchez et al., 2011). Work by our group has demonstrated the ability of PEA, in the absence of cells, to induce the formation of FN networks driven by the material interface (Cheng et al., 2018; Llopis-hernández et al., 2016). The

formation of these physiological-like networks of FN exposes the cell binding and GF binding domains of the molecule. Sequestered GFs can then be presented in native synergy with the cell binding domains of FN. Using the GF BMP-2, this simple polymer based system that supports spontaneous FN unfolding has been found to induce osteogenesis of MSCs *in vitro*, and implantation of coated constructs lead to full union of critical size defects in a mouse model and a non-healing fracture in a dog (Cheng et al., 2018; Llopis-hernández et al., 2016).

3.1.2 BMP-2

BMPs are potent growth factors, constituting the largest subfamily of the TGFß superfamily (Chen et al., 2004). Originally identified and related to bone formation, BMPs have now been shown to be ubiquitously expressed and to play essential roles in a wide variety of developmental and cellular processes (Obradovic Wagner et al., 2010). Extensive studies in cultured cells, knockout mice and humans with naturally occurring mutations in BMP-related genes have demonstrated that BMP signalling pathways are indispensable for embryogenesis, skeletal formation, neurogenesis and haematopoiesis (Chen et al., 2004).

BMPs signal through two different types of serine/threonine kinase receptors; three type I receptors (BMPR1A, BMPR1B and activin receptor-like kinase 2 (ALK2)), and three type II receptors (BMPR1, activin receptor 2 (ARTR2) and ACTR2B) (Wang et al., 2014). Both receptor types have a short extracellular domain, a single transmembrane domain and an intracellular domain with serine/threonine kinase activity (Wang et al., 2014). BMPs signal through canonical and non-canonical pathways. Canonical pathways are activated by BMP binding to a heterotetrameric receptor complex, comprised of two type I and type II receptors (Figure 3-2) (Heldin et al., 1997). The mechanism of formation of the signalling complex can vary – for example, BMP-2 and BMP-4 preferentially bind type I receptors and recruit type II, whereas BMP-6 and BMP-7 interact with type II and recruit type I (De Caestecker, 2004). Upon complex formation the type I receptor acts as a substrate for the constitutively active type II receptor (De Caestecker, 2004; Wang et al., 2014).

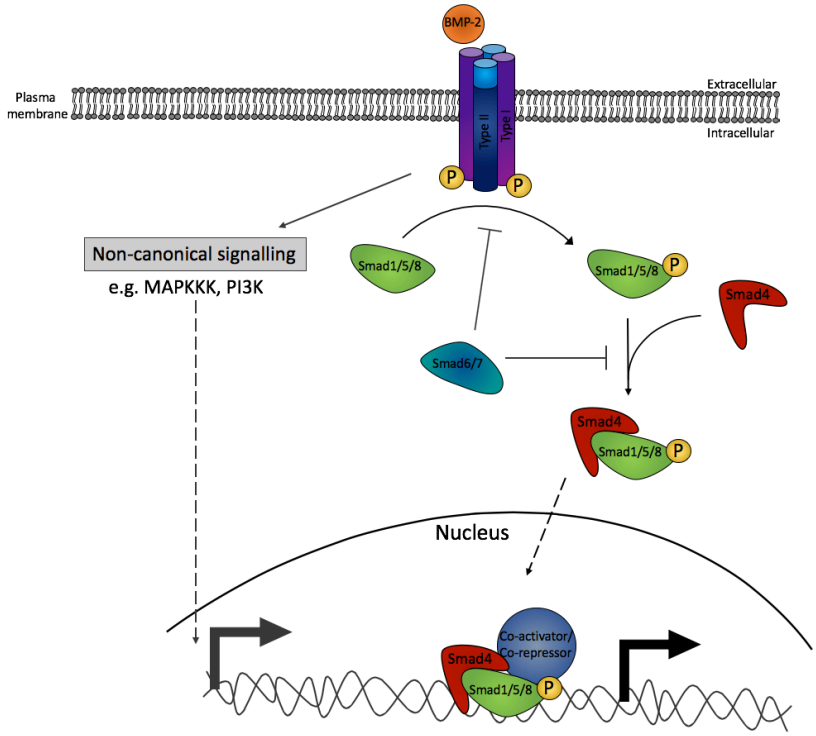

Figure 3-2 BMP-2 signalling. BMPs, such as BMP-2, signal via the Smad-dependent pathway or various non-canonical pathways. In the canonical pathway, BMP-2 initiates the signal transduction cascade by binding type I or II serine/threonine kinase receptors to form a heterotetrameric complex. Type II receptors are constitutively active, binding transphosphorylates the type I receptor. The type I receptor then phosphorylates the R-Smads (Smad1/5/8). Phosphorylated Smad1/5/8 associates with the co-Smad (Smad-4) and the complex translocates to the nucleus where it further associates with co-activators or co-repressors to regulate gene expression (Wang et al., 2014).

BMP-activated type I receptors relay the signal to the cytoplasm by phosphorylating their immediate downstream targets, Smad1, Smad5 and Smad8, which interact with Smad4 and translocate to the nucleus where the complex functions as a transcription factor with co-activators and co-repressors regulating gene expression (Wang et al., 2014). For osteogenesis, BMP-2 driven Smad phosphorylation activates RUNX2, the master regulator of the osteogenic response (Phimphilai et al., 2006). Although signalling may occur on multiple levels and non-canonical, Smad-independent, signalling pathways have been identified to include phosphoinositide 3- kinase (PI3K), Akt, protein kinase C (P/kc), Rho-GTPases, and the MAPKKK family. Crosstalk with other pathways, such as Wnt signalling, and involvement of co-receptors, such as endoglin, add a further layer of control and complexity (Derynck and Zhang, 2003).

The osteoinductive potential of BMP-2 has been demonstrated extensively in many *in vivo* and preclinical models of critical sized defects, and currently it is routinely used in the clinic for spinal bone fusions (Sayama et al., 2015). Although, recent focus on BMPs roles in processes throughout all organ systems have led to the

investigation and application of BMPs in non-bone related pathophysiology, from cancer to kidney disease (Bach et al., 2018; Tomita et al., 2013). This versatility of functions of BMPs has posed the suggestion the acronym be changed from bone to body morphogenetic proteins (Obradovic Wagner et al., 2010).

3.1.3 Collagen

Collagen, is a major component of the native ECM, as such, it is the most abundant protein in mammals, contributing ~25% of the total protein mass (Alberts et al., 2008). There are at least 19 different types of collagen, and type I collagen is the most prevalent *in* vivo as it is the principle collagen for bone and skin, accounting for 90% of all body collagen (Alberts et al., 2008). Due its abundance, adaptability and ease to extract, collagen I has proven popular for tissue engineering applications (Antoine et al., 2014).

The basic primary structure of all collagen is composed of three polypeptide chains, which wrap around each other into a rope-like helical structure (Alberts et al., 2008). Type I collagen triple-helical proteins are formed of 67 nm polypeptide chains (Mw ~ 300 kDa). These fibrils self-assemble at neutral pH into bundled fibres (~12 – 120 nm diameter), that crosslink to produce a matrix structure, that ultimately forms a hydrogel in the presence of a water-based solvent (Antoine et al., 2014; Kadler et al., 2007). Thus collagen fibres and scaffolds can be created or engineered and their mechanical properties can be accurately tuned by, for example, controlling the rate of polymerisation through temperature or pH, introducing crosslinkers, or blending with other polymers (Antoine et al., 2014; Drury and Mooney, 2003).

Early studies that aimed to recapitulate the BM microenvironment such as Dexter cultures, pointed to an abundance of collagen I synthesis by the adherent stromal cell feeder layers that were isolated from BM aspirates (Bentley, 1982; Dexter et al., 1977). As such, collagen based cultures and scaffolds have been employed in attempts to mimic both the cell-ECM interactions of the niche and the 3D architecture (Dhami et al., 2016; Lai et al., 2013) As discussed in Table 1-5, niche mimetic collagen scaffolds have taken the form of microspheres (Wang et al., 1995), hydrogels (Leisten et al., 2012) and decellularized constructs (Lai et al.,

2013), and have all shown promise in long-term HSC culture. Consequently, we chose to incorporate a collagen type I hydrogel into the niche model.

3.1.4 Objectives/aims

This chapter aims to characterise the material properties of the culture model. First, the FN adsorption onto polymer surfaces was analysed, then this previously developed system was extended for use with a collagen type I hydrogel. Finally, assessment of seeding of human adipose tissue derived pericytes into the system was carried out. This will be achieved by addressing the following objectives:

- Assessment of FN conformation on PEA and PMA.
- Assessment of BMP-2 binding to FN.
- Assessment of cell numbers on polymer substrates.
- Measurement of collagen hydrogel stiffness.

3.2 Materials and Methods

3.2.1 BCA protein assay

Pierce™ BCA Protein Assay Kit (Thermo Fischer, UK) was used to measure the amount of FN adsorbed onto polymer substrates, as per manufacturer's instructions. Polymer substrates were incubated for 1 h at RT with FN solution (20 μg/mL). Solution was aspirated and collected in Protein LoBind Tubes (Eppendorf), if required 10x dilutions of aspirated solution was performed. BSA standard (2000 μg/mL – 25 μg/mL) and FN standard (100 μg/mL – 0.5 μg/mL) were prepared by serial dilution in PBS. Samples were added in triplicate to a microplate with working reagent, incubated at 37°C for 30 mins, cooled to RT and absorbance measured at 562 nm on plate reader. Blank replicates (PBS + working reagent) measurements were subtracted from measurements of standards and replicate samples. Standard curves were generated by plotting blank-corrected measurements vs concentration. Unknown sample concentrations were then interpolated from the standard curve.

3.2.2 BMP-2 ELISA

For quantification of BMP-2 adsorption, (50 ng/ml) BMP-2 solution was added to FN coated polymers and after 2 h incubation the BMP-2 solution was aspirated from the samples and collected in Protein LoBind Tubes (Eppendorf). Enzyme-linked immunosorbent assay (ELISA) was then carried out as per manufacturer's instructions (R&D Systems). Briefly, ELISA plates were coated with capture antibody overnight, then blocked for 1 h with BSA. Standards, original solution, original solution at 20x dilution and sample aspirates were then added to the plate, and bound BMP-2 was detected with biotinylated anti-human BMP-2. Streptavidin-HRP was added to plates for 20 min in the dark, followed by substrate solution (tetramethylbenzidine and peroxide) for 20 min, the reaction was then stopped by adding stop solution. Absorbance measured at 450 nm with wavelength correction at 570 nm. The standard curve was calculated using a four-parameter logistic curve fit. The amount of BMP-2 was calculated from the standard curve based on the BMP-2 standards of known concentration.

3.2.3 Atomic Force Microscopy

FN conformation images were produced using atomic force microscopy (AFM) Polymers were incubated with FN solution (20 μg/mL) for 10 min, washed twice in PBS, once with deionised water and then dried under a stream of nitrogen before imaging. A JPK Nanowizard 4 (Zeiss Axio Observer A1; Accurion Halcyonics_i4 balance table) was used for imaging in tapping mode, using antimony-droped Si cantilevers with a nominal resonant frequency of 75 kHz (Bruker). The phase signal was set to 0 at a frequency 5-10% lower than the resonant frequency. Height and phase images were acquired from each scan JPK Data Processing software version 5 was used for image analysis.

3.2.4 Rheology

Rheological measurements were carried out using an Anton Paar Physical MCR301 rheometer. A parallel plate geometry (25 mm diameter, sandblasted) and 1.0 mm gap were used to measure time sweeps. For measuring the frequency and strain sweeps, 2 mL collagen gels were prepared as described in Chapter 2.3.1.3 in 6-well plates and placed in 37 °C incubator for 12 h for gelation to occur. After complete gelation, samples were transferred to the rheometer and the rheological

measurements were recorded at 25 ºC. To ensure the measurements were made in the viscoelastic range, a strain sweep was carried out. The dynamic modulus of the hydrogel was measured as a frequency function, frequency sweeps were carried out between 0.1 – 15 Hz, to measure the dynamic shear of the modulus as a function of strain. Measurements were repeated 3 times on gels from 3 different batches. Storage moduli (G') values were extracted from the accompanying Kinexus software. The Young's modulus was then determined by taking the G' and multiplying by 3, assuming a Poisson's ratio of 0.5 in accordance with Hooke's law.

3.2.5 Coomassie staining

After 7 days of culture on surfaces, cells were fixed for 15 min at 37ºC with fixative solution. After two washes with PBS, 1 mL of filtered Coomassie blue solution was added to each well for 2 min at RT. After two more washes with PBS images were acquired on a light microscope.

3.3 Results

3.3.1 Fibronectin conformation and availability of domains

To confirm that PEA surfaces promoted FN network formation, we compared it to the closely related PMA, which differs to PEA by one methyl group (Figure 3-3) but behaves similarly in terms of surface wettability and stiffness (Salmerón-Sánchez et al., 2011). AFM examination revealed FN formed interconnected fibrillar networks on PEA, but remained in a closed, globular conformation on PMA (Figure 3-3).

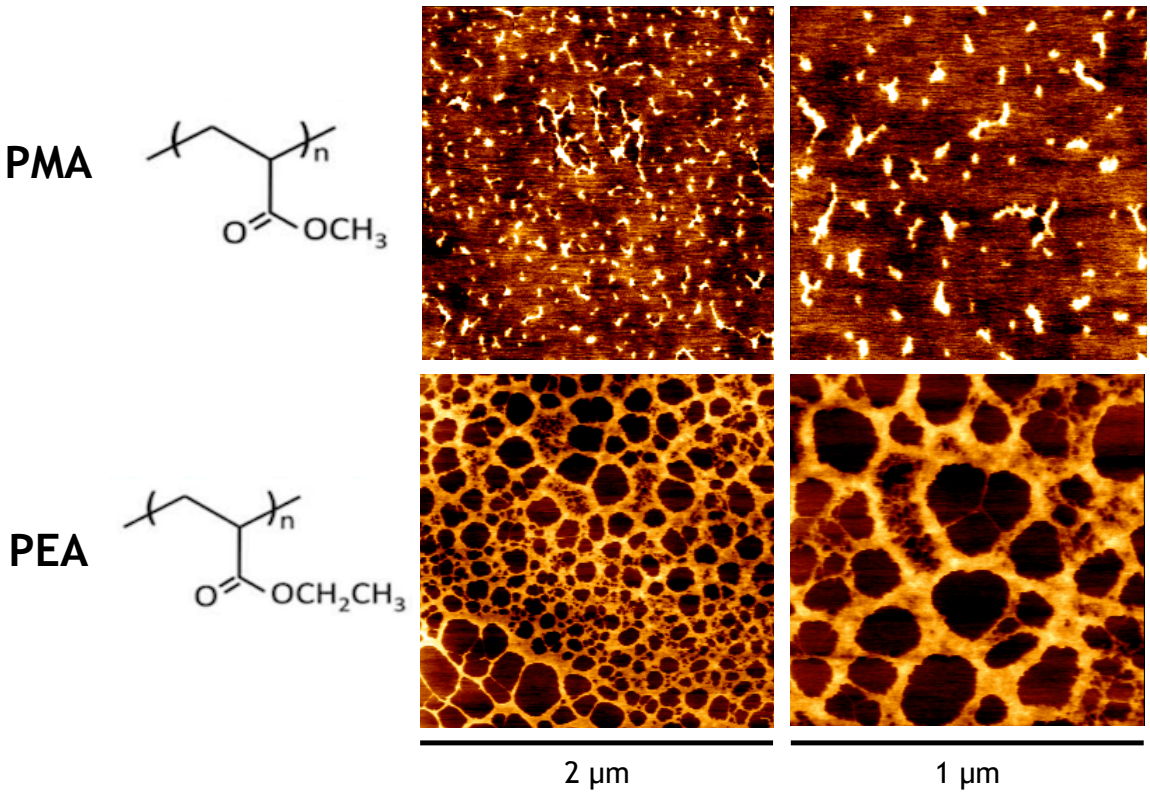

Figure 3-3 FN forms networks on PEA surfaces. AFM of FN adsorption onto polymer substrates. FN nanonetwork spontaneously assembled on the surface of PEA but not on closely related PMA. Chemical structures of polymers are represented. Chemical symbols reproduced under the terms of the Creative Commons Attribution NonCommercial License 4.0 (Llopis-hernández et al., 2016).

Total FN protein adsorption onto the surface was then quantified using a BCA assay, this indicated an increased mass of FN adsorbed on PMA (~775 ng/cm^2) compared to PEA (~520 ng/cm^2) (Figure 3-4A). The concentration of FN solution used was based on previous work from our group that demonstrated a minimum concentration of 10 μg/mL is needed for full interconnection of networks, and this has been optimised to a concentration of 20 μg/mL for more effective network formation (Cheng et al., 2018; Llopis-hernández et al., 2016).

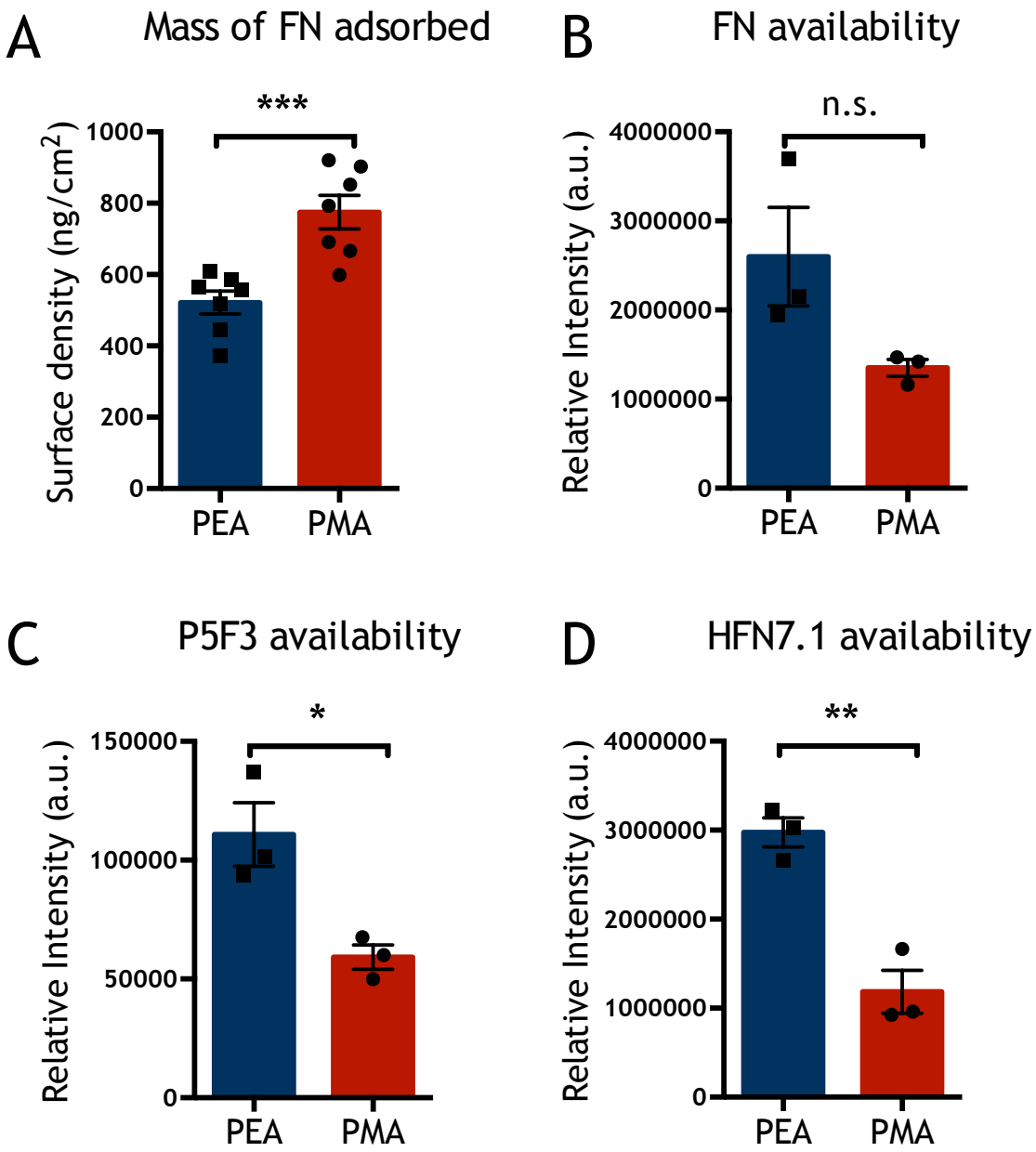

Figure 3-4 FN adsorption and domain availability on PEA and PMA. A. Surface density of FN on PEA and PMA per cm^2 coated from 20 μg/mL solution was determined using BCA assay, and indicates more FN adsorbs to PMA. B. In-cell western analysis was used to assess total FN availability demonstrated no significant differences; FN domains were tested in C. P5F3 (GF-binding domain) availability and D. HFN7.1 (RGD integrin-binding domain) availability were all increased on PEA substrates. Graphs show mean ± SEM, statistical analysis using unpaired two-tailed t-test, *= p<0.05, **= p<0.01, ***= p<0.001, n.s. = non-significant. A n=6, B-D n=3.

Although a higher density of FN adsorbed onto PMA, the AFM results depict network formation on PEA (Figure 3-4A and Figure 3-3). We therefore wanted to confirm FN was forming networks on PEA only, using in-cell western (ICW) techniques the availability of total FN was first assessed using a polyclonal antibody against total FN (Figure 3-4B), this showed no significant differences between PEA and PMA. Then antibodies against the GF binding domain (P5F3) (Figure 3-4C) and the integrin binding domain (HFN7.1) (Figure 3-4D) were used.

P5F3 is directed against the HepII GF binding domain in the type III_{12-14} region of FN, whereas HFN7.1 is directed to the flexible linker between the 9th and 10th type III repeats of FN (Vanterpool et al., 2014). Binding of both antibodies was increased on PEA compared to PMA, indicating increased exposure of these two domains. As both domains are concealed in globular FN molecules this data confirms FN network formation on PEA substrates.

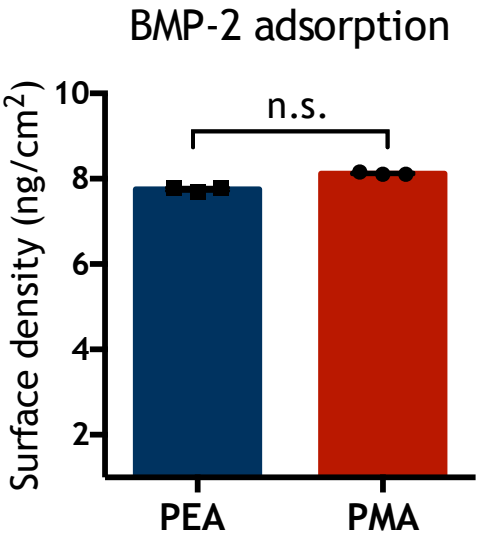

Figure 3-5 Surface density of BMP-2 on PEA FN and PMA FN. A 50 ng/mL BMP-2 solution was adsorbed onto PEA FN and PMA FN substrates, and BMP-2 surface density was quantified using ELISA. After incubation the amount of BMP-2 in the supernatant was determined using a standard curve, and the value was deducted from the concentration of the original solution to give the total mass adsorbed. Similar mass of BMP-2 was adsorbed onto both substrates. Graph shows mean ± SEM, n = 3, n.s. = non-significant using unpaired two-tailed t-test with Mann-Whitney test.

Exposure of the GF binding domain in FN networks has been previously exploited by our group to tether GFs, such as BMP-2 (Cheng et al., 2018; Llopis-hernández et al., 2016). To quantify BMP-2 adsorption an ELISA was carried out, although this revealed no significant differences in BMP-2 density between the two polymers (Figure 3-5). We have however previously demonstrated that only on PEA does BMP-2 co-localise to FN molecules, on PMA substrates BMP-2 is randomly dispersed and elutes from the substrate faster (Cheng et al., 2018; Llopis-hernández et al., 2016). The concentration of the BMP-2 solution used was 50 ng/mL, and ELISA analysis revealed ~8 ng/cm^2 to be adsorbed onto PEA and PMA substrates (Figure 3-5).

3.3.2 Cell adherence

To assess cell adherence to the polymers Coomassie blue staining was carried out after 3 days of culture of pericytes on the polymer substrates. The representative images in Figure 3-6A highlight lower levels of adherence and decreased cell-spreading on polymers containing no protein coating. To confirm this, ICW analysis of CellTag 700, a non-specific fluorescent protein stain, was used after 7 days of pericyte culture. Fluorescent intensity of each replicate was then measured and represented in the graphs in Figure 3-6B as fold change to a control glass coverslip. This demonstrated a significant decrease in fluorescence on PEA surfaces compared to those +FN and +FN BMP-2. A similar trend was observed for PMA, although this was not significant. This suggests cells on polymer substrates coated with FN and FN +BMP-2 could be greater in number or more spread, whereas on uncoated polymers cells may be less likely to adhere or spread.

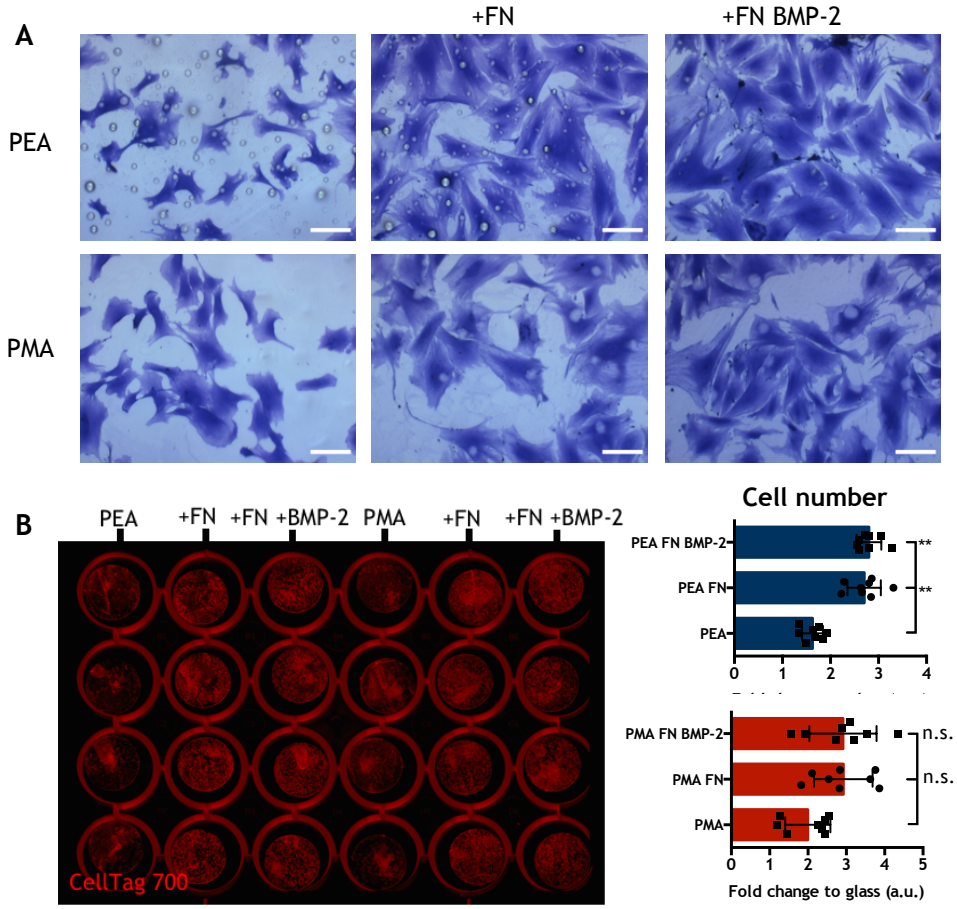

Figure 3-6 Cell adherence to PEA and PMA substrates. A. Coomassie blue staining of pericytes after 3 days culture on different polymer conditions. Scale bar is 100 µm, n = 3. B. ICW scan of CellTag 700 stain after 7 day culture, represented as fold change to glass control in graphs. Data suggests FN coating increases cell adhesion or spreading. N=8, data are shown as mean ± SEM, **= p<0.01, n.s. = non-significant, by one-way ANOVA followed by Kruskal-Wallis with multiple comparisons test.

3.3.3 Gel stiffness

We wanted to add a soft-matrix element to the model, therefore low-stiffness collagen type I gels were produced. To measure the stiffness of the gel, rheological measurements were carried out to determine the storage modulus (G') which could subsequently be converted into Young's modulus. To determine the Young's modulus (E) frequency sweeps were carried out between 1 and 10 Hz, and the storage modulus (G') converted using Hooke's law to Young's modulus (E = 3G').

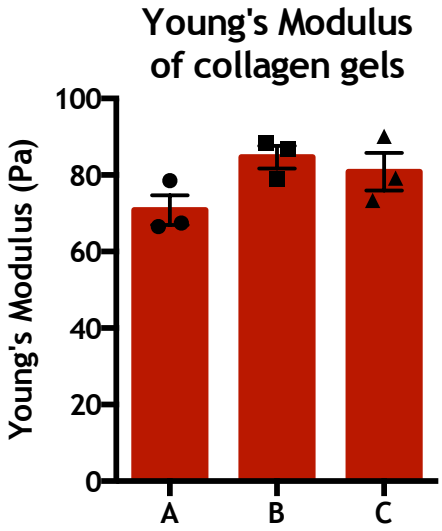

Figure 3-7 The Young's modulus of collagen type I gels. Rheological measurements were taken of 3 technical repeats of 3 batches of collagen gels (A-C). Storage modulus (G') were then converted to Young's modulus (E) using Hooke's law assuming a Poisson's ratio of 0.5 (E=3G'). Graph shows mean ± SEM. No statistical significance was observed, using non-parametric one-way ANOVA followed by Kruskal-Wallace multiple comparison test. Average Young's modulus is 78.8 Pa.

Three batches of gels (A-C) were produced, and 3 technical repeats taken for each batch, shown in Figure 3-7. The data suggests the mean Young's modulus of the gels to be around ~80 Pa. Some variation was observed between batches, although this was not significant, but could be due to inaccuracies in detecting the colour change upon adding volumes of NaOH to the gel mixture (Chapter 2.3.1.3). These measurements were in agreement with previous results from our group (Sweeten, 2019), and are slightly lower than that observed for measurements of intact bone marrow (Jansen et al., 2015).

3.4 Discussion

This chapter describes the characterisation of the different material components employed in the BM niche model used in this thesis.

3.4.1 PEA drives fibronectin fibrillogenesis

Using AFM imaging and antibody-based techniques we were able to confirm the polymer PEA could drive FN network formation (Figure 3-3 and Figure 3-4). This material-driven fibrillogenesis results in exposure of key binding sites on the FN molecule, such as the GF binding domain, FN III_{12-14}. Although an increased mass of FN was found to be adsorbed to PMA than PEA using BCA protein quantification, the AFM images and ICW analysis confirm network formation occurs only on PEA. We have previously confirmed 20 μg/mL as the optimum concentration for network formation on PEA; increasing the concentration of FN beyond this on PMA results only in a higher density of globular molecules, and not spontaneous unfolding (Cheng et al., 2018; Llopis-hernández et al., 2016).

To demonstrate material-driven network formation is driven by PEA, previous work employed random copolymer combinations of EA and MA. By modulating the EA/MA ratio the ability of adsorbed FN to form networks can be controlled, where increasing EA content leads to more interconnected FN networks, and a material composition that is >50% MA leads to significant decreases in the degree of fibrillogenesis (Mnatsakanyan et al., 2015). This cell-free network formation is rapid, it has been demonstrated FN organisation occurs within 1 min of adsorption (Gugutkov et al., 2010).

The increased availability of $FNIII_{9-10}$ domains on PEA was also correlated with increased measurements in cellular protein, as measured by Coomassie blue and CellTag protein stains, this suggests that FN adsorption influences cellular adherence and/or cell spreading on these surfaces. To quantify cell number more effectively DAPI counts could be carried out. Figure 3-6 shows when FN is present, there is a significant increase in cell number on PEA after 7 days (p<0.0005). Globular FN as presented on PMA follows a similar trend, although this was not significant, suggesting the increased availability of the cell binding domain on PEA is recognised and beneficial for cell adherence to the substrate.

3.4.1.1 Growth factor tethering

Similar levels of BMP-2 were found to be adsorbed to the PEA and PMA surfaces (Figure 3-5). However, our group has previously demonstrated by AFM and immunogold labelling that only open FN conformation supported by PEA is able to sequester the BMP-2 molecules; BMP-2 molecules were detected using an anti-BMP-2 antibody with a gold nanoparticle-labelled secondary antibody, depicted using height magnitude, then individual FN molecules were observed using phase magnitude (Cheng et al., 2018; Llopis-hernández et al., 2016). This revealed direct co-localisation of FN and BMP-2 molecules on PEA, whereas on PMA only random apposition of FN and BMP-2 molecules was observed, confirming FN sequestration of the GF on PEA. Very low release profiles have been demonstrated for both polymers over 14 days (>10% loss) (Cheng et al., 2018; Llopis-hernández et al., 2016). The results presented here, demonstrate BMP-2 can be adsorbed onto the polymer surfaces, however based on previous characterisation we show adsorption of FN onto PEA, but not PMA, allows controlled binding and presentation of the GF BMP-2 on the FN networks.

When considering the system for clinical application, the ability to deliver ultra-low doses of GFs is highly desirable, as discussed in Chapter 1.5.4. The controlled GF binding of the PEA system allows for GF delivery at nano-concentrations; 50 ng/mL BMP-2 coating was demonstrated to be sufficient to support osteogenesis both *in vitro* and *in vivo* (Cheng et al., 2018). We chose to employ BMP-2 at 50 ng/mL in this thesis based on these results, with the rationale of taking a system we had previously demonstrated to promote osteogenesis and bone formation, and manipulate different properties to more closely mimic aspects of the bone marrow microenvironment.

Bioinspired materials that focus on the interaction of GFs with the ECM have utilised GF sequestration in FN (Martino et al., 2011), vitronectin (Martino et al., 2014), tenascin c (De Laporte et al., 2013) and fibrinogen (Martino et al., 2013), and these have been applied to bone regeneration, wound healing and angiogenesis (Martino et al., 2011). Although collagen I is commonly used (typically in hydrogel format) as a vehicle for GF delivery, no GF binding site has yet been reported. In attempts to exploit these GF-ECM interactions, one study engineered GFs with supper-affinity to ECM binding sites (Martino et al., 2014).

Placental growth factor-2 (PlGF2) was found to most strongly bind to several ECM proteins through a heparin binding domain near its C-terminus, protein engineering techniques were then used to incorporate this domain onto clinically relevant GFs, such as BMP-2, VEGFA and PDGF-BB. Faster wound closure and tissue granulation was observed when these super-affinity GFs were applied to wound healing models at doses 40 – 250-fold lower (~200 ng) than that previously reported (Martino et al., 2014). This work underlines the importance and ability of efficient GF presentation to augment efficacy, although in this study delivery was without the use of a biomaterial carrier, engineering of the GFs to bind host ECM would be required to achieve potency in the clinical context.

3.4.1.2 Fibronectin networks present integrin- and growth factor- binding domains in close proximity

The coexistence of binding sites for integrin adhesion and high affinity GF binding in many ECM proteins allows for local concentrations of GFs near the cell surface. The data presented in Figure 3-4C-D indicates an increased availability of these two key binding sites on FN adsorbed onto PEA substrates. This arrangement leads to close localisation of integrin-mechanoreceptors and GFRs, stimulating integrin and GFR signalling in a confined space resulting in synergistic signalling, or integrin-GFR crosstalk (Figure 3-8) (Cheng et al., 2018; Llopis-hernández et al., 2016). For over a decade, the importance of integrin-GFR crosstalk has been investigated - cell adhesion is necessary to facilitate activation of GFRs, and GFs are necessary to stimulate cell adhesion, migration and integrin-dependent signals (Comoglio et al., 2003).

The work previously discussed by Martino et al (2011), was a landmark study for highlighting the potency of integrin-GFR crosstalk. Using the FN fragments incorporated into fibrin matrices to show that only when FN fragments $FNIII_{9-10}$/$FNIII_{12-14}$ were co-delivered was GF signalling significantly enhanced, integrin activation alone was not enough to activate proliferation or migration. Increased phosphorylation of GFRs and downstream signalling pathways (such as ERK1/2 - phosphoERK1/2) was observed for prolonged time periods (up to 40 minutes) post-stimulation with the $FNIII_{9-10}$/ $FNIII_{12-14}$ fragment, but not solubilised delivery $FNIII_{9-10}$ and $FNIII_{12-14}$ (not linked) or $FNIII_{9-10}$ alone. Suggesting the synergistic

effects of integrin-GFR crosstalk require co-localisation in the same nanoscale cluster (Martino et al., 2011).

Integrin and GFR synergistic signalling has been demonstrated to augment several biological processes, such as blood vessel formation, wound healing and bone regeneration (Table 3-1). Our previous work with MSCs in the PEA system demonstrated co-localisation of the BMPR1A receptor to focal adhesion plaques (Cheng et al., 2018), and coimmunoprecipitation confirmed specific interactions between BMPR1A and integrin β_1, part of $\alpha_5\beta_1$ FN receptor (Llopis-hernández et al., 2016). To confirm the colocalization in pericytes on PEA FN BMP-2 substrates, a proximity ligation assay (PLA) should be carried out. Low cell numbers are used in this system which would pose limitations for coimmunoprecipitation assays, whereas PLA allows for sensitive i*n situ* detection of protein interactions that can be detected using fluorescent microscopy.

The colocalization of BMPR1A and integrin $\beta1$ enables crosstalk, and our previous works shows this had significant effects on subsequent cell signalling; significant increases in Smad and integrin-associated FAK phosphorylation was observed with PEA conditions promoting simultaneous binding of integrins and GFRs compared to soluble BMP-2 administration. Blocking of the GF-binding region of FN lead to reversal to basal levels of phosphorylation. That these synergy promoting surfaces showed enhanced osteogenic effects *in vitro* and *in vivo* signifies how GFR/integrin cooperation may be exploited for accelerated regeneration (Cheng et al., 2018; Llopis-hernández et al., 2016).

To better understand the interplay between integrin-led mechanotransduction and GFR signalling, Crouzier et al, developed films made from poly(L-lysine) and HA with modulated stiffness and the ability to immobilise BMP-2 - enabling the ability to uncouple biochemical and matrix mechanical signals (Crouzier et al., 2011). They found C2C12 myoblast cells were able to respond to both soluble and matrix-bound BMP-2 on stiff substrates, but on softer substrates matrix-bound BMP-2 showed only migratory/adhesive responses, however with soluble BMP-2 poor spreading and cell rounding was observed. This study proposed bound BMP-2 encourages close localisation of adhesion receptors to GFRs, enabling cross-talk that may induce cytoskeletal remodelling and cell spreading (Crouzier et al., 2011). The group then used the same stiffness-modulated films to show matrix-

bound BMP-2 was sufficient to induce C2C12 cell spreading in a β_3 integrin-dependent manner, even on soft substrates. They found that BMP-2 stimulation activated Smad signalling through integrin $\alpha_v\beta_5$ (but not $\alpha_5\beta_1$), and that the colocalization of the receptors was driven by cell secreted FN which enabled the close localisation of FN adhesion sites with the matrix-bound BMP-2 (Fourel et al., 2016).

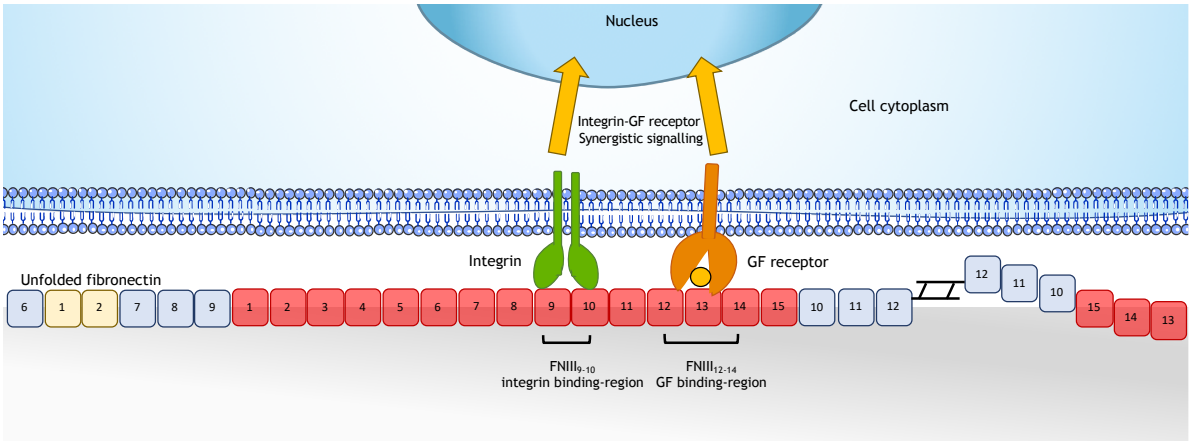

Figure 3-8 Integrin-GF receptor crosstalk. When FN is adsorbed onto the polymer PEA it causes spontaneous unfolding, simultaneously exposing integrin-binging ($FNIII_{9-10}$) and GF-binding ($FNIII_{12-14}$) domains. GFs can then be tethered to the FN molecules, promoting GFR and integrin colocalization, activating synergistic signalling pathways.

Table 3-1 Integrin and growth factor receptor synergistic signalling and biological effects.

Growth Factor	Integrin	Synergistic effect	Reference
BMP-2	$\alpha_5\beta_1$	Osteogenesis and bone regeneration	(Cheng et al., 2018; Llopis-hernández et al., 2016)
VEGF/PDGF	$\alpha_5\beta_1$	Wound healing	(Martino et al., 2014, 2011)
BMP-2/PDGF	$\alpha_5\beta_1$	Bone regeneration	(Martino et al., 2014, 2011)
VEGF	$\alpha_v\beta_3$	Increased cell adhesion and spreading *in vitro*, limited angiogenic response *in vivo*	(Traub et al., 2013)
BMP-2	$\alpha_v\beta_3$	Osteogenesis	(Fourel et al., 2016)
VEGF	α_v	Vasculogenesis	(Moulisová et al., 2017)

Together these studies and with those summarised in Table 3-1 provide further evidence for the cooperative effects of GFR and integrin signalling in biological contexts. However, they also demonstrate contradictions over which receptors are involved in synergy signalling. This is further complicated by studies demonstrating that removing the integrin binding domain enhanced wound healing

in a VEGF based system (Martino et al., 2013), and by evidence for activation of GFRs via integrin juxtaposition even in the absence of GFs (Veevers-Lowe et al., 2011). This suggests the need for well-defined model systems coupling mechanical and biochemical properties to understand the subtleties of the synergies between integrins and GFRs.

3.4.2 Low stiffness collagen gels in the range of bone marrow

The design of this system and the decision to add a collagen hydrogel was motivated by two observations: (I) the effects of matrix mechanics on MSPC phenotype, where soft/low-stiffness microenvironments have been demonstrated to maintain self-renewing, or niche-like phenotypes (Engler et al., 2006; Sweeten, 2019); and (II) that the BM is composed of discrete regions of heterogeneous physical and compositional properties (Jansen et al., 2015). Near to the bone surface, osteoid and collagenous bone are thought to define a stiffer microenvironment shown to be enriched with FN, whereas softer perivascular microenvironments have been shown as laminin-rich, with collagens I and IV found to be more generally distributed throughout the marrow cavity (Nilsson et al., 1998). The rationale behind the thickness of the gel was influenced by our previous work, where ~1 cm thick gels were demonstrated to have a niche-supporting effect on MSCs (Sweeten, 2019), but also with the aim of culturing gels that will remain at the cell-material interface for long-term culture. Work in our group has demonstrated lower volumes of gel are more readily contracted by cells leading to dissociation of gels from the well-plates and resulting in floating gels (Orapiriyakul, 2020).

These subtle gradations in matrix stiffness have proved difficult to measure accurately in an *in vivo*-like context. Although porcine models have shown the intact marrow is viscoelastic, with mechanical properties reported to range from 0.25 – 24.7 kPa (Young's modulus) (Jansen et al., 2015), the study was unable to correlate the heterogeneity in stiffness to specific endosteal/central marrow locations. The rheological data presented in Figure 3-7 shows collagen type I hydrogels used in this thesis display a mean Young's modulus of ~80 Pa, falling just outside the lower scale of the range measured for intact marrow, but similar to that of low stiffness systems previously reported to promote MSPC phenotype maintenance (Engler et al., 2006; Sweeten, 2019). However, future work would

aim to tune the stiffness of these gels to fall more accurately within the measured stiffness range of intact BM, this could be done by changes to cross-linking which may also affect the alignment of the collagen fibrils, or by investigation into the use of different concentrations of collagen. 2.05 mg/mL collagen I was used in this work as it is a concentration we have characterised and employed in previous studies (Lewis et al., 2017; Sweeten, 2019; Tsimbouri et al., 2017). In previous work in our group, we found that increasing the collagen concentration to 5 mg/mL did not significantly effect hydrogel stiffness compared to the 2.05 mg/mL hydrogels (Orapiriyakul, 2020). As such, other more readily tuneable materials have been considered for future work, such as synthetic PEG matrices, which is discussed further in Chapter 7.2.

It is of note that the Jansen et al, 2015 study is currently the only study to measure intact marrow, whilst this is important, it must also be considered that these measurements are carried out with cells *in situ*, which will contribute to rheological properties. Thus, perhaps the stiffness measured is not directly comparable to the cell free collagen matrices we employ here. However, measurements of decellularized marrow also prove difficult, as post-processing (such as chemical and temperature changes, length of post-mortem time) has been demonstrated to dramatically affect the elastic modulus of bone marrow other tissues (Davis and Praveen, 2006; Jansen et al., 2015; Rashid et al., 2013). These studies demonstrate that to truly measure the exact elastic and viscoelastic components of the BM microenvironment that cells interact with is difficult and will undoubtedly require synchronisation of several techniques.

Further to the impact of gel stiffness on cellular phenotype and behaviour, the fibrillar microstructure of collagen has been demonstrated to impact cell response. One study demonstrated short fibre length and high fibre stiffness limited the transfer of cellular traction forces to nearby fibres, thus reducing focal adhesion formation and cellular spreading and leading to preference for MSCs to undergo adipogenesis. Whilst cell migration, proliferation, spreading and thus osteogenesis, was associated with the ability to recruit fibres and produce long-range deformations in the matrix (Xie et al., 2017). As such, fibre microstructure is an important consideration, and could be further investigated in future work - by crosslinking collagen gels at different temperatures, inducing different

arrangements of collagen fibrils, the impact on cellular behaviour (e.g. on proliferation and expansion of MSPCs) could be explored.

3.4.2.1 HSC response to niche stiffness

Although the impact of matrix elasticity is well understood in stromal stem cells, comparatively less understood is the impact of biophysical signals on haematopoiesis. Similarly to MSCs, myosin-II plays a key role in generating actomyosin forces in adhesion and sensing the stiffness of the environment; where G-CFS stimulated BM osteoblast stiffening leads to HSC mobilisation, and soft or highly elastic matrices have been shown to drive expansion of HSC/HSPCs (Engler et al., 2006; Holst et al., 2010). Myosin-IIA (MIIA) and myosin-IIB (MIIB), contractile motor molecules, serve as matrix stiffness sensors in HSCs and influence HSC fate through regulation of asymmetric cell division (Shin et al., 2014). Stiff endosteum-like matrix activates MIIA increasing more symmetric divisions that lead to differentiation, whereas soft-matrices reduce MIIA activation leading to polarised MIIB expression in dividing cells, resulting in asymmetric self-renewing divisions (Shin et al., 2014). MIIB is known to interact directly with cell surface markers, and hence $MIIB^{high}$ cells could correlate with an increase in putative HSC markers, such as CD34 (Clark et al., 2006; Shin et al., 2013).

Gradients of cellular and ECM protein composition across the niche impact the biophysical environment to which HSCs are exposed. The study by Choi and Harley (2017) engineered marrow-inspired ECM ligand-coated PA substrates with tuneable stiffness and used these to demonstrate how different combinations of stiffness/ligand can influence HSC fate decisions. Here, they reported increased primitive myeloid proliferation in the substrates resembling endosteal niches (high FN content, stiff microenvironment ~40 kPa), whereas those resembling vascular zones (high laminin content) favoured erythroid lineages, although microenvironment stiffness displayed an undetermined role in combination with laminin. The effect was abrogated through inhibition of myosin-II or adhesion to FN via integrins $\alpha_5\beta_1$ and $\alpha_v\beta_3$, suggesting intracellular tension as a key regulator of HSC lineage specification (Choi and Harley, 2017). HSCs engage matrix components via integrins, and several integrins have been found to be enriched in specific sub-populations of HSCs, as discussed in Chapter 1.3.3. The study by Choi and Harley (2017) provides functional output on niche biophysical effects on HSC

fate decisions, and alongside the evidence suggesting HSC-ECM ligand interactions may be critical during different stages of haematopoiesis, further supports a direct link of the heterogeneity of BM niche matrix ligand composition and mechanical properties to the differential regulation of HSCs.

3.4.3 Summary

The results discussed in this chapter provide evidence and reason for using each material component in the development of a BM niche model. The initial rationale to employ the PEA system is based on previous results obtained from our group in using this system to (I) efficiently present GFs in synergy with integrins and (II) its ability to promote osteogenesis. The concept for this thesis was to take an environment that could promote bone formation, then add key niche factors such as low-stiffness ECM (in the form of the collagen type I hydrogel) to create a system that could promote, and allow us to investigate, BM-like regulation of stromal cells and HSCs.

Chapter 4 Characterising a Bone Marrow Niche MSPC Phenotype

4.1 Introduction

Chapter 3 described the materials used in this thesis to engineer model BM niche systems. This chapter characterises the phenotypic properties of the stromal cellular component of the model, with a view to introducing HSCs in co-culture.

As described in Chapter 1, MSPCs are tightly regulated by their niche microenvironment, and in turn also act as crucial support to HSCs in the BM where they co-reside. A growing understanding of the heterogeneity of niche cell types (Table 1-3) and their interactions, both cell-cell and cell-microenvironmental cues, are proving fundamental to harnessing stem cell potential *ex vivo* (Pinho and Frenette, 2019). Signalling molecules, such as GFs and cytokines, are released from nestin+ MSPCs and are central to homing, maintenance and retention of HSCs in the BM (Asada et al., 2017; Kunisaki et al., 2013; Nakahara et al., 2019; Pinho et al., 2013). The inclusion of nestin+ MSPCs is therefore highly favourable for an HSC niche model.

4.1.1 Nestin

Nestin is a type VI intermediate filament (IF) protein that, unlike most other IF proteins, cannot self-polymerise and instead relies on its interaction with its copolymerisation partner vimentin to form networks. The inability of nestin to form networks is presumably due to a very short N-terminal head domain, that in other IF proteins is essential for filament assembly (Park et al., 2010). Nestin was first identified as a neuroepithelial progenitor marker in the central nervous system (CNS) (Lendahl et al., 1990), as such, it was commonly used as a marker to identify neuronal precursor cells and as a marker of neurogenesis in other stem cell types, despite this its specific functions remain largely undetermined.

As highlighted in Chapter 1, more recently nestin+ stromal cells have been characterised as important BM niche cells. They are found close to vasculature and in tight association with adrenergic nerve fibres and HSCs *in vivo*, and are enriched for MSPC activity *ex vivo* (Méndez-Ferrer et al., 2010). Selective ablation

of nestin+ cells (Méndez-Ferrer et al., 2010) or CAR cells (Omatsu et al., 2010) led to significant aberrant effects on HSC and progenitor cell maintenance in mouse BM. However, the intracellular location of nestin limits its use as a potential marker to isolate naïve cells directly from live BM. As such, surface markers specific to nestin+ cells have been identified. A subset of nestin+ cells positively expressing CD51 (integrin α_V) and PDGFRα have been demonstrated by the Frenette group to be enriched for MSPC and HSC niche activity *in vivo* and *in vitro*. Cultured CD51+PDGFRα+ cells are self-renewing and able to express high levels of niche-related genes and maintain populations of haematopoietic progenitors *in vitro* (Pinho et al., 2013). This suggests that these markers could be evaluated as markers for identifying and isolating key niche MSPCs.

Seminal work from the Discher group used gels of varying stiffnesses to promote differentiation of MSCs down distinct tissue lineages, correlating gel stiffness to *in vivo* tissue stiffness and resulting cell phenotype. Here it was reported that soft (0.1 - 1 kPa) gels promote neurogenesis of MSCs, using increased nestin expression as a marker of neural commitment (Engler et al., 2006). However MSC capacity to undergo neural differentiation has remained somewhat contentious over the years (Lattanzi et al., 2015), and now it is suggested that the low stiffness previously correlated to neural environments, for MSCs is somewhat representative of BM stiffness (Jansen et al., 2015). In this regard, in this thesis we chose to add a low-stiffness gel component to the culture system, with the aim to mimic BM mechanics and increase nestin expression to promote a BM niche-like phenotype in a population of MSPCs. Hypothesising that a nestin+ stromal population would be enriched for BM niche activity, such as an elevated expression of HSC maintenance factors, allowing us to harness this for HSC support in co-culture and to investigate the mechanisms fundamental to this phenotype.

4.1.2 HSC maintenance cytokines

As described in (Table 1-4) soluble factors contribute to HSC maintenance within the BM niche. Known to direct chemotaxis of HSCs, CXCL12 signalling also contributes to maintaining HSCs in a slowly proliferative state and supports their retention in the BM (Ara et al., 2003; Nie et al., 2008; Sugiyama et al., 2006). CXCL12 is synthesized by several niche cell types, including CAR cells, endothelial cells and perivascular nestin+ cells (Table 1-4). Nestin+ MSPCs are tightly

associated with nerves and HSCs, and their CXCL12-expression is regulated in response to adrenergic signals from the sympathetic nervous system (SNS) in a circadian manner (Katayama et al., 2006; Lucas et al., 2008; Méndez-Ferrer et al., 2008). Nestin+ MSPCs and endothelial cells also express high levels of SCF, which can be both soluble and membrane-bound, and is required throughout BM development and for HSC maintenance in the adult BM (Ding et al., 2012; Pinho et al., 2013).

Gold standard conditions used for *in vitro* HSC culture require the addition of such soluble maintenance factors, primarily SCF at concentrations ranging from 10 to 150 ng/mL, TPO at 6 to 50 ng/mL and Flt3 at 5 to 25 ng/mL (Lewis, 2018). Therefore, we hypothesised that engineering a niche model that promotes and supports a population of stromal cells that are phenotypically similar to nestin+ MSPCs, this may lead to increased expression of HSC maintenance factors, and would ultimately be favourable for, and reduce the need for additional cytokine input, in HSC co-culture.

4.1.3 Aims and objectives

This chapter aims to recapitulate key aspects of the BM niche microenvironment and investigate support of defined niche phenotypes in a population of MSPCs. CD146+ pericytes were seeded onto glass or polymer coated substrates, with the addition of ECM factors (FN, BMP-2), factors that mimic BM stiffness (collagen I hydrogels) and the addition of an oxygen gradient (hypoxia, 1% O_2) to mimic the hypoxic niche, for up to 14 days (represented in Figure 4-1). Assessment of phenotypic changes were then carried out using RNA-seq, flow cytometry and immunofluorescence analysis. The aims of this chapter were as such:

- Assess support or changes in key niche phenotypic markers.
- Investigate if low-stiffness gels can be used to increase nestin expression.
- Assess if increased nestin expression correlates to HSC-support activities, such as maintenance factor production.

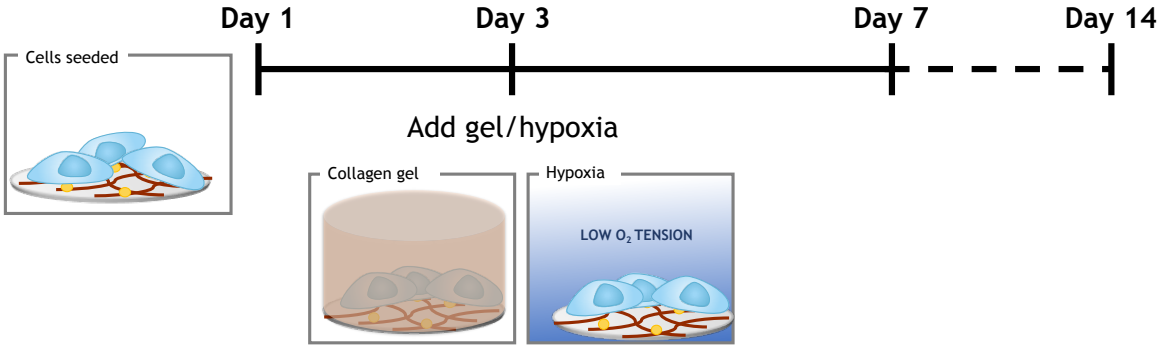

Figure 4-1 Timeline of model culture. Cells are seeded onto polymer or glass substrates, on day 3 collagen gels are added or samples added into hypoxia (1% oxygen). Models are then cultured for the desired time period (usually 7-14 days), media changed every 3 days.

4.2 Materials and Methods

4.2.1 Phenotyping of pericytes by flow cytometry

Pericytes were seeded in desired niche models, and gels/hypoxia added and cultured for 14 days, as per Figure 4-1. To obtain high numbers of cells for analysis 12 technical replicates were combined, and this was repeated for 3 biological replicates.

4.2.1.1 Flow cytometry staining

Cells were prepared for flow cytometry analysis as per Chapter 2.3.3. To assess expression of surface markers associated with niche phenotypes, two panels of antibodies were used and are shown in Table 4-1.

Table 4-1 Antibodies used for flow cytometry assessment of pericyte phenotype.

Fluorophore	Panel 1	Panel 2
APC	LepR	CD51
APC-Cy7	CD90	CD31
FITC	CD29	
eFluor 450		CD105
PE	NG2	CD140a
Cy7		CD140b
Cy5	CD146	CD166

4.2.1.2 Gating strategy

FlowJo™ software was used to analyse flow cytometry data after acquisition. A gate was added to the forward scatter area (FSC-A) versus side scatter area (SSC-A) plot to identify viable pericyte populations, shown in Figure 4-2. A significant proportion of dead cells were observed due to collagenase digest. At least 5 x 10^3

viable cells were analysed per condition. Unstained cells were used as a negative control. Figure 4-2 shows representative histograms for one biological replicate for panel A and panel B (Table 4-1).

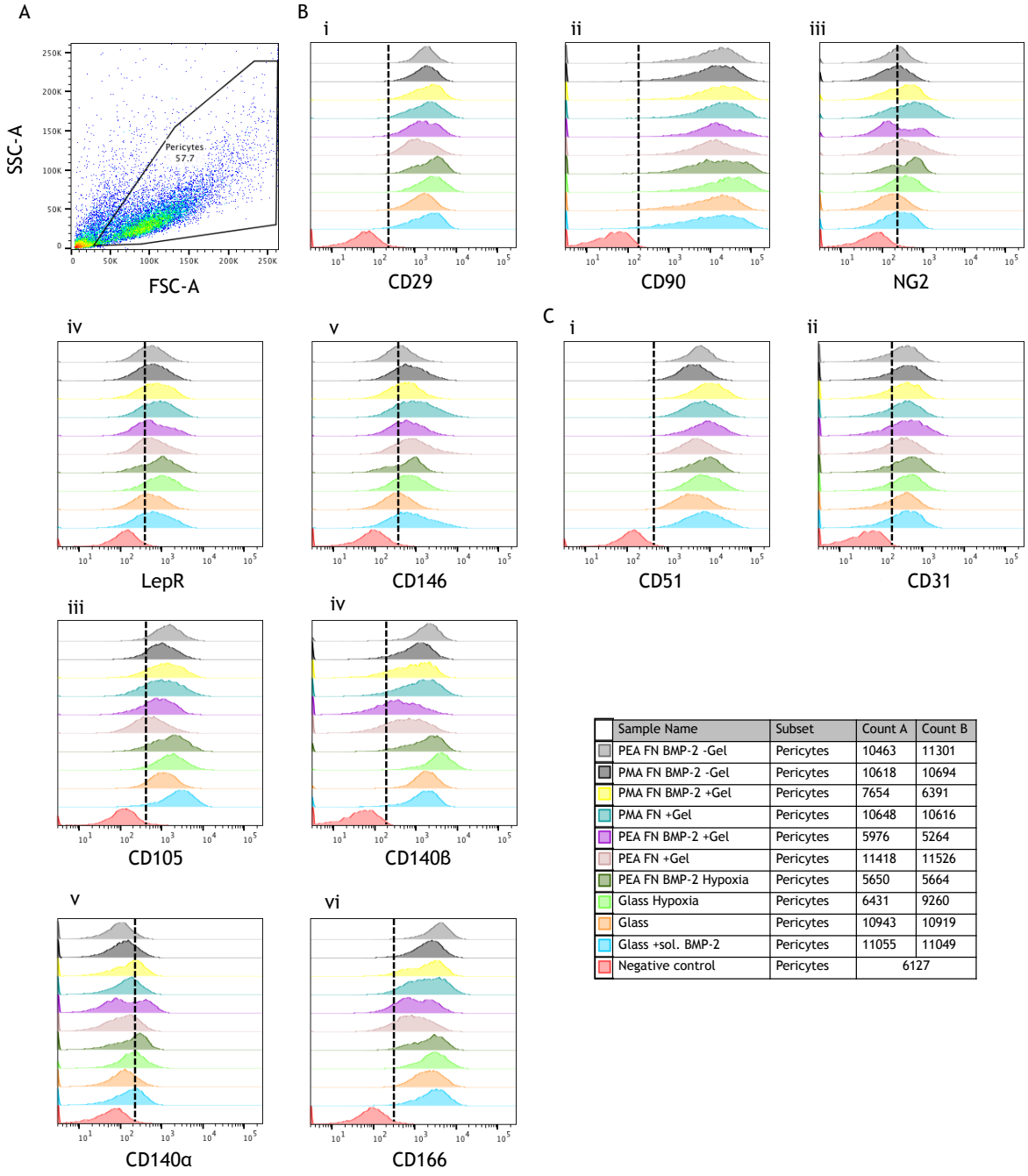

	Sample Name	Subset	Count A	Count B
	PEA FN BMP-2 -Gel	Pericytes	10463	11301
	PMA FN BMP-2 -Gel	Pericytes	10618	10694
	PMA FN BMP-2 +Gel	Pericytes	7654	6391
	PMA FN +Gel	Pericytes	10648	10616
	PEA FN BMP-2 +Gel	Pericytes	5976	5264
	PEA FN +Gel	Pericytes	11418	11526
	PEA FN BMP-2 Hypoxia	Pericytes	5650	5664
	Glass Hypoxia	Pericytes	6431	9260
	Glass	Pericytes	10943	10919
	Glass +sol. BMP-2	Pericytes	11055	11049
	Negative control	Pericytes	6127	

Figure 4-2 Gating strategy and representative histograms for analysis of pericyte phenotype. Sample data from one patient for flow cytometry of pericytes cultured in niche systems for 14 days. A. Representative gating strategy for pericytes from PEA FN BMP-2 -gel, which was then analysed for each marker in antibody panel A (B i-v) and panel B (C i-vi) represented by histograms. Unstained cells were used as the negative control (red). Dotted line is a visual representation of positive marker expression. Count A and Count B shown in the legend indicate numbers of cells analysed for panel A and panel B respectively.

4.2.1.3 Analysis

The median fluorescent intensity (MFI) values for each channel were recorded for analysis, the value for the negative control was subtracted from each sample. Values were then represented as fold change over pericytes cultured on glass, and 3 patients displayed as a heatmap using Cluster 3.0 and Java TreeView software.

4.2.2 Brefeldin A treatment

Cells were cultured in model systems for 14 days, for the last 24 h of culture the media was removed and fresh 2% media was added supplemented with 5 μg/mL of Brefeldin A. Brefeldin A inhibits protein transport, enhancing detection of intracellular cytokines. After 24h incubation with brefeldin A, samples were fixed, stained for immunofluorescent analysis of cytokines CXCL12 and SCF and visualised on the microscope as described in Chapter 2.3.4 and 2.3.5. Cytokine output was then quantified using ImageJ software, where a global threshold was applied and measurements of integrated intensity taken, this was then divided by the number of nuclei per image to give an average intensity. At least 10 representative images were analysed per replicate, n=3. Statistical analysis was carried out using GraphPad Prism 6 software.

4.3 Results

4.3.1 Support of a niche phenotype in MSPCs

4.3.1.1 Transcriptomics day 7

Global RNA-seq profiling was carried out on pericytes in each niche system at day 7 to gain a snapshot into changes in transcript levels of key phenotypic genes (Figure 4-3). Based on literature searches a list of 84 genes was generated including:

1. Osteogenesis markers (e.g. *BGLAP*, *SPP1* and *RUNX2*)

2. Stem cell and stem cell maintenance markers (e.g. *MCAM*, *THY1* and *ALCAM*)

3. Defined niche markers (e.g. *LEPR*, *NES*, *THPO* and *KITL*)

The RNA-seq analysis revealed only subtle changes between experimental conditions at day 7, as changes were no greater than ±3 fold when compared to the glass control. However, in PEA FN BMP-2 -gel some early osteogenic markers were elevated, such as *RUNX2,* or equal to expression on the glass control, such as *SPARC* (encoding the protein osteonectin, ON). Later osteogenic markers *BGLAP* (encoding the protein osteocalcin, OCN) and *ALPP* (alkaline phosphatase) were down regulated or unchanged in this condition, although this is expected as expression of these usually increases around days 14 - 21 during osteogenic differentiation of MSCs (Yang et al., 2014). Hypoxia induced an increase in several early and late osteogenic markers in cells on glass and PEA FN BMP-2, including *SP7* (encoding the protein osterix, OSX), *ALPP* and *BGLAP*. The hypoxic conditions also had elevated levels of transcription factors and marker proteins related to other lineages. For example *ADIPOQ* (adiponectin) related to adipogenesis (Amable et al., 2014), and several genes typically implicated in neuronal phenotypes but with broad roles, such as *NGF*, *NGFR* and *NCAM1* (Engler et al., 2006). Interestingly, BMP2 was strongly upregulated in all condition except PEA FN BMP-2 +gel and glass +sol. BMP-2 where it was only slightly elevated, and glass hypoxia where it was down-regulated. These results are represented as a heatmap in Figure 4-3 and broadly agree with previous work with MSCs that solid-phase BMP-2 presentation can promote osteogenesis.

Transcripts with increased expression in conditions with low-stiffness gels (+gel), were mostly related to stem cell maintenance or stem cell niches (Figure 4-3). Pericyte markers were either increased, e.g. *MCAM* (CD146) or maintained e.g. *CSPG4* (NG2) and *PDGFRA* (PDGFRα), with the addition of a gel. Niche genes, including *NES* (nestin), *CDH2* (N-Cadherin) and *ITGB1* (integrin β1, CD29) showed increased expression with gels. Expression of HSC maintenance cytokine *THPO* (TPO) levels were observed for all glass and PEA conditions, but not by PMA-based conditions, however down-regulation of *CXCL12* and *KITLG* (SCF) was observed for all conditions, which was unexpected (Figure 4-3).

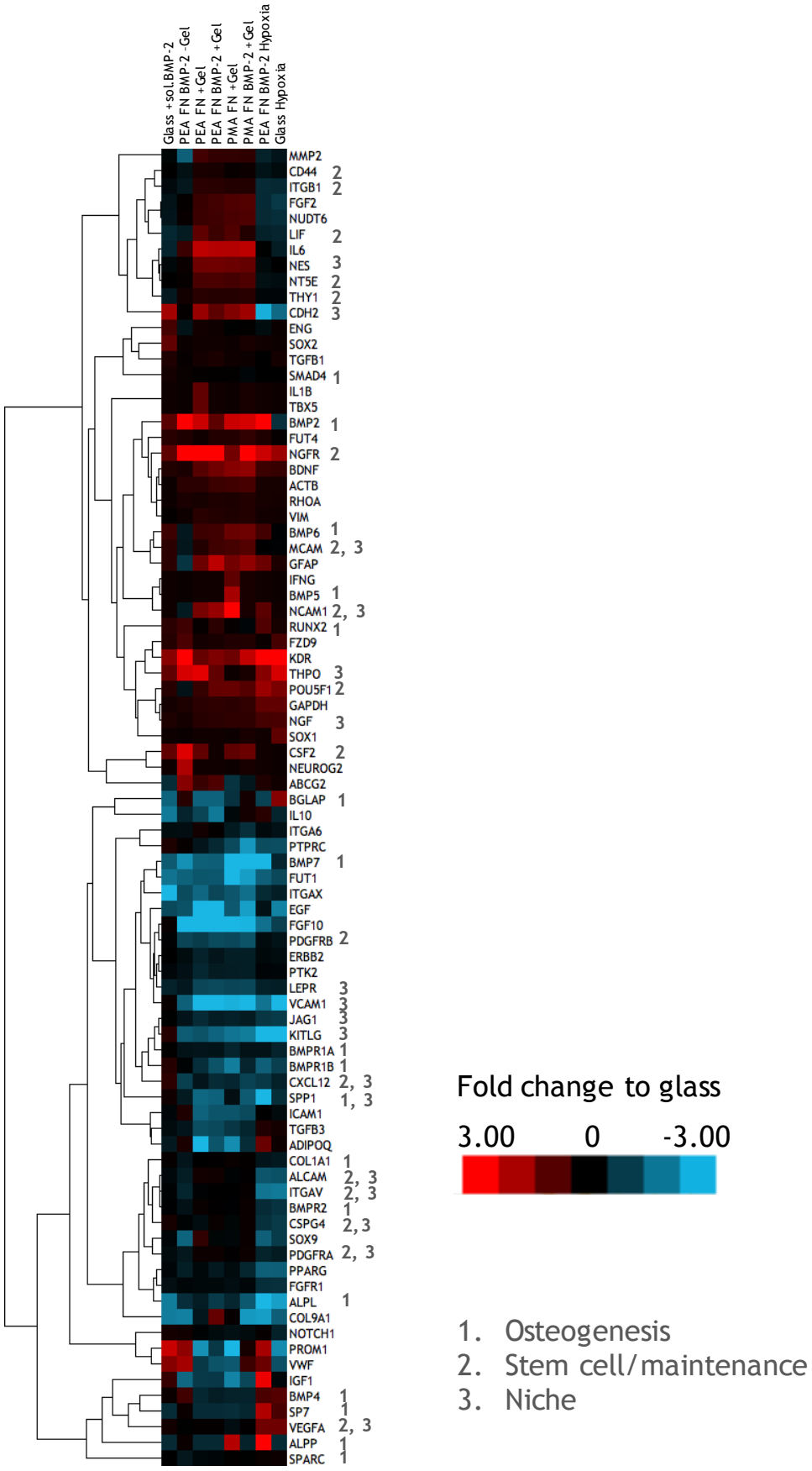

Figure 4-3 RNA-seq profiling of niche-related and differentiation markers at day 7. Change in transcript levels after 7 days culture in each niche system, compared to glass control. Genes are clustered through average linkage. Genes related to 1. Osteogenesis, 2. Stem cell markers/maintenance and 3. Niche markers are indicated. N = 2 for PEA FN BMP-2 hypoxia, n = 3 for all other conditions.

4.3.1.2 Surface marker expression day 14

The RNA-seq data gave us an overview into cell phenotypic response to the different niche models at day 7. To further characterise the phenotype and validate to changes observed at the transcript level, analysis of surface markers implicated in MSPC BM niche phenotypes was carried out using flow cytometry and is shown in Figure 4-4. This was carried out at day 14, as previous work in our group suggested a period of 'priming' of the stromal population is beneficial (Sweeten 2019). This provides cells time to respond to the microenvironmental cues presented by each system and allows for assessment of longer-term maintenance of phenotypic markers. Flow cytometry allowed us to assess several surface markers in the same population of cells (Table 4-1), and this data is displayed as a heatmap in Figure 4-4, represented as fold change to the glass control.

Analysis of each marker, and its relevance in the BM niche, is described in

Table 4-2. Taken together the data suggests that addition of low-stiffness gels to both PEA- and PMA-based systems supported expression of the markers studied, three of which have been implicated in HSC-regulating MSPCs in *in situ* mouse BM – NG2, CD146 and CD51 (Kunisaki et al., 2013; Pinho et al., 2013).

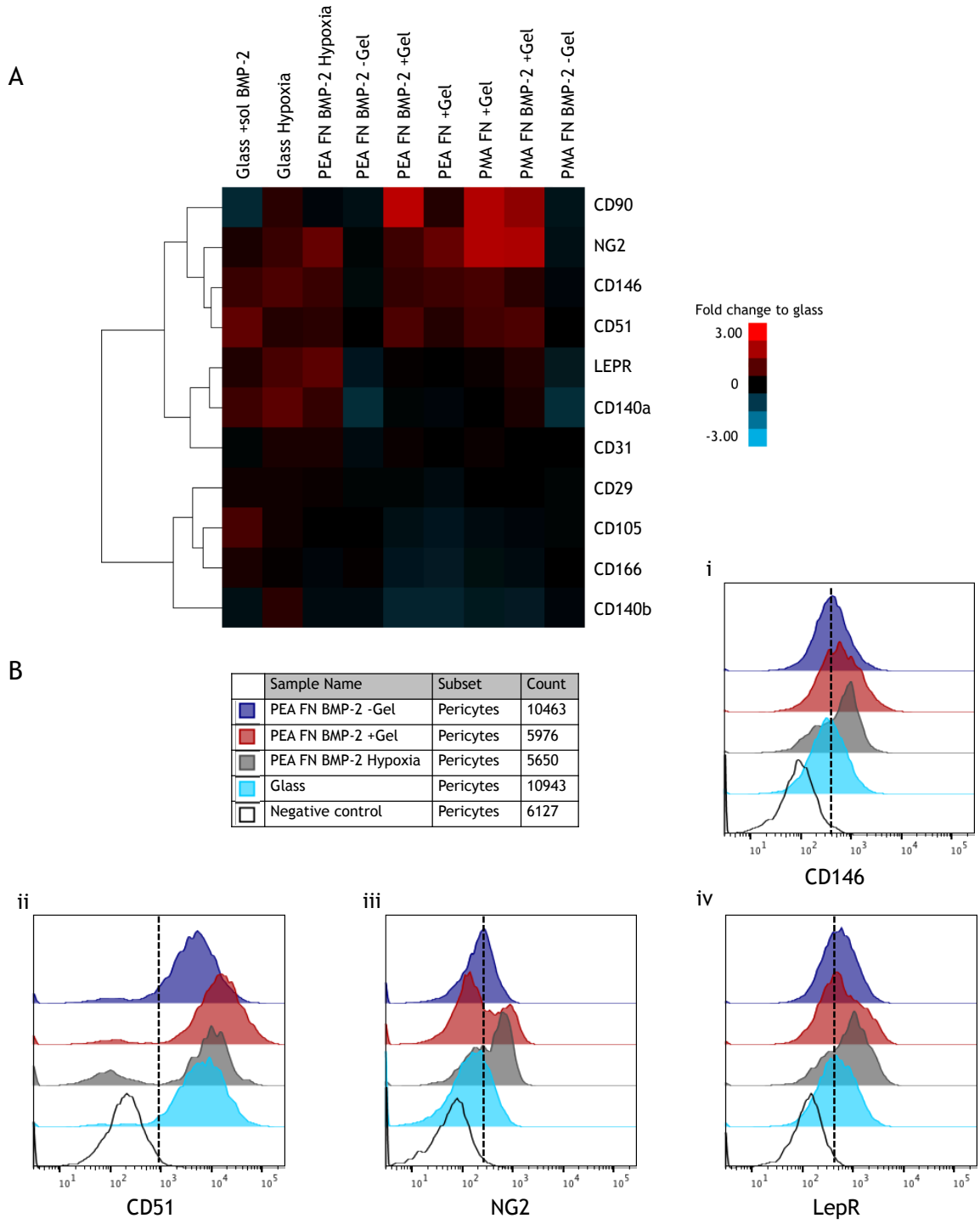

Figure 4-4 Assessment of pericyte phenotype after 14 day culture in niche models. A. Heatmap shows fold change over glass of median fluorescent values obtained by flow cytometry from 3 independent experiments with ≥5 x 10^3 cells from 3 biological replicates. Values are represented as fold change to pericytes seeded on glass controls. Markers are clustered by average linkage. B. Representative histograms of 4 markers from one patient for glass (cyan) PEA FN BMP-2 -gel (blue), PEA FN BMP-2 +gel (red) and PEA FN BMP-2 Hypoxia (grey) conditions. Unstained cells were used as the negative control (black line). i. CD146 is better retained by +gel and hypoxia; ii. All conditions retain CD51 expression; iii. +gel displays 2 populations, one of which are NG2+; iv. LepR expression is largely positive in hypoxia. Dotted line is a visual representation of positive marker expression. N = 3 biological repeats, at least 5x10^3 cells analysed per condition.

Table 4-2 Summary of changes in expression of surface markers assessed by flow cytometry at day 14. PECAM-1; platelet and endothelial adhesion molecule-1. ALCAM; activated leukocyte cell adhesion molecule.

Marker	Result	Relevance in the BM niche	Reference
CD90	Expression supported in PEA FN BMP-2 +gel, PMA FN +gel and PMA FN BMP-2 +gel. Suggests low-stiffness gels reduce differentiation.	Thy-1, required expression for defined MSCs. Loss of expression indicates differentiation.	(Dominici et al., 2006)
NG2	Expression supported with the addition of low-stiffness gel and hypoxia.	Expressed by rare subset of pericytes implicated in maintaining LT-HSCs	(Kunisaki et al., 2013)
CD146	Expression supported with addition of low-stiffness gel, hypoxia and soluble BMP-2 administration.	CD146+ nestin+ cells are enriched for HSC-support activity.	(Pinho et al., 2013)
CD51	Expression supported with addition of low-stiffness gel and soluble BMP-2 administration. Decreased with -gel.	Integrin α_v, surrogate marker for nestin+ MSPCs.	(Pinho et al., 2013)
LEPR	Expression supported in hypoxia. No change observed with gel addition.	Expressed by perisinusoidal MSPCs. Support HSC activation.	(Kunisaki et al., 2013)
CD140a	Increased expression supported in hypoxia, decreased in PEA FN BMP-2 and PMA FN BMP-2 -gel. No change +gel.	PDGFRα, surrogate marker for nestin+ MSPCs, expressed by perivascular cells.	(Pinho et al., 2013)
CD31	No change.	PECAM-1, endothelial marker.	(Crisan et al., 2008)
CD29	No change.	Integrin β_1, commonly expressed by MSPCs, used for isolation from tissues.	(Guimaraes-Camboa et al., 2017)
CD105	Slight decrease observed in PEA FN +gel and PEA FN BMP-2 +gel, whereas support observed with soluble BMP-2 administration.	Endoglin, expressed by subset of MSPCs shown to produce ectopic haematopoietic marrow.	(Chan et al., 2009)
CD166	Slight decrease observed in PEA FN +gel and PEA FN BMP-2 +gel, whereas subtle support observed with soluble BMP-2 administration.	ALCAM, commonly used to mark stromal cell multipotency.	(Boxall and Jones, 2012; Tsimbouri et al., 2014)
CD140b	Decreased in PEA FN +gel and PEA FN BMP-2 +gel, low level support in glass hypoxia.	PDGFRβ, commonly used to isolate MSPCs from tissues.	(Crisan et al., 2008; Guimaraes-Camboa et al., 2017)

At day 14, for the markers tested, the contribution of the low-stiffness gel or hypoxia is greater than that of FN network and BMP-2 availability, as no notable differences were observed between these conditions (Figure 4-4 and

Table 4-2). However, it suggests that low-stiffness gels are able to support a population of MSPCs that express similar markers to those described in the literature to act as HSC support cells, that is NG2+ CD51+ CD146+ pericytes (Pinho et al., 2013).

4.3.2 Intermediate filament expression

Nestin expression was observed to be increased in the RNA-seq screen at day 7 (Figure 4-3). One of the surrogate markers shown to correlate with nestin+ MSPCs in the BM, CD51 (Pinho et al., 2013), was found to be elevated in the flow cytometry analysis at day 14 (Figure 4-4) in cells exposed to gels (2 -fold PEA FN BMP-2 +gel). To confirm this finding, protein level analysis of nestin expression was carried out at both 7 and 14 days using immunofluorescence microscopy (Figure 4-5). The highest nestin expression levels were observed in PEA FN +gel and PEA FN BMP-2 +gel conditions at 7 days. A small increase was observed in the PMA FN +gel conditions, but this was not significant compared to similar polymer conditions in the absence of a gel. Nestin expression in cells on PEA FN +gel and PEA FN BMP-2 +gel systems were 9.6- and 8.5-fold greater, respectively, than MSPCs grown on identical polymer conditions in the absence of a gel at day 7 (Figure 4-5A).

By day 14, both PEA and PMA +gel-based systems exhibited similar levels of nestin expression that increased significantly compared to hypoxic and -gel systems (Figure 4-5A). Data from the two timepoints reveals that exposure to a preformed FN network (PEA) in combination with low-stiffness gels drives increased MSPCs nestin expression earlier than when FN is presented in globular conformation (PMA). However, by day 14 this effect is indistinguishable. The presence of BMP-2 tethered to FN networks did not produce any discernible differences to nestin expression. Figure 4-5B shows representative images at 14 days, where nestin network formation can be observed in the PEA FN BMP-2 +gel system.

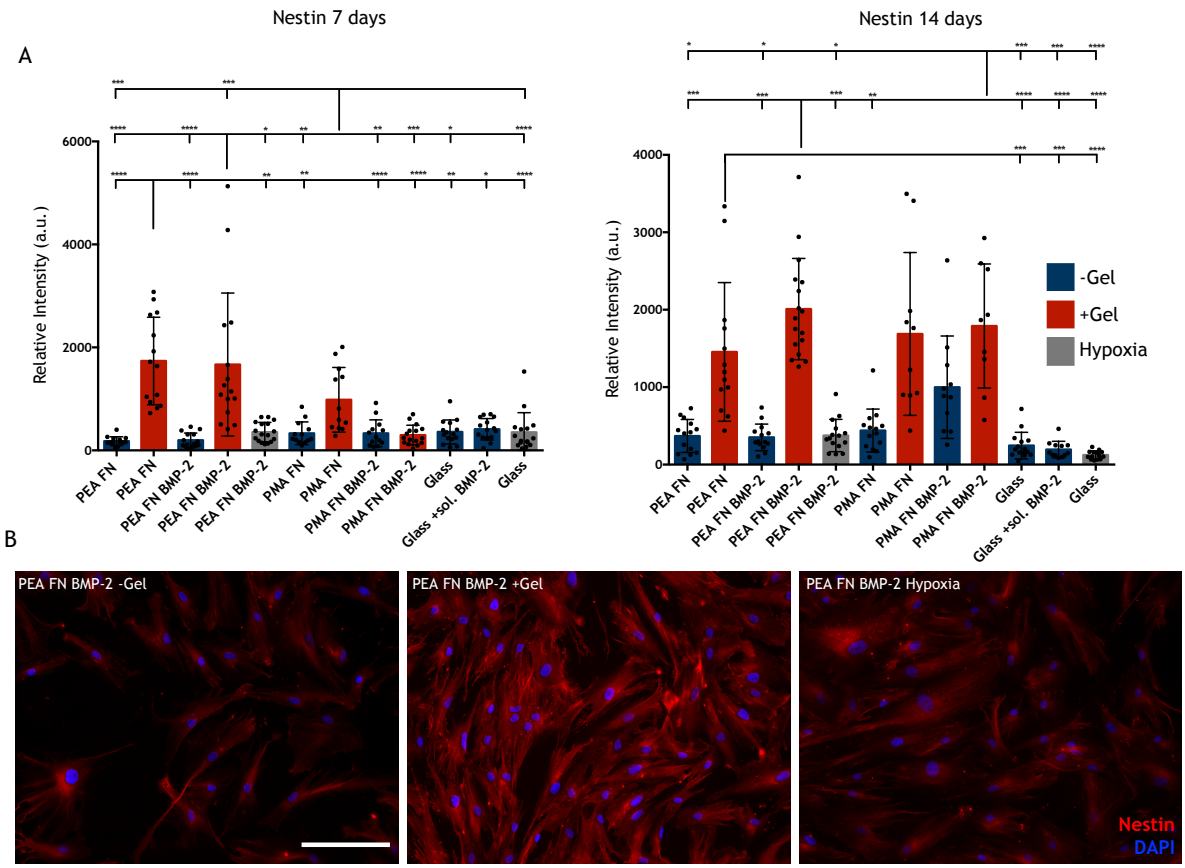

Figure 4-5 Nestin expression at 7 and 14 days. A. Analysis of nestin by immunofluorescence shows that the addition of low-stiffness gels to the model drives increased expression. This was more pronounced in PEA substrates than PMA at 7 days, and increased significantly on PEA and PMA substrates +gel by day 14. B. Representative images of nestin expression at day 7, scale bar is 100 μm, red = nestin, blue = DAPI. Graphs show mean integrated intensity of nestin ± SD (n=3 technical repeats), -gel = blue, +gel = red, hypoxia = grey, each point represents 1ximage field/number nuclei. One-way ANOVA followed by Kruskal-Wallis test with multiple comparisons, *= $p<0.05$, **= $p<0.01$, ***= $p<0.001$, ****= $p<0.0001$.

Nestin polymerisation and network formation requires its copolymerisation with vimentin, although vimentin network formation is not reliant on nestin (Park et al., 2010). Previous reports in NSCs indicate that changes in nestin levels have no significant effect on vimentin levels (Park et al., 2010). To investigate whether the increase in nestin observed in Figure 4-5 was specific to nestin, or to a general increase in IF proteins, vimentin levels were assessed. Immunofluorescence staining was carried out on PEA FN BMP-2 samples in the presence or absence of a gel, or in hypoxic conditions at day 7. Figure 4-6 indicates pericytes in all conditions express vimentin networks, with no significant changes in vimentin levels observed between the different conditions. Demonstrating that the increase in nestin expression observed with gel addition, is specific to nestin filaments and does not rely on changes in vimentin dynamics.

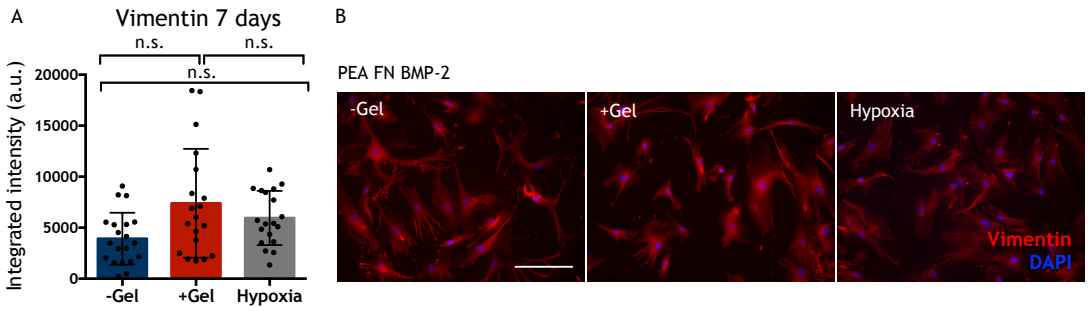

Figure 4-6 Vimentin expression on PEA FN BMP-2 at 7 days. A. Analysis of vimentin by immunofluorescence shows no significant increase with the addition of collagen gels or hypoxia. B. Representative images of vimentin expression, scale bar is 100 μm. Graphs show mean integrated intensity of nestin ± SD (n=3 technical repeats), each point represents 1ximage field/number nuclei. One-way ANOVA followed by Kruskal-Wallis test with multiple comparisons, n.s.= non-significant.

4.3.3 HSC maintenance factor expression

Nestin+ MSPCs have been shown to be enriched for HSC-supporting activity, with an increased expression of HSC maintenance cytokines (Kunisaki et al., 2013; Pinho et al., 2013). As such, we sought to determine if the nestin+NG2+CD51+CD146+ MSPCs supported by the +gel systems were able to produce the critical HSC maintenance factors SCF and CXCL12. Cells were cultured for 14 days total, and brefeldin A was added for the final 24h of culture. Brefeldin A inhibits intracellular protein transport by blocking transport to the Golgi complex, leading to accumulation of proteins in the endoplasmic reticulum, and is commonly used to study cytokine production. Previous work had indicated 24h as appropriate incubation time, allowing for significant cytokine build up without causing significant effects on cell viability (Sweeten, 2019).

Cells were then stained with anti- CXCL12 and SCF for immunofluorescence analysis (Figure 4-7). Figure 4-7A-C shows representative images for CXCL12 expression in PEA FN BMP-2 conditions (-gel, +gel, +hypoxia), and quantification (Figure 4-7D) revealed a significant increase in CXCL12 expression in PEA FN +gel and PEA FN BMP-2 +gel, compared to PEA FN BMP-2 -gel (3-fold), PEA FN BMP-2 hypoxia (2-fold), PMA +gel based conditions (>10-fold), and PMA FN BMP-2 -gel (5.5-fold). Glass hypoxia also had significantly increased expression compared to PMA, PEA FN BMP-2 hypoxia, glass and glass +sol. BMP-2.

Figure 4-7E-G show representative images for SCF expression in PEA FN BMP-2 conditions (-gel, +gel, +hypoxia). Quantification of SCF expression (Figure 4-7H) revealed SCF levels increased exclusively in PEA FN +gel and PEA FN BMP-2 +gel,

ranging from 8- to 25-fold increases. This was significant to all conditions, although no difference was observed ±BMP-2 in the PEA +gel conditions. This data demonstrates that the nestin+ NG2+ CD51+ CD146+ MSPCs maintained in the PEA FN/PEA FN BMP-2 +gel systems contain HSC-support activities. Interestingly, in contrast to the surface marker and nestin level analysis, CXCL12 and SCF expression was supported only when the cells were presented with FN networks and low-stiffness gels.

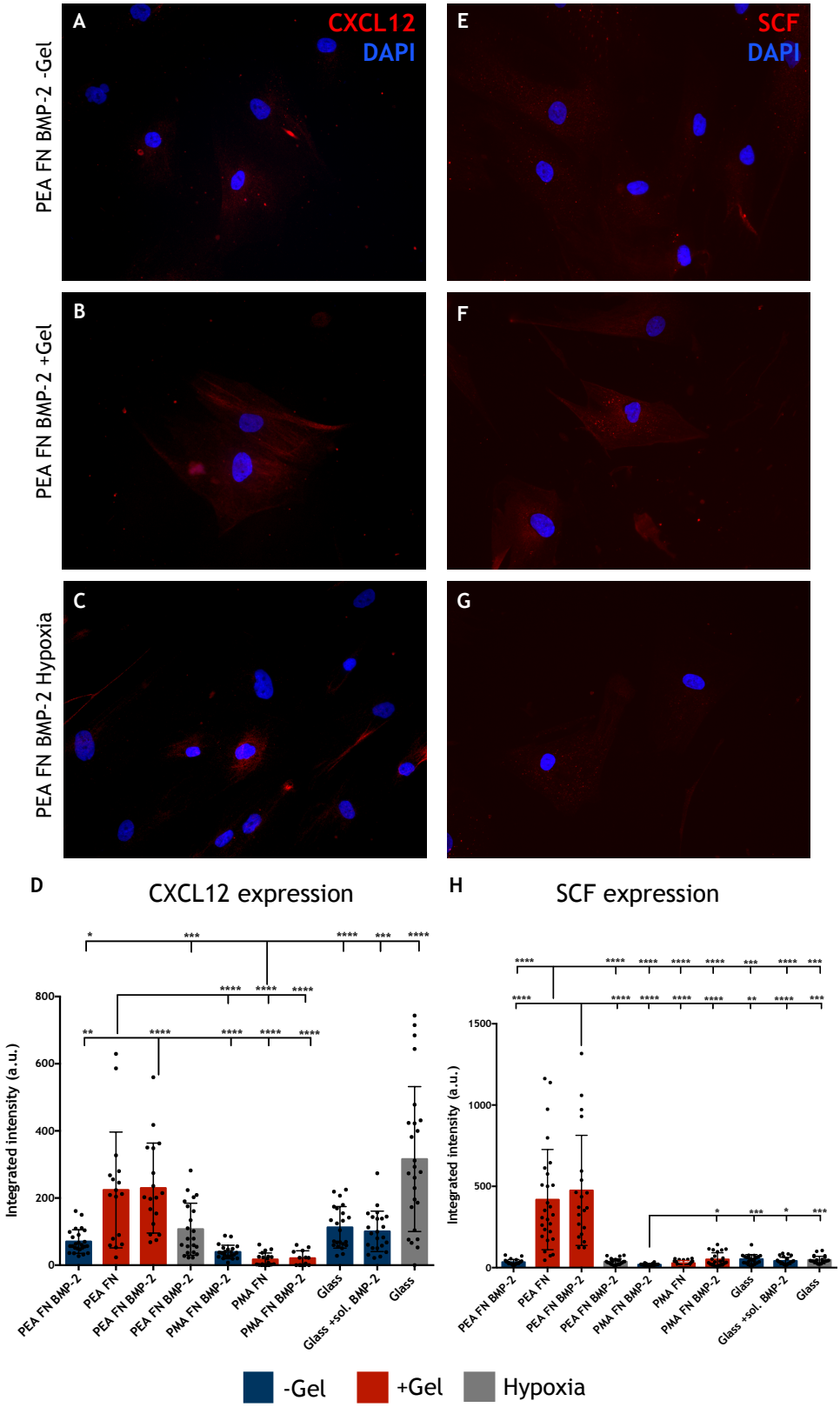

Figure 4-7 CXCL12 and SCF production in niche models. Cells were cultured in niche systems for 14 days with brefeldin A treatment (5 μg/mL in culture media) added for the final 24h to inhibit intracellular protein transport. Quantification of immunofluorescence staining with CXCL12 (A-D) and SCF (E-H) revealed significantly increased production of both cytokines in PEA FN +gel and PEA FN BMP-2 +gel, and in glass hypoxia for CXCL12. Scale bar = 100 μm, (A-C) red = CXCL12, blue = DAPI, (E-G) red = SCF, blue = DAPI. D & H show mean integrated intensity of CXCL12 and SCF ±SD (n=3 technical replicates), -gel = blue, +gel = red, hypoxia = grey, each point represents 1ximage field/number nuclei. One-way ANOVA followed by Kruskal-Wallis test with multiple comparisons, *= p<0.05, **= p<0.01, ***= p<0.001, ****= p<0.0001.

4.4 Discussion

The aim of this chapter was to assess the phenotype of pericytes seeded into our niche systems after up to 14 days culture. We wanted to assess the contribution of different niche properties, such as low-stiffness gels or hypoxia, on the ability to promote/maintain a niche-like MSPC phenotype *in vitro*.

4.4.1 Low-stiffness gels support expression of phenotypic niche markers

Transcriptomics performed at day 7 gave a snapshot of gene changes at an early time point in the MSPC niche model (Figure 4-3). The PEA FN BMP-2 -gel condition was predicted to show preference to osteo-commitment, and the data supports this hypothesis with an increase of the early osteogenic marker *RUNX2* observed. *RUNX2* is a key transcription factor which plays a central role in the regulation of bone matrix proteins (Hassan et al., 2006). A second important transcription factor that is required for bone matrix proteins is *SP7* (also called osterix; OSX), whose activation can be *RUNX2* dependent or independent. As such *SP7* activation is usually observed after *RUNX2* activity peaks (Yang et al., 2014). The RNA-seq data from this model (Figure 4-3) reveals in some conditions *SP7* levels increase in hypoxia, whilst PEA FN BMP-2 hypoxia also increased *RUNX2*. This reflects several reports where hypoxia can promote osteogenesis of MSPCs *in vitro* (Ejtehadifar et al., 2015; Hung et al., 2012). Other osteogenic markers such as *OCN* and *ALPP* were not observed to have increased. This was expected at day 7 as these are typically late osteogenic markers, indicative of a mature mineralised matrix, more typically elevated around day 16 – 28 in MSCs (Yang et al., 2014).

The results from the RNA-seq analysis provide an overview of cell phenotype, and are useful to direct further investigation, however changes in transcript abundance were only small, as such the regulation of these osteogenic transcripts would need to be confirmed by qPCR. Further to this, pericytes isolated from adipose tissue, as used in this thesis, and adipose-derived MSCs/MSPCs have been shown to display less potent osteogenic commitment *in vitro* than BM equivalents (Herrmann et al., 2016; Im et al., 2005). As such, the temporal gene expression of differentiation markers may be different between the published, characterised MSC time points and adipose-derived pericytes, and this may explain the only weak

up-regulation of these genes. A qPCR experiment at several time points would be required to elucidate peak RUNX2 activity in this system.

The list of genes produced for Figure 4-3 also included many genes implicated in stem cell maintenance and in the BM niche, such as surface markers *MCAM*, *NES*, *CSPG4*, several of which appeared to show increased expression in the presence of low-stiffness gels. We therefore chose to assess and confirm these trends by analysing protein levels. Other studies have demonstrated that a 'priming' period is beneficial when introducing HSCs into co-culture systems (Leisten et al., 2012; Sweeten, 2019). Therefore, we chose to carry out these assessments at the later time point of 14 days, in order to allow time for cells to establish responses to the different niche cues.

Flow cytometry was used to assess a panel of markers associated with MSPC and BM niche phenotypes. As for the RNA-seq analysis, mostly subtle changes were observed, with no fold change greater than ±3. Although this is perhaps expected in cultured stromal cell populations, for which no defined set of surface markers has been identified to robustly confirm phenotypes, and with further subsets of MSPCs being described in the literature (Dominici et al., 2006; Mo et al., 2016; Pinho et al., 2013).

The analysis demonstrated retention of CD90 in cells in systems containing gels, loss of which is associated with differentiation. Increased expression of the pericyte marker CD146 (*MCAM*) in systems containing gels was confirmed, and interestingly, these systems also demonstrated increase of the pericyte marker NG2 (*CSPG4)* which has been implicated as a marker of MSPCs that reside in periarteriolar locations and promote HSC quiescence (Figure 4-8) (Kunisaki et al., 2013). The expression of CD51 was also observed to increase in +gel conditions; CD51 has been implicated as a surrogate marker along with PDGFRα for a subset of MSPCs that are nestin+ and CD146+ (Pinho et al., 2013), although the cells lacked expression of PDGFRα. Interestingly, LepR expression was supported in hypoxic conditions, and LepR+ MSPCs have been shown to preferentially reside in the most hypoxic sinusoidal regions of mouse BM, suggesting low oxygen tensions may be adequate to support this phenotype (Figure 4-8) (Kunisaki et al., 2013).

The flow cytometry data confirmed expression of markers identified in the RNA-seq screen, and several of these markers suggested that the phenotype supported by the systems containing low-stiffness gels may be similar to nestin+ MSPCs in the BM.

However, for better comparison the cells should have been subject to the same flow cytometry analysis on the day of seeding, so changes from this phenotype could be assessed. Further, it should be noted that the percentage of recovery of cells from the niche systems to perform flow cytometry was low. Several replicates needed to be pooled to achieve statistically relevant numbers of cells to analyse. This was in part due to difficulties detaching cells from PEA surfaces using flow cytometry suitable detachment solutions (e.g. TrpLE or accuatse), and due to the time period required to digest the collagen gels (~90 minutes), which led to some cell death and cell debris. This could of course lead to bias in the population of cells retrieved and analysed. Therefore techniques that rely on fixation, isolation of cell RNA, or protein extraction, of cells directly on the materials may provide information more representative of the entire cell population. This also restricted the use of this data to assess changes in cell expansion and proliferation between the different systems, something likely effected by the different components of the system, and as such, is something that should be investigated in future work.

4.4.2 Low-stiffness gels promote nestin expression

We found that addition of a soft collagen hydrogel (~80 Pa) on top of pericytes seeded on polymer substrates led to increased nestin expression (Figure 4-5). Elevated expression was only observed at 7 days when pericytes were seeded onto substrates containing unfolded FN networks, where PEA FN +gel and PEA FN BMP-2 +gel increased nestin expression 9.6- and 8.5-fold respectively, when compared to cultures in the absence of low-stiffness gels. However, by day 14 increased expression was observed in these conditions and also in PMA FN +gel and PMA FN BMP-2 +gel (Figure 4-5). This suggests the addition of low-stiffness gels is able to drive nestin expression, but that the addition of FN networks drives expression earlier only when presented in a non-globular conformation on the PEA polymer. Suggesting that in order to promote a nestin+ niche-like phenotype of stromal cells in low-stiffness environments, early ECM attachment is required by the cells.

Nestin-expressing cells are frequently found in areas of regeneration, where they may function as a reservoir of stem/progenitor cells capable of proliferation and differentiation (Park et al., 2010). Nestin expression is observed during myogenic differentiation, in progenitor cells of the CNS and in highly proliferative tissues such as during neoplastic transformation e.g. glioma and neuroblastoma (Matsuda et al., 2015; Pallari et al., 2011; Sahlgren et al., 2003). As an IF, nestin function is often linked to its involvement in the cytoskeleton, however it has been shown in NSCs that nestin supports expansion of the stem cell pool by preventing apoptosis. This function was shown to be independent of nestin involvement in the cytoskeleton, as when vimentin was knocked down, preventing nestin from polymerising, no negative effects were observed. Whereas, nestin knock-down in NSCs significantly increased early apoptosis and *in vivo* nestin deficiency is known to be embryonically lethal (Park et al., 2010). This study suggests that nestin incorporation into the cytoskeleton enhances its function, and that nestin has roles that go beyond its structural function. Studies have implicated a role in the disassembly of vimentin during mitosis (Chou et al., 2003), and as a selective scaffolding protein for cyclin-dependent kinase 5 (Cdk5), a crucial signalling determinant during development and myogenic differentiation in neuronal and myogenic precursors (Pallari et al., 2011; Sahlgren et al., 2006, 2003).

Here, we observed a similar effect where nestin was significantly increased with gel addition, yet no significant changes in vimentin where observed (Figure 4-6). This perhaps supports the idea that the role of nestin in stem cells is independent of its involvement in the cytoskeleton. However, vimentin networks have physical properties likely to contribute to cell mechanics, for example they are characterised by a high degree of strain stiffening and ability to withstand large strains without breakage, in contrast to microtubules and microfilaments that rupture at more moderate strains (Janmey et al., 1991; Murray et al., 2014; Qin et al., 2009). Previous studies demonstrate that whilst substrate stiffness has been shown to alter many aspects of cell behaviour, changes in vimentin organisation were not reported. However, one more recent study investigating regulation of vimentin in response to substrate stiffness in MSCs, found that although the amount of total vimentin protein remains constant, the amount of protein that becomes soluble significantly increases with decreasing stiffness (Murray et al., 2014). This could explain the results observed in Figure 4-6, and suggests

investigation into the fraction of soluble vimentin rather than total protein could be investigated in future work.

The functional role of nestin expression in the BM remains to be elucidated. The 2013 study by Pinho et al, suggests that cell surface markers CD51 and PDGFRα can be used to identify Nestin+ MSPCs (Pinho et al., 2013). Interestingly, the expression of nestin at day 14 observed in the immunofluorescence analysis (Figure 4-5) correlated with increased expression of CD51 obtained from flow cytometry, but not PDGFRα (Figure 4-4). Nestin+ CD51+ PDGFRα+ cells isolated from human BM were also found to homogeneously express CD146. This correlates to nestin expression driven by low-stiffness gels (Figure 4-3, Figure 4-4, Figure 4-5). The nestin+ CD51+ PDGFRα+ cells isolated by Pinho et al, were enriched for HSC supporting niche activity and contained colony forming units-fibroblast (CFU-F) activity compared to nestin- CD51- PDGFRα- cells. However, only a small proportion of CD146+ cells expressed all 3 markers, suggesting further heterogeneities in the stromal population in human marrow. It is of note, that most studies demonstrating PDGFRα+ as a marker for MSPCs, use it as a method for isolation from tissues, whether PDGFRα expression is supported upon *in vitro* culture is unclear (Sá da Bandeira et al., 2016). This data suggests the phenotype of pericytes seeded in the +gel systems is similar to that of HSC-maintaining periarteriolar MSPCs identified in the BM, illustrated in Figure 4-8.

In context of the *in vivo* murine BM, distinct nestin+ MSPC distribution has been demonstrated. Based on cell fluorescence intensity and morphology, two distinct types of Nes-GFP+ cells (Nes-GFP^{bright} and Nes-GFP^{dim}) have been identified and characterised (Kunisaki et al., 2013). Both populations displayed mesenchymal progenitor (CFU-F) activities *in vitro*, but Nes-GFP^{bright} cells contained most CFU-F activity and increased expression of genes associated with HSC maintenance. However, Nes-GFP^{bright} cells are much fewer in number (~0.002% of total BM). The two nestin+ populations revealed physiological differences in localisation, with Nes-GFP^{bright} exclusively associating along arterioles, while Nes-GFP^{dim} were associated with sinusoids. Interestingly, Nes-GFP^{dim} cells were enriched for genes associated with DNA replication and cell cycle. Proliferation analysis revealed a significant decrease in Nes-GFP^{bright} cells, suggesting these cells are largely quiescent within the niche (Kunisaki et al., 2013). This is perhaps in contrast to

evidence in other cell types that proposes roles for nestin in supporting cell proliferation, and further highlights the discrepancies in function associated to nestin expression in different cell types. In future work, it would be of interest to characterise the proliferation of the pericytes in the BM niche model used in this thesis, to further characterise the phenotypic state of the stromal cells.

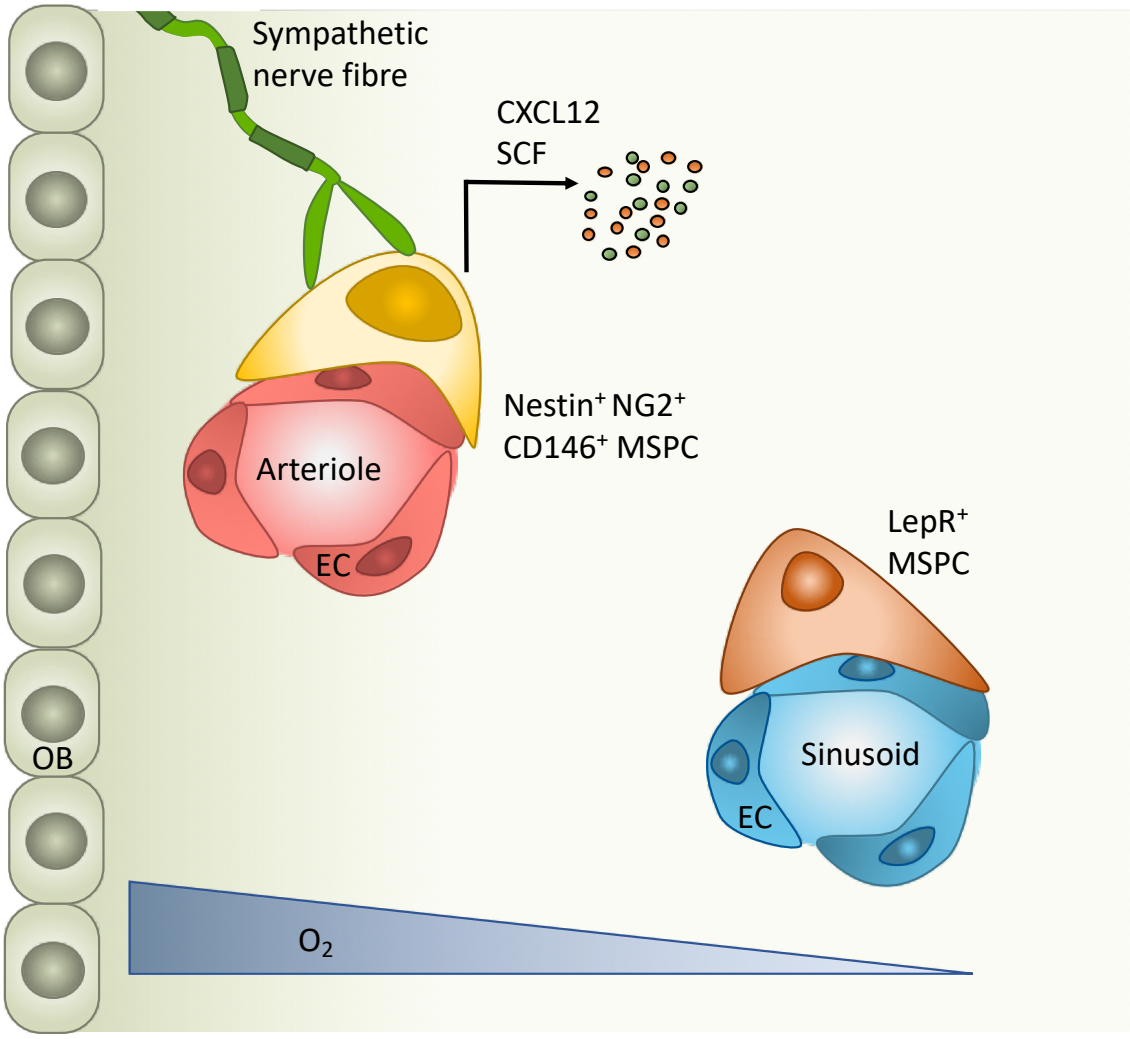

Figure 4-8 MSPC phenotypes in the BM niche. Nestin+ NG2+ CD146+ MSPCs are reside on arterioles near the endosteal surface, they express high levels of HSC-maintenance cytokines SCF and CXCL12 and are in close association with sympathetic nerve fibres. LepR+ MSPCs reside on more hypoxic sinusoids. MSPC; mesenchymal stromal and perivascular cells. OB; osteoblast. EC; endothelial cell.

4.4.3 Fibronectin +gel driven nestin expression correlates with HSC maintenance cytokine production

We hypothesised that by promoting a nestin+ MSPC phenotype we would also see elevated expression in HSC maintenance cytokines, primarily CXCL12 and SCF. Although Figure 4-3 suggests that transcription levels for both cytokines were low at day 7 we sought to investigate this at the protein level, to examine if cytokine

production was detectable in culture media ELISAs were initially carried out. However, inconsistencies with repeatability led us to believe the gel may have been capturing significant levels of cytokines, resulting in unreliable readings. Instead we chose to investigate cytokine expression by blocking protein transport for the final 24h of culture during the 'priming' period of 14 days.

Figure 4-7 shows CXCL12 production was most significantly elevated in PEA FN BMP-2 +gel, PEA FN +gel and also glass hypoxia. SCF was significantly elevated in PEA FN BMP-2 +gel and PEA FN +gel only. Firstly, this suggests that the combination of FN networks and low-stiffness gels are proficient to stimulate cytokine expression, and that the addition of BMP-2 is not required. Secondly, this increased HSC-maintenance factor phenotype is concomitant with the nestin+ CD51+ CD146+ MSPC phenotype we observed in these conditions. Nestin+ MSPCs are known to demonstrate enhanced HSC support activity (Table 1-3). Therefore, this data supports our hypothesis that using specific microenvironmental cues we can direct pericyte physiology towards a niche-like phenotype (Figure 4-8).

Surprisingly, although similar phenotypes were maintained on the PEA- and PMA-based +gel systems in all previous analysis, this did not correlate to increased cytokine production on PMA substrates (Figure 4-7). This could correlate with the delayed onset of nestin expression on PMA substrates observed in Figure 4-5, and suggests a longer priming period would be required for cytokine production in these conditions.

Interestingly, TPO, another important maintenance cytokine, displayed elevated transcript levels in the RNA-seq analysis (Figure 4-3). TPO production was similarly tested by ELISA at day 7 and 14, levels of the cytokine were undetectable in all conditions at both time points (Appendix Figure 7-3). TPO production in the niche is primarily from osteoblasts and osteoprogenitors, although it is believed systemic production from hepatocytes also has a major contribution to levels *in vivo* (Qian et al., 2007; Yoshihara et al., 2007). As the stromal phenotype supported by the niche model appears to be suggestive of nestin+ MSPCs, which do not produce significant TPO (Pinho and Frenette, 2019), this was not pursued further. However, in future, similar investigations using brefeldin A should be carried out, as the PEA FN BMP-2 -gel condition which has been previously demonstrated with MSCs to promote osteogenesis (Cheng et al., 2018; Llopis-hernández et al., 2016;

Sweeten, 2019), may promote TPO production at a later time point when a mature osteogenic state is reached.

4.5 Summary

This chapter describes the analysis of cell phenotype in response to engineered niche systems. We wanted to assess which microenvironmental cues presented to cells were able to support specific phenotypes of MSPCs, with the aim to identify those that enhance BM niche properties and drive an HSC supporting phenotype. The results in this chapter demonstrate:

- The addition of low-stiffness collagen gels directs pericyte phenotype towards that of periarteriolar MSPCs described in the BM niche. This phenotype is nestin+ NG2+ CD51+ CD146+.

- When in contact with preformed FN networks on PEA FN +gel and PEA FN BMP-2 +gel this MSCP population produces cytokines CXCL12 and SCF. Suggesting these systems may drive an HSC-supportive MSPC phenotype.

- FN networks drive earlier nestin expression, suggesting ECM interactions are important for nestin regulation.

- Nestin expression can be driven by the addition of low-stiffness matrices, suggesting this is a mechanosensitive response.

- The addition of the GF BMP-2 had no significant effect on the PEA FN +gel-based systems.

In the next chapter, these models are used further to investigate how the different microenvironmental cues influence stem cell metabolism, and how this relates to the phenotypes observed in this chapter.

Chapter 5 Hypoxia and Metabolism

5.1 Introduction

Low oxygen tension (hypoxia) is a key niche characteristic in maintaining quiescent or self-renewing states of embryonic, haematopoietic, mesenchymal, neural and cancer stem cells (Mohyeldin et al., 2010). This low oxygen environment is tolerated by stem cells, and appears to be essential for their function. It is thought that the 'hypoxic niche' offers an adaptive advantage to the stem cell, as in hypoxia anaerobic metabolism is utilised, avoiding mitochondrial OXPHOS and the resulting generation of ROS that can be damaging to DNA. The energy demand of self-renewing stem cells is less than that of cells undergoing differentiation, and it has been shown that MSCs in standard culture are more glycolytic, a phenomenon also known as the Warburg effect (Pattappa et al., 2011; Warburg, 1925). Then as differentiating cells begin to migrate out of the niche, metabolism shifts to OXPHOS to meet increased energy demands (Figure 5-1) (Mohyeldin et al., 2010; Pattappa et al., 2011; Simsek et al., 2010; Suda et al., 2011). Thus, hypoxic niches are thought to have an important role in regulating stem cell differentiation and self-renewal, thereby avoiding exhaustion of the stem cell pool (Yoon-Young and Sharkis, 2007).

It has been well studied that hypoxia is a hallmark of the BM niche, with studies identifying genetic and metabolic profiles that reflect adaption to low oxygen environments in HSCs (Simsek et al., 2010; Takubo et al., 2013, 2010). As discussed in Chapter 1.4.4, although the BM is a highly vascularized tissue, direct measurements of oxygen tension *in vivo* have found the absolute pO_2 of the cavity to be quite low (ranging from 1.5 - 4.2% oxygen). The most hypoxic zones have been revealed to be the deep sinusoidal regions, with the highly vascularised endosteal region displaying a slightly higher pO_2 (Figure 5-2) (Spencer et al., 2014).

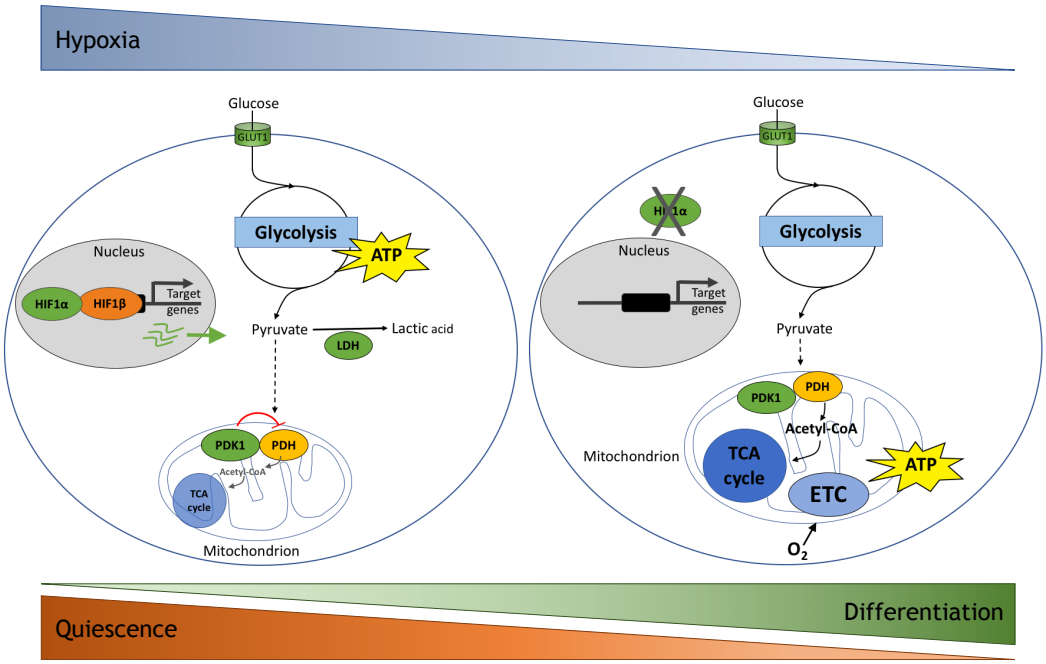

Figure 5-1 Stem cells reside in and adapt to hypoxic niches. In hypoxic environments, such as stem cell niches, stem cells switch their metabolism to anaerobic glycolysis. This is controlled by the master transcriptional regulator of the hypoxic response HIF1α, which in hypoxia translocates to the nucleus and activates target genes. Several of these genes are glycolytic enzymes, such as LDH (lactate dehydrogenase) and PDK1 (pyruvate dehydrogenase kinase 1). This metabolises pyruvate to lactate, preventing it from entering the mitochondria, and ATP is generated from glycolysis. As cells move out of hypoxic niches they lose quiescence and begin to differentiate. HIF1α is no longer active and pyruvate is able to enter the mitochondria via PDH (pyruvate dehydrogenase), where it moves through the citric acid cycle (TCA) and electron transport chain (ETC) to generate a greater ATP output than glycolysis alone.

Isolation and *in vitro* culture of stem cells along with biomaterials strategies have greatly accelerated our understanding of fundamental niche mechanisms and behaviours. Initially little attention was paid to the metabolic milieu of native niches, and as for all other established cell lines, culture was typically at normoxic pO_2 levels on tissue culture plastic. However, as culture at low oxygen of stem cells began to be investigated, active hypoxia-related signalling pathways were shown to be important for retaining naive phenotypes (Pattappa et al., 2011). Coupled with direct measurements of pO_2 levels of native niches, the importance of the low oxygen environment and its impact on cellular metabolism is now being widely investigated.

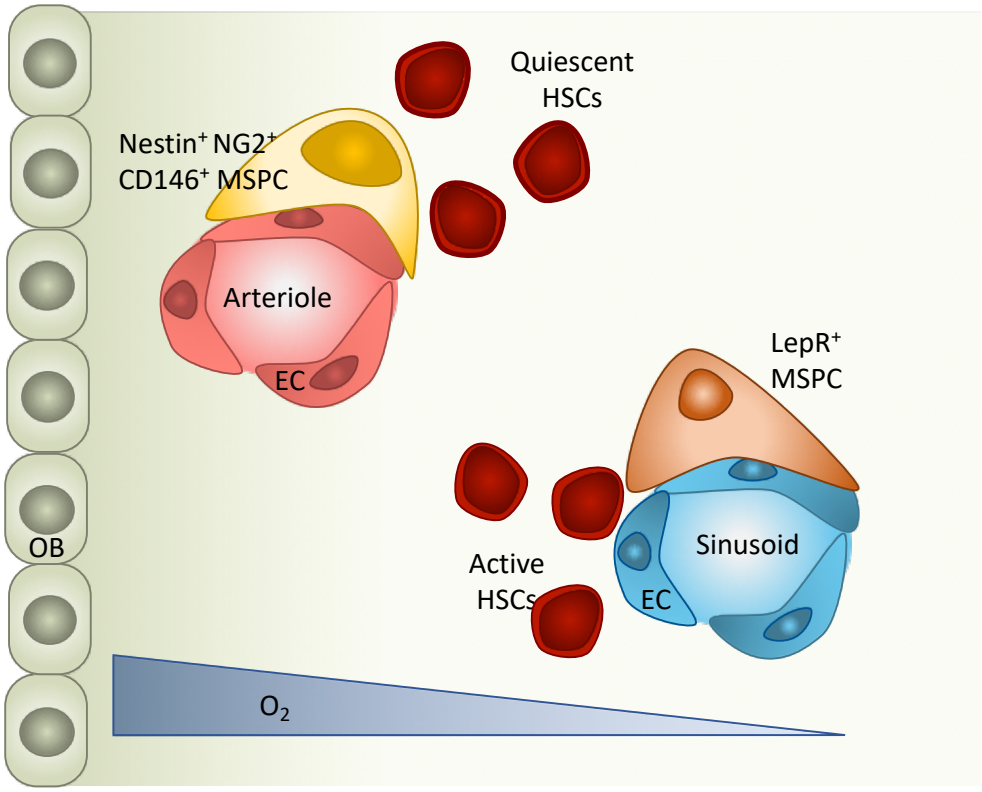

Figure 5-2 Oxygen gradient in the bone marrow niche. More hypoxic sinusoidal regions house LepR+ MSPCs that regulate active HSCs. The endosteal region is highly populated with arterioles, which house Nestin+ CD146+ NG2+ MSPCs that regulate quiescent HSCs.

5.1.1 HIF1α

Response to low oxygen tensions is mediated by the transcriptional complex hypoxia-inducible factor (HIF) proteins at the cellular level (Wang and Semenza, 1995). HIF is a heterodimeric DNA-binding complex composed of two basic-helix-loop-helix proteins of the PAS family (PER, AHR, ARNT and SIM family) (Semenza et al., 1997). The HIFβ subunits are non-oxygen responsive nuclear proteins and levels are stably maintained in cells, whereas the HIFα subunits (HIF1α and HIF2α) are constitutively turned over in the cytoplasm and are highly oxygen responsive (Weidemann and Johnson, 2008). Under hypoxia the α/β heterodimer binds to hypoxia response elements (HRE) of target genes via a core pentanucleotide sequence (RCGTG; arginine, cysteine, glycine, threonine, glycine). HIF related activity is key in regulating a broad range of responses to hypoxia both cellular and systemically, and is known to directly or indirectly regulate over 100 genes. HIF-mediated pathways influence genes that are themselves non-oxygen responsive, but that also influence metabolic adaption, angiogenesis, cell growth, differentiation, survival and apoptosis (Weidemann and Johnson, 2008).

HIF1α subunits have a short half-life under normoxia (Salceda and Caro, 1997). The continually produced α-subunits are degraded through oxygen-dependent hydroxylation of two prolyl residues in their oxygen-dependent degradation domains (ODDD), by HIF prolyl hydroxylases (PHDs) (Ivan et al., 2001; Jaakkola et al., 2001). PHD enzymes are 2-oxoglutarate dependent, non-heme FE(II)-dioxygenases, and hence split molecular oxygen - one atom is inserted into the HIF1α peptide at the prolyl residue, the other reacts with 2-oxoglutarate, producing CO_2 and succinate as by products. PHDs remain unmodified under low oxygen, and hence the effects of hypoxia are often simulated in culture by iron chelation, most commonly cobalt chloride (CoCl) (Bruick and McKnight, 2001).

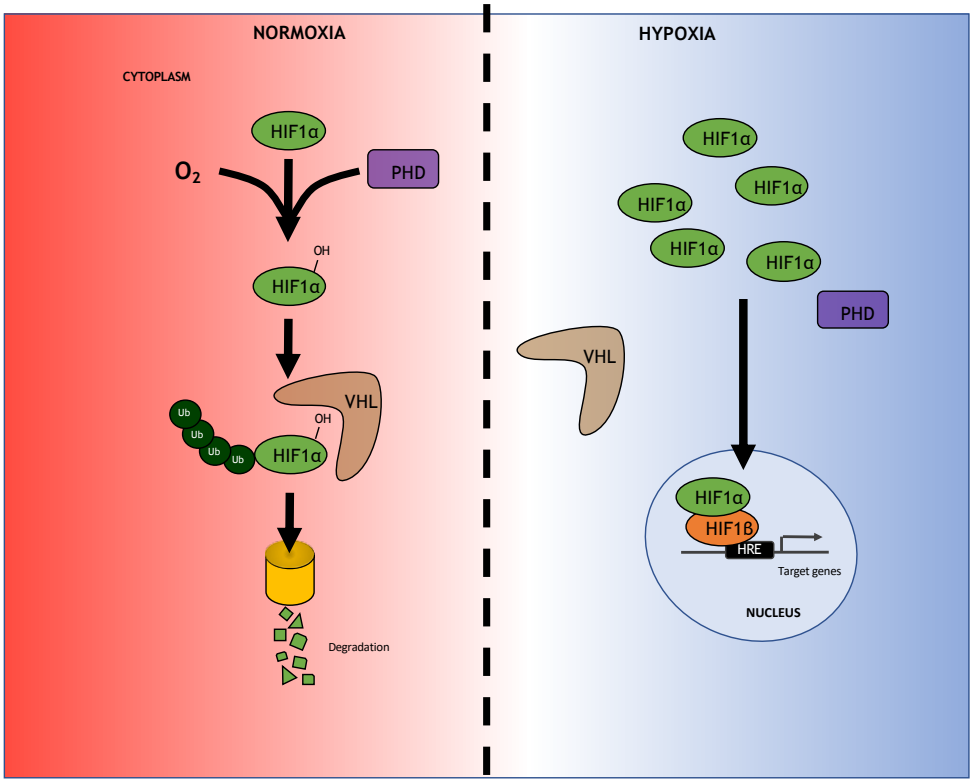

Figure 5-3 HIF1α regulation by oxygen tension. HIF1α contains hydroxylation sites on two prolyl residues in the oxygen-dependent degradation domain (ODDD). In the presence of oxygen, prolyl hydroxylation is catalysed by the Fe(II)-, oxygen- and 2-oxoglutarate-dependent PHDs. The hydroxylated prolyl residues allow capture of HIF1α by the von Hippel-Lindau protein (VHL), an E3 ubiquitin ligase. Ubiquitination leads to subsequent proteasomal degradation. In the absence of hydroxylation, i.e. in low oxygen or PHD inhibition, HIF1α translocates to the nucleus, heterodimerizes with HIF1β and binds to hypoxia-response elements (HREs) in the regulatory regions of target genes.

In normoxia, the hydroxylated ODDD is recognised by the E3 ubiquitin ligase von Hippel-Lindau (VHL), which facilitates polyubiquitination and subsequent proteasomal degradation of HIF1α. Consequently, in hypoxic conditions hydroxylation is supressed and HIF1α protein can accumulate. Subsequently,

HIF1α subunits translocate to the nucleus where they can dimerise with HIF1β (Staller et al., 2003), the heterodimeric protein complex then binds the HREs on promoter or enhancer sequences on target genes that facilitate adaption to hypoxia (Figure 5-3) (Weidemann and Johnson, 2008).

The role of HIF1α as a regulator of metabolic adaption is important for many cellular processes. It has been shown to play an important role in both MSCs and HSCs in their niches, where the balance between self-renewal and differentiation requires distinct metabolic programs to meet the changing energy demands (Guarnerio et al., 2014; Morikawa and Takubo, 2016; Pattappa et al., 2011; Simsek et al., 2010; Takubo et al., 2010), which will be discussed and investigated in this chapter.

5.1.1.1 HIF2α and HIF3α

HIF1α was the first hypoxia-inducible factor described, it is believed to be the master regulator of the hypoxic response and initial characterisation was focussed on this subunit. However, there are two other oxygen-dependent HIFα subunits, HIF2α (also known as EPAS1) and HIF3α, that remain to be fully characterised (Ivan et al., 2001; Masson et al., 2001). The three HIFα isoforms are encoded by distinct gene loci but retain some similarities; all possess the ODDD and HIFβ-dimerising domain. HIF1α is ubiquitously expressed, whereas HIF2α and HIF3α are found in a subset of tissues. HIF2α also binds to HRE and upregulates gene expression but its expression is more limited and appears to be tissue or cell type-specific and limited to e.g. endothelium (Tian et al., 1997), kidney (Wiesener et al., 2002), lungs (Ema et al., 1997) and small intestine (Wiesener et al., 2002). HIF1α and HIF2α show some functional overlap, but have also been shown to regulate unique genes and physiological functions (Covello et al., 2006). HIF1α uniquely activates glycolytic enzyme genes, while HIF2α preferentially activates VEGF (Hu et al., 2003), Oct4 (Covello et al., 2006) and Cyclin D1 (Baba et al., 2003).

HIF2α is known to be an upstream regulator of POU5F1 (OCT4) in mouse ESCs suggesting an important role in maintenance of ESC pluripotency (Covello et al., 2006). OCT4 expression, along with other ESC markers (NANOG, SOX2), is lost upon culture at 20% oxygen (Chen et al., 2010). One study investigated the levels of the

three HIFα subunits in ESCs and found transient HIF1α expression at low oxygen, whereas the HIF2α and HIF3α subunits although initially low, were significantly upregulated and localised to the nucleus in long-term exposure to hypoxia. Silencing of HIF2α lead to a loss of ESC pluripotency genes and proliferation, whereas HIF3α knockdown decreased HIF2α expression, but promoted HIF1α levels (Forristal et al., 2010). This demonstrates complex interactions between the 3 subunits is necessary to maintain ESC pluripotency under hypoxic culture, where HIF3α regulates expression of both HIF2α and HIF1α, but HIF2α is required for proliferation and pluripotency regulation.

HIF3α is less closely related to HIF1α, it lacks the C-terminal activation domain required for co-activator binding, meaning it is unable to recruit the basal transcriptional machinery to target genes. Little is known is about which genes HIF3α regulates, although it has also been shown to act as a dominant negative regulator of HIF1α in the corneal epithelium of the eye (Makino et al., 2001). For MSPCs, one recent study illustrated HIF3α pro-inflammatory activation that is oxygen-independent (Cuomo et al., 2018), and another implicated it as a regulator of chondrogenesis (Markway et al., 2015). As such, the role of the less well studied HIF3α subunit remains unclear.

5.1.2 MSPCs and hypoxia

Hypoxia has been indicated as a key caveat in all stem cell niches, requiring tight metabolic regulation to maintain long-term quiescence and self-renewal of stem cell populations (Mohyeldin et al., 2010). As such, MSPC response and regulation in hypoxia has been of great focus, with the aim of maintaining niche-like phenotypes that would allow for longer term culture and ultimately use for tissue engineering or immune suppressive purposes (Ejtehadifar et al., 2015).

There exists conflict in reports of the effects of hypoxia and hypoxia-relating signalling on MSPC differentiation capacity *in vitro*. For example some studies demonstrate BM-derived MSCs showed decreased osteogenic commitment in hypoxic culture (D'Ippolito et al., 2006; Fehrer et al., 2007), with one study highlighting even after long-term culture no osteoblastic markers or mineralisation could be observed compared to actively differentiating normoxic

counterparts, instead upregulation of naïve markers could be observed, such as OCT-4, telomerase reverse transcriptase and HIF1α (D'Ippolito et al., 2006). Another report shows culture for short periods in hypoxia can significantly augment beneficial therapeutic characteristics of MSCs, increased modulation of key genes and self-renewal capacity has been observed with hypoxic exposure for just 48h (Antebi et al., 2018)

Contrastingly, there have been reports of hypoxic culture of BM MSCs promoting chondrogenic, osteogenic and adipogenic differentiation capacity (Müller et al., 2011; Tsai et al., 2011; Wagegg et al., 2012). Reports on MSCs from other sources have corroborated these findings, where one study evidenced an increase of oxygen from just 1% to 3% was shown to restore the osteogenic potential of MSPCs from various tissues (Holzwarth et al., 2010), and 'hypoxic priming' has been shown to increase chondrogenic potential of adipose-derived MSPCs (Mohyeldin et al., 2010). Bone formation during fracture healing operates in a hypoxic environment due to disruption of vasculature (Dimitriou et al., 2005), and a recent study demonstrated both HIF1α and HIF2α are highly expressed in osteoblasts (Merceron et al., 2019). The study by Merceron et al, indicated HIF1α was a positive regulator of osteogenesis, whereas HIF2α was found to inhibit osteoblast formation through upregulation of chondrogenic marker SOX9 (Merceron et al., 2019).

Reports on the effect of hypoxia specifically on BM pericytes are fewer, however, the *in situ* localisation of CD146+ pericytes predominantly to arteriolar walls suggests preference for the less hypoxic regions of the BM. This was confirmed in a study that correlated CD146 expression to perivascular cells surrounding vessel endothelium. Upon isolation and hypoxic *in vitro* culture CD146 expression was markedly decreased in these cells after 2 weeks, although the loss was reversible when cells were reintroduced into normoxic culture for a further 2 weeks (Tormin et al., 2011).

Stem cell expansion and lifespan has been shown to increase in cultures at low oxygen tensions; the glycolytic phenotype, driven primarily by HIF1α, limits oxidative stress, DNA damage and chromosomal aberrations, which compromise the safety and viability of long-term cultures. Despite faster growth, studies have

shown MSPCs can be passaged up to 10x more under hypoxic conditions. It is thought that hypoxia reduces the rate of telomere shortening per cell division, suggesting these oxidative stress protection mechanisms help maintain an increased lifespan (Estrada et al., 2012; Fehrer et al., 2007).

Overall, the effects of hypoxic culture on MSPCs remains unclear, this could be due to i. ill-defined isolation profiles of MSPCs leading to heterogeneities in the cell types used, and ii. ill-defined methods of hypoxic culture, some studies use ion-chelators, others hypoxic incubators at varying oxygen concentrations. With recent reports suggesting differences in pO_2 gradients sensed by cells will differ even with uneven media heights, means making comparisons between studies can perhaps be inconsistent (Wenger et al., 2015).

5.1.3 HSCs and hypoxia

HSCs are thought to be localised to the hypoxic regions of the BM niche, and indeed hypoxic *ex vivo* culture of primitive haematopoietic progenitors or HSCs has been shown to maintain cell cycle quiescence (Hermitte et al., 2006), and stemness (Danet et al., 2003). How HSCs adapt to this environment has been well studied, and was revealed in two landmark studies from 2010, that used complementary approaches to provide important insights into the role of hypoxia and HIF1α signalling in regulating HSC function (Simsek et al., 2010; Takubo et al., 2010).

Simsek et al, demonstrated HSCs adapt to and utilise chronic hypoxia through stabilisation of HIF1α, activating transcription of target genes that are involved in adaption to glycolysis as the main source of energy. They showed HSCs exhibit elevated levels of HIF1α, increased rates of glucose consumption and lactate production, with correspondingly decreased rates of mitochondrial OXPHOS when compared to mature cells (Simsek et al., 2010). Takubo et al (2010), corroborated these findings, presenting conditional deletion of HIF1α in HSCs led to loss of quiescence and of long-term repopulation capacity in serial transplantation assays. Then, by conditionally deleting VHL this landmark study revealed that monoallelic deletion of the E3 ubiquitin ligase leads to HIF1α stabilisation, increasing the population of LT-HSCs. However, complete ablation of VHL appears to lead to over stabilisation of HIF1α, leading to a loss of HSC activity in transplantation assays (Takubo et al., 2010). Collectively these two studies

provide genetic evidence that HIF1α is an essential regulator for HSC long-term maintenance, and that tight regulation of HIF1α levels are essential for maintaining this function.

Takubo et al, went on to further investigate the metabolic implications of HIF1α regulation in HSCs using metabolomic analysis (Takubo et al., 2013). High flux through the glycolytic pathway was characterised through accumulation of fructose-1,6-bisphosphate (F1,6BP), a product of the rate-limiting step of glycolysis, reflecting irreversible commitment to the pathway. Elevated levels of pyruvate corresponded with low levels of phosphoenolpyruvate, the by-product and substrate for the final ATP-generating step in the glycolytic pathway. Alongside this, high glycolytic enzyme expression and activity, such as pyruvate kinase, in LT-HSCs confirmed a reliance on anaerobic metabolism for energy production. Presenting striking differences in metabolic wiring of LT-HSCs compared to their committed progeny. Engagement with the citric acid (TCA) cycle, and therefore OXPHOS, is prevented in these HSCs through HIF1α driven expression of pyruvate dehydrogenase kinase (PDK) 2 and 4, which suppresses pyruvate dehydrogenase (PDH) activity, preventing the conversion of pyruvate to acetyl-CoA (Takubo et al., 2013).

Reliance on tight regulation of distinct metabolic profiles in HSCs is not only essential for maintenance of quiescence, but a timely shift is required for activation and differentiation to committed progeny, which was highlighted in a further complementary study by Yu et al, in 2013. Here they showed disruption of mitochondrial OXPHOS was achieved through depletion of a PTEN-like phosphatase, PTPMT1 which is located on the inner membrane of mitochondria, and was found to completely block HSC differentiation. The decrease in differentiation observed was not due to loss of the HSC compartment, but to the inability of *Ptpmt1*-deficient HSCs to undergo differentiation-associated divisions both *in vitro* and *in vivo*, leading to rapid haematopoietic failure in a mouse model (Yu et al., 2013).

However, the hypoxic state of HSCs has been demonstrated to be not entirely due to a hypoxic niche, but also regulated through cell-autonomous mechanisms. one recent study demonstrated that HSC hypoxic status is independent of location

within the BM cavity (Nombela-Arrieta et al., 2013). Here they demonstrated that HIF1α was stably expressed, and hypoxic probe pimonidazole was stably incorporated in HSCs isolated from throughout distinct BM regions, and this profile was retained in human circulating HSCs. Indicating the hypoxic phenotype of HSCs is cell-specific rather than location dependent. The importance of HIF1α stability in HSCs is further demonstrated by non-cell-autonomous niche microenvironmental factors able to drive its stabilisation. Both SCF (Pedersen et al., 2008) and TPO (Kirito et al., 2005) have been shown to drive HIF1α stabilisation and hypoxic response profile in HSCs cultured in normoxia. In addition, MSPCs exhibiting elevated HIFs and a hypoxic profile have been shown to inhibit HSC expansion and differentiation *in vitro* (Guarnerio et al., 2014).

Collectively, this landmark series of studies implicate the importance in tight regulation of HIF1α levels in HSCs, and how this supports a metabolic phenotype that is required for self-renewing HSCs and functional haematopoiesis. HIF1α drives expression of key genes that allow adaption to hypoxia through utilisation of anaerobic glycolysis, and by preventing entry into OXPHOS. However, this program may rapidly switch to utilise mitochondrial OXPHOS to facilitate the increased energy demands associated with differentiation. Current *in vitro* culture of HSCs is limited by loss of self-renewing ability after only a few days, highlighting the importance of signals provided by the native niche. Studies such as these explain the importance of building culture systems that more accurately mimic stem cell native microenvironments to successfully expand populations *in vitro*.

5.1.4 Investigating cellular metabolism with metabolomics

Measurable shifts in energy demand and metabolic activities occur as cells respond to their physical and chemical microenvironment. Metabolites are small molecules that are transformed during these metabolic processes, as such, they can provide a functional readout of cellular biochemistry. Genes and protein functions are subject to epigenetic regulation and post-translational modifications, whereas metabolites serve as direct signatures of biochemical activity, offering mechanistic insights for understanding, and interrogating, how cellular biochemistry correlates to phenotype (Patti et al., 2012). Progression in mass spectrometry (MS) technologies now offers tools for global metabolite profiling, known as untargeted metabolomics. This can be performed using either nuclear

magnetic resonance (NMR), or liquid chromatography followed by mass spectrometry (LC/MS) which has become the technique of choice for global profiling. LC/MS provides higher sensitivity and enables the detection of thousands of peaks measured from minimal amount of biological material, requiring minimal sample preparation (for example, <25 mg of tissue, several thousands of cells, or ~50 μL of biofluids) (Buscher et al., 2009; Jonsson et al., 2005; Patti et al., 2012).

MS distinguishes metabolites based on the mass-to-charge ratios (*m*/*z*) of the intact metabolite and their fragmentation patterns. Coupling this with chromatography provides an additional dimension of identification, whereby metabolites can be differentiated by their retention times. LC/MS has been widely used in metabolite profiling studies of human urine, or other biofluids, for biomarker discovery. Metabolic signatures have been assigned that correlate with insulin resistance (Newgard et al., 2009), increased risk of cardiovascular disease (Shah et al., 2012) and non-alcoholic fatty liver disease (Luukkonen et al., 2016).

There has also been recent focus on global profiling of stem cells permitting systems-level analysis to uncover biochemical effectors of cellular behaviours. For example, metabolic profiling was carried out on pericytes and MSCs as differentiation was directed down distinct lineages, or their stemness maintained (Alakpa et al., 2017a, 2016; McMurray et al., 2011; Tsimbouri et al., 2012). By using material-based platforms to direct cellular behaviour, such as gels ranging in stiffness, or nanotopographies to direct self-renewal or osteogenesis, rather than biochemical components (such as GFs or defined medias) our group has identified metabolites involved in these processes. By feeding these bioactive molecules into stem cell cultures, differentiation could be induced (Alakpa et al., 2016). This approach highlights critical biochemical pathways for investigation, and a method for identifying individual metabolites of therapeutic significance using reproducible biomaterial strategies.

5.1.5 Objectives and aims

Metabolic adaption is a requirement of stem cells in their niches. We aimed to investigate if we could mimic aspects of this metabolic phenotype in our BM model systems using low-stiffness gels. The aims of this chapter were to investigate cellular metabolism as such:

- Investigate changes in HIF1α levels and activation in hypoxia and with low-stiffness gel addition.

- Assess the effects on downstream targets of HIF1α, such as glycolytic enzymes and GFs.

- Use metabolomics to identify differences/similarities between the niche model systems at the biochemical pathway level.

5.2 Materials and Methods

5.2.1 HIF1α co-localisation analysis

To assess levels of active HIF1α in cell nuclei, cultures of 3 days were initiated (gel added after 24h), then fixed and stained with rabbit anti-HIF1α followed by secondary anti-rabbit fluorescent probes, nuclei stained with DAPI and samples mounted and visualised on a fluorescent microscope (Chapter 2.3.5). The images captured were uploaded to CellProfiler software (version 2.1.1), using a custom developed pipeline. Using the DAPI image, a mask was drawn around the nucleus, then imposed onto the corresponding raw HIF1α image and the integrated intensity measured, demonstrated in Figure 5-4. The value for each nucleus measured was then plotted as an individual point and subject to statistical analysis using GraphPad Prism 6 software.

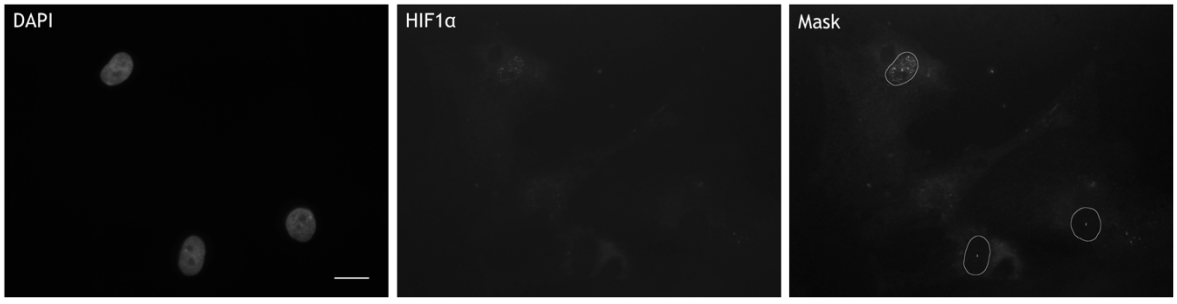

Figure 5-4 HIF1α analysis using CellProfiler script. The DAPI image was used to create a mask, which was overlaid to the HIF1α image and integrated intensity of this area measured. This ensures activated HIF1α that was co-localised with the nucleus was measured. Images from PEA FN BMP-2 Hypoxia. Scale bar is 20 μm.

5.2.2 Hypoxyprobe™

After 6 days culture in the model, medium was changed to a fresh medium containing 200 μM pimonidazole (Chen et al., 2010; Genetos et al., 2010; Raheja

et al., 2008), and cultured for a further 24 h. Cells were then fixed, blocked and stained with mouse anti-pimonidazole as in Chapter 2.3.4. Secondary Texas Red anti-mouse was added, and samples visualised on the fluorescent microscope. Integrated intensity was measured using imageJ software and subject to statistical analysis using GraphPad Prism 6 software.

5.2.3 Metabolomics analysis

Whole cell metabolomic analysis was performed on cell lysates isolated from pericytes cultured in niche systems for 7 or 14 days. Substrates were washed with ice-cold PBS, and cells lysed in extraction buffer (PBS/methanol/chloroform at 1:3:1 ratio) for 60 mins at 4˚C with constant agitation. Lysates were then transferred to cold Eppendorfs and spun at 13000 g at 4˚C for 5 mins to remove debris, and stored at -80˚C. Cleared extracts were used for hydrophilic interaction LC/MS analysis (UltiMate 3000 RSLC, (ThermoFisher), with a 6 150 x 4.6 mm ZIC-pHILIC column running at 300 µl/min-1 and Orbitrap Exactive). A standard pipeline, consisting of XCMS (peak picking), MzMatch (filtering and grouping) and IDEOM (further filtering, post-processing and identification) was used to process the raw mass spectrometry data. Identified core metabolites were validated against a panel of unambiguous standards by mass and predicted retention time. Further putative identifications were generated by mass and predicted retention times. Heatmaps of selected metabolites and principle component analysis (PCA) plots were generated using MetaboAnalyst software (version 4.0).

5.2.4 $^{13}C_6$-Glucose metabolomic tracing

Pericytes were seeded onto PEA FN BMP-2 niche systems and allowed to grow for 72 h. Cells were then washed and media was changed to basal media comprising 25% normal glucose and 75% $^{13}C_6$-Glucose (Cambridge Isotopes Ltd), for +gel conditions collagen gels were generated as in Chapter 2.3.1.3, where 0.5 mL 2% DMEM was substituted with 0.5 mL $^{13}C_6$-Glucose containing 2% DMEM, hypoxic samples were added to hypoxic workstation. After 3 days incubation extractions were performed as in section 5.2.3 and LC-MS was performed. The LC-MS platform consisted of an Accela 600 HPLC system combined with an Exactive (Orbitrap) mass spectrometer (ThermoFisher). Two complementary columns were used; the zwitterionic ZICpHILLIC column (150 mm x 4.6 mm; 3.5 µm, Merck) and the

reversed phase ACE C18-AR column (150 mm x 4.6 mm; 3.5 µm Hichrom) and in both cases sample volume was 10 µl at a flow rate of 0.3 ml/min. Eluted samples were then analysed by mass spectrometry. Raw data from LC-MS of ^{13}C-labelled extracts was processed to generate a combined PeakML file (Westrop et al., 2017). Further analysis using mzMatch-ISO in R (Chokkathukalam et al., 2013) generated a PDF file containing chromatograms used to check peak-shape and retention time, and a tabdelineated file detailing peak height for each isopotologue, which was used to calculate percentage labelling. Cell number measurements were taken by ICW CellTag700 staining of duplicate samples and used to standardise samples. Total $^{13}C_6$-Glucose incorporation was calculated by totalling incorporation excluding up to C_2 to eliminate natural incorporation.

5.3 Results

5.3.1 Analysis of HIF1α levels and its downstream targets

Using RNA-seq, a list of genes involved in hypoxic adaption was generated (Figure 5-5). This list includes regulators of hypoxic response HIFs (HIF1α and HIF3α), and downstream targets such as growth factors (VEGFA, VEGFB), and glycolytic or mitochondrial OXPHOS enzymes (PDK1, PTPMT1, PDK2, PDK3, PDK4). An increase in HIF1α expression was observed in all polymer +gel conditions compared to polymers or glass -gel or +hypoxia, whereas HIF3α appeared to increase in hypoxia and in PEA FN +gel and PEA FN BMP-2 +gel specifically.

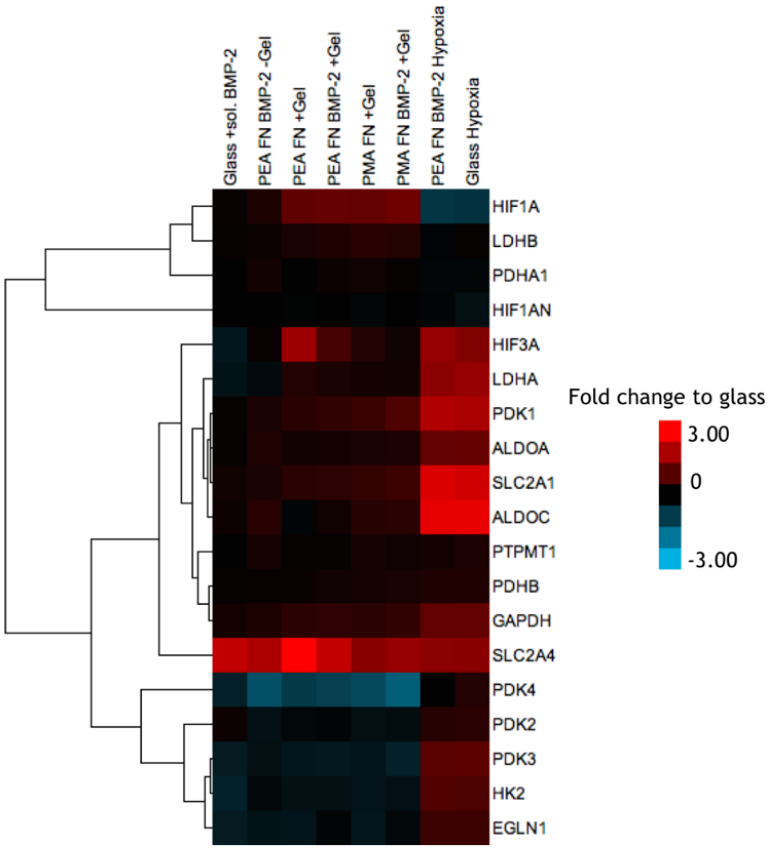

Figure 5-5 RNA-Seq profiling of pericyte transcripts relating to hypoxic adaption after 7 days. Results are shown as fold change to glass control. The hypoxic systems show up regulation of most genes, except HIF1A which is increased in +gel conditions only. Genes are clustered by average linkage. N = 2 for PEA FN BMP-2 hypoxia, n = 3 for all other conditions.

To confirm this effect of HIF1α, immunofluorescence microscopy was carried out. As HIF1α is constitutively produced and degraded in the cytoplasm, only active levels were measured, that is, HIF1α protein co-localised with the nucleus (Figure 5-4). Measurements of the integrated intensity of a masked area corresponding to the nucleus were compared (Figure 5-6). For the protein level analysis glass +gel condition was included. The increase in HIF1α observed with gel addition in Figure 5-5 was corroborated in PEA FN BMP-2 +gel at the protein level (Figure 5-6). Although a similar trend was observed with PMA FN BMP-2 +gel, it was not significant. To confirm this effect, the same experiment was carried out using Stro1+ MSCs, where a significant increase in HIF1α with gel addition was observed (Appendix Figure 7-2). These results suggest the addition of the low-stiffness gel increases stimulation, or accumulation, of active HIF1α to levels higher than those required for steady state or chronic hypoxia. Figure 5-6B shows representative images for each PEA FN BMP-2 condition, where increased HIF1α localised to the nucleus in gel conditions.

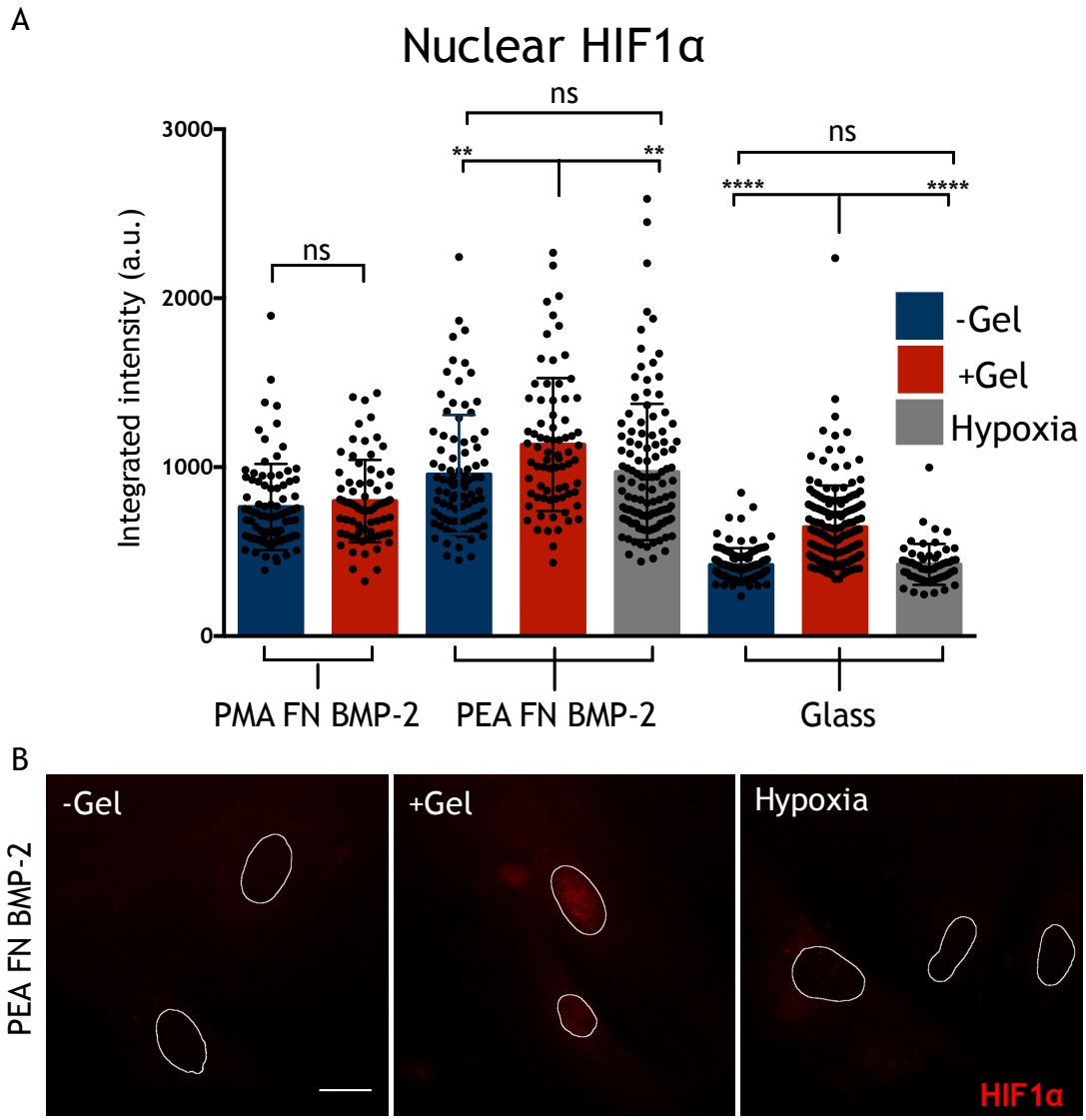

Figure 5-6 Nuclear HIF1α levels increase with low-stiffness gels. HIF1α is active when localised to the nucleus. Immunofluorescence analysis was carried out after 3 days, and the integrated intensity of HIF1α in cell nuclei measured. A. Shows increased HIF1α levels were observed on PEA FN BMP-2 substrates, and that addition of a low-stiffness gel increases HIF1α levels in glass and PEA FN BMP-2. B. Representative images of HIF1α, red = HIF1α, white = nuclear outline. Scale is 20 μm. Graph shows mean integrated intensity of nuclear HIF1α ± SD (n=3), each point represents 1 nuclei. One-way ANOVA followed by Kruskal-Wallis test with multiple comparisons, n.s. = non-significant, *= p<0.05, **= p<0.01, ***= p<0.001, ****= p<0.0001.

To further investigate the observed increase in HIF1α levels, analysis of downstream targets was carried out. Lactate dehydrogenase (LDH) is a glycolytic enzyme catalysing the conversation of pyruvate to lactate. LDH levels were investigated using ICW. A significant increase of LDH levels was observed in the PEA FN BMP-2 hypoxia condition compared to glass and glass +sol. BMP-2, with a trend towards increasing levels in glass hypoxia, although this was not significant (Figure 5-7A). This was consistent with the increase observed in *LDHA* expression

in the RNA-seq analysis in Figure 5-5. Glass +gel was excluded from analysis as cells migrated into the gel, making techniques such as ICW unreliable.

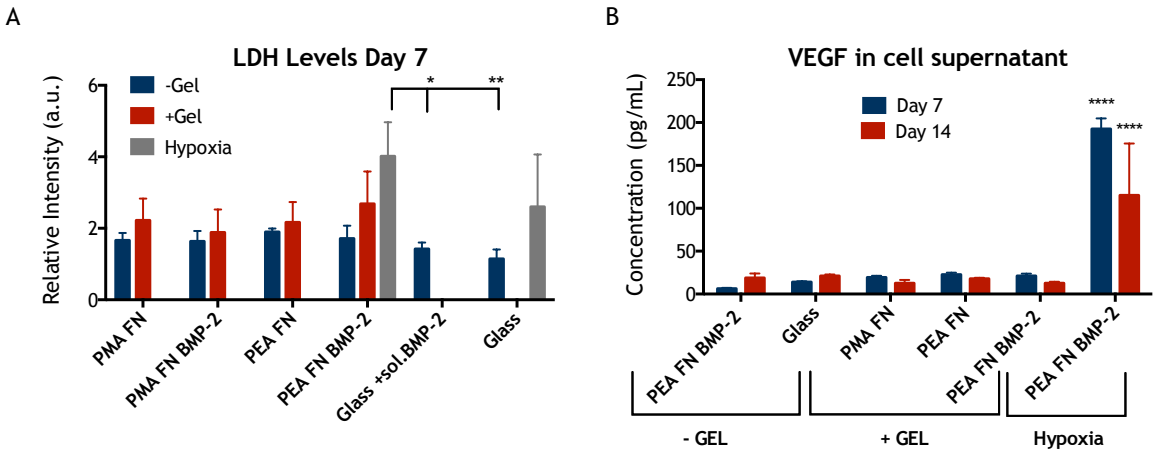

Figure 5-7 Analysis of HIF1α downstream targets LDH and VEGF. A. LDH levels assessed after 7 days culture by in cell western analysis (n=4) . B. Cell supernatant was collected at day 7 and 14 and VEGF levels assessed using ELISA (n=3). Data reported as means ± SD. One-way ANOVA followed by Kruskal-Wallis test with multiple comparisons, *p<0.05, **p<0.001, ****p<0.0001. Data suggests both LDH and VEGF are increased in hypoxia, but no significant changes are observed in the -/+gel conditions.

A further downstream HIF1α target is VEGF, to assess changes in levels an ELISA was carried out on cell supernatant collected at both 7 and 14 days (Figure 5-7B). As expected, a significant increase in VEGF was observed in PEA FN BMP-2 hypoxia, where VEGF levels were increased ~30-fold compared to PEA FN BMP-2 -gel. VEGF levels in -gel, +gel and glass conditions were comparably low, ranging from ~5 - 26 ng/mL.

5.3.2 Hypoxia gradient analysis

To distinguish whether the increasing HIF1α levels observed in the conditions with low-stiffness gels was due to a potential oxygen gradient at the interface, Hypoxyprobe™ was used. Hypoxyprobe™ (pimonidazole hydrochloride) indirectly measures cellular hypoxia, by forming thiol adducts with proteins. The probe can only bind at pO_2 < 10 mmHg (1.4% oxygen), these adducts can then be detected using an anti-pimonidazole antibody (Genetos et al., 2010).

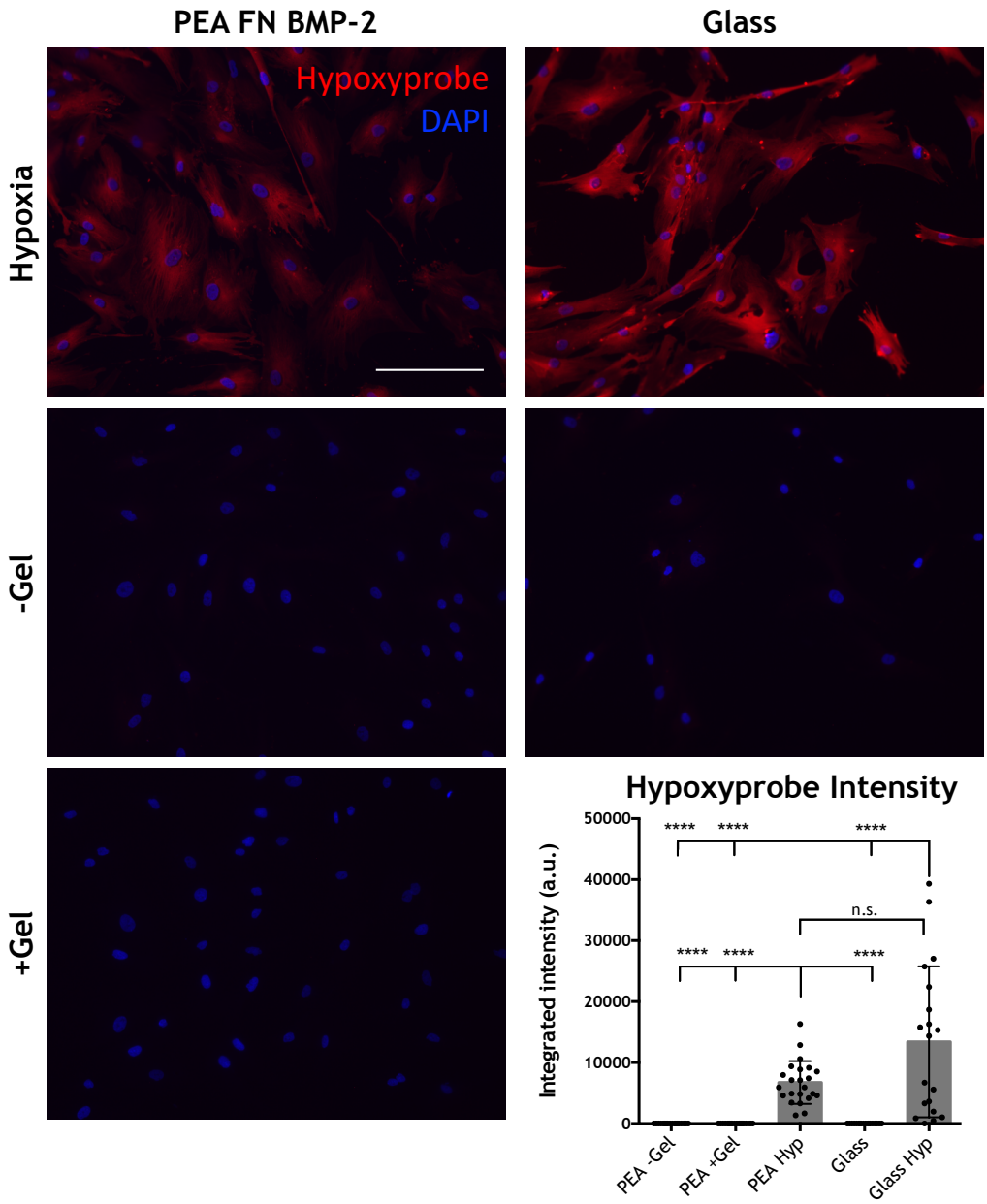

Figure 5-8 Hypoxia gradient analysis. Hypoxyprobe™ forms antibody-detectable adducts in cellular proteins at 1.4% oxygen, positive detection was observed only in hypoxia, not with low-stiffness gel addition (+Gel). Red is Hypoxyprobe™, blue is DAPI, scale bar is 100 μm. Integrated intensity of Hypoxyprobe™ for immunofluorescence images shown on graph, bar is mean ±SD, each point represents 1ximage field/number nuclei, n=4. **** $p< 0.0001$, n.s. = non-significant; by one-way ANOVA followed by Kruskal-Wallis test with multiple comparisons.

Immunofluorescence analysis revealed positive staining in the conditions in hypoxia (PEA FN BMP-2 and glass, $p<0.0001$), with no positive detection of the probe in PEA FN BMP-2 or glass +/- gels (Figure 5-8). Indicating the polymer/gel interface does not generate a local hypoxia gradient.

5.3.3 Analysis of the cell metabolome in response to material mechanics and hypoxia

To gain further insight into the effects of the HIF1α regulation exhibited in the different niche models, analysis of the entire cell metabolome was carried out by LC-MS. The abundance of each metabolite detected (peak intensities) was then subject to PCA (Figure 5-9). In Figure 5-9, differences in the entire metabolome for each condition (n = 3 or 4, where one replicate of PEA FN BMP-2 +gel 7d was excluded from analysis due to inconsistent ion chromatograms) are represented in a two-dimensional space composed of the principle component (PC) vectors PC1 and PC2. Figure 5-9A represents analysis at 7 days, and Figure 5-9B at 14 days, in which PC1 represents 40.7% and 20.5%, and PC2 represents 15.1% and 17.8% of the observed variance between conditions, respectively. The projection of substrate conditions onto PC1 and PC2 separates their metabolic signatures into distinct clusters. Clustering at both time points is relatively similar, with conditions with low-stiffness gels (+gel) forming a distinctly similar clustering pattern, regardless of underlying polymer or presence of GFs. Whereas, the glass, glass +sol.BMP-2 and PEA FN BMP-2 conditions -/+ hypoxia show similar clustering in PC1, but can be distinguished in PC2 at both time points. +gel conditions are distinct at both time points in PC1, but in PC2 they cluster at the intersection between the -/+ hypoxia conditions, suggesting metabolic properties that are both distinct to the presence of the gel, but also share some similarities with both normoxic and hypoxic signatures.

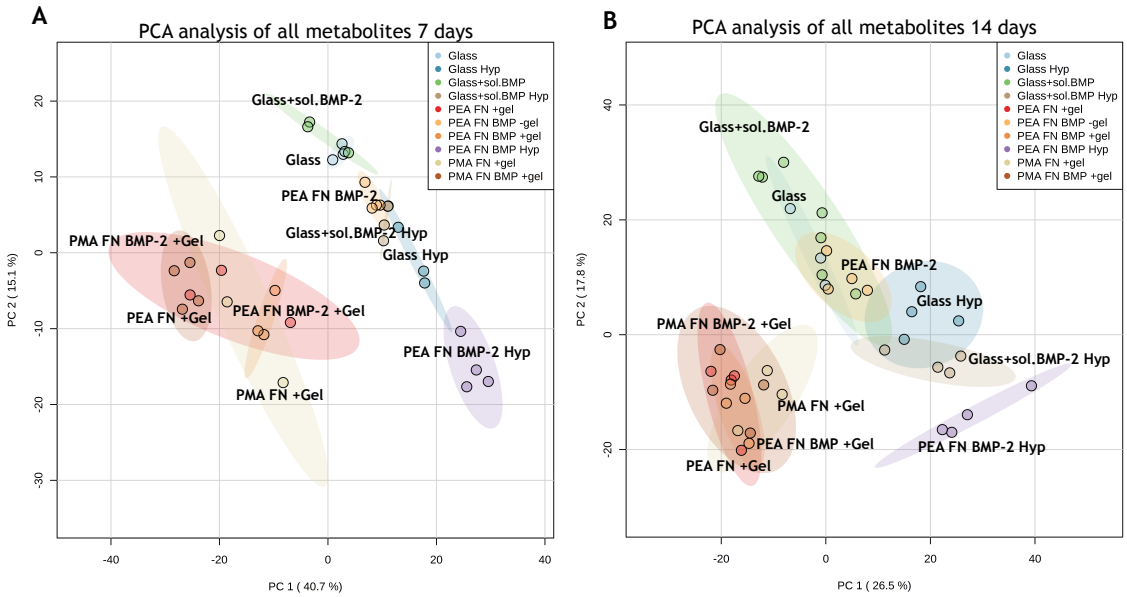

Figure 5-9 Principle component analysis (PCA) of entire metabolome in all niche systems. Pericytes were cultured in niche systems for 7 and 14 days, and all detectable metabolites were subject to PCA. Each point represented 1 replicate (n=4 or 3 where 1 failed sample was removed), ellipses represent the spatial borders associated with each condition with a 95% confidence interval. Data shows similar clustering at both time points, with all +gel conditions clustering, and hypoxia and -gel clustering closely in PC1.

To better consider these effects, PEA FN BMP-2 -/+gel/hypoxia conditions were subject to PCA. Analysis of the entire cell metabolome at each time point, this time including a third PC (PC3), presented a similar trend. Where +gel conditions exhibited more similarities to hypoxic counterparts in PC1 and PC3, and to -gel in PC2 (Figure 5-10A).

The identified metabolites were then filtered based on pathway. As HIF1α primarily regulates adaption to anaerobic respiration, metabolites involved in glycolysis and OXPHOS were analysed. Figure 5-10B shows the PCA of these filtered results, where +gel clustering appears more similar to hypoxia in PC1 (50.3%), and intermediate of hypoxia/normoxia in PC2 (26.7%) and PC3 (10.8%).

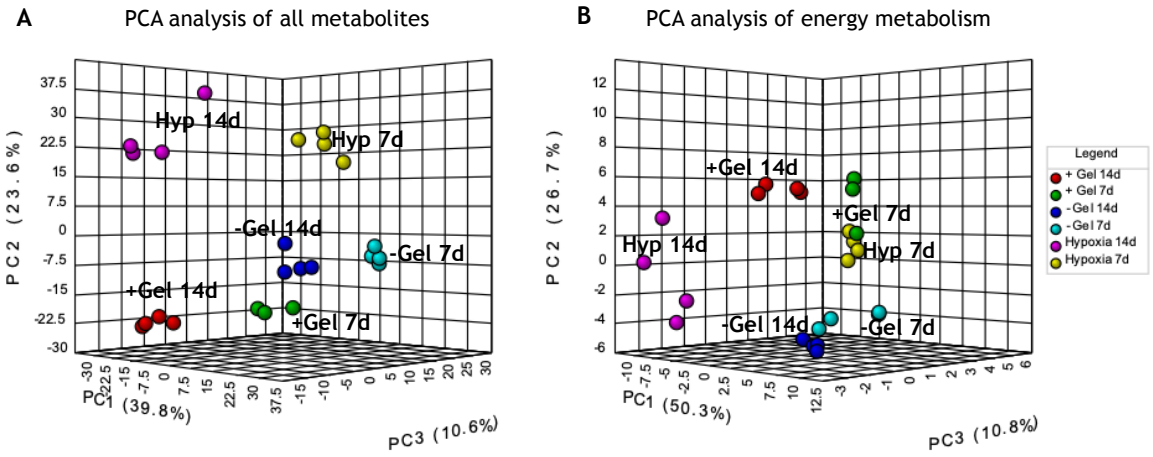

Figure 5-10 PCA of PEA FN BMP-2 conditions. Pericytes were cultured in PEA FN BMP-2 -gel/+gel/hypoxia niche systems for 7 and 14 days. A. All detectable metabolites and B. identified metabolites involved in energy metabolism were subject to PCA. Each point represented 1 replicate (n=4 or 3 where 1 failed sample was removed). Both plots show distinct clustering based on system and time point, PC1 separates both time points, whereas PC2 separates system condition. In both A and B, hypoxia and +gel show similar clustering in PC1.

To observe what these similarities/differences in energy metabolism were at the pathway level, a heatmap of individual metabolite abundance was generated from the filtered list. In Figure 5-11 assessment of individual metabolite abundance revealed an increase in metabolites associated with glycolysis in hypoxic samples, and an increase in the TCA cycle metabolites in-gel conditions. The PEA FN BMP-2 +gel conditions showed a similarly low regulation of glycolytic metabolites to –gel, however there was also down regulation of TCA cycle metabolites - similar to the regulatory pattern observed in hypoxia. This suggests that the addition of the low-stiffness gel promotes a degree of glycolytic adaption, where glycolysis is not up regulated, but the TCA cycle appears to be down regulated.

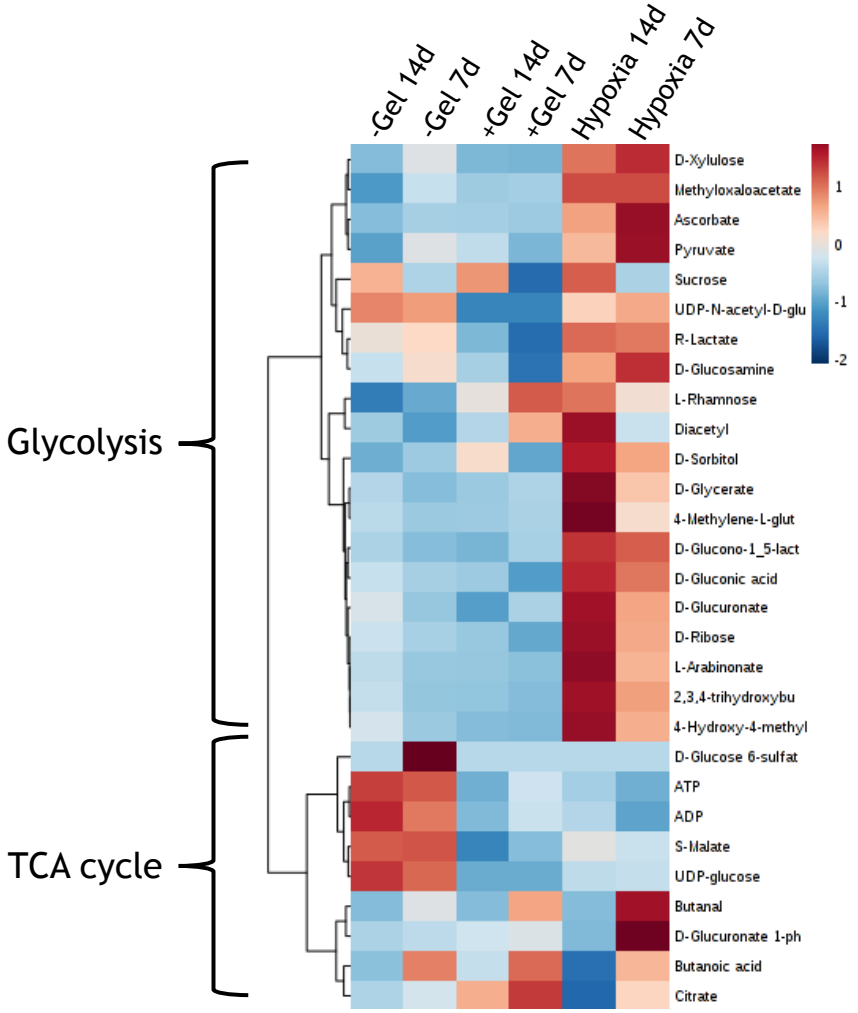

Figure 5-11 Glycolytic and TCA cycle metabolite profile in PEA FN BMP-2 -gel/+gel/hypoxia. Heatmap shows group averages of log transformed peak intensities of each replicate at 7 and 14 days. Hypoxia related metabolites show increased abundance (red) in PEA FN BMP-2 hypoxia 7 and 14 days, whereas TCA cycle metabolites are increased in PEA FN BMP-2 -gel 7 and 14 days. PEA FN BMP-2 +gel conditions show no increase in hypoxia, but similar down regulation of TCA cycle associated metabolites as for hypoxic samples. N =3 for +gel 7 d, n=4 for all other samples. Clustered through average linkage.

5.3.4 Flux of heavy glucose in glycolysis

To further investigate changes in cellular metabolism in pericytes in response to different niche systems, we used MS to follow the conversion of ^{13}C-labelled glucose. To investigate differences between the effects of gels and hypoxia we assessed only PEA FN BMP-2 -gel/+gel/hypoxia samples. Cells were cultured in standard 2% DMEM for 3 days followed by 3 days incubation with ^{13}C-glucose containing media. As illustrated in Figure 5-12 pericytes cultured in hypoxia and +gel significantly increased glucose uptake compared to -gel. As expected, hypoxia then led to significant increases in lactate and pyruvate production to -gel, although, interestingly a similar trend was not observed in +gel for these downstream metabolites. This is interesting and indicates that while there is

increased glucose uptake, it agrees with trends in Figure 5-11 where glycolysis does not appear to be enhanced but, importantly, neither does TCA (no TCA intermediates were labelled). It is tempting to suggest that respiration is just slowed as cells become more quiescent, and in slowing, the cells accumulate more glucose but don't use it.

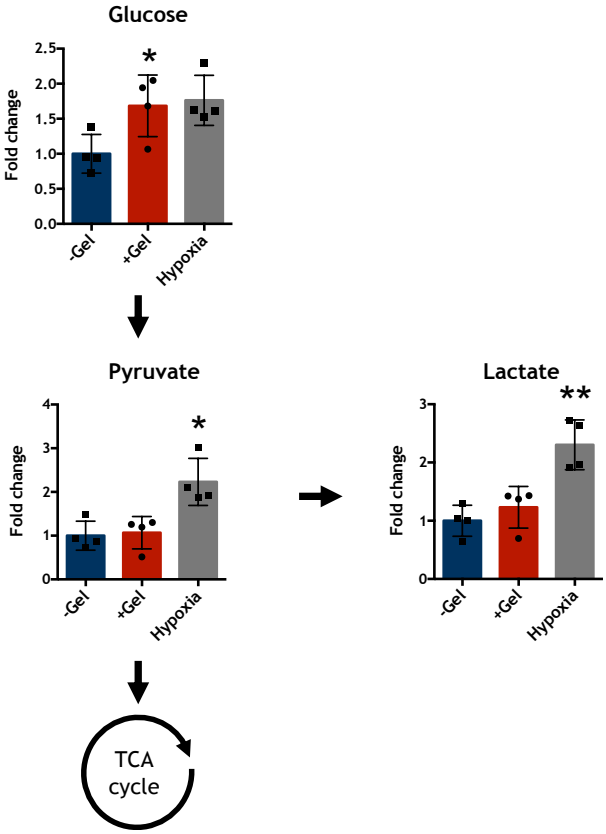

Figure 5-12 $^{13}C_6$-Glucose metabolomic tracing. Pericytes were seeded for 7 days in PEA FN BMP-2 niche systems in the presence of $^{13}C_6$-glucose for 72h. LC-MS was then used to measure the conversion and abundance of $^{13}C_6$-labelled metabolites in the glycolysis pathway. Graphs show a fold change relative to $^{13}C_6$-labelled metabolites in pericytes cultured in the PEA FN BMP-gel system. Graphs show means ± SD, n=4. One-way ANOVA followed by Kruskal-Wallis test with multiple comparisons to -gel control, *p< 0.05, **p<0.001.

5.4 Discussion

The aim of this chapter was to investigate whether the maintenance of pericyte phenotype by low-stiffness gels was due to similarities in metabolic programmes utilised in hypoxia. The *in vivo* BM niche exhibits low oxygen tensions, to which stromal and haematopoietic stem cells adapt through a specific response primarily controlled by HIFs.

5.4.1 HIF1α increases with gel addition

Hypoxia is known to affect MSPC self-renewal capacity. Basal HIF1α levels are upregulated in MSCs in normoxia compared to established tissue-specific cell lines (Palomäki et al., 2013). However, this effect will dissipate with long term culture as self-renewal capacity is lost in standard normoxic cell culture conditions (~20% O_2).

In the BM niche, hypoxia is thought to maintain enhanced glycolysis in MSPCs and HSCs via HIF1α (Ejtehadifar et al., 2015; Mohyeldin et al., 2010). HIF1α promotes the expression of glycolytic enzymes such as pyruvate dehydrogenase kinase (PDK1, 2 and 4), which prevents pyruvate from entering the TCA cycle and thereby inhibiting OXPHOS (Weidemann and Johnson, 2008). In Figure 5-5 we show that HIF1α transcript levels are increased at 7 days in all PEA/PMA conditions that are cultured with low-stiffness gels, this suggests the soft environment supports the stem cell-like phenotype characterised by stabilisation of the protein. Interestingly, in conditions cultured in hypoxia HIF1α expression was observed to be down regulated, however PDK1 was increased in hypoxia and small increases were observed in PEA/PMA +gel conditions, but not -gel.

During periods of prolonged exposure to hypoxia, transient HIF1α activation has been observed (Forristal et al., 2010); HIF1α activates an auto-negative feedback loop to avert over accumulation, in which PHD2 and 3 expression is induced by HIF1α, leading to stabilisation of its levels (Marxsen et al., 2004), and PHD2 (*EGLN1*) transcript levels were observed to be increased in Figure 5-5. Factor inhibiting HIF (FIH, *HIFA1N*) is a further factor regulating HIF1α post-translationally, however no changes in transcript levels were observed (Figure 5-5). HIF1α is also subject to other post-translational modifications, such as oxygen independent pathways, as such, transcript level analysis of HIF1α can often be an unreliable marker for assessing its activity (Dengler et al., 2014).

Consequently, we then investigated HIF1α protein levels in Figure 5-6, where a similar trend was observed to the RNA-seq data. A significant increase in active HIF1α in the conditions with a gel was observed. We confirmed this effect is non-pericyte specific, as the same trend was observed in MSCs (Appendix Figure 7-2).

Hypoxyprobe™ staining revealed this effect is not due to an oxygen gradient presented at the gel/material interface (Figure 5-8), suggesting this response could be related to matrix mechanics sensing, where soft-ECM leads to increased stem cell niche-like HIF1α activation.

Analysis of downstream targets such as HIF1α-controlled VEGF production and glycolytic enzyme LDH levels showed up-regulation at both transcript (Figure 5-5) and protein levels only in hypoxia (Figure 5-7). LDH mRNA expression was increased in PEA FN BMP-2 hypoxia and glass hypoxia conditions, though at the protein level this trend was only significant in PEA FN BMP-2 hypoxia to glass and glass +sol.BMP-2 (p<0.005, p<0.05) (Figure 5-7). This could be due to a low level of maintenance of stem cell metabolic phenotype in the other conditions at 7 days and hence maintenance of increased LDH protein, as regardless of the substrate there was a slight trend towards higher levels in conditions with gels. However, in the future, a more suitable method to investigate this would be an LDH enzyme activity assay, rather than gene or protein level analysis, as protein levels may remain similar whilst enzyme activity regulated or increased.

That HIF1α mRNA and protein levels are not elevated in hypoxia, but the response programme it initiates is still active (Figure 5-7 and Figure 5-11). This suggests its regulation in response to prolonged/chronic hypoxia. As illustrated in both untargeted and targeted metabolomic analysis, the up regulation of metabolites involved in the glycolytic pathway, such as lactate and pyruvate, in the hypoxic conditions also confirms the hypoxic anaerobic glycolysis response was active (Figure 5-11 and Figure 5-12). It is likely no significant increase in active HIF1α levels were observed at the protein level in hypoxia due to this negative feedback loop leading to HIF1α-levels cycling.

The elevated HIF1α phenotype is important for stem cell maintenance as it drives the glycolytic metabolic profile associated with self-renewing stem cells in the BM niche. In MSCs, HIF1α translocation to the nucleus is mediated by a motor adaptor protein, Bicaudal D homolog 1 (BICD1). BICD1 interaction with HIF1α is regulated through the Akt/GSK3β pathway, in which hypoxia-inactivation of GSK3β is induced by Akt, resulting in increased interaction between BICD1 and HIF1a (Beitner-Johnson et al., 2001; Deguchi et al., 2009; Lee et al., 2018).

Interestingly, Akt activation has been linked to increased nestin expression in several types of cancer stem cells (Z. Chen et al., 2014; Hambardzumyan et al., 2008; Matsuda et al., 2017), taken together with results from Chapter 4 this pathway could be investigated as a potential mechanism for supporting this niche-like metabolic phenotype with low-stiffness gels.

5.4.2 Gel addition down regulates TCA cycle

Our group has previously studied the effects of physical microenvironment properties, such as matrix stiffness and nanotopography, on cellular metabolism (Alakpa et al., 2017a, 2016; Tsimbouri et al., 2012). In these studies it was shown that pericytes grown on top of gels of varying stiffness showed distinct metabolic signatures, with high percentages of variance observed in carbohydrate, amino acid and lipid metabolism pathways (Alakpa, 2014). Similarly, here the global analysis of the cellular metabolome for all conditions revealed distinct clustering patterns, with most apparent differences observed between the presence of low-stiffness gels or hypoxia, rather than the chemistry of the underlying substrate (PEA/PMA/glass) or availability of GFs (Figure 5-9), suggesting the significance of the mechanical environment.

To assess if the HIF1α regulation we observed with the addition of gels was promoting a hypoxic-like metabolic profile, a list of metabolites involved in glycolysis and the TCA cycle was generated. PCA presented a similar pattern of clustering for this metabolic pathway as had been observed in PCA of the entire metabolome, with +gel clustering midway of hypoxia and –gel conditions (Figure 5-10B). Here we chose to focus analysis on only PEA FN BMP-2 -gel/+gel/hypoxia samples, in order to direct the comparison of hypoxic and low-stiffness environments. Analysis of individual metabolite abundance illustrated where similarities in metabolism lay. Figure 5-11 highlights the pericytes in +gel conditions do not appear to up regulate glycolysis but instead suggests repression of mitochondrial OXPHOS in a way that is similar to those in hypoxic conditions. This metabolic signature closely resembles the Warburg effect. First identified in cancer cells, it describes a method of energy production in which glycolysis is induced and mitochondrial OXPHOS repressed in normoxic conditions (Warburg, 1925), often referred to as oxidative glycolysis. It is suggested this enables more efficient conversion of glucose into biomass rather than ATP, supporting the

characteristic rapid proliferation of cancer cells. This shift is perhaps counterintuitive in fast-growing cancer cells, as oxidative glycolysis is less efficient than OXPHOS in terms of ATP production (the main source of cellular energy), however, this is predominantly problematic when glucose is deficient, whereas in the body or cell culture, glucose is in ready supply (Vander Heiden et al., 2009). It is thought that the Warburg effect is exhibited in MSPCs, and other stem cells, in order to preserve the beneficial effects of a predominantly glycolytic metabolic programme on maintenance of stem cell phenotypes (Ross et al., 2019).

To investigate this in more detail, we carried out heavy labelled glucose tracing. Interestingly, we found that the pericytes cultured in +gel conditions significantly increased their glucose uptake compared to -gel (Figure 5-12). However, this elevated consumption did not result in increased pyruvate and lactate production, as is characteristic of anaerobic glycolysis and as was predictably observed in the hypoxic samples. Increased glucose uptake is a hallmark of the hypoxic response, where the inhibition of OXPHOS results from hypoxic exposure and leads to a stimulation of glucose transport (Zhang et al., 1999). Increased glucose uptake is primarily through stimulation of transcription of glucose transporters (Glut) Glut1, Glut3 and Glut 4, which is activated through i. HIF1α activation leading to enhanced transcription, and ii. enhanced Glut transcription secondary to inhibition of OXPHOS (Zhang et al., 1999). Our RNA-Seq data suggested increased transcript levels of Glut1 (SLC2A1) in hypoxic samples, whereas Glut 3 and 4 were elevated in +gel conditions (Figure 5-5). Glut1 is the only Glut that retains enhanced transcription in response to chronic hypoxia, whereas 3 and 4 are initially expressed upon OXPHOS inhibition. This would need to be confirmed in future work by qPCR analysis, however may be suggestive of a hypoxic response similar to early hypoxic exposure in the gel samples, whereas those cultured in prolonged hypoxia show a response signature to chronic hypoxic exposure.

The heavy labelled glucose metabolomic analysis would have benefited from analysis of more glycolysis intermediates and TCA cycle intermediates; this would have provided deeper insight into the flux of glucose in the systems. However, these metabolites were unreliably detected, and hence future work would use more defined standards in LC-MS in order to better detect their abundance.

Overall, the metabolomic data presented the expected increased glycolytic response in the hypoxic niche system, -gel also presented expected increased OXPHOS more similar to the profile of actively differentiating cells. The +gel system appears to inhibit OXPHOS and increase glucose uptake, however we did not observe a similar increase in all glycolytic metabolites as observed for the hypoxic system. Hypoxic systems were exposed to chronic low pO_2 which presents a defined metabolic phenotype, the inhibition of OXPHOS in +gel conditions is suggestive of an oxidative glycolytic phenotype which presents some overlap with the response to chronic hypoxia, but may be more similar to early hypoxic exposure.

5.4.3 Summary

Taken together, the data presented in this chapter highlights a system where low-stiffness gels that maintain BM niche like MSPC phenotypes constitutively activate HIF1α, in a way that is dissimilar to exposure to chronic hypoxia (Figure 5-6). In response to hypoxia, elevation of glycolytic effectors, such as Glut1, is second to inhibition of OXPHOS, and our metabolomic data suggests pericytes cultured in +gel systems inhibit flux through the TCA cycle (Figure 5-11 and Figure 5-12). This could suggest a mechanism where the elevated levels of HIF1α in +gel niche systems are constitutively active in order to inhibit OXPHOS. This response is different to chronic hypoxic exposure, and may explain why hallmark downstream effectors, such as VEGF and LDH, are not elevated in the same way (Figure 5-7). Suggesting the +gel systems promote a 'pseudo-hypoxia/hypoxia-like' response in order to inhibit OXPHOS, which is beneficial for protecting self-renewing stem cells against DNA-damaging ROS produced as by-products from the TCA cycle. Or indeed, the pericytes in this system may be in a more quiescent state, and hence they do not need to meet the high energy demand produced via OXPHOS. To investigate this further a cell proliferation experiment should be carried out.

Further to this, to investigate in more detail how this pseudo-hypoxia is regulated at the pathway level, functional assays would be useful to distinguish activity levels of certain glycolytic and OXPHOS enzymes, as this will give a more accurate overview of metabolic activity than transcript or protein level analysis of the enzymes. Also of interest for future work would be investigation of the protein level and potential activity of the HIF3α subunit, as increased transcript levels

were observed in hypoxia and PEA +gel conditions (Figure 5-5). HIF3α has been shown to directly regulate HIF1α activity in ESCs, yet other studies have shown differing cell-type specific responses. Currently little evidence exists of the role of HIF3α in MSPCs, or the stem cell niche.

Chapter 6 HSC Co-Culture and Characterisation

6.1 Introduction

HSCs are the best-characterised population of ASCs, where individual stages of lineage commitment and differentiation have been characterised by surface marker expression (Seita and Weissman, 2010), illustrated in Figure 6-1. Their differentiation potential is hierarchal in structure, where lineage commitment leads to progressive loss of multipotency (Figure 1-6 and Figure 6-1) (Chao et al., 2008). The mammalian blood system contains more than 10 distinct mature cell types all derived from a common progenitor cell i.e. HSCs; including red blood cells (erythrocyte), megakaryocytes/platelets, myeloid cells (monocyte/macrophage and granulocytes), mast cells, T- and B-lymphocytes, natural killer (NK) cells and dendritic cells (Eaves, 2015; Zhang et al., 2018). However, despite the term self-renewal being prevalent in HSC literature, this process remains to be fully defined on a molecular level (Zon, 2008).

6.1.1 The HSC phenotype

HSCs were originally isolated from mice in 1988 by FACS using combinations of monoclonal antibodies to cell surface markers (Spangrude et al., 1988). Since then, a wealth of knowledge has formed through the use of functional readout assays and investigations of multiple combinations of cell surface markers, leading to the development of a well-characterised HSC hierarchy in humans (Figure 6-1) (Chao et al., 2008; Notta et al., 2011).

The first positive marker used to identify human HSCs was CD34, which is also expressed in non-haematopoietic endothelial cells (Krause et al., 1996). CD34+ cells constitute 0.5 – 5% of the total bone marrow and are the only cells to possess *in vitro* self-renewal capacity (Murray et al., 1995). However, the CD34+ cell population is itself heterogeneous, with 90 - 99% co-expressing CD38; these CD34+CD38+ cells are able to generate myeloid and lymphoid progeny but have lost clonogenic capacity (Hao et al., 1995). Whereas, CD34+CD38- cells show long-term repopulating potential and this phenotype has been employed routinely for several decades to identify HSC populations (Chao et al., 2008). Loss of CD34 expression is associated with uni-lineage differentiation (Civin et al., 1984;

DiGiusto et al., 1994). As the field has developed, further markers have been elucidated to characterise the different stages of haematopoiesis, the most common marker panels used to differentiate between HSCs and progenitor cells are shown in Figure 6-1.

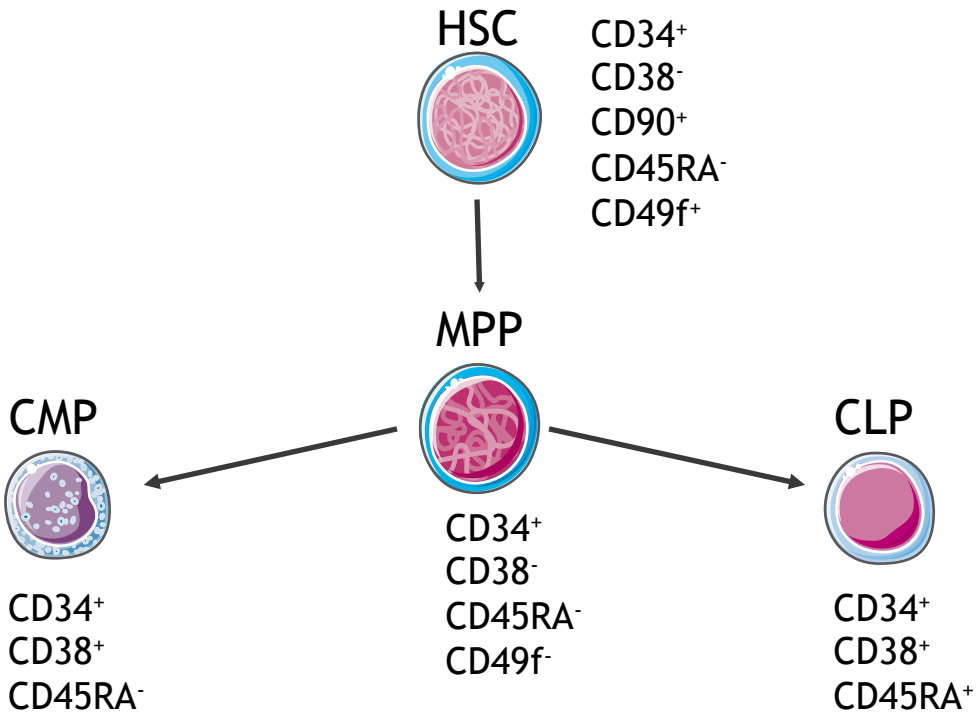

Figure 6-1 Surface markers associated with human haematopoietic stem cell (HSC) differentiation into lineage progenitors. Self-renewing HSCs differentiate producing multipotent progenitors (MPP), that will further commit to common myeloid progenitors (CMP) and common lymphoid progenitors (CLP) (Chao et al., 2008; Notta et al., 2011). This figure was created using Servier Medical Art, licensed under a Creative Commons Attribution 3.0 Generic License

It should be noted that although murine haematopoiesis reflects human haematopoiesis in many ways, the immunophenotypic markers of human HSCs (CD34+ CD38-) differ from functionally similar mouse counterparts (Larochelle et al., 2011). Mouse HSCs use a different set of markers to define HSC subsets. They use Lineage- (Lin-), Sca-1+ and c-Kit+ to identify the naïve HSC heterogenous population, followed by a combination of signalling lymphocyte activation molecule (SLAM) family receptors (CD150+ CD244- CD48-) markers to define the subsets, which have previously been associated with lymphocyte activation and proliferation (Kiel et al., 2005; Yilmaz et al., 2006). Whereas for human HSCs SLAM markers alone can be used to identify HSCs (Mikkola and Orkin, 2006).

6.1.2 HSC *ex vivo* culture

As discussed in Chapter 1.3.3.1 HSCs have been employed clinically for over 50 years (Aljurf et al., 2019). HSCTs are the gold standard treatment for many haematological disorders and have shown further promise in clinical trials for the treatment of autoimmune diseases (Radaelli et al., 2014). The multilineage differentiation capacity and ability to repopulate the entire blood system in recipients means the clinical relevance of these cells is enormous. Although, whilst HSCTs are currently routinely used for therapy the demand for donor HSCTs cannot currently be met. HSCTs require hosts to be heavily immunosuppressed, donor cells have to be closely immunologically matched to prevent graft-versus-host disease (Park and Seo, 2012) and the relative inability to expand naïve pluripotent HSCs in the laboratory (Kumar et al., 2017) means their true clinical potential remains to be fully realised.

HSCTs are life-saving, however insufficient numbers of HSCs in the graft is a common problem, leading to graft failure (Brunstein et al., 2010). This is a critical problem for both autologous and matched allogeneic HSCTs. Some clinical studies have attempted to increase success rates using grafts from multiple donors and have shown that even a 2- to 3-fold expansion would have great clinical impact (Boitano et al., 2010; Brunstein et al., 2010). As such, research has focussed on methods of *ex vivo* expansion of HSCs for clinical use, which itself has proved difficult. For *ex vivo* expansion, symmetric cell division is required, thus avoiding robust proliferation which ultimately leads to differentiation and apoptosis (Morrison and Kimble, 2006).

HSCs lose their self-renewal capacity when they are removed from their native niche (Jones and Wagers, 2008; Morrison and Scadden, 2014; Pinho and Frenette, 2019). The current gold standard culture conditions for HSC expansion use complex media formulations, the most common being serum-free supplemented with TPO, SCF, Flt3 ligand, G-CSF and IL-6 (interleukin-6) (Kumar and Geiger, 2017). This media is expensive and ineffective for long term maintenance; typically only leading to 2- to 4-fold expansions before differentiation and exhaustion of the stem cell pool, meaning inability to increase cell yield to clinically relevant levels (Patterson and Pelus, 2018). Thus, efforts have focussed on HSC expansion using other strategies such as genetic manipulation (Wang and

Rivière, 2017), small molecules (Zon, 2008) and to recapitulate aspects of the native niche using material engineering (Bello et al., 2018; Lee-Thedieck and Spatz, 2012). Methods such as these aim to produce clinically relevant yields of HSCs, and also allow investigation into functional mechanisms involved in important niche cellular processes.

6.1.3 Aims and objectives

The aim of this chapter is to investigate the potential of the developed BM niche systems for HSCs regulation. Analysis of surface marker expression using flow cytometry will be used to assess the ability of each model to support the HSC population, in terms of maintenance, expansion and differentiation.

Pericytes were seeded into the models and cultured for 14 days to allow robust response to the model components, or 'priming' time. At day 14, HSCs were added in three different media formulations; 100 % – full concentration of cytokines, considered gold standard HSC culture conditions, 10% – 10x dilution of cytokines and 0% – culture media containing no cytokines (detailed in Table 6-1). For the +gel conditions HSCs were seeded on top of the gel. After 5 days of co-culture the HSCs are removed for analysis by flow cytometry.

Then, to examine the impact of the different niche systems ability to maintain the long-term repopulating progenitors and potential impact on direct lineage specification, HSCs were sorted into long term culture initiating cell (LTC-IC) assays for 6 weeks (Liu et al., 2013), harvested and plated into colony-forming unit (CFU) assays for 5 days and resulting colonies counted. A schematic of the cell culture timeline is shown in Figure 6-2.

The LTC system assesses the ability of CD34+ cells capacity to initiate and sustain proliferation for long periods *in vitro* as a surrogate definition of self-renewing long-term repopulating cells (Sutherland et al., 1990). The assay provides the appropriate feeder layer, medium, supplements and culture conditions to support this. Already committed progenitors in the test sample will proliferate and die out due to clonal expansion. The resulting cells capable of long-term culture share functional and phenotypic properties with *in vivo* LT-HSCs, and are referred to as LTC-ICs. LTC-ICs are then added to methylcellulose semi-solid culture media to

assess their differentiation potential using a colony forming assay. This media contains all the necessary factors to allow progenitors to differentiate into all mature progenitor types which BM LT-HSCs can differentiate into. Therefore, using this assay we can quantify both the number of CFUs from the LTC-ICs and reveal any lineage bias in the expanded cells (Lemieux et al., 1995; Sutherland et al., 1990).

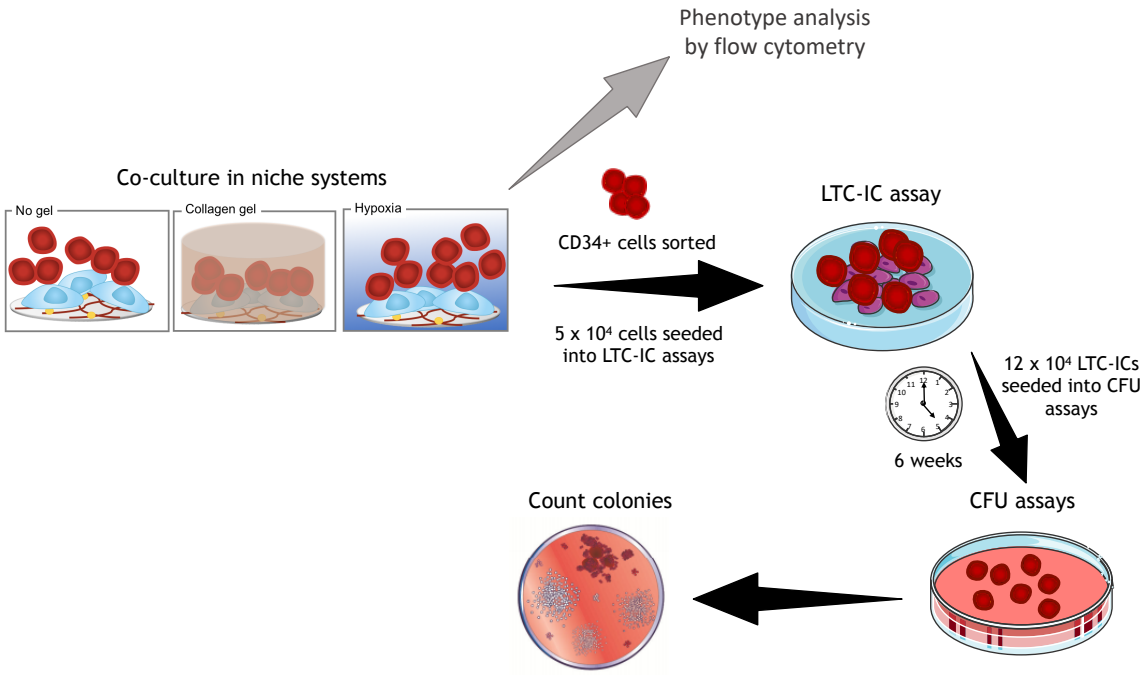

Figure 6-2 Schematic of HSC co-culture in niche systems. Pericytes were seeded for a 14 day priming period in niche systems. On day 14 HSCs were added and co-culture and maintained for 5 days. At day 5 cells were either subject to phenotypic analysis by flow cytometry, or CD34+ cells were sorted and seeded into long term culture-initiating cell (LTC-IC) assay, which were maintained for 6 weeks. LTC-ICs were then seeded into colony forming unit (CFU) assays and after 5 days colonies were counted.

6.2 Materials and Methods

6.2.1 HSC culture

BM HSCs were obtained from CalTag MedSystems, UK and stored in liquid nitrogen until required. To thaw cells, they were immediately placed in a 37°C water bath, transferred to a 15 mL falcon tube. 10 mL of pre-warmed IMDM+BIT media was added drop wise for the first 5 mL. The cell suspension was centrifuged for 10 mins at 400 g, and the cell pellet re-suspended in 1 mL. Cell counts were performed and the cell suspension was seeded into one well of a 24-well plate at $5x10^5$ cells/mL, and left to rest overnight in an incubator at 37°C and 5% CO_2 in 100% cytokine media (Table 6-1).

After overnight incubation, cells were recounted and seeded into the niche models outlined in Chapter 4, where a population of MSPCs had been cultured for 14 days. HSCs were seeded into the 24-well plated models at 5 x 10^4 cells/mL at 0.5 mL/well, in the appropriate media type (Table 6-1). For conditions containing gels the HSCs were seeded on top of the gel. Separate control wells with 5 x 10^4 cells/well in media only were also setup (cells only control). Seeded cells were then cultured for 5 days. At least 1 x 10^3 cells were transferred to an Eppendorf and subsequently phenotyped at day 0 using flow cytometry.

Table 6-1 HSC media formulations.

Media type	SCF (ng/mL)	TPO (ng/mL)	Flt3 (ng/mL)
100% cytokine	100	50	100
10% cytokine	10	5	10
0% cytokine	0	0	0

6.2.2 HSC phenotyping by flow cytometry

6.2.2.1 HSC flow cytometry staining

HSCs were harvested from niche systems after 5 days culture. Collagen gels were digested as in Chapter 2.3.1.3 and collagenase solution was added to all other conditions. Supernatants were passed through 70 μm filters and collected in 50 mL falcon tubes. Accutase™ was then added for 5-10 mins to detach cells and pooled into the same 50 mL falcon tube. Cells were centrifuged for 5 mins at 400 g and transferred to 96 well plates for staining. The antibodies used for staining are detailed in Table 6-2.

Table 6-2 Antibodies used for flow cytometry assessment of HSC phenotype

Fluorophore	Marker	Supplier
Am Cyan	CD45	BD Biosciences
PE	CD34	BD Biosciences
Cy7	CD38	BD Biosciences

6.2.2.2 Gating strategy and data analysis

Flow cytometry analysis of stained HSC phenotype was then carried out using BD FACS Canto II analyser. The gating strategy used for analysis is shown in Figure 6-3.

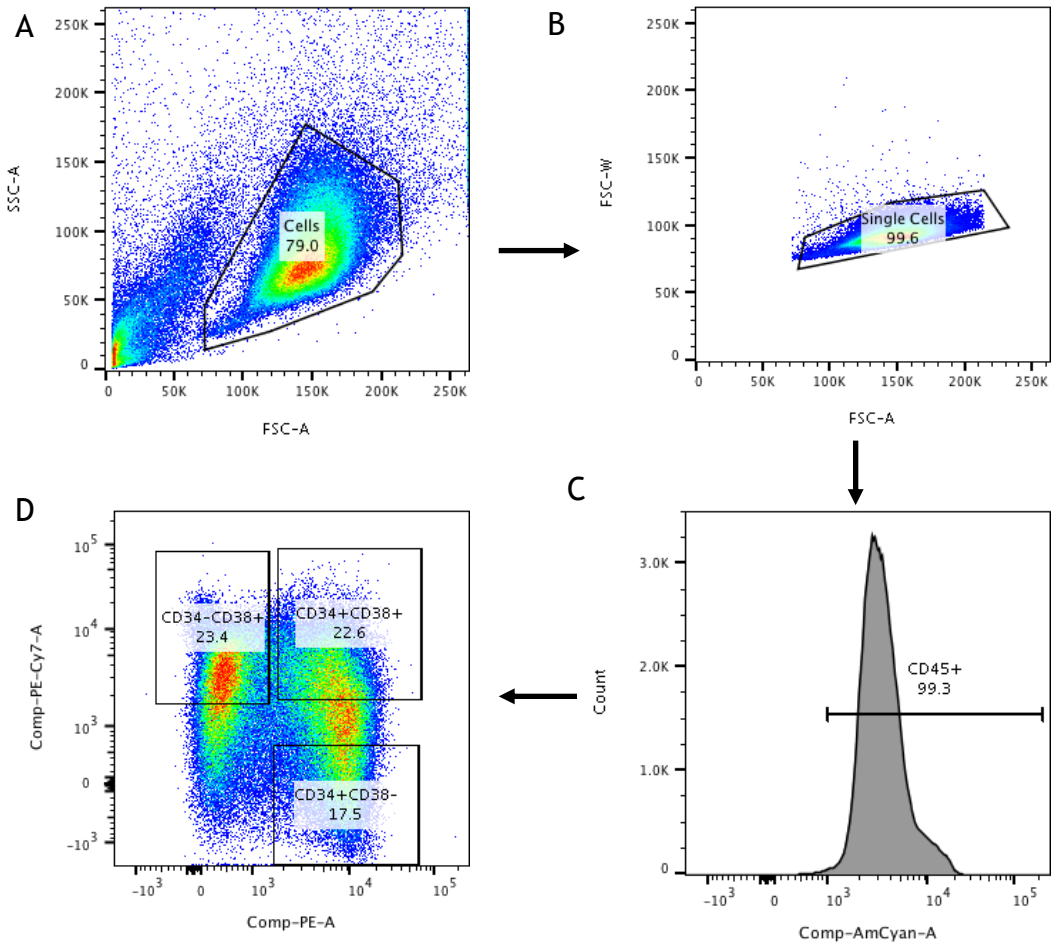

Figure 6-3 Gating strategy for analysis of HSC identification. Sample data taken from glass control. A. Forward scatter area (FSC-A) versus side scatter area (SSC-A) plot used to identify viable cells; B. FSC-A versus FSC width (FSC-W) plot used to identify single cells; C. A gate was added on CD45+ cells to remove any pericytes and D. 3 gates used to identify CD34+CD38 -, CD34+CD38- and CD34-CD38+. The CD34+CD38- population represents both LT- and ST-HSCs, whereas CD34+CD38+ and CD34-CD38+ populations represent HSPCs and committed progenitors.

6.2.3 LTC-IC

LTC-ICs were carried out on CD34+ HSC harvested from niche systems after 5 days. Engineered stromal fibroblast feeder layers were first established. M2-10B4 (overexpressing IL-3 and G-CSF) was maintained in RPMI containing 10% FBS, and Sl/Sl (overexpressing IL-3 and SCF) in DMEM containing 10% FBS, and were passaged at ~90% confluence. Cells were grown for 2 weeks prior to use in selection agents to select stromal cells expressing long-term cell maintenance factors (M2-10B4, 0.4mg/ml G418 and 0.06mg/ml Hygromycin B; Sl/Sl, 0.8mg/ml G418 and 0.15mg/ml Hygromycin B). On the final passage, cells at ~80% confluence were irradiated with 8000 cGy, trypsinised and counted. M2-10B4 and Sl/Sl were mixed at 1:1 ratio at a final concentration of $1.5x10^6$/ml. Cells were then seeded into

collagen coated 24-well plates (Stem Cell Technologies, UK) for 24 hours before adding CD34+ cells.

6.2.3.1 Cell sorting from niche systems

Collagen gels were digested as in Chapter 2.3.1.3, surfaces treated with accutase™ and cells collected from all niche systems after 5 days of pericyte-HSC co-culture. Populations were then stained with the antibodies detailed in Table 6-3.

Table 6-3 Antibodies used for cell sorting to LTC-IC.

Fluorophore	Marker	Supplier
PE	CD34	BD Biosciences
FITC	Lin-	BD Biosciences
Am Cyan	CD45	BD Biosciences
PE-Cy7	CD38	BD Biosciences

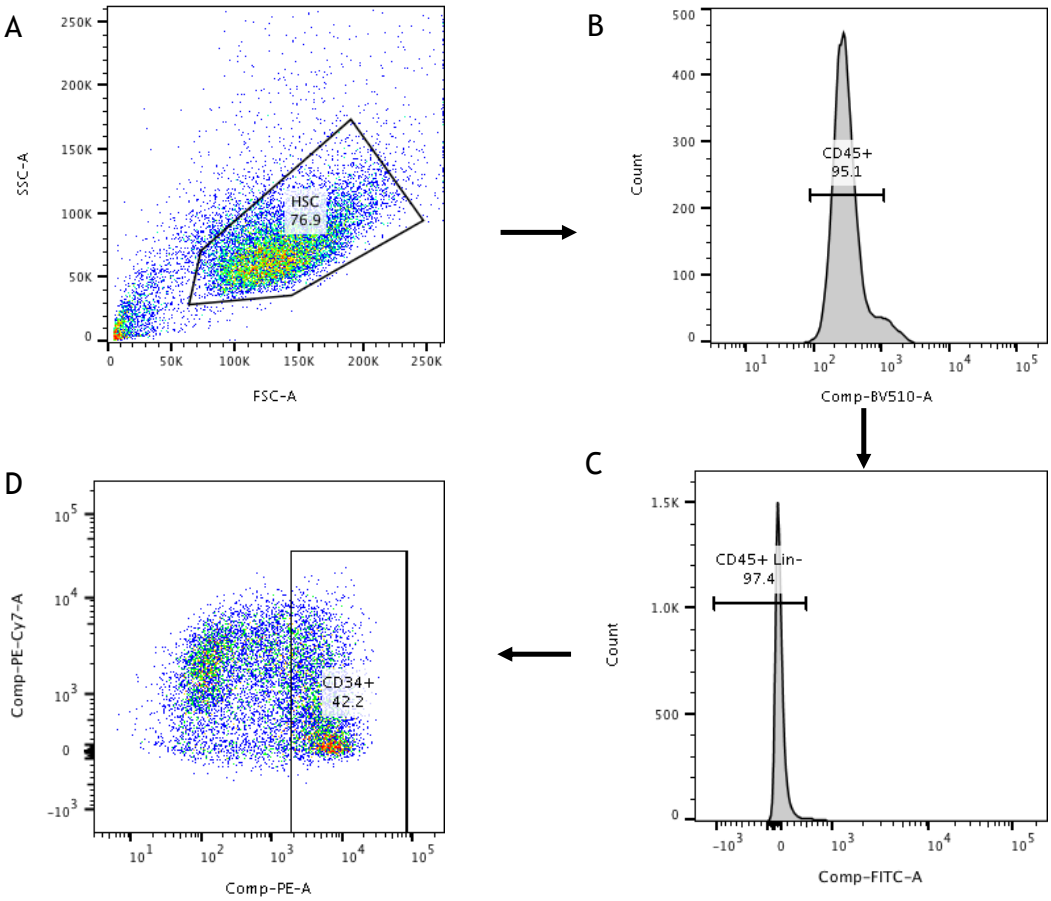

Figure 6-4 Gating strategy used for cell sorting for LTC-IC. Sample data taken from PEA FN BMP-2 -gel, patient 1. A. FSC-A versus SSC-A plot used to identify viable cells; B. Gate added on CD45+ cells to remove any pericytes; C. Lin- gate used to remove any committed progenitors and D. Gate added on CD34+ population, and these cells were collected and used in the LTC-IC assay.

BD FACSAria cell sorter (BD Biosciences) was used to sort single CD34+ cells by FACS. Lin- was used to remove any committed progenitors, CD45 to remove any pericytes and cells were selected based on CD34+ expression, the gating strategy used is represented in Figure 6-4. CD34+ cells were sorted into suspension and were resuspended at 5 x 10^4 cells/mL in HLTM+10^{-6}M Hydrocortisone (HC). Media was removed from feeder layers, and 5 x 10^4 CD34+ cells were seeded/well. Duplicates were seeded for each condition; when enough cells were unable to be collected in certain conditions, only single replicates were used. Cultures were then incubated at 37ºC in 5% CO_2 for 6 weeks. 0.5 mL HLTM was removed and 0.5 mL fresh HLTM+10^{-6}M HC added weekly.

6.2.4 CFU assay

To harvest cells from LTC-IC cultures after 6 weeks, HLTM was removed containing any non-adherent cells and added to a 5 mL sterile tube. Each well was then washed with 0.1 mL HBSS, then trypsin added for 5 mins at 37ºC in 5% CO_2. Once adherent layer had started to detach cells were resuspended and added to the 5 mL tubes. Wells were subsequently washed once with IMDM containing 2 % FBS and added to the appropriate tubes. Tubes were filled with IMDM with 2% FBS and centrifuged at 300 g for 8 mins. Supernatant was removed without disturbing the cell pellet, leaving 0.1 mL of medium. Cells were then counted, and 2.4 x 10^5 cells added to bijou tubes containing 2.5 mL of Methocult™. Bijoux tubes were briefly vortexed and left at RT for 5 mins to allow bubbles to dissipate. 1.1 mL from each tube was then plated into duplicate 35 mm culture dishes using a 3 mL syringe with a blunt needle. The 2 replicate dishes were placed within a 100 mm Petri dish containing a third 35 mm dish (without lid) containing 3 mL of sterile water. Cultures were incubated at 37ºC in 5% CO_2 for 5 days.

After 7 days total colonies were counted using a light microscope. Scores were taken for detection of classes of colonies, summarised in Table 6-4. Each CFU assay was counted by two independent researchers and an average taken. Averages were then plotted in graphs using GraphPad Prism 6.0 software.

6.3 Results

Flow cytometry analysis was used to determine whether our engineered niche systems could support LT-HSCs in culture. In brief, HSCs were added into 'primed' niche systems and co-culture was maintained for 5 days in the 3 different media types outlined in Table 6-1. CD34+ cells in 100% media on TCP were used as the control (cells only). At day 5 cells were harvested for phenotypic analysis, or further experimentation in the LTC-IC functional assays (Figure 6-2).

6.3.1 Low-stiffness gels reduce HSC/HSPC proliferation

Analysis of the CD34+CD38- population revealed that the addition of low-stiffness gels or hypoxia significantly reduced proliferation or expansion of this population when compared to the cells only control and PEA FN BMP-2 -gel, in all 3 media conditions (Figure 6-5). Both cells only and PEA FN BMP-2 -gel led to an increase of ~4- to 8-fold when compared to the number of CD34+CD38- cells input at day 0. Interestingly, in cells only, when cytokine concentration in the media was reduced there was a significant decrease in proliferation of this population. Whereas for the PEA FN BMP-2 -gel system the opposite is true – reducing cytokine concentration significantly increased CD34+ CD38- numbers, this was indistinguishable between 10% and 0% media. This data suggests that both the cells only control and the PEA FN BMP-2 -gel system cause robust proliferation or expansion of the CD34+CD38- population, whereas in the presence of low-stiffness gels or hypoxia, proliferation appears to be lowered.

Further to this, although not significant, a similar trend was observed in the PEA FN +gel and PEA FN BMP-2 +gel to PEA FN BMP-2 -gel in response to cytokine concentration in the media (Figure 6-5). In these conditions in 10% and 0% media, the CD34+ CD38- population appears to be maintained (i.e. 1-fold change), yet numbers slightly reduce in the presence of 100% cytokine concentrations. This suggests that in the presence of pericytes in the PEA systems, it is perhaps beneficial to reduce or remove the supplemented cytokines in the culture media (Figure 6-5).

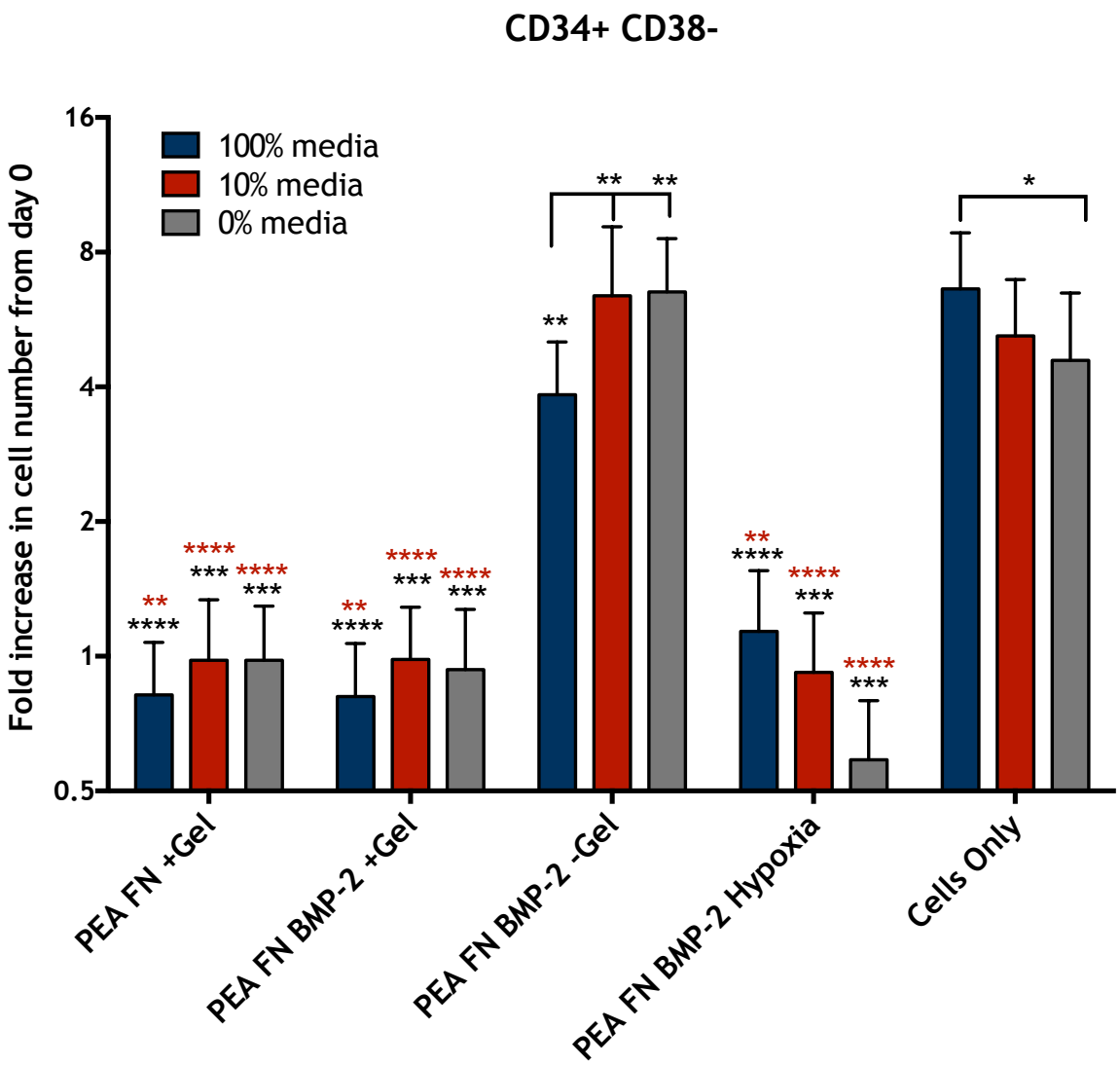

Figure 6-5 Fold increase of CD34+CD38- cells at day 5 in 3 media types. Data shows proliferation/maintenance of CD34+CD38- population, represented as a fold change to the number of CD34+CD38- cells added at day 0. Data shows that cells only control and the PEA FN BMP-2 -gel system lead to significant proliferation of this population. When in the presence of pericytes in the PEA systems, the addition of cytokines in the media is not beneficial to proliferation or maintenance of this population. Whereas the opposite is true for cells only. Data also suggests that the addition of low-stiffness gels does not induce proliferation, but instead leads to maintenance of the population. Graph shows mean ±SEM. N = 3, with 3 HSCs donors and one pericyte donor. Two-way ANOVA followed with multiple comparisons, Tukey's post-test, *= $p \leq 0.05$, **= $p \leq 0.01$, ***= $p \leq 0.001$, ****= $p \leq 0.0001$. Unless otherwise indicated, black * compared to cells only, red * compared to PEA FN BMP-2 -Gel.

We then analysed the CD34+ CD38+ subset to assess expansion of early committed progenitors (this population contains the CMP and CLP compartment) (Figure 6-6A). Similar to Figure 6-5, the PEA +gel systems in 0% media did not lead to expansion or proliferation of this population compared to starting numbers at day 0, but only when there were no additional cytokines in the media (Figure 6-6A). Addition of full (100%) or dilute (10%) media significantly increased proliferation of progenitors in the PEA FN BMP-2 +gel system. PEA FN BMP-2 -gel displayed a similar trend, with additional cytokines leading to increased proliferation of this

population, although this system also significantly increased the progenitor population when compared to +gel and hypoxia. Hypoxia was the only condition that significantly reduced the number of cells in this compartment. Overall, this data further suggests that removing or reducing cytokines in media when in PEA systems is beneficial, in that proliferation of this early committed population is reduced. However, only when in the presence of low-stiffness gels is the population maintained, as no significant expansion is observed (Figure 6-6A).

The CD34- CD38+ subset represents lineage committed cells with little/no progenitor activity remaining (Chao et al., 2008). We saw significant levels of proliferation of these cells in all PEA conditions except hypoxia, reflecting their highly proliferative nature (Figure 6-6B) (Passegué et al., 2005). Although proliferation was observed, similar results regarding supplemental cytokines were observed. In PEA FN BMP-2 -gel, PEA FN +gel and PEA FN BMP-2 +gel systems, there was a significant reduction in proliferation of this population when cytokines were reduced or removed. There were no significant differences between the +gel and -gel, however hypoxia and cells only systems had significantly lower numbers of cells in this population. This suggests that the mechanical environment does not directly influence this compartment, but that reducing or removing exogenous cytokines from the media helps to reduce its proliferation (Figure 6-6B).

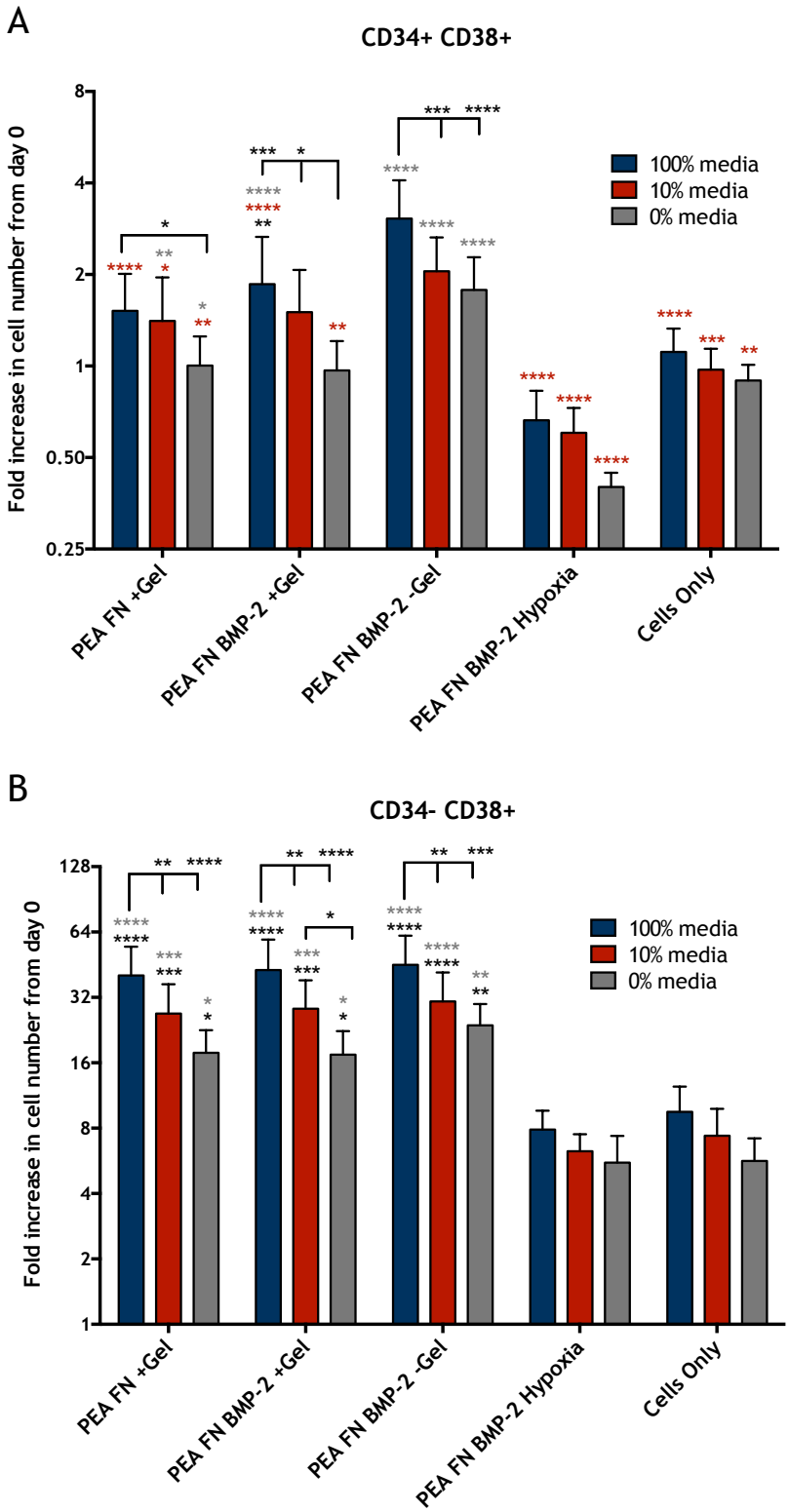

Figure 6-6 Fold increase of CD34+CD38+ and CD34-CD38+ cells at day 5 in 3 media types. 100% media leads to an increase in proliferation of early and committed progenitors in both (A) CD34+CD38+ and (B) CD34-CD38+ populations, when compared to 10% or 0% media. (A) demonstrates maintenance of this population in PEA +gel systems, but only when exogenous cytokines are removed from culture media. PEA FN BMP-2 -gel leads to proliferation of this compartment, yet this is also reduced in 10% and 0% cytokine media. (B) demonstrates expansion of this highly proliferative compartment in PEA -gel/+gel systems, however removal of cytokines from the media reduced significantly this expansion. Graph shows mean ±SEM. N = 3, with 3 HSCs donors and one pericyte donor. Two-way ANOVA followed with multiple comparisons, Tukey's post-test, *= $p \leq 0.05$, **= $p \leq 0.01$, ***= $p \leq 0.001$, ****= $p \leq 0.0001$. Unless otherwise indicated, black * compared to cells only, red * compared to PEA FN BMP-2 -gel, grey * compared to PEA FN BMP-2 hypoxia.

Overall, this data suggests that the PEA FN BMP-2 -gel co-cultures and the cells only control led to increases in fold changes of the number of the most phenotypically naïve cells identified by expression of CD34+CD38- (Figure 6-5). The PEA FN BMP-2 -gel system also influenced proliferation of both early progenitors (CD34+CD38+) and lineage committed cells (CD34-CD38+). However, when exogenous cytokines were removed from the media, the expansions were more favourable – that is increased CD34+CD38- (naïve compartment) (Figure 6-5), but reduced CD34+CD38+ and CD34-CD38+ (early and committed progenitors) (Figure 6-6). A similar trend was also observed for PEA +gel conditions, however these systems appeared to maintain the population rather than induce proliferation. The systems with gels maintained the CD34+CD38- and CD34+CD38+ populations similar to that input at day 0, however this was only when in the absence of supplemental cytokines, suggesting this system could be limiting cell proliferation thus maintaining - but not expanding - HSCs in culture (Figure 6-5 and Figure 6-6). The PEA FN BMP-2 hypoxia system displayed the lowest fold changes of all systems, displaying no proliferation or expansion in any compartment. This is in line with quiescent HSCs residing in hypoxic niches (Ito and Suda, 2014).

6.3.2 Low-stiffness gels support LT-HSCs

To assess the ability of these systems to maintain or expand functional LT-HSCs in culture, we carried out LTC-IC assays followed by CFU assays (outlined in Figure 6-2). These assays were carried out on PEA FN BMP-2 systems -/+gel in both 100% and 0% media types, with cells only in gold standard 100% media used as the control (Kumar and Geiger, 2017). Gold standard medium with 0% cytokines was also tested but insufficient cell numbers were obtained after LTC-IC to perform reliable CFUs. We selected these conditions as they showed the most pertinent changes in CD34+ subset numbers during co-culture, in the presence or absence of exogenous cytokines. Hereafter PEA FN BMP-2 -gel and PEA FN BMP-2 +gel will be referred to as -gel and +gel, respectively.

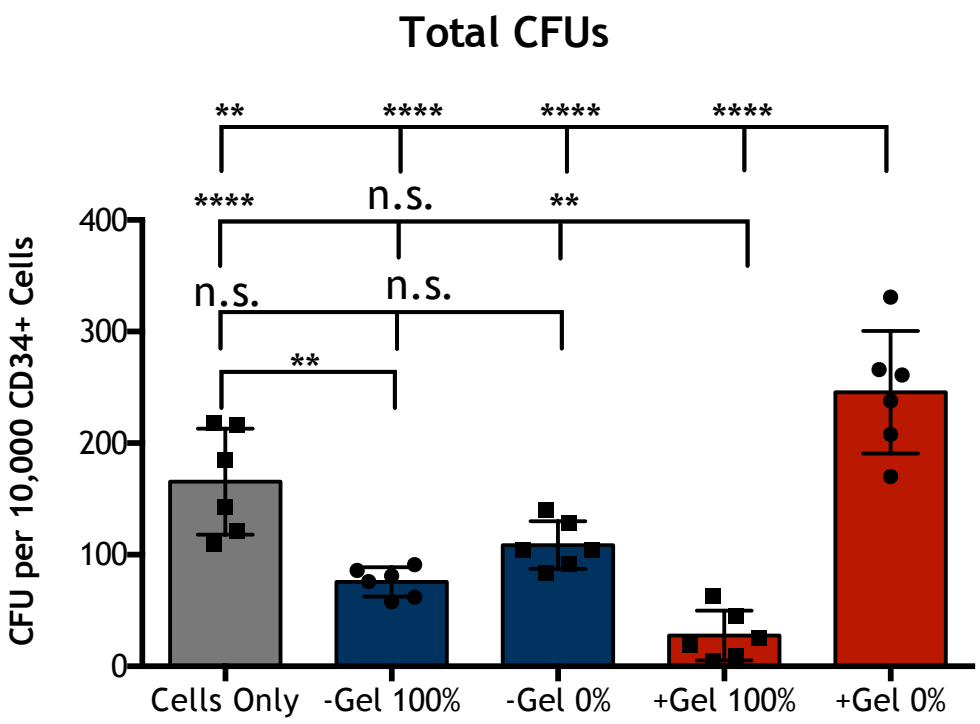

Figure 6-7 Total number of colonies maintained from niche systems. CD34+ cells were harvested from PEA FN BMP-2 -/+ gel niche systems after 5 days culture in 0% or 100% medias. CD34+ cells were then added to LTC-IC assays for 6 weeks and resulting LTC-ICs subject to CFU assay. Total number of colonies were counted and are represented as CFUs per 1 x 10^4 CD34+ cells. The resulting data indicates PEA FN BMP-2 +gel 0% media is able to maintain the highest number of CFUs. Graph shows mean ±SD. One-way ANOVA with Tukey's post-test with multiple comparisons, **= $p \leq 0.01$, ****= $p \leq 0.0001$, n.s. (non-significant). Data from 2 donors, n=3.

After transfer to methylcellulose, the total number of colonies were counted after 5 days to reveal the number of long-term repopulating, colony-forming cells that were present in the cell population used to inoculate the assay. The +gel 0% media significantly produced the highest average number of CFUs per 1 x 10^4 CD34+ cells (245 ± 55) (Figure 6-7). The total number of CFUs was significantly higher than that maintained by the cells only control in 100% media (165 ± 47). Interestingly, +gel 100% media led to a significant decrease in CFUs (28 ± 22), indicating the pericytes in the +gel system possess HSC maintenance activity that is dampened when high concentrations of cytokines are added (Figure 6-7). The -gel systems followed a similar trend, where more CFUs were observed in 0% (108 ± 21) compared to 100% media (75 ± 13), although this was significantly less than CFUs supported by +gel and by the control. This is in line with the data presented in Figure 6-6, where increase in the committed progenitor compartment was observed in 100% media conditions, and robust expansion of progenitor compartments is associated with loss of the naïve HSC compartment (Morrison and Kimble, 2006).

Progenitor lineage potential was further assessed from CFUs. Each CFU was identified by specific morphological features as one of the 6 colony types described in Table 6-4 and represented in Figure 6-8. Quantification of the number of colonies associated with discrete fate specification events allowed us to assess if there was a degree of lineage bias as a function of matrix environment and cytokine concentration. The colonies correspond to stages of myeloid, granulocytic and erythroid/megakaryocytic specification.

Table 6-4 Colony types counted in colony-forming unit assay

Abbreviation	Colony type	Represent
CFU-E	Colony-forming unit – erythroid	Late stage myeloid progenitors restricted to single lineage
CFU-G	Colony-forming unit – granulocyte	Myeloid progenitors restricted to single lineage
CFU-GM	Colony-forming unit – granulocyte, macrophage	Myeloid specification
BFU-E	Burst-forming unit -erythroid	Primitive erythroid progenitors
CFU-M	Colony-forming unit – macrophage	Late stage myeloid progenitors restricted to single lineage
CFU-GEMM	Colony-forming unit – granulocyte, erythrocyte, macrophage, megakaryocyte	Early stages of myeloid specification

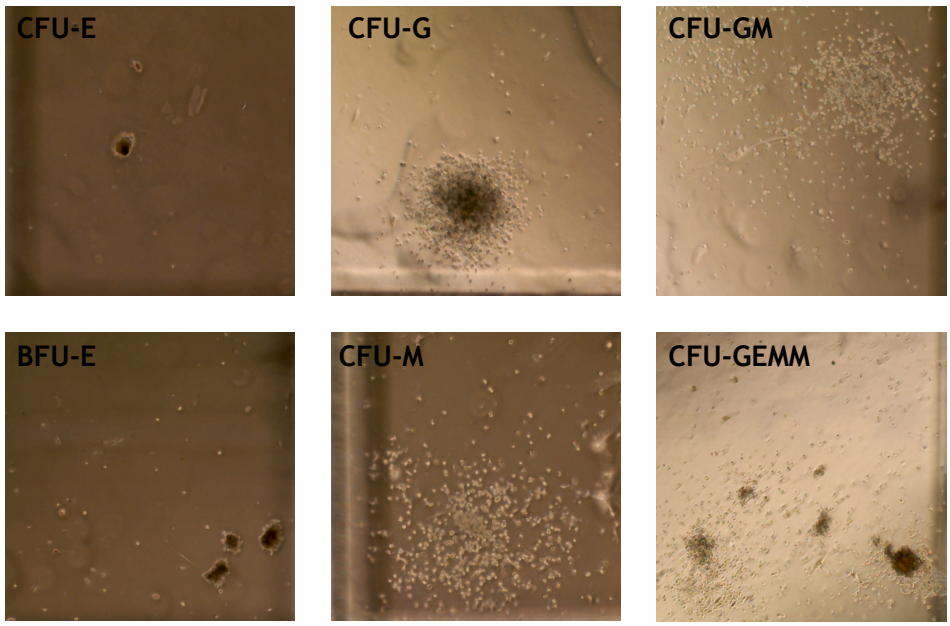

Figure 6-8 Representative colony types in CFU assay after 7 days. Cells harvested from LTC-IC assay were added to CFU assay, and colonies counted after 7 days. CFU-E; contain ~8-200 haemoglobinised erythroblasts. BFU-E; clusters of erythroid progenitors with high proliferative capacity. CFU-G; homogenous population of granulocyte progenitors. CFU-M; homogenous population of macrophage progenitors. CFU-GM; heterogenous population of macrophages and granulocytes. CFU-GEMM; multilineage progenitors that give rise to erythroid, granulocyte, macrophage and megakaryocyte lineages.

The cells only population represents a control distribution of lineage specification with each of the 6 lineage specifications represented (Figure 6-9). This distribution of specification is closely resembled only by +gel 0% media, which also retains specification for all 6 lineages. Whereas, +gel 100% media has lost all BFU-E colony forming capacity and shows an increase in CFU-Es compared to control and +gel 0% media. Both conditions -gel also show a marked decrease in BFU-E colonies. Similarly, to +gel 100% media, -gel 100% media shows increased specification to CFU-E (Figure 6-8).

Overall the CFU assays indicate that +gel 0% media is able to support LTC-ICs that also retain multipotency in terms of lineage specification comparable to the same capacity as the current gold standard media control.

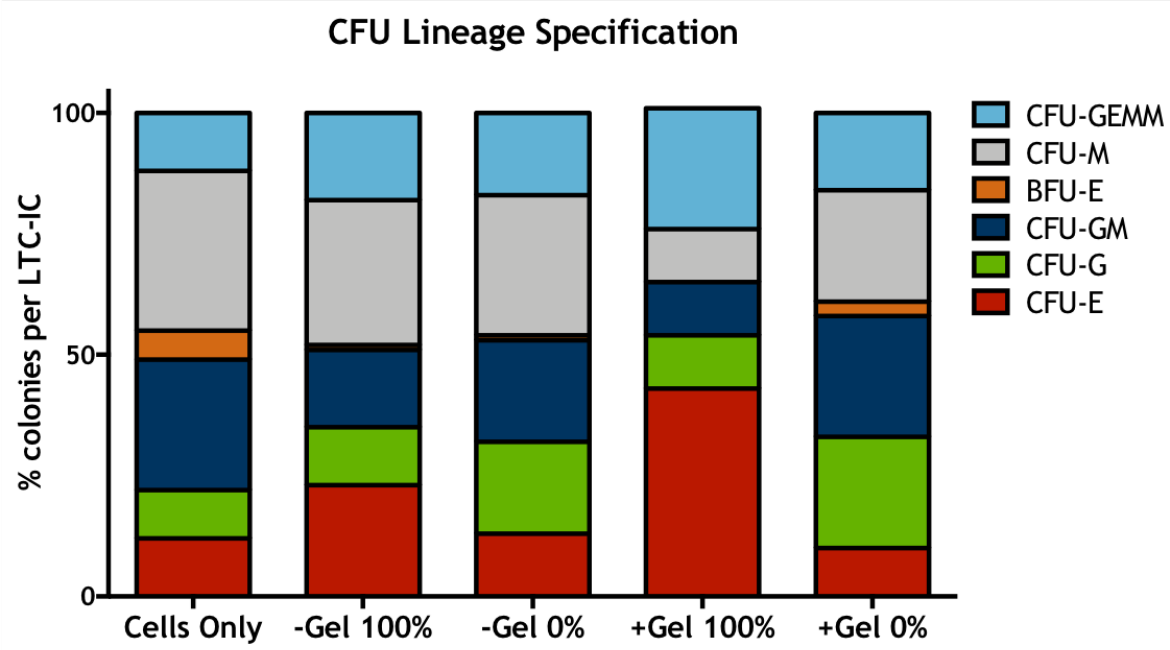

Figure 6-9 Lineage specification state of CD34+ cells cultured in niche systems. CFU assay was used to assess myeloid and erythroid lineage specification of the CD34+ cells cultured in PEA FN BMP-2 -/+gel niche systems in 100% and 0% cytokine medias. CD34+ cells cultured in 100% media were used as the control (cells only). PEA FN BMP-2 +gel 0% media (+Gel 0%) retains commitment to all lineages at similar distribution to the control. +gel 100% shows preference to CFU-E commitment and has lost BFU-E activity. Both -gel 0% and 100% similarly showed a decrease in BFU-E commitment. Data is represented as percentage (%) of total CFUs counted for each condition. 1 biological replicate, 3 technical replicates.

6.4 Discussion

This chapter investigated the response of HSCs co-cultured in the niche systems. The aim was to assess if the MSPC phenotypes observed in previous chapters to retain BM niche-like properties were able to support HSC activity.

6.4.1 PEA FN BMP-2 systems support proliferation (-gel) or maintenance (+gel) of the CD34+ CD38- population

Analysis of HSC phenotype by flow cytometry after pericyte co-culture revealed significant proliferation of the CD34+ CD38- population when cultured with pericytes seeded in PEA FN BMP-2 -gel systems and in the cells only control (Figure 6-5). Whereas in PEA +gel and hypoxic systems the population was maintained at numbers similar to those input at day 0. This proliferation with pericytes on PEA -gel is consistent with previous work using adipose-derived CD146+ pericytes as a feeder layer to successfully expand CD34+ cells *ex vivo* (Corselli et al., 2013). This 2013 study highlighted that the pericytes, which expressed key niche markers such as CXCL12 and nestin, were able to support human Lin- CD34+ cells in long-term culture that retained CFU activity. This was significantly higher than CD146- MSCs which had lost all CFU capacity by week 6, suggesting that within heterogeneous populations of MSCs the ability to support HSCs may be confined to the CD146+ perivascular cells. This is consistent with previous observations from our group that used a similar PEA+GF based system to co-culture HSCs with Stro1+ MSCs (Sweeten, 2019). After co-culture with Stro1+ MSCs, large degrees of variability were observed between patient samples upon analysis of HSC phenotype, which could be explained by populations of Stro1+ MSCs that may retain CD146+ expression (Lv et al., 2014; Tormin et al., 2011).

Interestingly, proliferation of the CD34+ CD38- population was significantly increased on PEA FN BMP-2 -gel when cytokines supplemented in the media were reduced (10%) or removed (0%) (Figure 6-5). A similar trend was observed in the PEA +gel systems regarding maintenance of the population (Figure 6-5). Whereas the opposite was observed in the cells only control, removing cytokines decreased proliferation. Although it should be noted, although proliferation was reduced, the cells only control was able to support relative expansion of both CD34+ CD38- and CD34- CD38+ populations even in the absence of maintenance cytokines (Figure 6-5 and Figure 6-6). This was unexpected as it is well accepted in the field that HSC culture requires complex media formulations. However after the LTC-IC assay, insufficient cell numbers were obtained to perform CFU assays, indicating the supplemented GFs are required to support the LT-HSC population. The length of culture for this system may also help explain this observation, as perhaps 5 days is too short to significantly effect HSC behaviour in these conditions, and a longer

time in culture would be required to observe phenotypic changes in response to absent cytokines.

We then went on to investigate the differentiation state of these cells by analysing both the CD34+ CD38+ and CD34- CD38+ populations. CD34+ CD38+ cells still retain differentiation capacity in accordance with the HSC hierarchy (Figure 6-1) whereas this capacity is lost in the CD34- CD38+ population. Interestingly, analysis of these compartments also revealed in the PEA -/+gel systems, it is favourable to remove exogenous cytokines from the media (Figure 6-6). These populations are highly proliferative but lack long-term functionality, hence reduced proliferation or expansion of them is desirable. The 0% PEA +gel systems maintained the CD34+ CD38- population, and significantly reduced CD34- CD38+ proliferation in the absence of exogenous cytokines compared to the PEA +gel system with 100% cytokines.

This analysis suggests that overall, removal of exogenous cytokines from media is beneficial in co-cultured systems using PEA 'primed' pericytes. Further, the PEA FN BMP-2 -gel system leads to robust proliferation of all populations investigated, including the most naïve CD34+CD38- population. Whereas the addition of low-stiffness gels and hypoxia to the system appears to reduce excess proliferation and maintain the naïve compartment, whilst reducing expansion of committed progenitors.

6.4.2 Low-stiffness gels and fibronectin networks support maintenance of LT-HSCs in the absence of supplemented cytokines

We used flow cytometry to assess changes in numbers of CD34+ subsets, then to show a functional effect in the niche systems an LTC-IC and CFU assay was used (Figure 6-7). Interestingly, this revealed the CD34+ CD38- proliferation induced in the PEA FN BMP-2 -gel system did not result in an increase in the number of functional LT-HSCs (CFUs). Whereas, the PEA FN BMP-2 +gel 0% that in the flow cytometry analysis maintained the most naïve compartment, resulted in significantly increased number of CFUs (~1.5-fold compared to the gold standard cells only control, and ~2.3-fold compared to -gel 0% cytokines) (Figure 6-7). The CFUs from this system were also able to retain lineage specification comparable

to the control (Figure 6-9). This capacity was only seen in the absence of additional HSC maintenance cytokines in the medium, as use of 100% cytokine media had a detrimental effect on the number of CFUs (Figure 6-7) and led to aberrant lineage specification (Figure 6-9). Taken together this data demonstrates the PEA FN BMP-2 +gel system is able to effectively maintain a significant population of LT-HSCs, but only in the absence of additional maintenance cytokines.

This data implies that the PEA FN BMP-2 +gel system that we have shown to support a population of nestin+ MSPCs, retains HSC support activity. It is able to maintain a population of HSCs that retain self-renewal capacity long-term in culture, without the addition of exogenous support cytokines in the media. Although the system with -gel resulted in expansion of the desirable CD34+ CD38- phenotype, these cells were not retained long term, suggesting loss of self-renewal capacity.

The results presented in Chapter 4 demonstrate that the PEA FN BMP-2 +gel system supports a nestin+ MSPC phenotype. *In vivo* these nestin+ MSPCs are present in close proximity to HSCs and express high levels of HSC maintenance factors, and have been shown in standard TCP *in vitro* culture to form mesenspheres that self-renew, expand in serial transplantation and support HSC activity (Méndez-Ferrer et al., 2010; Nakahara et al., 2019; Pinho et al., 2013). However, the Frenette group identified when nestin+ MSPCs were cultured, downregulation of HSC maintenance genes was observed. This loss of 'stemness' as a result of removal from the native niche, leads to limited success in long-term HSC co-cultures (Nakahara et al., 2019). The data presented in this chapter has demonstrated that use of biomaterial strategies can support the niche-like activity of nestin+ MSPCs during *in vitro* culture. These nestin+ MSPCs retain HSC supporting activities that are able to maintain a population of naïve CD34+CD38- progenitors which contain a higher frequency of LT-HSCs in co-culture than current gold standard culture conditions.

As biomaterial strategies have advanced, there has been a focus on engineering the BM niche microenvironment, moving away from simpler traditional Dexter-style co-culture stromal cells types and instead incorporating one or more material properties (Lee-Thedieck and Spatz, 2012). Results, however, are varied, with

similar systems leading to diverse findings. For example, reports on the use of perfusion cultures have demonstrated HSC expansion (Bourgine et al., 2018), maintenance (Torisawa et al., 2014) and differentiation (Rödling et al., 2017). Yet several biomaterial strategies have demonstrated differences in HSC location and homing within the engineered systems. The study by Bourgine et al, used porous HA-based scaffolds populated with MSCs and CD34+ cells in perfusion culture. They reported an increase in HSCs and progenitor cells in this system, and interestingly, identified the most naïve HSCs (CD34+CD38-) localised and adhered to the MSC-seeded scaffold surface whereas committed cells remained in the perfused supernatant (Bourgine et al., 2018). Similar to this, a study by Leisten et al, used a collagen hydrogel seeded with MSCs and HSCs seeded above the gel in suspension (both the collagen gel and HSC seeding method are akin to that used in this thesis). After 14 days culture they identified two sub-populations of HSCs, more differentiated HSPCs were identified to have remained in suspension above the collagen gel (CD34+CD38+), whereas more naïve HSCs (CD34+CD38-) had migrated into the MSC-seeded gel (Leisten et al., 2012). Both of these reports indicate HSC-MSC homing, or cell-cell contact is important for retaining the most desirable population of HSCs in culture. It would be of interest to investigate the migration of the HSCs in our gel system and identify if the LT-HSCs maintained in this system are homing to the nestin+ MSPCs at the gel-FN network interface. It may also be of interest to investigate other methods of HSC seeding to ensure closer proximity of the stromal layer and the HSCs - encapsulation of the HSCs within the gel was not possible with our system as we used a 14 day priming period for the stromal compartment, however future work may consider this.

With the aim of engineering supportive MSPC-based environments, the study by Nakahara et al, induced retention of HSC maintenance factors by targeting Nestin+ MSPC transcriptional machinery (Nakahara et al., 2019). RNA sequencing was used to identify transcription factors that were downregulated in mouse Nestin+ MSPCs after *in vitro* culture compared to freshly isolated Nestin+ MSPCs. From a list of 28 genes, a combination of 5 genes was subsequently identified to elevate HSC maintenance factor genes upon viral integration (*Ostf1, Xbp1, Irf3, Irf7* and *Klf7*). The transfected, or 'revitalised', cells exhibited significant elevation of niche genes such as *Scf, Cxcl12, Vcam1* and *Angpt1*. Upon *in vitro* co-culture of the revitalised MSPCs a 1.7-fold expansion of HSCs was observed (Nakahara et al.,

2019). After co-culture with the revitalised MSPCs, HSCs were expanded and transplanted into lethally irradiated mice. This demonstrated functionality of these HSCs through their ability to reconstitute multilineages long-term in the irradiated recipient mice. They found higher repopulation capacity for all the mature lineages in HSCs from the co-cultures, an ability that was retained even after secondary transplantation. The study went further to investigate if these revitalised mouse niche cells were able to confer similar effects when co-cultured with human HSCs. The system was increasingly effective, as demonstrated by the significant 28-fold expansion of the human HSCs, corroborated by an increased repopulating capacity. Demonstrating and ability of these revitalised mouse MSPCs to expand both mouse and human HSCs (Nakahara et al., 2019).

The above technique relies on lentiviral vectors for insertional mutagenesis, and although results are promising there are large safety risks that will need to be addressed before launching clinical trials. Whereas, the work presented in this thesis similarly engineers a MSPC phenotype that retains HSC support activity, yet by using only material and ECM-based cues. Optimisation of biomaterial-based strategies to maintain a more efficient feeder layer have the potential to circumvent the safety concerns associated with e.g. genetic transformations.

Over the past decade, small molecules that target multiple transcription factors have also been a focus for *ex vivo* HSC expansion. The use of small molecules to target cellular signalling evades the use of potentially dangerous strategies required by genetic manipulation. Nicotinamide (Horwitz et al., 2014), prostaglandin E2 (PGE2) (North et al., 2007), StemRegenin 1 (SR1) (Boitano et al., 2010) and a PPAR-γ antagonist GW9662 (Guo et al., 2018) have all been identified through chemical genetic screens or screening of large small molecule libraries. They have all demonstrated *in vitro* potential to induce robust proliferation of CD34+ cells, summarised in Table 6-5. Three of these molecules - PGE2, nicotinamide and SR1 - have resulted in relatively successful phase I clinical trials, where the safety of *ex vivo* expanded cells were confirmed (Cutler et al., 2013; Horwitz et al., 2014; Wagner et al., 2016).

Perhaps of greatest success is SR1, an agonist of the aryl hydrocarbon receptor (AhR) which regulates genes that are involved in haematopoiesis, thus blocking HSC differentiation (Boitano et al., 2010). Treatment of CD34+ cells with SR1 in

combination with the standard HSC cytokine cocktail (SCF, Flt3, TPO and interleukin-6 (IL-6)) led to a remarkable >300-fold expansion of human umbilical cord blood (UCB) CD34+ cells *in vitro* after 15 days treatment (Boitano et al., 2010; Wagner et al., 2016). In a phase I/II clinical trial these expanded cells were transplanted into patients alongside an untreated unit of UCB (Wagner et al., 2016). SR1 treatment demonstrated successful, safe and rapid engraftment in all patients. However, simple manipulation of HSCs expansion in this way often does not provide the correct combination of signals to promote naïve, multipotent, undifferentiated therapeutically useful stem cells. The expansion observed from SR1 treatment is predominantly in the progenitor compartment, and upon HSCT a transient burst of myeloid cells was observed after 7 days. It is also of note that the most naïve CD34+ (LT-HSC) fraction that engrafted was derived not from the SR1 treated UCBs, but from the untreated UCB unit that was co-administered. Suggesting the SR1 cells may contribute more to the progenitor pool than to the long-term repopulating fraction (Wagner et al., 2016).

Table 6-5 Summary of current small molecules used for ex vivo HSC expansion.

Compound	Biological rationale	Media cytokines	Culture Time	Effect	Reference
PGE2	Enhanced prostaglandin E2 synthesis	None	24–48 h	Enhanced neutrophil recovery, leading to enhanced homing, survival and proliferation of HSCs.	(Cutler et al., 2013; Goessling et al., 2009)
SR1	Inhibits AhR	SCF, Flt3, TPO, IL-6	7-21 days	>300-fold increase in CD34+ cells. Blocks differentiation. Enhanced neutrophil recovery and engraftment.	(Boitano et al., 2010; Wagner et al., 2016)
Nicotinamide	SIRT1 inhibitor	SCF, Flt3, TPO, IL-6	21 days	Inhibits HSC differentiation, facilitates HSC homing and engraftment.	(Horwitz et al., 2014; Peled et al., 2012)
PPAR-γ antagonist	Enhanced glycolysis	SCF, Flt-3, TPO	4 days	3-fold expansion of HSCs. Contained LT repopulating potential. Decrease in differentiation associated genes.	(Guo et al., 2018)

Although some of these small molecule strategies have seen success in early stage clinical trials, culturing HSCs in this manner remains a double-edged sword; robust proliferation will undoubtedly always be accompanied by differentiation and a resulting loss of stemness (Pollard and Kranc, 2010). These molecules may provide the correct biochemical signal to stimulate HSC expansion, however virtually all other niche constituents are removed from these culture methods (Table 6-5). It could therefore be easily envisioned that a combinatorial approach using small molecule strategies employed in tandem with biomaterial approaches, that recapitulate physical aspects of the BM niche microenvironment (discussed in Table 1-5) could be beneficial. This could have the potential to drive the robust proliferation achieved through small molecule addition, whilst integrating the multiple signalling components that make up the BM microenvironment to reduce differentiation.

Future work could investigate this in our PEA FN BMP-2 +gel system, as we have demonstrated the ability to maintain LT-HSCs using this strategy in the absence of maintenance cytokines, the addition of e.g. SR1, could be used to drive expansion whilst providing cues for long term maintenance. Further investigation into longer culture periods of HSCs in this system, and into HSC proliferation and cell cycle should also be investigated. Additionally, the resulting CD34+ cells should be investigated for repopulation capacity and in serial transplantation studies in irradiated recipient mice, considered the gold standard test for functionality (Domen et al., 2006).

6.4.3 Summary

HSC expansion is an area of great focus due to an increased demand for HSCTs to treat increasing blood-related disorders and insufficient donor availability (Brunstein et al., 2010; Lane et al., 2014; Radaelli et al., 2014). Successful HSCT require higher numbers of HSCs than are usually successfully obtained, revived or engrafted from single donors (Kumar et al., 2017). Understanding the cell-intrinsic mechanisms and extrinsic niche-regulatory mechanisms that are fundamental to HSC homeostasis are essential for establishing effective and safe methods for expanding HSCs *ex vivo* for clinical use. As insights into these properties have been gained over the past decade, strategies for HSC expansion are now promising, with encouraging results from some later stage clinical trials (Wagner et al., 2016).

However, many of these studies rely on HSC control using genetic manipulation or small molecule stimulation, the widespread intrinsic effects of which are not yet fully understood (Boitano et al., 2010; Nakahara et al., 2019; North et al., 2007). Large risks associated with the safety of these processes will need to be addressed before these cells find their way into the clinic.

Our study presents a method to maintain a population of LT-HSCs in culture using only physiological-mimetic matrix cues. Although the co-culture period used was relatively short, the results are promising and indicate optimisation of the system could be investigated for long-term HSC culture (outlined in Chapter 7). Further to this, if future work were able to manipulate this engineered environment to promote expansion of this LT-HSC population, the risk associated with cells from this system would potentially be significantly less than that of, for example, insertional mutagenesis strategies (Nakahara et al., 2019). The results from this chapter suggest that currently the system offers a platform in which multiple niche properties can be manipulated, constructed and de-constructed, and their intrinsic and extrinsic effects on both MSPCs and HSCs studied in detail. Platforms such as this would allow for more *in vivo*-like study of downstream effects of small molecule strategies, genetic engineering and drug toxicity testing.

Chapter 7 Discussion

7.1 Project Summary

As outlined in Chapter 1, this thesis aimed to recapitulate aspects of the BM niche microenvironment. The system was then used to investigate key regulatory mechanisms for maintaining niche-like phenotypes in MSPCs, and for maintaining a population of HSCs *in vitro*. Key achievements are described below:

- Cell source: pericytes derived from adipose tissue were used throughout this project. Adipose tissue is deemed clinical waste and as such is more easily acquired than e.g. BM samples. Although it would be of interest to assess the use of BM pericytes in this model, adipose-derived cells were demonstrated to express key BM niche markers and ultimately maintain LT-HSCs in culture.

- The rationale for using a low-stiffness matrix in the form of the collagen hydrogel to drive nestin expression was effective.

- Preformed FN networks presented on the PEA substrates in combination with low-stiffness gels also led to increased expression of key phenotypic niche markers. The system supported an MSPC population that was nestin+ CD146+ CD51+ and NG2+. This population was supported to degrees on other substrates, such as PMA, however the PEA FN +gel systems were the only systems able to support expression of the 2 key maintenance factors, CXCL12 and SCF.

- The modular nature of the system allowed detailed investigation into metabolic mechanisms in response to each niche component. From this we identified a 'hypoxic-like' mechanism induced by the use of low-stiffness gels. This may be important for regulation of the nestin+ MSPCs maintained by this system.

- The PEA FN BMP-2 +gel system was able to maintain a population of LT-HSCs *in vitro*, in the absence of additional maintenance cytokines in the

media. This was significantly increased compared to the current gold standard method for *in vitro* HSC maintenance.

In conclusion, the *in vitro* BM niche model developed here was capable of maintaining and supporting populations of MSPCs and HSCs in niche-like states. The system allowed easy construction and deconstruction of multiple niche properties, providing a platform on which to investigate their impact on fundamental cell processes and contribution to the desired niche phenotype. However, the ultimate goal for *in vitro* BM models will be to achieve HSC expansion, or maintenance in culture for longer time periods. As such, further work is needed to achieve these goals.

7.2 Recommendations for Future Work

Along with the experiments detailed in chapter discussions, considerations for future work are detailed below.

The use of glass coverslips as a control surface would be changed to a more appropriate surface, such as TCP and TCP +FN. As discussed, glass was used as a control as a result of the method of substrate fabrication. PEA was coated onto glass coverslips by spin coating and hence plain glass was chosen as the control. Although, when comparing cell behaviour in standard culture conditions, plain TCP options would be more appropriate and allow comparison against stem cell behaviours in standard culture conditions, and should be used in future work.

In this thesis, we employed MSPCs, or pericytes, isolated from human adipose tissue, which is considered clinical waste and thus is easily sourced. There is evidence for this cell source containing HSC supportive properties *in vitro* (Corselli et al., 2013), and much evidence for adipose-sourced stem cells retaining similar properties to BM isolated counterparts (da Silva Meirelles et al., 2015; Paduano et al., 2017; Sá da Bandeira et al., 2016), although there are also reports on discrepancies in potency for e.g. osteogenic differentiation (Herrmann et al., 2016; Im et al., 2005). For future work, it would be of interest to employ BM-derived MSPCs in this system. This would more closely mimic the native *in vivo* compartment, which could lead to different, or perhaps more potent effects, on both the support of the MSPC phenotype, and HSC regulation.

Future work may also consider investigations into different levels of hypoxia. In this thesis we used 1% O_2, this was based on current studies both measuring BM oxygen (Spencer et al., 2014) and what is widely used in similar studies investigating *ex vivo* BM niche recapitulation and HSC culture (Antebi et al., 2018; Danet et al., 2003; Guarnerio et al., 2014; Kobayashi et al., 2019; Lee et al., 2018; Shima et al., 2009). However, some studies have demonstrated beneficial effects on HSC regulation at slightly higher oxygen tensions, still within that measured for the BM niche cavity, ranging from 2-5% O_2 (Hammoud et al., 2012; Mantel et al., 2015; Roy et al., 2012). It may also be considered that due to the distinct locations and thus oxygen tensions of the endosteal and sinusoidal niches, that altering oxygen tension may be used to replicate specific niches that ultimately will have implications on HSC behaviour.

Investigation into using the PEA FN system to efficiently present GFs focussed only on the use of BMP-2. However, as discussed, often no significant results were obtained when compared to the FN network alone. We know from our previous work that using this system to present GFs to cells is effective (Cheng et al., 2018; Llopis-hernández et al., 2016; Moulisová et al., 2017), however the addition of other major cues, such as hypoxia and low-stiffness gels, may have dampened effects of the GF. However, it is also of consideration that the FN GF binding domain has high affinity to many other GFs and some HSC regulatory cytokines, which may be increasingly effective in promoting the niche-like phenotype we aimed to engineer in this thesis (Martino and Hubbell, 2010; Pelletier et al., 2000). Some of these are discussed in Table 7-1 below. Future work would investigate these factors independently and in combination, with the aim to achieve a more mimetic niche environment. The system could also offer a platform in which to study the different GF/cytokine signals contribution to MSPC and HSC phenotypes within the niche environment.

Table 7-1 GFs and cytokines to be considered for future model development.

Growth Factor/Cytokine	Rationale	References
NGF	Likely secreted by sympathetic nerve fibres in the BM niche. NGFR (CD271) expressed by a population of naïve MSCs. Previous work from our group demonstrated a niche-phenotype promoting effect in MSPCs.	(Álvarez-Viejo et al., 2015; Lv et al., 2014; Mo et al., 2016; Sweeten, 2019)
VEGF	Present in the BM niche. VEGFR highly expressed by endothelial cells in the vascular niche.	(Kunisaki et al., 2013)
PDGFα	PDGFRα is expressed by pericytes *in vivo* but is quickly lost in culture. PDGFRα is associated with the nestin+ MSPC phenotype.	(Pinho et al., 2013; Sá da Bandeira et al., 2016)
CXCL12	Important HSC maintenance cytokine. Produced in the niche by MSPCs and CAR cells.	(Sugiyama et al., 2006)
TGF-B	Secreted by nonmyelinating Schwann cells in the niche and leads to regulation of HSC dormancy. This could be added to a PEA system with HSCs only.	(Yamazaki et al., 2011)

A limitation to investigation into different GFs and cytokine combinations is acquisition of materials, leading to time constraints. A strategy to overcome this is, however, easily envisaged; our group has developed and characterised a plasma polymerisation method for PEA coatings (Cheng et al., 2018). This method is both time effective and permits coating of a range of 2D and 3D surfaces and constructs. Using plasma PEA polymerisation 96-well plates could be coated, FN adsorbed, and FN networks formed. Combinations of GFs and cytokines discussed in Table 7-1 could then be tethered and presented in a physiological-like manner to the cells, in an efficient multi-well microarray style format.

The 96-well plate style format would also offer other critical benefits. The coverslip-based system used in this thesis was limited in terms of length of HSC co-culture due to an inability to exchange media during periods of co-culture. Typically, HSC culture is performed in 96-well plates that can be centrifuged and media exchanged without disrupting HSCs (Corselli et al., 2013). Transferring the system to a PEA coated 96-well plate would therefore not only allow the user to

test multiple conditions, but the ability to exchange media would permit longer culture periods for investigation.

The plasma polymerisation technique also has the ability to PEA coat 3D scaffolds. The use of 3D printed scaffolds such as those used in our previous work (Cheng et al., 2018) would offer a viable strategy to take this system into 3-dimensions. One recent study reported MSCs seeded onto 3D scaffolds in a perfused bioreactor system resulted in increased nestin expression when compared to static culture (Bourgine et al., 2018). The lattice structures, coated with PEA FN and GF combinations, could easily be incorporated into such a system. Offering a platform on which to further investigate additional niche properties such as fluid flow.

As will be discussed later, there is a drive towards creating NATs for both pharmaceutical and clinical use. The current system uses a rat-tail collagen type I gel to promote nestin+ MSPCs, which will inevitably suffer batch-to-batch variability, leading to problems with reproducibility. A next step would be to replace the collagen gel with a rationally designed synthetic matrix, such as PEG. The gel would ideally retain similar stiffness to that in the range of the BM microenvironment (Jansen et al., 2015), and the ability to accurately tune PEG matrix stiffness through various techniques make it desirable for this application (Caliari and Burdick, 2016; Garcia, 2014; Trujillo et al., 2019a). PEG gels also offer further opportunity to reproducibly tune additional biochemical and physical cues in a modular fashion, unpublished work from our group has demonstrated PEG can be functionalised with ECM molecules such as FN or laminin (Trujillo et al., 2019b). This would offer further sites for GF binding, where different GF/cytokine presentation could be applied in the hydrogel component and the underlying PEA coated coverslip.

Further, the work presented in this thesis assessed MSPC phenotype in the absence of HSCs in co-culture. Undoubtedly HSC addition will lead to changes in fundamental MSPC mechanisms. MSPC-HSC co-culture and interaction more accurately represents the native microenvironment, investigation in to phenotypic and mechanistic differences of MSPCs when in contact with HSCs in this system would be vital to gain understanding into such important cell-intrinsic regulatory mechanisms. This investigation would help elucidate the beneficial signals

supported by MSPCs cultured in 0% cytokines in the PEA FN BMP-2 +gel system that permit effective LT-HSC maintenance.

7.3 Prospective Applications of Bone Marrow Niche Models

A model of the BM niche microenvironment has several potential research, clinical and pharmaceutical applications. These are summarised in Figure 7-1 and are discussed in detail below.

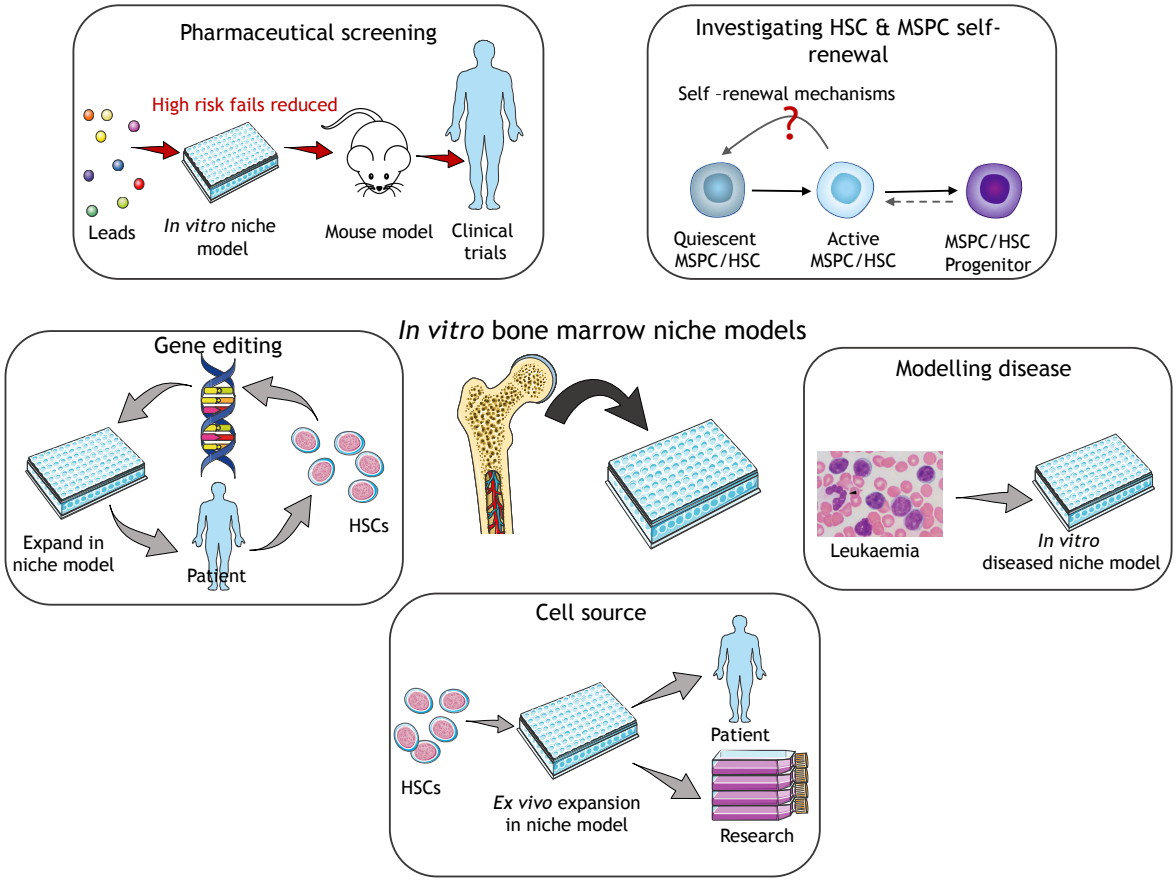

Figure 7-1 Potential applications of an *in vitro* BM niche model. These include a more humanised method for screening pharmaceutical leads, reducing the need for animal models and the number of high risk fails entering costly clinical trials. Platforms on which to model and study HSC and MSPC processes at the molecular level, such as haematopoiesis and self-renewal mechanisms. More humanised models of diseases such as leukaemia, modelling disease progression and drug efficacy. Robust ex vivo expansion would offer better cell sources for research and clinical use. Gene editing platforms, that would increase efficacy and promote expansion of the therapeutic cells. Leukaemia image from (Li et al., 2016) with permissions, other images from Servier Medical Art, licensed under a Creative Commons Attribution 3.0 Generic License.

7.3.1 Probing haematopoiesis and niche dynamics

Although HSCs are the most studied, easily isolated and clinically relevant ASC, the problems associated with their *ex vivo* culture mean a greater understanding of their biology is needed to fully realise their potential (Eaves, 2015). Many signals that contribute to HSC homeostasis have been identified and are discussed in earlier chapters. However, many still remain incompletely defined, for example, the HSC self-renewal process remains to be fully elucidated at the molecular level (Zon, 2008). Study of HSC biology and haematopoiesis in humans is limited. Although mouse models have offered invaluable alternatives, discrepancies do exist, in part due to the differences between human and murine immune systems (Chao et al., 2008).

Furthermore, MSPCs have shown great therapeutic potential in both the ability to regenerate damaged or diseased tissues (Dalby et al., 2018), and for their immunosuppressive capacity for transplant operations (Ito et al., 2010). MSPCs also lose their stem cell potential in *in vitro* culture (McMurray et al., 2011), and although the mechanisms of differentiation have been extensively investigated, relatively little is still know about how the native physical environment modulates self-renewal of these cells.

An *in vitro* BM niche model, such as that developed in this thesis, would offer a platform on which to study these processes, and gain further understanding of fundamental regulatory processes in both HSCs and MSPCs. For example, the study by Roch et al, (discussed in Chapter 1.5.5) demonstrates this for HSCs, where the engineered niche system was used to systematically probe early HSC fate choices, identifying specific gene signatures associated with lineage commitment (Roch et al., 2017). For MSPCs, our group has demonstrated control over self-renewal using nanotopographies (McMurray et al., 2011). The topographical controlled system was then used as a platform to investigate and harness the immunomodulatory capacity of MSPCs (Ross et al., 2019). Studies such as these, will ultimately lead to the development of novel methods to harness HSC and MSPC behaviours.

7.3.2 Modelling disease

Many haematological disorders involve HSCs, and are consistent with the regulation of haematopoiesis by the BM niche, current evidence suggests that the niche can also drive neoplasia, or be remodelled to support malignant cells (Pinho and Frenette, 2019). In leukaemias, stem or progenitor cell damage leads to overproduction of one type of white blood cell, fundamentally changing the cellular composition of the marrow. Just as healthy HSPCs can modulate the microenvironment, leukemic stem cells (LSCs) can remodel it further to create a cancer-supportive environment (Pinho and Frenette, 2019). Some of these modifications lead to upregulation of surface receptors that mediate cell adhesion and survival in LSCs, that can confer chemoresistance. LSCs also share quiescent and self-renewing properties with HSCs, meaning developing treatments that target only LSCs is difficult (Bonnet, 2005). An *in vitro* BM niche model could not only be used to study these interactions and processes in detail, but also to explore therapeutic targets. Furthermore, as the origin of such malignancies are heterogenous in terms of phenotypic changes, an *in vitro* model could be employed to model the patients' own tumour microenvironment and identify the most appropriate therapeutic strategy on a personalised medicine basis. A study employing a co-culture with MSCs and patient derived multiple myeloma cells has demonstrated this, where patients could be screened for clinical response to therapeutic compounds (Pak et al., 2015).

7.3.3 NAT pharmaceutical screening

In recent decades, advances in the molecular understanding of disease processes has underpinned new potential therapeutic targets. However, there is a lack of corresponding increase in drug discovery and manufacture. It is notable that in small molecule drug discovery, the drive for high throughput has led to the use of overly simplified cell models that do not recreate aspects of native cell microenvironments and testing of compounds in non-human models. This has fuelled productivity crisis, where high numbers of drug candidates are taken forwards, yet the attrition rate is high with many ultimately failing in Phase I/II clinical trials. Almost half of fails are not predicted by traditional *in vitro* and pre-clinical *in vivo* screens (Cook et al., 2014). In fact, AstraZeneca reported that from 2011 to 2016, 66% of its small molecule projects failed, critically only 23% before

clinical trial stages (i.e. cheap fails) (Cook et al., 2014). This demonstrates that current techniques lack the ability to accurately predict success at the pre-clinical trial stage.

This is driving Pharma to look to NATs (Ewart et al., 2018), built using human cells and likely requiring the tissue complexity that stem cells and tissue engineering strategies can produce (Donnelly et al., 2018). Systems such as these can be used to better predict drug mechanism, toxicity and efficacy in a biomimetic setting. These *in vitro* models would allow leads with high risk of failure to be dropped quickly, ultimately reducing the number of fails that reach costly clinical trial stages, saving the pharmaceutical industry enormous amounts of time and money.

In this regard, organ-on-a-chip (OOC) platforms that recapitulate multifaceted tissue-specific microenvironments are being developed and employed. OOC techniques aim not to build whole living organs, but to establish the minimally functional units representing aspects of human physiology in a controlled system (Ronaldson-Bouchard and Vunjak-Novakovic, 2018). The bone marrow-on-a-chip developed by the Ingber group in 2014 is a promising step toward realising these biomimetic drug testing platforms (Torisawa et al., 2014).

7.3.4 Cell source for clinical applications and research

Despite the success of HSCT, the limited number of HSCs available still poses a major obstacle for the wider application of HSC-based therapies (Brunstein et al., 2010). Efficient expansion of HSCs remains a major goal in the field (Kunisaki and Frenette, 2012). As discussed in Chapter 6, an *in vitro* BM model that could maintain HSCs in long-term culture and stimulate expansion of the population on demand would overcome these obstacles to getting HSCs safely and successfully into the clinic. These systems could ultimately be developed to induce *ex vivo* expansion of autologous patient HSCs for transplant. Currently there is a reliance on allogenic donors in order to achieve sufficient cell number for engraftment, however the patient's own cells could be isolated, maintained and expanded in an *in vitro* BM niche system, while the patient undergoes myeloablative therapy. This would enable higher yields and negate the need for a donor, circumventing the need to find an HLA match and avoiding risks of graft-versus-host disease.

7.3.5 Gene editing platform

Gene editing of HSCs is an area of particular interest, and has shown promising results in recent clinical trials for patients affected by primary immunodeficiencies, malignancies, haemoglobinopathies or inborn metabolic errors (Naldini, 2015). These treatments are based on the transplantation of *ex vivo*-engineered, autologous HSCs that are then transplanted back into patients. However, there are reports of such strategies leading to delayed recovery periods, that may be associated with the *ex vivo* culture of the cell therapy product (Aiuti et al., 2013; Zonari et al., 2017). As such, improved *ex vivo* culture conditions, such as biomimetic BM models, could improve the success rate of these procedures. Further, *in vitro* models that support HSC expansion could both provide a platform on which to successfully genetically edit patient HSCs, but also expand this population for implantation.

7.4 Conclusion

The past decade has seen extraordinary growth in the understanding of BM niches and the specific cellular and molecular components that regulate MSPC and HSC activity (Pinho and Frenette, 2019). However much still remains to be elucidated before the enormous potential of these cell types is fully harnessed. The development of *in vitro* models that are more permissive for human BM niche studies than current *in vivo* murine models will be beneficial, as currently it is difficult to recapitulate certain haematological malignancies in mice. These advances would enable the development of improved, chemically and physically defined, culture systems and the design of *ex vivo* MSPC and HSC expansion protocols that will ultimately improve research and clinical applications of these valuable cell types.

Appendices

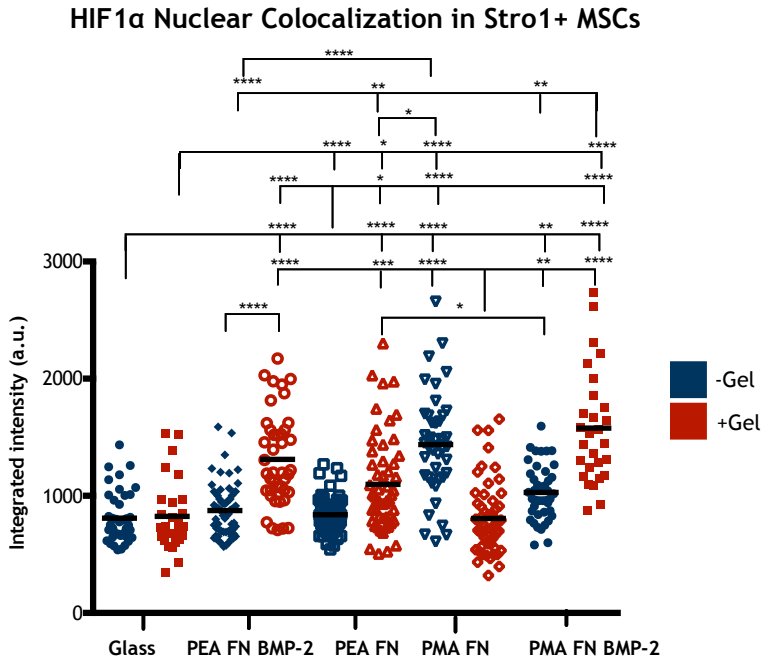

Figure 7-2 Nuclear HIF1α levels increase with low-stiffness gels in Stro1+ MSCs. HIF1α is active when localised to the nucleus. Immunofluorescence analysis was carried out after 3 days, and the integrated intensity of HIF1α in cell nuclei measured. Data shows increased HIF1α levels were observed on PEA FN and PEA FN BMP-2 substrates, and that addition of a collagen type 1 gel increases HIF1α levels in glass, PEA FN and PEA FN BMP-2. Graph shows mean integrated intensity of nuclear HIF1α (n=3), each point represents 1 nuclei. One-way ANOVA followed by Kruskal-Wallis test with multiple comparisons, *= p<0.05, **= p<0.01, ***= p<0.001, ****= p<0.0001.

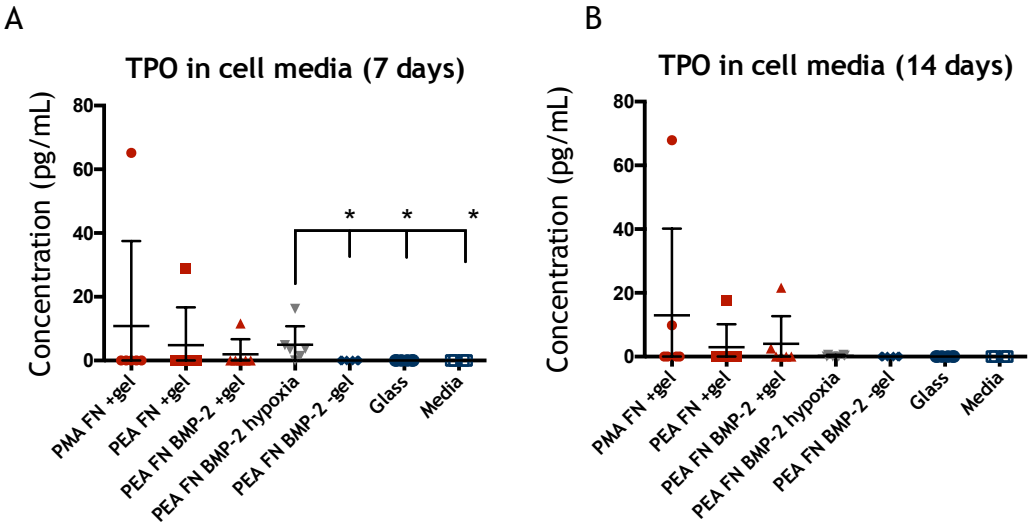

Figure 7-3 TPO in cell media. TPO concentrations in cell media measured by ELISA at (A) day 7 and (B) 14 of culture. Data indicates no TPO was detected in most samples but shows variations in the technical repeats. Graph shows individual data points for technical repeats, average ± SEM. Statistics by one-way ANOVA with Kruskal-Wallis test for multiple comparisons, *=p<0.05.

List of References

Agarwal, R., González-García, C., Torstrick, B., Guldberg, R.., Salmerón-Sánchez, M., García, A.J., 2015. Simple Coating with Fibronectin Fragment Enhances Stainless Steel Screw Osseointegration in Healthy and Osteoporotic Rats. Biomaterials 63, 137–145. https://doi.org/10.1016/bs.mcb.2015.01.016.Observing

Ahmed, E.M., 2015. Hydrogel: Preparation, characterization, and applications: A review. J. Adv. Res. 6, 105–121. https://doi.org/10.1016/j.jare.2013.07.006

Aiuti, A., Biasco, L., Scaramuzza, S., Ferrua, F., Cicalese, M.P., Baricordi, C., Dionisio, F., Calabria, A., Giannelli, S., Castiello, M.C., Bosticardo, M., Evangelio, C., Assanelli, A., Casiraghi, M., Di Nunzio, S., Callegaro, L., Benati, C., Rizzardi, P., Pellin, D., Di Serio, C., Schmidt, M., Von Kalle, C., Gardner, J., Mehta, N., Neduva, V., Dow, D.J., Galy, A., Miniero, R., Finocchi, A., Metin, A., Banerjee, P.P., Orange, J.S., Galimberti, S., Valsecchi, M.G., Biffi, A., Montini, E., Villa, A., Ciceri, F., Roncarolo, M.G., Naldini, L., 2013. Lentiviral hematopoietic stem cell gene therapy in patients with wiskott-aldrich syndrome. Science (80-.). 341. https://doi.org/10.1126/science.1233151

Al-jarsha, M., Moulisova, V., Leal-egana, A., Connell, A., Naudi, K.B., Ayoub, A., Dalby, M.J., Salmerón-sánchez, M., 2018. Engineered coatings for titanium implants to present ultra-low doses of BMP-7. ACS Biomater. Sci. Eng. 4, 1812–1819. https://doi.org/10.1021/acsbiomaterials.7b01037

Alakpa, E. V., Burgess, K.E.V., Chung, P., Riehle, M.O., Gadegaard, N., Dalby, M.J., Cusack, M., 2017a. Nacre Topography Produces Higher Crystallinity in Bone than Chemically Induced Osteogenesis. ACS Nano 11, 6717–6727. https://doi.org/10.1021/acsnano.7b01044

Alakpa, E. V., Jayawarna, V., Burgess, K.E.V., West, C.C., Péault, B., Ulijn, R. V., Dalby, M.J., 2017b. Improving cartilage phenotype from differentiated pericytes in tunable peptide hydrogels. Sci. Rep. 7, 1–11. https://doi.org/10.1038/s41598-017-07255-z

Alakpa, E. V., Jayawarna, V., Lampel, A., Burgess, K. V., West, C.C., Bakker, S.C.J., Roy, S., Javid, N., Fleming, S., Lamprou, D.A., Yang, J., Miller, A., Urquhart, A.J., Frederix, P.W.J.M., Hunt, N.T., Péault, B., Ulijn, R. V., Dalby, M.J., 2016. Tunable Supramolecular Hydrogels for Selection of Lineage-Guiding Metabolites in Stem Cell Cultures /j.chempr.2016.07.001)). Chem 1, 512. https://doi.org/10.1016/j.chempr.2016.08.001

Alakpa, E. V, 2014. Cell metabolism in response to biomaterial mechanics.

Alberti, K., Davey, R.E., Onishi, K., George, S., Salchert, K., Seib, F.P., Bornhäuser, M., Pompe, T., Nagy, A., Werner, C., Zandstra, P.W., 2008. Functional immobilization of signaling proteins enables control of stem cell fate. Nat. Methods 5, 645–650. https://doi.org/10.1038/nmeth.1222

Alberts, B., Johnson, A., Lewis, J., Raff, M., Roberts, K., Walter, P., 2008. Molecular Biology of the Cell. Garland Science.

Aljurf, M., Weisdorf, D., Alfraih, F., Szer, J., Müller, C., Confer, D., Hashmi, S., Kröger, N., Shaw, B.E., Greinix, H., Kharfan-Dabaja, M.A., Foeken, L., Seber, A., Ahmed, S., El-Jawahri, A., Al-Awwami, M., Atsuta, Y., Pasquini, M., Hanbali, A., Alzahrani, H., Okamoto, S., Gluckman, E., Mohty, M., Kodera, Y., Horowitz, M., Niederwieser, D., El Fakih, R., 2019. "Worldwide Network for Blood & Marrow Transplantation (WBMT) special article, challenges facing emerging alternate donor registries." Bone Marrow Transplant. https://doi.org/10.1038/s41409-019-0476-6

Álvarez-Viejo, M., Menendez-Menendez, Y., Otero-Hernandez, J., 2015. CD271 as a marker to identify mesenchymal stem cells from diverse sources before culture. World J. Stem Cells 7, 470. https://doi.org/10.4252/wjsc.v7.i2.470

Amable, P.R., Teixeira, M.V.T., Carias, R.B.V., Granjeiro, J.M., Borojevic, R., 2014. Gene expression and protein secretion during human mesenchymal cell differentiation into adipogenic cells. BMC Cell Biol. 15, 1–10. https://doi.org/10.1186/s12860-014-0046-0

Antebi, B., Rodriguez, L.A., Walker, K.P., Asher, A.M., Kamucheka, R.M., Alvarado, L., Mohammadipoor, A., Cancio, L.C., 2018. Short-term physiological hypoxia potentiates the therapeutic function of mesenchymal stem cells. Stem Cell Res. Ther. 9, 1–15. https://doi.org/10.1186/s13287-018-1007-x

Antoine, E.E., Vlachos, P.P., Rylander, M.N., 2014. Review of Collagen I Hydrogels for Bioengineered Tissue Microenvironments: Characterization of Mechanics, Structure, and Transport. Tissue Eng. Part B Rev. 20, 683–696. https://doi.org/10.1089/ten.teb.2014.0086

Aota, S., Nomizu, M., Yamada, K.M., 1994. the Short Amino-Acid-Sequence Pro-His-Ser-Arg-Asn in Human Fibronectin Enhances Cell-Adhesive Function. J. Biol. Chem. 269, 24756–24761.

Ara, T., Tokoyoda, K., Sugiyama, T., Egawa, T., Kawabata, K., Nagasawa, T., 2003. Long-term hematopoietic stem cells require stromal cell-derived factor-1 for colonizing bone marrow during ontogeny. Immunity 19, 257–67.

Aragona, M., Panciera, T., Manfrin, A., Giulitti, S., Michielin, F., Elvassore, N., Dupont, S., Piccolo, S., 2013. A mechanical checkpoint controls multicellular growth through YAP/TAZ regulation by actin-processing factors. Cell 154, 1047–1059. https://doi.org/10.1016/j.cell.2013.07.042

Arai, F., Hirao, A., Ohmura, M., Hidetaka, S., Matsuoka, S., Takubo, K., Ito, K., Gou Young Koh, T.S., 2004. Tie2 / Angiopoietin-1 Signaling Regulates Hematopoietic Stem Cell Quiescence in the Bone Marrow Niche. Cell 118, 149–161.

Asada, N., Kunisaki, Y., Pierce, H., Wang, Z., Fernandez, N.F., Birbrair, A., Ma, A., Frenette, P.S., 2017. Differential cytokine contributions of perivascular haematopoietic stem cell niches. https://doi.org/10.1038/ncb3475

Avolio, E., Meloni, M., Spencer, H.L., Riu, F., Katare, R., Mangialardi, G., Oikawa, A., Rodriguez-Arabaolaza, I., Dang, Z., Mitchell, K., Reni, C., Alvino, V. V., Rowlinson, J., Livi, U., Cesselli, D., Angelini, G., Emanueli, C., Beltrami, A.P., Madeddu, P., 2015. Combined intramyocardial delivery of human pericytes and cardiac stem cells additively improves the healing of mouse infarcted hearts through stimulation of

vascular and muscular repair. Circ. Res. 116, e81–e94. https://doi.org/10.1161/CIRCRESAHA.115.306146

Baba, M., Hirai, S., Yamada-Okabe, H., Hamada, K., Tabuchi, H., Kobayashi, K., Kondo, K., Yoshida, M., Yamashita, A., Kishida, T., Nakaigawa, N., Nagashima, Y., Kubota, Y., Yao, M., Ohno, S., 2003. Loss of von Hippel-Lindau protein causes cell density dependent deregulation of CyclinD1 expression through Hypoxia-inducible factor. Oncogene 22, 2728–2738. https://doi.org/10.1038/sj.onc.1206373

Bach, D.H., Park, H.J., Lee, S.K., 2018. The Dual Role of Bone Morphogenetic Proteins in Cancer. Mol. Ther. - Oncolytics 8, 1–13. https://doi.org/10.1016/j.omto.2017.10.002

Banfi, A., Muraglia, A., Dozin, B., Mastrogiacomo, M., Cancedda, R., Quarto, R., 2000. Proliferation kinetics and differentiation potential of ex vivo expanded human bone marrow stromal cells: Implications for their use in cell therapy. Exp. Hematol. 28, 707–715. https://doi.org/10.1016/S0301-472X(00)00160-0

Bazan, J.., 1990. Haemopoietic receptors and helical cytokines. Immunol. Today 11, 350–354. https://doi.org/doi.org/10.1016/0167-5699(90)90139-Z

Beitner-Johnson, D., Rust, R.T., Hsieh, T.C., Millhorn, D.E., 2001. Hypoxia activates Akt and induces phosphorylation of GSK-3 in PC12 cells. Cell. Signal. 13, 23–27. https://doi.org/10.1016/S0898-6568(00)00128-5

Bello, A.B., Park, H., Lee, S.H., 2018. Current approaches in biomaterial-based hematopoietic stem cell niches. Acta Biomater. 72, 1–15. https://doi.org/10.1016/j.actbio.2018.03.028

Benoit, D.S.W., Schwartz, M.P., Durney, A.R., Anseth, K.S., 2008. Small functional groups for controlled differentiation of hydrogel-encapsulated human mesenchymal stem cells. Nat. Mater. 7, 816–23. https://doi.org/10.1038/nmat2269

Bentley, S.A., 1982. Collagen synthesis by bone marrow stromal cells: a quantitative study. Br. J. Haematol. 50, 491–497. https://doi.org/10.1111/j.1365-2141.1982.tb01945.x

Bertet, C., Sulak, L., Lecuit, T., 2004. Myosin-dependent junction remodelling controls planar cell intercalation and axis elongation. Nature 429, 667–671. https://doi.org/10.1038/nature02581.1.

Bian, L., Guvendiren, M., Mauck, R.L., Burdick, J.A., 2013. Hydrogels that mimic developmentally relevant matrix and N-cadherin interactions enhance MSC chondrogenesis. Proc. Natl. Acad. Sci. 110, 10117–10122. https://doi.org/10.1073/pnas.1214100110

Bianco, J.E.R., Rosa, R.G., Congrains-Castillo, A., Joazeiro, P.P., Waldman, S.D., Weber, J.F., Saad, S.T.O., 2019. Characterization of a novel decellularized bone marrow scaffold as an inductive environment for hematopoietic stem cells. Biomater. Sci. 7, 1516–1528. https://doi.org/10.1039/c8bm01503a

Biggs, M.J.P., Richards, R.G., Gadegaard, N., Wilkinson, C.D.W., Oreffo, R.O.C., Dalby, M.J., 2009. The use of nanoscale topography to modulate the dynamics of adhesion

formation in primary osteoblasts and ERK/MAPK signalling in STRO-1+ enriched skeletal stem cells. Biomaterials 30, 5094–103. https://doi.org/10.1016/j.biomaterials.2009.05.049

Boitano, A.E., Wang, J., Romeo, R., Bouchez, L.C., Parker, A.E., Sutton, S.E., Walker, J.R., Flaveny, C.A., Perdew, G.H., Denison, M.S., Schultz, P.G., Cooke, M.P., 2010. Aryl Hydrocarbon Receptor Antagonists Promote the Expansion of Human Hematopoietic Stem Cells. Science (80-.). 329, 1345–1348.

Bonnet, D., 2005. Cancer stem cells: Lessons from leukaemia. Cell Prolif. 38, 357–361. https://doi.org/10.1111/j.1365-2184.2005.00353.x

Boulais, P.E., Frenette, P.S., 2015. Making sense of hematopoietic stem cell niches [WWW Document]. Blood J. URL http://www.bloodjournal.org/content/bloodjournal/125/17/2621.full.pdf (accessed 10.5.15).

Bourgine, P.E., Klein, T., Paczulla, A.M., Shimizu, T., Kunz, L., Kokkaliaris, K.D., Coutu, D.L., Lengerke, C., Skoda, R., Schroeder, T., Martin, I., 2018. In vitro biomimetic engineering of a human hematopoietic niche with functional properties. Proc. Natl. Acad. Sci. 115, E5688–E5695. https://doi.org/10.1073/pnas.1805440115

Boxall, S.A., Jones, E., 2012. Markers for Characterization of Bone Marrow Multipotential Stromal Cells. Stem Cells Int. 2012, 1–12. https://doi.org/10.1155/2012/975871

Brahimi-Horn, M.C., Pouysségur, J., 2007. Oxygen, a source of life and stress. FEBS Lett. 581, 3582–3591. https://doi.org/10.1016/j.febslet.2007.06.018

Bray, N.L., Pimentel, H., Melsted, P., Pachter, L., 2016. Near-optimal probabilistic RNA-seq quantification. Nat. Biotechnol. 34, 525–527. https://doi.org/10.1038/nbt.3519

Bruick, R.K., McKnight, S.L., 2001. A Conserved Family of Prolyl-4-Hydroxylases That Modify HIF. Science (80-.). 294, 1337–1340. https://doi.org/10.1126/science.1066373

Brunstein, C.G., Gutman, J.A., Weisdorf, D.J., Woolfrey, A.E., DeFor, T.E., Gooley, T.A., Verneris, M.R., Appelbaum, F.R., Wagner, J.E., Delaney, C., 2010. Allogeneic hematopoietic cell transplantation for hematologic malignancy: Relative risks and benefits of double umbilical cord blood. Blood 116, 4693–4699. https://doi.org/10.1182/blood-2010-05-285304

Bucaro, M.A., Vasquez, Y., Hatton, B.D., Aizenberg, J., 2012. Fine-tuning the degree of stem cell polarization and alignment on ordered arrays of high-aspect-ratio nanopillars. ACS Nano 6, 6222–6230. https://doi.org/10.1021/nn301654e

Buscher, J.., Czernik, D., Ewald, J.., Sauer, U., Zamboni, N., 2009. Cross-Platform Comparison of Methods for Quantitative Metabolomics of Primary Metabolism. Anal. Chem. 81, 2135–2143.

Butler, J.M., Nolan, D.J., Vertes, E.L., Varnum-Finney, B., Kobayashi, H., Hooper, A.T., Seandel, M., Shido, K., White, I.A., Kobayashi, M., Witte, L., May, C., Shawber, C., Kimura, Y., Kitajewski, J., Rosenwaks, Z., Bernstein, I.D., Rafii, S., 2010.

Endothelial Cells Are Essential for the Self-Renewal and Repopulation of Notch-Dependent Hematopoietic Stem Cells. Cell Stem Cell 6, 251–264. https://doi.org/10.1016/j.stem.2010.02.001

Caliari, S.R., Burdick, J.A., 2016. A Practical Guide to Hydrogels for Cell Culture Steven. Nat. Methods 14, 405–414. https://doi.org/10.1038/nmeth.3839.A

Calvi, L.M., Adams, G.B., Weibrecht, K.W., Weber, J.M., Olson, D.P., Knight, M.C., Martin, R.P., Schipani, E., Divieti, P., Bringhurst, F.R., Milner, L.A., Kronenberg, H.M., Scadden, D.T., 2003. Osteoblastic cells regulate the haematopoietic stem cell niche. Nature 425, 841–846. https://doi.org/10.1038/nature02041.1.

Cano, E., Gebala, V., Gerhardt, H., 2017. Pericytes or Mesenchymal Stem Cells: Is That the Question? Cell Stem Cell 20, 296–297. https://doi.org/10.1016/j.stem.2017.02.005

Caplan, A.I., 1991. Mesenchymal stem cells. J. Orthop. Res. 9, 641–650. https://doi.org/10.1016/j.arcmed.2003.09.007

Cavalcanti-Adam, E.A., Aydin, D., Hirschfeld-Warneken, V.C., Spatz, J.P., 2008. Cell adhesion and response to synthetic nanopatterned environments by steering receptor clustering and spatial location. HFSP J. 2, 276–285. https://doi.org/10.2976/1.2976662

Cavalcanti-Adam, E.A., Volberg, T., Micoulet, A., Kessler, H., Geiger, B., Spatz, J.P., 2007. Cell Spreading and Focal Adhesion Dynamics Are Regulated by Spacing of Integrin Ligands. Biophys. J. 92, 2964–2974. https://doi.org/10.1529/biophysj.106.089730

Cavo, M., Fato, M., Peñuela, L., Beltrame, F., Raiteri, R., Scaglione, S., 2016. Microenvironment complexity and matrix stiffness regulate breast cancer cell activity in a 3D in vitro model. Sci. Rep. 6, 35367. https://doi.org/10.1038/srep35367

Celiz, A.D., Smith, J.G.W., Langer, R., Anderson, D.G., Winkler, D.A., Barrett, D.A., Davies, M.C., Young, L.E., Denning, C., Alexander, M.R., 2014. Materials for stem cell factories of the future. Nat. Mater. 13, 570–579. https://doi.org/10.1038/nmat3972

Chan, C.K.F., Chen, C.C., Luppen, C.A., Kim, J.B., DeBoer, A.T., Wei, K., Helms, J.A., Kuo, C.J., Kraft, D.L., Weissman, I.L., 2009. Endochondral ossification is required for haematopoietic stem-cell niche formation. Nature 457, 490–494. https://doi.org/10.1038/nature07547

Chao, M.P., Seita, J., Weissman, I.L., 2008. Establishment of a normal hematopoietic and leukemia stem cell hierarchy. Cold Spring Harb. Symp. Quant. Biol. 73, 439–449. https://doi.org/10.1101/sqb.2008.73.031

Chen, C.S., Mrksich, M., Huang, S., Whitesides, G.M., Ingber, D.E., 1997. Geometric Control of Cell Life and Death. Science (80-.). 276, 1425–1428. https://doi.org/10.1126/science.276.5317.1425

Chen, D., Zhao, M., Mundy, G.R., 2004. Bone morphogenetic proteins. Growth Factors

22, 233–241. https://doi.org/10.1007/978-1-4471-5451-8_118

Chen, H.-F., Kuo, H.-C., Lin, S.-P., Chien, C.-L., Chiang, M.-S., Ho, H.-N., 2010. Hypoxic Culture Maintains Self-Renewal and Enhances Embryoid Body Formation of Human Embryonic Stem Cells. Tissue Eng. Part A 16, 2901–2913. https://doi.org/10.1089/ten.tea.2009.0722

Chen, W.C., Baily, J.., Corselli, M., Diaz, M.., Sun, B., Xiang, G., Gray, G.., Huard, J., Péault, B., 2014. Human Myocardial Pericytes : Multipotent Mesodermal Precursors Exhibiting Cardiac. Stem Cells 557–573.

Chen, Z., Wang, J., Cai, L., Zhong, B., Luo, H., Hao, Y., Yu, W., Wang, B., Su, C., Lei, Y., Bella, A.E., Xiang, A.P., Wang, T., 2014. Role of the stem cell-associated intermediate filament nestin in malignant proliferation of non-small cell lung cancer. PLoS One 9, 1–10. https://doi.org/10.1371/journal.pone.0085584

Cheng, Z.A., Alba-Perez, A., Gonzalez-Garcia, C., Donnelly, H., Llopis-Hernandez, V., Jayawarna, V., Childs, P., Shields, D.W., Cantini, M., Ruiz-Cantu, L., Reid, A., Windmill, J.F.C., Addison, E.S., Corr, S., Marshall, W.G., Dalby, M.J., Salmeron-Sanchez, M., 2018. Nanoscale Coatings for Ultralow Dose BMP-2-Driven Regeneration of Critical-Sized Bone Defects. Adv. Sci. 1800361, 1800361. https://doi.org/10.1002/advs.201800361

Choi, J.S., Harley, B.A.C., 2017. Marrow-inspired matrix cues rapidly affect early fate decisions of hematopoietic stem and progenitor cells. Sci. Adv. 3. https://doi.org/10.1126/sciadv.1600455

Chokkathukalam, A., Jankevics, A., Creek, D.J., Achcar, F., Barrett, M.P., Breitling, R., 2013. MzMatch-ISO: An R tool for the annotation and relative quantification of isotope-labelled mass spectrometry data. Bioinformatics 29, 281–283. https://doi.org/10.1093/bioinformatics/bts674

Chou, Y.H., Khuon, S., Herrmann, H., Goldman, R.., 2003. Modulation of Fibroblast Morphology and Adhesion during Collagen Matrix Remodeling. Mol. Biol. Cell 14, 1468–1478. https://doi.org/10.1091/mbc.E02

Chow, D.C., Wenning, L.A., Miller, W.M., Papoutsakis, E.T., 2009. Modeling pO2 Distributions in the Bone Marrow Hematopoietic Compartment. I. Krogh's Model. Biophys. J. 81, 675–684. https://doi.org/10.1016/s0006-3495(01)75732-3

Chow, D.C., Wenning, L.A., Miller, W.M., Papoutsakis, E.T., 2001. Modeling pO2 distributions in the bone marrow hematopoietic compartment. II. Modified Kroghian models. Biophys. J. 81, 685–696. https://doi.org/10.1016/S0006-3495(01)75733-5

Civin, C.I., Strauss, L.C., Brovall, C., Fackler, M.J.O., Schwartz, J.F., Shaper, J.H., 1984. Antigenic analysis of hematopoiesis . III . A hematopoietic progenitor cell surface antigen defined by a monoclonal antibody raised against KG-1a cells . Information about subscribing to The Journal of Immunology is online at : . A Hematopoietic Progenito. J. Immunol. 133, 157–165.

Clark, K., Langeslag, M., Van Leeuwen, B., Ran, L., Ryazanov, A.G., Figdor, C.G., Moolenaar, W.H., Jalink, K., Van Leeuwen, F.N., 2006. TRPM7, a novel regulator of

actomyosin contractility and cell adhesion. EMBO J. 25, 290–301. https://doi.org/10.1038/sj.emboj.7600931

Clarke, B., 2008. Normal bone anatomy and physiology. Clin. J. Am. Soc. Nephrol. 3 Suppl 3, S131-9. https://doi.org/10.2215/CJN.04151206

Comoglio, P.M., Boccaccio, C., Trusolino, L., 2003. Interactions between growth factor receptors and adhesion molecules: Breaking the rules. Curr. Opin. Cell Biol. 15, 565–571. https://doi.org/10.1016/S0955-0674(03)00096-6

Cook, D., Brown, D., Alexander, R., March, R., Morgan, P., Satterthwaite, G., Pangalos, M.N., 2014. Lessons learned from the fate of AstraZeneca's drug pipeline: A five-dimensional framework. Nat. Rev. Drug Discov. 13, 419–431. https://doi.org/10.1038/nrd4309

Corselli, M., Chin, C.J., Parekh, C., Sahaghian, A., Wang, W., Ge, S., Evseenko, D., Wang, X., Montelatici, E., Lazzari, L., Crooks, G.M., Bruno, P., 2013. Perivascular support of human hematopoietic stem / progenitor cells. Blood 121, 2891–2901. https://doi.org/10.1182/blood-2012-08-451864.The

Cosgrove, B.D., Mui, K.L., Driscoll, T.P., Caliari, S.R., Mehta, K.D., Assoian, R.K., Burdick, J.A., Mauck, R.L., 2016. N-cadherin adhesive interactions modulate matrix mechanosensing and fate commitment of mesenchymal stem cells. Nat. Mater. 15, 1297–1306. https://doi.org/10.1038/nmat4725

Covello, K., Kehler, J., Yu, H., Gordan, J., Arsham, A., Hu, C., Labosky, P., Simon, M., Keith, B., 2006. HIF-2alfa regulates Oct-4: effects of hypoxia on stem cell function , embryonic development , and tumor growth. Genes Dev. 20, 557–570. https://doi.org/10.1101/gad.1399906.Sox2

Crisan, M., Yap, S., Casteilla, L., Chen, C.-W., Corselli, M., Park, T.S., Andriolo, G., Sun, B., Zheng, B., Zhang, L., Norotte, C., Teng, P.-N., Traas, J., Schugar, R., Deasy, B.M., Badylak, S., Bűhring, H.-J., Giacobino, J.-P., Lazzari, L., Huard, J., Péault, B., 2008. A Perivascular Origin for Mesenchymal Stem Cells in Multiple Human Organs. Cell Stem Cell 3, 301–313. https://doi.org/10.1016/j.stem.2008.07.003

Crouzier, T., Fourel, L., Boudou, T., Albigès-Rizo, C., Picart, C., 2011. Presentation of BMP-2 from a soft biopolymeric film unveils its activity on cell adhesion and migration. Adv. Mater. 23, 111–118. https://doi.org/10.1002/adma.201004637

Cuomo, F., Coppola, A., Botti, C., Maione, C., Forte, A., Scisciola, L., Liguori, G., Caiafa, I., Ursini, M.V., Galderisi, U., Cipollaro, M., Altucci, L., Cobellis, G., 2018. Pro-inflammatory cytokines activate hypoxia-inducible factor 3α via epigenetic changes in mesenchymal stromal/stem cells. Sci. Rep. 8, 1–12. https://doi.org/10.1038/s41598-018-24221-5

Curtis, A.S., Varde, M., 1964. Control of cell behaviour: Topological factors. J. Natl. Cancer Inst. 33, 15–26.

Cutler, C., Kim, H.T., Armand, P., Koreth, J., Glotzbecker, B., Ho, V.T., Alyea, E., Isom, M., Kao, G., Soiffer, R.J., Ritz, J., Goessling, W., North, T.E., Zon, L.I., Antin, J.H., Hoggatt, J., Silberstein, L., Scadden, D.T., Multani, P., Robbins, D.,

Le, T., Desponts, C., Rezner, B., Mendlein, J., Shoemaker, D.D., Chen, Y.-B., Ballen, K., Pelus, L.M., Hu, P., Armant, M., 2013. Prostaglandin-modulated Umbilical cord blood hematopoietic stem cell transplantation. Blood 122, 3074–3081. https://doi.org/10.1182/blood-2013-05-503177

Cutler, S.M., Garcia, A.J., 2003. Engineering cell adhesive surfaces that direct integrin a5B1 binding using a recombinant fragment of fibronectin. Biomaterials 24, 1759–1770. https://doi.org/10.1016/S0142-9612(02)00570-7

D'Ippolito, G., Diabira, S., Howard, G.A., Roos, B.A., Schiller, P.C., 2006. Low oxygen tension inhibits osteogenic differentiation and enhances stemness of human MIAMI cells. Bone 39, 513–522. https://doi.org/10.1016/j.bone.2006.02.061

D'Souza, A., Fretham, C., 2018. Current Uses and Outcomes of Hematopoietic Cell Transplantation (HCT): CIBMTR Summary Slides, 2018.

Da Cruz, L., Fynes, K., Georgiadis, O., Kerby, J., Luo, Y.H., Ahmado, A., Vernon, A., Daniels, J.T., Nommiste, B., Hasan, S.M., Gooljar, S.B., Carr, A.J.F., Vugler, A., Ramsden, C.M., Bictash, M., Fenster, M., Steer, J., Harbinson, T., Wilbrey, A., Tufail, A., Feng, G., Whitlock, M., Robson, A.G., Holder, G.E., Sagoo, M.S., Loudon, P.T., Whiting, P., Coffey, P.J., 2018. Phase 1 clinical study of an embryonic stem cell-derived retinal pigment epithelium patch in age-related macular degeneration. Nat. Biotechnol. 36, 1–10. https://doi.org/10.1038/nbt.4114

da Silva Meirelles, L., Maistro Malta, T., de Deus Wagatsuma, V.M., Palma, P.V.B., Araujo, A.G., Ribeiro Malmegrim, K.C., Morato de Oliveira, F., Panepucci, R.A., Silva-Jr, W., Kashima Haddad, S., Covas, D.T., 2015. Cultured human adipose tissue pericytes and mesenchymal stromal cells display a very similar gene expression profile. Stem Cells Dev. 00. https://doi.org/10.1089/scd.2015.0153

Dalby, M.J., Gadegaard, N., Herzyk, P., Sutherland, D., Agheli, H., Wilkinson, C.D.W., Curtis, A.S.G., 2007a. Nanomechanotransduction and interphase nuclear organization influence on genomic control. J. Cell. Biochem. 102, 1234–1244. https://doi.org/10.1002/jcb.21354

Dalby, M.J., Gadegaard, N., Oreffo, R.O.C., 2014. Harnessing nanotopography and integrin-matrix interactions to influence stem cell fate. Nat. Mater. 13, 558–569. https://doi.org/10.1038/nmat3980

Dalby, M.J., Gadegaard, N., Tare, R., Andar, A., Riehle, M.O., Herzyk, P., Wilkinson, C.D.W., Oreffo, R.O.C., 2007b. The control of human mesenchymal cell differentiation using nanoscale symmetry and disorder. Nat. Mater. 6, 997–1003. https://doi.org/10.1038/nmat2013

Dalby, M.J., García, A.J., Salmeron-Sanchez, M., 2018. Receptor control in mesenchymal stem cell engineering. Nat. Rev. Mater. 3, 17091. https://doi.org/10.1038/natrevmats.2017.91

Dalby, M.J., Riehle, M.O., Johnstone, H., Affrossman, S., Curtis, A.S.G., 2004. Investigating the limits of filopodial sensing: A brief report using SEM to image the interaction between 10 nm high nano-topography and fibroblast filopodia. Cell Biol. Int. 28, 229–236. https://doi.org/10.1016/j.cellbi.2003.12.004

Daley, W.P., Gulfo, K.M., Sequeira, S.J., Larsen, M., 2009. Identification of a mechanochemical checkpoint and negative feedback loop regulating branching morphogenesis. Dev. Biol. 336, 169–182. https://doi.org/10.1016/j.ydbio.2009.09.037

Daley, W.P., Kohn, J.M., Larsen, M., 2011. A focal adhesion protein-based mechanochemical checkpoint regulates cleft progression during branching morphogenesis. Dev. Dyn. 240, 2069–2083. https://doi.org/10.1002/dvdy.22714

Danet, G.., Pan, Y., Luongo, J.., Bonnet, D.., Celest Simon, M., 2003. Expansion of human SCID-repopulating cells under hypoxic conditions. J. Clin. Invest. 112, 126–135. https://doi.org/10.1172/JCI17669 [doi]\r112/1/126 [pii]

Davis, B.L., Praveen, S.S., 2006. Nonlinear Versus Linear Behavior of Calcaneal Bone Marrow At Different Shear Rates. Proc. Annu. Meet. Am. Soc. Biomater. 1–2. https://doi.org/papers://82E9EA27-E255-4A82-9E40-6DAC45A310F4/Paper/p687

De Caestecker, M., 2004. The transforming growth factor-β superfamily of receptors. Cytokine Growth Factor Rev. 15, 1–11. https://doi.org/10.1016/j.cytogfr.2003.10.004

De Laporte, L., Rice, J.J., Tortelli, F., Hubbell, J.A., 2013. Tenascin C Promiscuously Binds Growth Factors via Its Fifth Fibronectin Type III-Like Domain. PLoS One 8. https://doi.org/10.1371/journal.pone.0062076

Decker, M., Leslie, J., Liu, Q., Ding, L., 2018. Hepatic thrombopoietin is required for bone marrow hematopoietic stem cell maintenance. Science (80-.). 360, 106–110. https://doi.org/10.1126/science.aap8861

DeForest, C.A., Anseth, K.S., 2012. Photoreversible patterning of biomolecules within click-based hydrogels. Angew. Chemie - Int. Ed. 51, 1816–1819. https://doi.org/10.1002/anie.201106463

Deforest, C.A., Polizzotti, B.D., Anseth, K.S., 2009. Sequential click reactions for synthesizing and patterning three-dimensional cell microenvironments. Nat. Mater. 8, 659–664. https://doi.org/10.1038/nmat2473

Deguchi, J.O., Yamazaki, H., Aikawa, E., Aikawa, M., 2009. Chronic hypoxia activates the akt and β-catenin pathways in human macrophages. Arterioscler. Thromb. Vasc. Biol. 29, 1664–1670. https://doi.org/10.1161/ATVBAHA.109.194043

Dellavalle, A., Sampaolesi, M., Tonlorenzi, R., Tagliafico, E., Sacchetti, B., Perani, L., Innocenzi, A., Galvez, B.., Messina, G., Morosetti, R., Sheng, L., Belicchi, M., Peretti, M., Chamberlain, J.., Wright, E., Torrente, Y., Bianco, P., Cossu, G., 2007. Pericytes of human skeletal muscle are myogenic precursors distinct from satellite cells. Nat. Cell Biol. 9, 255–267. https://doi.org/http://dx.doi.org/10.1038/ncb1542

Dengler, V.L., Galbraith, M.D., Espinosa, J.M., 2014. Transcriptional regulation by hypoxia inducible factors. Crit. Rev. Biochem. Mol. Biol. 49, 1–15. https://doi.org/10.3109/10409238.2013.838205

Derynck, R., Zhang, Y.E., 2003. Smad-dependent and Smad-independent pathways in

TGF-B family signalling. Nature 425. https://doi.org/10.1038/nature02006

Dexter, T.., Moore, M.A.., Sheridan, A.P.., 1977. Maintenance of hemopoietic stem cells and production of differentiated progeny in allogeneic and semiallogeneic bone marrow chimeras in vitro. J. Exp. Med. 145, 1612–1616. https://doi.org/10.1084/jem.173.4.1021

Dhami, S.P.S., Kappala, S.S., Thompson, A., Szegezdi, E., 2016. Three-dimensional ex vivo co-culture models of the leukaemic bone marrow niche for functional drug testing. Drug Discov. Today 21, 1464–1471. https://doi.org/10.1016/j.drudis.2016.04.019

Diehlmann, A., Horn, P., Saffrich, R., Ho, A.D., Wagner, W., Eckstein, V., Walenda, T., Bork, S., Wein, F., 2010. Co-culture with mesenchymal stromal cells increases proliferation and maintenance of haematopoietic progenitor cells. J. Cell. Mol. Med. 14, 337–350. https://doi.org/10.1111/j.1582-4934.2009.00776.x

DiGiusto, D., Chen, S., Combs, J., Webb, S., Namikawa, R., Tsukamoto, A., Chen, B.P., Galy, A.H., 1994. Human fetal bone marrow early progenitors for T, B, and myeloid cells are found exclusively in the population expressing high levels of CD34. Blood 84, 421–32.

Dimitriou, R., Tsiridis, E., Giannoudis, P. V., 2005. Current concepts of molecular aspects of bone healing. Injury 36, 1392–1404. https://doi.org/10.1016/j.injury.2005.07.019

Ding, L., Morrison, S.J., 2013. Haematopoietic stem cells and early lymphoid progenitors occupy distinct bone marrow niches. Nature 495, 231–235. https://doi.org/10.1038/nature11885

Ding, L., Saunders, T.L., Enikolopov, G., Morrison, S.J., 2012. Endothelial and perivascular cells maintain haematopoietic stem cells. Nature 481, 457–62. https://doi.org/10.1038/nature10783

Domen, J., Wagers, A., Weissman, I.L., 2006. Bone Marrow (Hematiopoietic) Stem Cells, in: Stem Cell Information: The National Institutes of Health Resource for Stem Cell Research. NIH, pp. 13–34.

Dominici, M., Le Blanc, K., Mueller, I., Slaper-Cortenbach, I., Marini, F., Krause, D., Deans, R., Keating, A., Prockop, D., Horwitz, E., 2006. Minimal criteria for defining multipotent mesenchymal stromal cells. The International Society for Cellular Therapy position statement. Cytotherapy 8, 315–7. https://doi.org/10.1080/14653240600855905

Donnelly, H., Dalby, M.J., Salmeron-Sanchez, M., Sweeten, P.E., 2016. Current approaches for modulation of the nanoscale interface in the regulation of cell behavior. Nanomedicine Nanotechnology, Biol. Med. 1–10. https://doi.org/10.1016/j.nano.2017.03.020

Donnelly, H., Salmerón-Sánchez, M., Dalby, M.J., 2018. Designing stem cell niches for differentiation and self-renewal. J. R. Soc. Interface.

Donnelly, H., Smith, C.-A., Sweeten, P.E., Gadegaard, N., Meek, R.D., D'Este, M., Mata,

A., Eglin, D., Dalby, M.J., 2017. Bone and cartilage differentiation of a single stem cell population driven by material interface. J. Tissue Eng. 8. https://doi.org/10.1177/2041731417705615

Driscoll, T.P., Cosgrove, B.D., Heo, S.J., Shurden, Z.E., Mauck, R.L., 2015. Cytoskeletal to Nuclear Strain Transfer Regulates YAP Signaling in Mesenchymal Stem Cells. Biophys. J. 108, 2783–2793. https://doi.org/10.1016/j.bpj.2015.05.010

Drury, J.L., Mooney, D.J., 2003. Hydrogels for tissue engineering: Scaffold design variables and applications. Biomaterials 24, 4337–4351. https://doi.org/10.1016/S0142-9612(03)00340-5

Dupont, S., Morsut, L., Aragona, M., Enzo, E., Giulitti, S., Cordenonsi, M., Zanconato, F., Le Digabel, J., Forcato, M., Bicciato, S., Elvassore, N., Piccolo, S., 2011. Role of YAP/TAZ in mechanotransduction. Nature 474, 179–184. https://doi.org/10.1038/nature10137

Eaves, C.J., 2015. Hematopoietic stem cells : concepts, definitions, and the new reality. Blood 125, 2605–2614. https://doi.org/10.1182/blood-2014-12-570200.Lessons

Ehninger, A., Trumpp, A., 2011. The bone marrow stem cell niche grows up: mesenchymal stem cells and macrophages move in. J. Exp. Med. 208, 421–428. https://doi.org/10.1084/jem.20110132

Ejtehadifar, M., Shamsasenjan, K., Movassaghpour, A., Akbarzadehlaleh, P., Dehdilani, N., Abbasi, P., Molaeipour, Z., Saleh, M., 2015. The effect of hypoxia on mesenchymal stem cell biology. Adv. Pharm. Bull. 5, 141–149. https://doi.org/10.15171/apb.2015.021

Elosegui-Artola, A., Andreu, I., Beedle, A.E., Lezamiz, A., Uroz, M., Kosmalska, A.J., Oria, R., Kechagia, J.Z., Rico-Lastres, P., Le Roux, A.-L., Shanahan, C.M., Trepat, X., Navajas, D., Garcia-Manyes, S., Roca-Cusachs, P., 2017. Force triggers YAP nuclear entry by mechanically regulating transport across nuclear pores. Cell (in press). https://doi.org/10.1016/j.cell.2017.10.008

Elosegui-Artola, A., Trepat, X., Roca-Cusachs, P., 2018. Control of Mechanotransduction by Molecular Clutch Dynamics. Trends Cell Biol. xx, 1–12. https://doi.org/10.1016/j.tcb.2018.01.008

Ema, M., Taya, S., Yokotani, N., Sogawa, K., Matsuda, Y., Fujii-Kuriyama, Y., 1997. A novel bHLH-PAS factor with close sequence similarity to hypoxia-inducible factor 1a regulates the VEGF expression and is potentially involved in lung and vascular development. Proc. Natl. Acad. Sci. 94, 4273–4278.

Engler, A.J., Sen, S., Sweeney, H.L., Discher, D.E., 2006. Matrix elasticity directs stem cell lineage specification. Cell 126, 677–89. https://doi.org/10.1016/j.cell.2006.06.044

Estrada, J.C., Albo, C., Benguría, A., Dopazo, A., López-Romero, P., Carrera-Quintanar, L., Roche, E., Clemente, E.P., Enríquez, J.A., Bernad, A., Samper, E., 2012. Culture of human mesenchymal stem cells at low oxygen tension improves growth and genetic stability by activating glycolysis. Cell Death Differ. 19, 743–55. https://doi.org/10.1038/cdd.2011.172

Ewart, L., Dehne, E.-M., Fabre, K., Gibbs, S., Hickman, J., Hornberg, E., Ingelman-Sundberg, M., Jang, K.-J., Jones, D.R., Lauschke, V.M., Marx, U., Mettetal, J.T., Pointon, A., Williams, D., Zimmermann, W.-H., Newham, P., 2018. Application of Microphysiological Systems to Enhance Safety Assessment in Drug Discovery. Annu. Rev. Pharmacol. Toxicol. 58, 65–82. https://doi.org/10.1146/annurev-pharmtox-010617-052722

Fan, V.H., Tamama, K., Au, A., Littrell, R., Richardson, L.B., Wright, J.W., Wells, A., Griffith, L.G., 2007. Tethered epidermal growth factor provides a survival advantage to mesenchymal stem cells. Stem Cells 25, 1241–1251. https://doi.org/10.1634/stemcells.2006-0320

Fehrer, C., Brunauer, R., Laschober, G., Unterluggauer, H., Reitinger, S., Kloss, F., Gülly, C., Gaßner, R., Lepperdinger, G., 2007. Reduced oxygen tension attenuates differentiation capacity of human mesenchymal stem cells and prolongs their lifespan. Aging Cell 6, 745–757. https://doi.org/10.1111/j.1474-9726.2007.00336.x

Feng, J., Mantesso, A., De Bari, C., Nishiyama, A., Sharpe, P.T., 2011. Dual origin of mesenchymal stem cells contributing to organ growth and repair. Proc. Natl. Acad. Sci. 108, 6503–6508. https://doi.org/10.1073/pnas.1015449108

Flaim, C.J., Chien, S., Bhatia, S.N., 2005. An extracellular matrix microarray for probing cellular differentiation. Nat. Methods 2, 119–125. https://doi.org/10.1038/nmeth736

Forristal, C.E., Wright, K.L., Hanley, N.A., Oreffo, R.O.C., Houghton, F.D., 2010. Hypoxia inducible factors regulate pluripotency and proliferation in human embryonic stem cells cultured at reduced oxygen tensions. Reproduction 139, 85–97. https://doi.org/10.1530/REP-09-0300

Fourel, L., Valat, A., Faurobert, E., Guillot, R., Bourrin-reynard, I., Ren, K., Lafanechère, L., Planus, E., Picart, C., Albiges-Rizo, C., 2016. β3 integrin–mediated spreading induced by matrix-bound BMP-2 controls Smad signaling in a stiffness-independent manner. J. Cell Biol. 212, jcb.201508018. https://doi.org/10.1083/jcb.201508018

Frenette, P.S., Subbarao, S., Mazo, I.B., von Andrian, U.H., Wagner, D.D., 1998. Endothelial selectins and vascular cell adhesion molecule-1 promote hematopoietic progenitor homing to bone marrow. Proc. Natl. Acad. Sci. 95, 14423–14428. https://doi.org/10.1073/pnas.95.24.14423

Friedenstein, A.J., 1976. Precursor Cells of Mechanocytes. Int. Rev. Cytol. 47, 327–359.

Fuentealba, L.C., Obernier, K., Alvarez-Buylla, A., 2012. Adult neural stem cells bridge their niche. Cell Stem Cell 10, 698–708. https://doi.org/10.1016/j.stem.2012.05.012

Garcia, A.J., 2014. PEG-Maleimide Hydrogels for Protein and Cell Delivery in Regenerative Medicine. Ann. Biomed. Eng. 42, 312–322. https://doi.org/10.1038/jid.2014.371

Gaziev, J., Sodani, P., Polchi, P., Andreani, M., Lucarelli, G., 2005. Bone marrow transplantation in adults with thalassemia: Treatment and long-term follow-up.

Ann. N. Y. Acad. Sci. 1054, 196–205. https://doi.org/10.1196/annals.1345.024

Genetos, D.C., Toupadakis, C.A., Raheja, L.F., Wong, A., Papanicolaou, S.E., Fyhrie, D.P., Loots, G.G., Yellowley, C.E., 2010. Hypoxia decreases sclerostin expression and increases Wnt signaling in osteoblasts. J. Cell. Biochem. 110, 457–467. https://doi.org/10.1002/jcb.22559

Gobaa, S., Hoehnel, S., Roccio, M., Negro, A., Kobel, S., Lutolf, M.P., 2011. Artificial niche microarrays for probing single stem cell fate in high throughput. Nat. Methods 8, 949–955. https://doi.org/10.1038/nmeth.1732

Goessling, W., North, T.E., Loewer, S., Lord, A.M., Lee, S., Stoick-cooper, C.L., Weidinger, G., Puder, M., Daley, G.Q., Moon, R.T., Zon, L.I., 2009. Genetic Interaction of PGE2 and Wnt Signaling Regulates Developmental Specification of Stem Cells and Regeneration. Cell 136, 1136–1147. https://doi.org/10.1016/j.cell.2009.01.015

Gong, J. k., 1978. Edosteal Marrow: A Rich Source of Hematopoietic Stem Cells. Science (80-.). 562, 1443–1445.

Gortiz, C., Dias, D.., Tomilin, N., Barbacid, M., Shupliakov, O., Frisen, J., 2011. A Pericyte Origin of Spinal Cord Scar Tissue. Science (80-.). 238–243.

Greenbaum, A., Hsu, Y.S., Day, R.B., Schuettpelz, L.G., Christopher, M.J., Borgerding, J.N., Nagasawa, T., Link, D.C., 2013. CXCL12 in early mesenchymal progenitors is required for haematopoietic stem-cell maintenance. Nature 495, 227–230. https://doi.org/10.1038/nature11926

Guarnerio, J., Coltella, N., Ala, U., Tonon, G., Pandolfi, P.P., Bernardi, R., 2014. Bone Marrow Endosteal Mesenchymal Progenitors Depend on HIF Factors for Maintenance and Regulation of Hematopo. Stem Cell Reports 2, 794–809. https://doi.org/10.1016/j.stemcr.2014.04.002

Gugutkov, D., Altankov, G., Rodríguez Hernández, J.C., Monleón Pradas, M., Salmerón-Sánchez, M., 2010. Fibronectin activity on substrates with controlled -OH density. J. Mater. Res. Part A 92, 332–331. https://doi.org/10.1002/jbm.a.32374

Guimaraes-Camboa, N., Cattaneo, P., Sun, Y., Moore-morris, T., Gu, Y., Dalton, N.D., Rockenstein, E., Masliah, E., Stallcup, W.B., Chen, J., Evans, S.M., 2017. Pericytes of Multiple Organs Do Not Behave as Article Pericytes of Multiple Organs Do Not Behave as Mesenchymal Stem Cells In Vivo. Cell Stem Cell 20, 1–15. https://doi.org/10.1016/j.stem.2016.12.006

Guo, B., Huang, X., Lee, M.R., Lee, S.A., Broxmeyer, H.E., 2018. Antagonism of PPAR-γ signaling expands human hematopoietic stem and progenitor cells by enhancing glycolysis. Nat. Med. https://doi.org/10.1038/nm.4477

Hadden, W.J., Young, J.L., Holle, A.W., McFetridge, M.L., Kim, D.Y., Wijesinghe, P., Taylor-Weiner, H., Wen, J.H., Lee, A.R., Bieback, K., Vo, B.-N., Sampson, D.D., Kennedy, B.F., Spatz, J.P., Engler, A.J., Choi, Y.S., 2017. Stem cell migration and mechanotransduction on linear stiffness gradient hydrogels. Proc. Natl. Acad. Sci. 114, 5647–5652. https://doi.org/10.1073/pnas.1618239114

Hagedorn, E.J., Durand, E.M., Fast, E.M., Zon, L.I., 2015. Getting more for your marrow: boosting hematopoietic stem cells numbers with PGE2 329, 220–226. https://doi.org/10.1016/j.yexcr.2014.07.030.Getting

Hambardzumyan, D., Becher, O.J., Rosenblum, M.K., Pandolfi, P.P.P., Manova-Todorova, K., Holland, E.C., 2008. PI3K pathway regulates survival of cancer stem cells residing in the perivascular niche following radiation in medulloblastoma in vivo. Genes Dev. 22, 436–448. https://doi.org/10.1101/gad.1627008

Hammoud, M., Vlaski, M., Duchez, P., Chevaleyre, J., Lafarge, X., Boiron, J.M., Praloran, V., Brunet de la Grange, P., Ivanovic, Z., 2012. Combination of low O 2 concentration and mesenchymal stromal cells during culture of cord blood CD34 + cells improves the maintenance and proliferative capacity of hematopoietic stem cells. J. Cell. Physiol. 227, 2750–2758. https://doi.org/10.1002/jcp.23019

Hao, Q.L., Shah, A.J., Thiemann, F.T., Smogorzewska, E.M., Crooks, G.M., 1995. A functional comparison of CD34 + CD38- cells in cord blood and bone marrow. Blood 86, 3745–53.

Hao, Q.L., Zhu, J., Price, M.A., Payne, K.J., Barsky, L.W., Crooks, G.M., 2001. Identification of a novel, human multilymphoid progenitor in cord blood. Blood 97, 3683–3690. https://doi.org/10.1182/blood.V97.12.3683

Hassan, M.Q., Tare, R.S., Lee, S.H., Mandeville, M., Morasso, M.I., Javed, A., Wijnen, A.J. Van, Stein, J.L., Stein, G.S., Lian, J.B., 2006. BMP2 Commitment to the Osteogenic Lineage Involves Activation of. J. Biol. Chem. 281, 40515–40526. https://doi.org/10.1074/jbc.M604508200

Hayashi, I., Vuori, K., Liddington, R.C., 2002. The focal adhesion targeting (FAT) region of focal adhesion kinase is a four-helix bundle that binds paxillin. Nat. Struct. Biol. 9, 101–106. https://doi.org/10.1038/nsb755

Heldin, C.-H., Kohei, M., Peter, D., 1997. TFG-beta signalling from cell membrane to nucleas through SMAD proteins. Nature 390, 465–71.

Hermitte, F., Brunet de la Grange, P., Belloc, F., Praloran, V., Ivanovic, Z., 2006. Very Low O_2 Concentration (0.1%) Favors G_0 Return of Dividing $CD34^+$ Cells. Stem Cells 24, 65–73. https://doi.org/10.1634/stemcells.2004-0351

Herrera, M.B., Bussolati, B., Bruno, S., Morando, L., Mauriello-Romanazzi, G., Sanavio, F., Stamenkovic, I., Biancone, L., Camussi, G., 2007. Exogenous mesenchymal stem cells localize to the kidney by means of CD44 following acute tubular injury. Kidney Int. 72, 430–441. https://doi.org/10.1038/sj.ki.5002334

Herrmann, M., Bara, J., Sprecher, C., Menzel, U., Jalowiec, J., Osinga, R., Scherberich, A., Alini, M., Verrier, S., 2016. Pericyte plasticity – comparative investigation of the angiogenic and multilineage potential of pericytes from different human tissues. Eur. Cells Mater. 31, 236–249. https://doi.org/10.22203/ecm.v031a16

Hofmeister, C.C., Zhang, J., Knight, K.L., Le, P., Stiff, P.J., 2007. Ex vivo expansion of umbilical cord blood stem cells for transplantation: Growing knowledge from the hematopoietic niche. Bone Marrow Transplant. 39, 11–23. https://doi.org/10.1038/sj.bmt.1705538

Holst, J., Watson, S., Lord, M.S., Eamegdool, S.S., Bax, D. V., Nivison-Smith, L.B., Kondyurin, A., Ma, L., Oberhauser, A.F., Weiss, A.S., Rasko, J.E.J., 2010. Substrate elasticity provides mechanical signals for the expansion of hemopoietic stem and progenitor cells. Nat. Biotechnol. 28, 1123–1128. https://doi.org/10.1038/nbt.1687

Holzwarth, C., Vaegler, M., Gieseke, F., Pfister, S.M., Handgretinger, R., Kerst, G., Müller, I., 2010. Low physiologic oxygen tensions reduce proliferation and differentiation of human multipotent mesenchymal stromal cells. BMC Cell Biol. 11. https://doi.org/10.1186/1471-2121-11-11

Horwitz, M.E., Kurtzberg, J., Peled, T., Horwitz, M.E., Chao, N.J., Rizzieri, D.A., Long, G.D., 2014. Umbilical cord blood expansion with nicotinamide provides long-term multilineage engraftment Clinical medicine Umbilical cord blood expansion with nicotinamide provides long-term multilineage engraftment. J. Clin. Invest. 124, 3121–3128. https://doi.org/10.1172/JCI74556.transplantation

Hu, C., Wang, L., Chodosh, L. a, Keith, B., Simon, M.C., 2003. Differential Roles of Hypoxia-Inducible Factor 1 alpha and HIF-2 alpha in Hypoxix Gene Regulation. Mol Cell Biol 23, 9361–9374. https://doi.org/10.1128/MCB.23.24.9361

Huebsch, N., Arany, P.R., Mao, A.S., Shvartsman, D., Ali, O.A., Bencherif, S.A., Rivera-Feliciano, J., Mooney, D.J., 2010. Harnessing traction-mediated manipulation of the cell/matrix interface to control stem-cell fate. Nat. Mater. 9, 518–526. https://doi.org/10.1038/nmat2732

Hung, S.P., Ho, J.H., Shih, Y.R. V, Lo, T., Lee, O.K., 2012. Hypoxia promotes proliferation and osteogenic differentiation potentials of human mesenchymal stem cells. J. Orthop. Res. 30, 260–266. https://doi.org/10.1002/jor.21517

Hynes, R.O., 2002. Integrins: Bidirectional, allosteric signaling machines. Cell 110, 673–687. https://doi.org/10.1016/S0092-8674(02)00971-6

Im, G. Il, Shin, Y.W., Lee, K.B., 2005. Do adipose tissue-derived mesenchymal stem cells have the same osteogenic and chondrogenic potential as bone marrow-derived cells? Osteoarthr. Cartil. 13, 845–853. https://doi.org/10.1016/j.joca.2005.05.005

Ingber, D.E., 2003a. Tensegrity I. Cell structure and hierarchical systems biology. J. Cell Sci. 116, 1157–1173. https://doi.org/10.1242/jcs.00359

Ingber, D.E., 2003b. Tensegrity II. How structural networks influence cellular information processing networks. J. Cell Sci. 116, 1397–1408. https://doi.org/10.1242/jcs.00360

Ishikawa, T., Wondimu, Z., Oikawa, Y., Gentilcore, G., Kiessling, R., Egyhazi Brage, S., Hansson, J., Patarroyo, M., 2014. Laminins 411 and 421 differentially promote tumor cell migration via α6ß1 integrin and MCAM (CD146). Matrix Biol. 38, 69–83. https://doi.org/10.1016/j.matbio.2014.06.002

Ito, K., Suda, T., 2014. Metabolic requirements for the maintenance of self-renewing stem cells. Nat. Rev. Mol. Cell Biol. 15, 243–256. https://doi.org/10.1038/nrm3772

Ito, T., Itakura, S., Todorov, I., Rawson, J., Asari, S., Shintaku, J., Nair, I., Ferreri, K., Kandeel, F., Mullen, Y., 2010. Mesenchymal stem cell and islet co-transplantation

promotes graft revascularization and function. Transplantation 89, 1438–1445. https://doi.org/10.1097/TP.0b013e3181db09c4

Ivan, M., Kondo, K., Yang, H.F., Kim, W., Valiando, J., Ohh, M., Salic, A., Asara, J.M., Lane, W.S., Kaelin, W.G., 2001. HIF alpha targeted for VHL-mediated destruction by proline hydroxylation: Implications for O-2 sensing. Science (80-.). 292, 464–468.

Jaakkola, P., Mole, D.R., Tian, Y.M., Wilson, M.I., Gielbert, J., Gaskell, S.J., von Kriegsheim, A., Hebestreit, H.F., Mukherji, M., Schofield, C.J., Maxwell, P.H., Pugh, C.W., Ratcliffe, P.J., 2001. Targeting of HIF-alpha to the von Hippel-Lindau ubiquitylation complex by O-2-regulated prolyl hydroxylation. Science (80-.). 292, 468–472. https://doi.org/10.1126/science.1059796

Jagannathan-Bogdan, M., Zon, L.I., 2013. Hematopoiesis. Development 140, 2463–2467. https://doi.org/10.1016/B978-0-12-374984-0.00686-0

Jain, N., Vogel, V., 2018. Spatial confinement downsizes the inflammatory response of macrophages. Nat. Mater. 17, 1134–1144. https://doi.org/10.1038/s41563-018-0190-6

Janmey, P.A., Euteneuer, U., Traub, P., Schliwa, M., 1991. Viscoelastic properties of vimentin compared with other filamentous biopolymer networks. J. Cell Biol. 113, 155–160. https://doi.org/10.1083/jcb.113.1.155

Jansen, K.A., Atherton, P., Ballestrem, C., 2017. Mechanotransduction at the cell-matrix interface. Semin. Cell Dev. Biol. 71, 75–83. https://doi.org/10.1016/j.semcdb.2017.07.027

Jansen, L.A., Birch, N.P., Schiffman, J.D., Crosby, A.J., Peyton, S.R., 2015. Mechanics of intact bone marrow. J. Mech. Behav. Biomed. Mater. 50, 299–307. https://doi.org/10.1016/j.jmbbm.2015.06.023

Jiang, Y., Chen, J., Deng, C., Suuronen, E.J., Zhong, Z., 2014. Click hydrogels, microgels and nanogels: Emerging platforms for drug delivery and tissue engineering. Biomaterials 35, 4969–4985. https://doi.org/10.1016/j.biomaterials.2014.03.001

Jones, D.L., Wagers, A.J., 2008. No place like home: anatomy and function of the stem cell niche. Nat. Rev. Mol. Cell Biol. 9, 11–21. https://doi.org/10.1038/nrm2319

Jonsson, P., Bruce, S.J., Moritz, T., Trygg, J., Sjöström, M., Plumb, R., Granger, J., Maibaum, E., Nicholson, J.K., Holmes, E., Antti, H., 2005. Extraction, interpretation and validation of information for comparing samples in metabolic LC/MS data sets. Analyst 130, 701–707. https://doi.org/10.1039/b501890k

Kadler, K.E., Baldock, C., Bella, J., Boot-Hanford, R.P., 2007. Collagens at a glance. J. Cell Sci. 120, 1955–1958. https://doi.org/10.1007/b103817

Kanchanawong, P., Shtengel, G., Pasapera, A.M., Ramko, E.B., Davidson, M.W., Hess, H.F., Waterman, C.M., 2010. Nanoscale architecture of integrin-based cell adhesions. Nature 468, 580–4. https://doi.org/10.1038/nature09621

Kasemo, B., Lausmaa, J., 1988. Biomaterial and Implant Surfaces: A Surface Science Approach. Int. J. Oral Maxillofac. Implant. 3, 247–259.

Katayama, Y., Battista, M., Kao, W.M., Hidalgo, A., Peired, A.J., Thomas, S.A., Frenette, P.S., 2006. Signals from the sympathetic nervous system regulate hematopoietic stem cell egress from bone marrow. Cell 124, 407–421. https://doi.org/10.1016/j.cell.2005.10.041

Kaushansky, K., 2006. Lineage-Specific Hematopoietic Growth Factors. N. Engl. J. Med. 354, 2034–2045. https://doi.org/10.1056/NEJMra052706

Keselowsky, B.G., Collard, D.M., Garcia, A.J., 2005. Integrin binding specificity regulates biomaterial surface chemistry effects on cell differentiation. Proc. Natl. Acad. Sci. U. S. A. 102, 5953–5957. https://doi.org/10.1073/pnas.0407356102

Keselowsky, B.G., Collard, D.M., García, A.J., 2004. Surface chemistry modulates focal adhesion composition and signaling through changes in integrin binding. Biomaterials 25, 5947–5954. https://doi.org/10.1016/j.biomaterials.2004.01.062

Keselowsky, B.G., Collard, D.M., Garcı, J., 2002. Surface chemistry modulates fibronectin conformation and directs integrin binding and specificity to control cell adhesion. J Biomed Mat Res 66, 247–259. https://doi.org/10.1002/jbm.a.10537

Khetan, S., Guvendiren, M., Legant, W.R., Cohen, D.M., Chen, C.S., Burdick, J.A., 2013. Degradation-mediated cellular traction directs stem cell fate in covalently crosslinked three-dimensional hydrogels. Nat. Mater. 12, 458–465. https://doi.org/10.1038/nmat3586

Kiel, M.J., Acar, M., Radice, G.L., Morrison, S.J., 2009. Hematopoietic Stem Cells Do Not Depend on N-Cadherin to Regulate Their Maintenance. Cell Stem Cell 4, 170–179. https://doi.org/10.1016/j.stem.2008.10.005

Kiel, M.J., Yilmaz, Omer H, Iwashita, T., Yilmaz, Osman H, Terhorst, C., Morrison, S.J., 2005. SLAM family receptors distinguish hematopoietic stem and progenitor cells and reveal endothelial niches for stem cells. Cell 121, 1109–21. https://doi.org/10.1016/j.cell.2005.05.026

Kikuchi, T., Morizane, A., Doi, D., Magotani, H., Onoe, H., Hayashi, T., Mizuma, H., Takara, S., Takahashi, R., Inoue, H., Morita, S., Yamamoto, M., Okita, K., Nakagawa, M., Parmar, M., Takahashi, J., 2017. Human iPS cell-derived dopaminergic neurons function in a primate Parkinson's disease model. Nature 548, 592–596. https://doi.org/10.1038/nature23664

Kilian, K. a, Bugarija, B., Lahn, B.T., Mrksich, M., 2010. Geometric cues for directing the differentiation of mesenchymal stem cells. Proc. Natl. Acad. Sci. U. S. A. 107, 4872–7. https://doi.org/10.1073/pnas.0903269107

Kirito, K., Fox, N., Komatsu, N., Kaushansky, K., 2005. Thrombopoietin enhances expression of vascular endothelial growth factor (VEGF) in primitive hematopoietic cells through induction of Thrombopoietin enhances expression of vascular endothelial growth factor (VEGF) in primitive hematopoietic cells thro 105, 4258–4263. https://doi.org/10.1182/blood-2004-07-2712

Kirkpatrick, C.A., Selleck, S.B., 2007. Heparan sulfate proteoglycans at a glance. J. Cell Sci. 120, 1829–1832. https://doi.org/10.1242/jcs.03432

Klamer, S., Voermans, C., 2014. The role of novel and known extracellular matrix and adhesion molecules in the homeostatic and regenerative bone marrow microenvironment. Cell Adhes. Migr. 8, 563–577. https://doi.org/10.4161/19336918.2014.968501

Kloxin, A.M., Kasko, A.M., Salinas, C.N., Anseth, K.S., 2009. Photodegradable hydrogels for dynamic tuning of physical and chemical properties. Science (80-.). 324, 59–63. https://doi.org/10.1126/science.1169494

Kobayashi, H., Morikawa, T., Okinaga, A., Hamano, F., Hashidate-Yoshida, T., Watanuki, S., Hishikawa, D., Shindou, H., Arai, F., Kabe, Y., Suematsu, M., Shimizu, T., Takubo, K., 2019. Environmental Optimization Enables Maintenance of Quiescent Hematopoietic Stem Cells Ex Vivo. Cell Rep. 28, 145-158.e9. https://doi.org/10.1016/j.celrep.2019.06.008

Kokkaliaris, K.D., Loeffler, D., Schroeder, T., 2012. Advances in tracking hematopoiesis at the single-cell level. Curr. Opin. Hematol. 19, 243–249. https://doi.org/10.1097/MOH.0b013e32835421de

Krause, D.S., Fackler, M.., Civin, C.I., May, W.S., 1996. CD34: Structure, biology, and clinical use. Blood 87.

Kumar, S., Geiger, H., 2017. HSC Niche Biology and HSC Expansion Ex Vivo. Trends Mol. Med. 23, 799–819. https://doi.org/10.1016/j.molmed.2017.07.003

Kumar, S., If, T.D., Geiger, H., 2017. Feature Review HSC Niche Biology and HSC Expansion Ex Vivo. Trends Mol. Med. xx, 1–21. https://doi.org/10.1016/j.molmed.2017.07.003

Kunisaki, Y., Bruns, I., Scheiermann, C., Ahmed, J., Pinho, S., Zhang, D., Mizoguchi, T., Wei, Q., Lucas, D., Ito, K., Mar, J.C., Bergman, A., Frenette, P.S., 2013. Arteriolar niches maintain haematopoietic stem cell quiescence. Nature 502, 637–643. https://doi.org/10.1038/nature12612

Kunisaki, Y., Frenette, P.S., 2012. The secrets of the bone marrow niche: Enigmatic niche brings challenge for HSC expansion. Nat. Med. 18, 864–865. https://doi.org/10.1038/nm.2825

Lai, W.Y., Li, Y.Y., Mak, S.K., Ho, F.C., Chow, S.T., Chooi, W.H., Chow, C.H., Leung, A.Y., Chan, B.P., 2013. Reconstitution of bone-like matrix in osteogenically differentiated mesenchymal stem cell-collagen constructs: A three-dimensional in vitro model to study hematopoietic stem cell niche. J. Tissue Eng. 4, 1–14. https://doi.org/10.1177/2041731413508668

Lane, S.W., Williams, D. a, Watt, F.M., 2014. Modulating the stem cell niche for tissue regeneration. Nat. Biotechnol. 32, 795–803. https://doi.org/10.1038/nbt.2978

Larochelle, A., Savona, M., Wiggins, M., Anderson, S., Ichwan, B., Keyvanfar, K., Morrison, S.J., Dunbar, C.E., 2011. Human and rhesus macaque hematopoietic stem cells cannot be purified based only on SLAM family markers. Blood 117, 1550–1554.

https://doi.org/10.1182/blood-2009-03-212803

Lattanzi, W., Parolisi, R., Barba, M., Bonfanti, L., 2015. Osteogenic and Neurogenic Stem Cells in Their Own Place: Unraveling Differences and Similarities Between Niches. Front. Cell. Neurosci. 9. https://doi.org/10.3389/fncel.2015.00455

Lee-Thedieck, C., Spatz, J.P., 2012. Artificial niches: Biomimetic materials for hematopoietic stem cell culture. Macromol. Rapid Commun. 33, 1432–1438. https://doi.org/10.1002/marc.201200219

Lee, H.J., Jung, Y.H., Oh, J.Y., Choi, G.E., Chae, C.W., Kim, J.S., Lim, J.R., Kim, S.Y., Lee, S.-J., Seong, J.K., Han, H.J., 2018. BICD1 mediates HIF1α nuclear translocation in mesenchymal stem cells during hypoxia adaptation. Cell Death Differ. https://doi.org/10.1038/s41418-018-0241-1

Leisten, I., Kramann, R., Ventura Ferreira, M.S., Bovi, M., Neuss, S., Ziegler, P., Wagner, W., Knüchel, R., Schneider, R.K., 2012. 3D co-culture of hematopoietic stem and progenitor cells and mesenchymal stem cells in collagen scaffolds as a model of the hematopoietic niche. Biomaterials 33, 1736–1747. https://doi.org/10.1016/j.biomaterials.2011.11.034

Lemieux, B.M.E., Rebel, V.I., Lansdorp, P.M., Eaves, C.J., 1995. Characterization and Purification 86, 1339–1347.

Lendahl, U., Zimmerman, L., McKay, R., 1990. CNS stem cells express a new class of intermediate... [Cell. 1990] - PubMed result. Cell 60, 585–595.

Lewis, E.E.L., Wheadon, H., Lewis, N., Yang, J., Mullin, M., Hursthouse, A., Stirling, D., Dalby, M.J., Berry, C.C., 2016. A Quiescent, Regeneration-Responsive Tissue Engineered Mesenchymal Stem Cell Bone Marrow Niche Model via Magnetic Levitation. ACS Nano 10, 8346–8354. https://doi.org/10.1021/acsnano.6b02841

Lewis, N.S., 2018. Development of a three-dimensional haematopoietic stem cell-permissive bone marrow niche model using magnetic levitation. University of Glasgow.

Lewis, N.S., Lewis, E. EL, Mullin, M., Wheadon, H., Dalby, M.J., Berry, C.C., 2017. Magnetically levitated mesenchymal stem cell spheroids cultured with a collagen gel maintain phenotype and quiescence. J. Tissue Eng. 8, 204173141770442. https://doi.org/10.1177/2041731417704428

Li, Y., Hu, S., Wang, S.A., Li, S., Huh, Y.O., Tang, Z., Medeiros, L.J., Tang, G., 2016. The clinical significance of 8q24/MYC rearrangement in chronic lymphocytic leukemia. Mod. Pathol. 29, 444–451. https://doi.org/10.1038/modpathol.2016.35

Liu, J., Wang, Y., Goh, W.I., Goh, H., Baird, M.A., Ruehland, S., Teo, S., Bate, N., Critchley, D.R., Davidson, M.W., Kanchanawong, P., 2015. Talin determines the nanoscale architecture of focal adhesions. Proc. Natl. Acad. Sci. 112, E4864–E4873. https://doi.org/10.1073/pnas.1512025112

Liu, M., Miller, C.L., Eaves, C.., 2013. Human Long-Term Culture Initiating Cell Assay, in: Helgason C., Miller C. (Eds) Basic Cell Culture Protocols. Methods in Molecular Biology (Methods and Protocols). Humana Press, Totowa, NJ.

https://doi.org/10.1027/0838-1925.17.6.228

Llopis-hernández, V., Cantini, M., González-garcía, C., Cheng, Z.A., Yang, J., Tsimbouri, P.M., García, A.J., Dalby, M.J., Salmerón-sánchez, M., 2016. Material-driven fibronectin assembly for high-efficiency presentation of growth factors. Sci. Adv. 1–11. https://doi.org/10.1126/sciadv.1600188

Lo Celso, C., Fleming, H.E., Wu, J.W., Zhao, C.X., Miake-Lye, S., Fujisaki, J., Côté, D., Rowe, D.W., Lin, C.P., Scadden, D.T., 2009. Live-animal tracking of individual haematopoietic stem/progenitor cells in their niche. Nature 457, 92–96. https://doi.org/10.1038/nature07434

Love, M.I., Huber, W., Anders, S., 2014. Moderated estimation of fold change and dispersion for RNA-seq data with DESeq2. Genome Biol. 15, 1–21. https://doi.org/10.1186/s13059-014-0550-8

Lucas, D., Battista, M., Shi, P.A., Isola, L., Frenette, P.S., 2008. Mobilized Hematopoietic Stem Cell Yield Depends on Species-Specific Circadian Timing. Cell Stem Cell 3, 364–366. https://doi.org/10.1016/j.stem.2008.09.004

Lutolf, M.P., Gilbert, P.M., Blau, H.M., 2009. Designing materials to direct stem-cell fate. Nature 462, 433–441. https://doi.org/10.1038/nature08602

Lutolf, M.P., Lauer-Fields, J.L., Schmoekel, H.G., Metters, A.T., Weber, F.E., Fields, G.B., Hubbell, J.A., 2003. Synthetic matrix metalloproteinase-sensitive hydrogels for the conduction of tissue regeneration: Engineering cell-invasion characteristics. Proc. Natl. Acad. Sci. 100, 5413–5418. https://doi.org/10.1073/pnas.0737381100

Luukkonen, P.K., Zhou, Y., Sädevirta, S., Leivonen, M., Arola, J., Orešič, M., Hyötyläinen, T., Yki-Järvinen, H., 2016. Hepatic ceramides dissociate steatosis and insulin resistance in patients with non-alcoholic fatty liver disease. J. Hepatol. 64, 1167–1175. https://doi.org/10.1016/j.jhep.2016.01.002

Lv, F.J., Tuan, R.S., Cheung, K.M.., Leung, V.Y.., 2014. Concise Review: The Surface Markers and Identity of Human Mesenchymal Stem Cells. Stem Cells 32, 1881–1897. https://doi.org/10.1634/stemcells.2007-0544

Makino, Y., Cao, R., Svensson, K., Bertilsson, G., Asman, M., Tanaka, H., Cao, Y., Berkenstam, A., Poellinger, L., 2001. Inhibitory PAS domain protein is a negative regulator of hypoxia-inducible gene expression. Nature 414, 550–554. https://doi.org/10.1038/35107085

Mantel, C.R., O'Leary, H.A., Chitteti, B.R., Huang, X., Cooper, S., Hangoc, G., Brustovetsky, N., Srour, E.F., Lee, M.R., Messina-Graham, S., Haas, D.M., Falah, N., Kapur, R., Pelus, L.M., Bardeesy, N., Fitamant, J., Ivan, M., Kim, K.S., Broxmeyer, H.E., 2015. Enhancing Hematopoietic Stem Cell Transplantation Efficacy by Mitigating Oxygen Shock. Cell 161, 1553–1565. https://doi.org/10.1016/j.cell.2015.04.054

Manz, M.G., Miyamoto, T., Akashi, K., Weissman, I.L., 2002. Prospective isolation of human clonogenic common myeloid progenitors. Proc. Natl. Acad. Sci. 99, 11872–11877. https://doi.org/10.1073/pnas.172384399

Markway, B.D., Cho, H., Zilberman-Rudenko, J., Holden, P., McAlinden, A., Johnstone, B., 2015. Hypoxia-inducible factor 3-alpha expression is associated with the stable chondrocyte phenotype. J. Orthop. Res. 33, 1561–1570. https://doi.org/10.1002/jor.22930

Martello, G., Smith, A., 2014. The Nature of Embryonic Stem Cells. Annu. Rev. Cell Dev. Biol. 30, 647–675. https://doi.org/10.1146/annurev-cellbio-100913-013116

Martin, M., 2011. Cutadapt removes adapter sequences from high-throughput sequencing reads. EMBnet.journal 17, 10. https://doi.org/10.14806/ej.17.1.200

Martino, M.M., Briquez, P.S., Güç, E., Tortelli, F., Kilarski, W.W., Metzger, S., Rice, J.J., Kuhn, G.A., Müller, R., Swartz, M.A., Hubbell, J.A., 2014. Growth Factors Engineerd for Super-Affinity to the Extracellular Matrix Enhance Tissue Engineering. Science (80-.). 343, 885–888. https://doi.org/10.1126/science.1247663

Martino, M.M., Briquez, P.S., Ranga, A., Lutolf, M.P., Hubbell, J.A., 2013. Heparin-binding domain of fibrin(ogen) binds growth factors and promotes tissue repair when incorporated within a synthetic matrix. Proc. Natl. Acad. Sci. 110, 4563–4568. https://doi.org/10.1073/pnas.1221602110

Martino, M.M., Hubbell, J.A., 2010. The 12th-14th type III repeats of fibronectin function as a highly promiscuous growth factor-binding domain. FASEB J. 24, 4711–4721. https://doi.org/10.1096/fj.09-151282

Martino, M.M., Tortelli, F., Mochizuki, M., Traub, S., Ben-David, D., Kuhn, G. a, Müller, R., Livne, E., Eming, S. a, Hubbell, J. a, 2011. Engineering the growth factor microenvironment with fibronectin domains to promote wound and bone tissue healing. Sci. Transl. Med. 3, 100ra89. https://doi.org/10.1126/scitranslmed.3002614

Marxsen, J.., Stengel, P., Doege, K., Heikkinen, P., Jokilehto, T., Wagner, T., Jelkmann, W., Jaakkola, P., Metzen, E., 2004. Hypoxia-inducible factor-1 (HIF1-) promotes its degradation by induction of HIF-a-prolyl-4-hydroxylases. N. Engl. J. Med. 382, 761–767. https://doi.org/10.1056/NEJMcpc069038

Masson, N., Willam, C., Maxwell, P.H., Pugh, C.W., Ratcliffe, P.J., 2001. Independent function of two destruction domains in hypoxia-inducible factor-a chains activated by prolyl hydroxylation. EMBO J. 20, 5197–5206. https://doi.org/10.1093/emboj/20.18.5197

Matsuda, Y., Ishiwata, T., Yoshimura, H., Hagio, M., Arai, T., 2015. Inhibition of nestin suppresses stem cell phenotype of glioblastomas through the alteration of post-translational modification of heat shock protein HSPA8/HSC71. Cancer Lett. 357, 602–611. https://doi.org/10.1016/j.canlet.2014.12.030

Matsuda, Y., Ishiwata, T., Yoshimura, H., Yamahatsu, K., Minamoto, T., Arai, T., 2017. Nestin phosphorylation at threonines 315 and 1299 correlates with proliferation and metastasis of human pancreatic cancer. Cancer Sci. 108, 354–361. https://doi.org/10.1111/cas.13139

Matsuzaki, Y., Mabuchi, Y., Okano, H., 2014. Leptin receptor makes its mark on MSCs. Cell Stem Cell 15, 112–114. https://doi.org/10.1016/j.stem.2014.07.001

McBeath, R., Pirone, D.M., Nelson, C.M., Bhadriraju, K., Chen, C.S., 2004. Cell shape, cytoskeletal tension, and RhoA regulate stem cell lineage commitment. Dev. Cell 6, 483–95.

McCutchen, J.W., Collier, J.P., Mayor, M.B., 1990. Osseointegration of titanium implants in total hip arthroplasty. Clin. Orthop. Relat. Res. 114–125.

McMurray, R.J., Gadegaard, N., Tsimbouri, P.M., Burgess, K. V, McNamara, L.E., Tare, R., Murawski, K., Kingham, E., Oreffo, R.O.C., Dalby, M.J., 2011. Nanoscale surfaces for the long-term maintenance of mesenchymal stem cell phenotype and multipotency. Nat. Mater. 10, 637–44. https://doi.org/10.1038/nmat3058

McNamara, L.E., Burchmore, R., Riehle, M.O., Herzyk, P., Biggs, M.J.P., Wilkinson, C.D.W., Curtis, A.S.G., Dalby, M.J., 2012. The role of microtopography in cellular mechanotransduction. Biomaterials 33, 2835–47. https://doi.org/10.1016/j.biomaterials.2011.11.047

McNamara, L.E., Sjöström, T., Seunarine, K., Meek, R.D., Su, B., Dalby, M.J., 2014. Investigation of the limits of nanoscale filopodial interactions. J. Tissue Eng. 5, 2041731414536177. https://doi.org/10.1177/2041731414536177

McWhorter, F.Y., Wang, T., Nguyen, P., Chung, T., Liu, W.F., 2013. Modulation of macrophage phenotype by cell shape. Proc. Natl. Acad. Sci. 110, 17253–17258. https://doi.org/10.1073/pnas.1308887110

Mei, Y., Saha, K., Bogatyrev, S.R., Yang, J., Hook, A.L., Kalcioglu, Z.I., Cho, S.W., Mitalipova, M., Pyzocha, N., Rojas, F., Van Vliet, K.J., Davies, M.C., Alexander, M.R., Langer, R., Jaenisch, R., Anderson, D.G., 2010. Combinatorial development of biomaterials for clonal growth of human pluripotent stem cells. Nat. Mater. 9, 768–778. https://doi.org/10.1038/nmat2812

Mendelson, A., Frenette, P.S., 2014. Hematopoietic stem cell niche maintenance during homeostasis and regeneration. Nat. Med. 20, 833–846. https://doi.org/10.1038/nm.3647.

Méndez-Ferrer, S., Lucas, D., Battista, M., Frenette, P.S., 2008. Haematopoietic stem cell release is regulated by circadian oscillations. Nature 452, 442–447. https://doi.org/10.1038/nature06685

Méndez-Ferrer, S., Michurina, T. V, Ferraro, F., Mazloom, A.R., Macarthur, B.D., Lira, S. a, Scadden, D.T., Ma'ayan, A., Enikolopov, G.N., Frenette, P.S., 2010. Mesenchymal and haematopoietic stem cells form a unique bone marrow niche. Nature 466, 829–834. https://doi.org/10.1038/nature09262

Merceron, C., Ranganathan, K., Wang, E., Tata, Z., Makkapati, S., Khan, M.P., Mangiavini, L., Yao, A.Q., Castellini, L., Levi, B., Giaccia, A.J., Schipani, E., 2019. Hypoxia-inducible factor 2α is a negative regulator of osteoblastogenesis and bone mass accrual. Bone Res. 7. https://doi.org/10.1038/s41413-019-0045-z

Mikkola, H.K.A., Orkin, S.., 2006. The journey of developing hematopoietic stem cells. Development 133, 3733–3744. https://doi.org/10.1242/dev.02568

Miroshnikova, Y.A., Le, H.Q., Schneider, D., Thalheim, T., Rübsam, M., Bremicker, N.,

Polleux, J., Kamprad, N., Tarantola, M., Wang, I., Balland, M., Niessen, C.M., Galle, J., Wickström, S.A., 2017. Adhesion forces and cortical tension couple cell proliferation and differentiation to drive epidermal stratification. Nat. Cell Biol. 1. https://doi.org/10.1038/s41556-017-0005-z

Mitchison, T., Kirschner, M., 1988. Cytoskeletal dynamics and nerve growth. Neuron 1, 761–772. https://doi.org/0896-6273(88)90124-9 [pii]

Mnatsakanyan, H., Rico, P., Grigoriou, E., Candelas, A.M., Rodrigo-Navarro, A., Salmeron-Sanchez, M., Sabater i Serra, R., 2015. Controlled Assembly of Fibronectin Nanofibrils Triggered by Random Copolymer Chemistry. ACS Appl. Mater. Interfaces 7, 18125–18135. https://doi.org/10.1021/acsami.5b05466

Mo, M., Wang, S., Zhou, Y., Li, H., Wu, Y., 2016. Mesenchymal stem cell subpopulations: phenotype, property and therapeutic potential. Cell. Mol. Life Sci. 73, 3311–3321. https://doi.org/10.1007/s00018-016-2229-7

Mohyeldin, A., Garzón-Muvdi, T., Quiñones-Hinojosa, A., 2010. Oxygen in stem cell biology: A critical component of the stem cell niche. Cell Stem Cell 7, 150–161. https://doi.org/10.1016/j.stem.2010.07.007

Monteiro A., I., Kollmetz, T., Malmström, J., 2018. Engineered systems to study the synergistic signaling between integrin-mediated mechanotransduction and growth factors (Review). Biointerphases 13, 06D302. https://doi.org/10.1116/1.5045231

Mooney, D.J., Lee, K.Y., Peters, M.C., Anderson, K.W., 2000. Controlled growth factor release from synthetic extracellular matrices. Nature 408, 998–1000. https://doi.org/10.1038/35050141

Morikawa, T., Takubo, K., 2016. Hypoxia regulates the hematopoietic stem cell niche. Pflugers Arch. Eur. J. Physiol. 468, 13–22. https://doi.org/10.1007/s00424-015-1743-z

Moroishi, T., Hansen, C.G., Guan, K.L., 2015. The emerging roles of YAP and TAZ in cancer. Nat. Rev. Cancer 15, 73–79. https://doi.org/10.1038/nrc3876

Morrison, S.J., Kimble, J., 2006. Asymmetric and symmetric stem-cell divisions in development and cancer. Nature. https://doi.org/10.1038/nature04956

Morrison, S.J., Scadden, D.T., 2014. The bone marrow niche for haematopoietic stem cells. Nature 505, 327–34. https://doi.org/10.1038/nature12984

Moulisová, V., Gonzalez-García, C., Cantini, M., Rodrigo-Navarro, A., Weaver, J., Costell, M., Sabater i Serra, R., Dalby, M.J., García, A.J., Salmerón-Sánchez, M., 2017. Engineered microenvironments for synergistic VEGF – Integrin signalling during vascularization. Biomaterials 126, 61–74. https://doi.org/10.1016/j.biomaterials.2017.02.024

Müller, E., Ansorge, M., Werner, C., Pompe, T., 2014. Mimicking the Hematopoietic Stem Cell Niche by Biomaterials, in: Bio-inspired Materials for Biomedical Engineering. John Wiley & Sons, Ltd, pp. 309–326. https://doi.org/10.1002/9781118843499.ch16

Müller, E., Pompe, T., Freudenberg, U., Werner, C., 2017. Solvent-Assisted Micromolding of Biohybrid Hydrogels to Maintain Human Hematopoietic Stem and Progenitor Cells Ex Vivo. Adv. Mater. 29, 1–7. https://doi.org/10.1002/adma.201703489

Müller, J., Benz, K., Ahlers, M., Gaissmaier, C., Mollenhauer, J., 2011. Hypoxic conditions during expansion culture prime human mesenchymal stromal precursor cells for chondrogenic differentiation in three-dimensional cultures. Cell Transplant. 20, 1589–1602. https://doi.org/10.3727/096368910X564094

Murray, L., Chen, B., Galy, A., Chen, S., Tushinski, R., Uchida, N., Negrin, R., Tricot, G., Jagannath, S., Vesole, D., 1995. Enrichment of human hematopoietic stem cell activity in the CD34+Thy-1+Lin- subpopulation from mobilized peripheral blood. Blood 85, 368–78.

Murray, L.J., Young, J.C., Osborne, L.J., Luens, K.M., Scollay, R., Hill, B.L., 1999. Thrombopoietin, flt3, and kit ligands together suppress apoptosis of human mobilized CD34+ cells and recruit primitive CD34+Thy-1+ cells into rapid division. Exp. Hematol. 27, 1019–1028. https://doi.org/10.1016/S0301-472X(99)00031-4

Murray, M.E., Mendez, M.G., Janmey, P.A., 2014. Substrate stiffness regulates solubility of cellular vimentin. Mol. Biol. Cell 25, 87–94. https://doi.org/10.1091/mbc.E13-06-0326

Nagasawa, T., Hirota, S., Tachibana, K., Takakura, N., Nishikawa, S., Kitamura, Y., Yoshida, N., Kikutani, H., Kishimoto, T., 1996. Defects of B-cell lymphopoiesis and BM myelopoiesis in mice lacking the CXC. Nature 382, 635–638.

Nakahara, F., Borger, D.K., Wei, Q., Pinho, S., Maryanovich, M., Zahalka, A.H., Suzuki, M., Cruz, C.D., Wang, Z., Xu, C., Boulais, P.E., Ma'ayan, A., Greally, J.M., Frenette, P.S., 2019. Engineering a haematopoietic stem cell niche by revitalizing mesenchymal stromal cells. Nat. Cell Biol. 21, 560–567. https://doi.org/10.1038/s41556-019-0308-3

Nakauchi, H., Sudo, K., Ema, H., 2006. Quantitative Assessment of the Stem Cell Self-Renewal Capacity. Ann. N. Y. Acad. Sci. 938, 18–25. https://doi.org/10.1111/j.1749-6632.2001.tb03570.x

Naldini, L., 2015. Gene therapy returns to centre stage. Nature 526, 351–360. https://doi.org/10.1038/nature15818

Naveiras, O., Nardi, V., Wenzel, P.L., Hauschka, P. V., Fahey, F., Daley, G.Q., 2009. Bone-marrow adipocytes as negative regulators of the haematopoietic microenvironment. Nature 460, 259–263. https://doi.org/10.1038/nature08099

Nehls, V., Drenckhahn, D., 1991. Heterogeneity of microvascular pericytes for smooth muscle type alpha- actin. J. Cell Biol. 113, 147–154. https://doi.org/10.1083/jcb.113.1.147

Newgard, C.B., An, J., Bain, J.R., Muehlbauer, M.J., Stevens, R.D., Lien, L.F., Haqq, A.M., Shah, S.H., Arlotto, M., Slentz, C.A., Rochon, J., Gallup, D., Ilkayeva, O., Wenner, B.R., Yancy, W.S., Eisenson, H., Musante, G., Surwit, R.S., Millington, D.S., Butler, M.D., Svetkey, L.P., 2009. A Branched-Chain Amino Acid-Related

Metabolic Signature that Differentiates Obese and Lean Humans and Contributes to Insulin Resistance. Cell Metab. 9, 311–326. https://doi.org/10.1016/j.cmet.2009.02.002

Ngandu Mpoyi, E., Cantini, M., Reynolds, P.M., Gadegaard, N., Dalby, M.J., Salmerón-Sánchez, M., 2016. Protein Adsorption as a Key Mediator in the Nanotopographical Control of Cell Behavior. ACS Nano 10, 6638–6647. https://doi.org/10.1021/acsnano.6b01649

Nie, Y., Han, Y.-C., Zou, Y.-R., 2008. CXCR4 is required for the quiescence of primitive hematopoietic cells. J. Exp. Med. 205, 777–783. https://doi.org/10.1084/jem.20072513

Nilsson, S.K., Debatis, M.E., Dooner, M.S., Madri, J.A., Quesenberry, P.J., Becker, P.S., 1998. Immunofluorescence characterization of key extracellular matrix proteins in murine bone marrow in situ. J. Histochem. Cytochem. 46, 371–377. https://doi.org/10.1177/002215549804600311

Nilsson, S.K., Johnston, H.M., Coverdale, J. a, 2001. Spatial localization of transplanted hemopoietic stem cells: Inferences for the localization of stem cell niches. Blood 97, 2293–2299. https://doi.org/10.1182/blood.V97.8.2293

Nilsson, S.K., Johnston, H.M., Whitty, G.A., Williams, B., Webb, R.J., Denhardt, D.T., Bertoncello, I., Bendall, L.J., Simmons, P.J., Haylock, D.N., 2005. Osteopontin, a key component of the hematopoietic stem cell niche and regulator of primitive hematopoietic progenitor cells. Blood 106, 1232–1239. https://doi.org/10.1182/blood-2004-11-4422.Supported

Nombela-Arrieta, C., Pivarnik, G., Winkel, B., Canty, K.J., Harley, B., Mahoney, J.E., Park, S.Y., Lu, J., Protopopov, A., Silberstein, L.E., 2013. Quantitative imaging of haematopoietic stem and progenitor cell localization and hypoxic status in the bone marrow microenvironment. Nat. Cell Biol. 15, 533–543. https://doi.org/10.1038/ncb2730

North, T.E., Goessling, W., Walkley, C.R., Lengerke, C., Kopani, K.R., Lord, A.M., Weber, G.J., Bowman, T. V, Jang, I., Grosser, T., Fitzgerald, G.A., Daley, G.Q., Orkin, S.H., Zon, L.I., 2007. Prostaglandin E2 regulates vertebrate haematopoietic stem cell homeostasis. Nature 447, 1007–1012. https://doi.org/10.1038/nature05883

Notta, F., Doulatov, S., Laurenti, E., Poeppl, A., Jurisica, I., Dick, J.E., 2011. Isolation of Single Human Hematopoietic. Science (80-.). 333, 218–222. https://doi.org/10.1126/science.1201219

Obara, M., Kang, M.S., Yamada, K.M., 1988. Site-directed mutagenesis of the cell-binding domain of human fibronectin: Separable, synergistic sites mediate adhesive function. Cell 53, 649–657. https://doi.org/10.1016/0092-8674(88)90580-6

Obradovic Wagner, D., Sieber, C., Bhushan, R., Borgermann, J.H., Graf, D., Knaus, P., 2010. BMPs: From Bone to Body Morphogenetic Proteins. Sci. Signal. 3. https://doi.org/10.1126/scisignal.3107mr1

Ogawa, M., Matsuzaki, Y., Nishikawa, S., Hayashi, S., Kunisada, T., Sudo, T., Kina, T.,

Nakauchi, H., Nishikawa, S., 1991. Expression and function of c-kit in hemopoietic progenitor cells. 174. https://doi.org/10.12681/eadd/1834

Oldershaw, R. a., 2012. Cell sources for the regeneration of articular cartilage: The past, the horizon and the future. Int. J. Exp. Pathol. 93, 389–400. https://doi.org/10.1111/j.1365-2613.2012.00837.x

Omatsu, Y., Sugiyama, T., Kohara, H., Kondoh, G., Fujii, N., Kohno, K., Nagasawa, T., 2010. The Essential Functions of Adipo-osteogenic Progenitors as the Hematopoietic Stem and Progenitor Cell Niche. Immunity 33, 387–399. https://doi.org/10.1016/j.immuni.2010.08.017

Orapiriyakul, W., 2020. Nanovibrational stimulation for 3D osteogenesis in biphasic 3D scaffold; A new option for bone tissue engineering. The University of Glasgow.

Oria, R., Wiegand, T., Escribano, J., Elosegui-Artola, A., Uriarte, J.J., Moreno-Pulido, C., Platzman, I., Delcanale, P., Albertazzi, L., Navajas, D., Trepat, X., García-Aznar, J.M., Cavalcanti-Adam, E.A., Roca-Cusachs, P., 2017. Force loading explains spatial sensing of ligands by cells. Nature 552, 219–224. https://doi.org/10.1038/nature24662

Orkin, S.H., Zon, L.I., 2008. Hematopoiesis: an evolving paradigm for stem cell biology. Cell 132, 631–44. https://doi.org/10.1016/j.cell.2008.01.025

Ozerdem, U., Grako, K.A., Dahlin-Huppe, K., Monosov, E., Stallcup, W.B., 2001. NG2 proteoglycan is expressed exclusively by mural cells during vascular morphogenesis. Dev. Dyn. 222, 218–227. https://doi.org/10.1002/dvdy.1200

Paduano, F., Marrelli, M., Amantea, M., Rengo, C., Rengo, S., Goldberg, M., Spagnuolo, G., Tatullo, M., 2017. Adipose tissue as a strategic source of mesenchymal stem cells in bone regeneration: A topical review on the most promising craniomaxillofacial applications. Int. J. Mol. Sci. 18. https://doi.org/10.3390/ijms18102140

Pak, C., Callander, N.S., Young, E.W.K., Titz, B., Kim, K.M., Saha, S., Chng, K., Asimakopoulos, F., Beebe, D.J., Miyamoto, S., 2015. MicroC 3 : an ex vivo microfluidic cis-coculture assay to test chemosensitivity and resistance of patient multiple myeloma cells. Integr. Biol. (United Kingdom) 7, 643–654. https://doi.org/10.1039/c5ib00071h

Pak, J., Lee, J.H., Park, K.S., Park, M., Kang, L.W., Lee, S.H., 2017. Current use of autologous adipose tissue-derived stromal vascular fraction cells for orthopedic applications. J. Biomed. Sci. 24, 1–12. https://doi.org/10.1186/s12929-017-0318-z

Pallari, H.-M., Lindqvist, J., Torvaldson, E., Ferraris, S.E., He, T., Sahlgren, C., Eriksson, J.E., 2011. Nestin as a regulator of Cdk5 in differentiating myoblasts. Mol. Biol. Cell 22, 1539–1549. https://doi.org/10.1091/mbc.E10-07-0568

Palomäki, S., Pietilä, M., Laitinen, S., Pesälä, J., Sormunen, R., Lehenkari, P., Koivunen, P., 2013. HIF-1α is upregulated in human mesenchymal stem cells. Stem Cells 31, 1902–1909. https://doi.org/10.1002/stem.1435

Pankov, R., Yamada, K.M., 2002. Fibronectin at a glance. J. Cell Sci. 115, 3861–3863.

https://doi.org/10.1242/jcs.00059

Park, D., Xiang, A.P., Mao, F.F., Zhang, L., Di, C.G., Liu, X.M., Shao, Y., Ma, B.F., Lee, J.H., Ha, K.S., Walton, N., Lahn, B.T., 2010. Nestin is required for the proper self-renewal of neural stem cells. Stem Cells 28, 2162–2171. https://doi.org/10.1002/stem.541

Park, M., Seo, J.J., 2012. Role of HLA in Hematopoietic Stem Cell Transplantation. Bone Marrow Res. 2012, 1–7. https://doi.org/10.1155/2012/680841

Parmar, K., Mauch, P., Vergilio, J., Sackstein, R., Down, J.D., 2007. Distribution of hematopoietic stem cells in the bone marrow according to regional hypoxia. Proc. Natl. Acad. Sci. 104, 5431–5436.

Passegué, E., Wagers, A.J., Giuriato, S., Anderson, W.C., Weissman, I.L., 2005. Global analysis of proliferation and cell cycle gene expression in the regulation of hematopoietic stem and progenitor cell fates. J. Exp. Med. 202, 1599–1611. https://doi.org/10.1084/jem.20050967

Pattappa, G., Heywood, H.K., de Bruijn, J.D., Lee, D.A., 2011. The metabolism of human mesenchymal stem cells during proliferation and differentiation. J. Cell. Physiol. 226, 2562–2570. https://doi.org/10.1002/jcp.22605

Patterson, A.M., Pelus, L.M., 2018. Spotlight on Glycolysis: A New Target for Cord Blood Expansion. Cell Stem Cell 22, 792–793. https://doi.org/10.1016/j.stem.2018.04.023

Patti, G.J., Yanes, O., Siuzdak, G., 2012. Innovation: Metabolomics: the apogee of the omics trilogy. Nat. Rev. Mol. Cell Biol. 13, 263–269. https://doi.org/10.1038/nrm3314

Pedersen, M., Löfstedt, T., Sun, J., Holmquist-Mengelbier, L., Påhlman, S., Rönnstrand, L., 2008. Stem cell factor induces HIF-1α at normoxia in hematopoietic cells. Biochem. Biophys. Res. Commun. 377, 98–103. https://doi.org/10.1016/j.bbrc.2008.09.102

Peled, T., Shoham, H., Aschengrau, D., Yackoubov, D., Frei, G., Rosenheimer G, N., Lerrer, B., Cohen, H.Y., Nagler, A., Fibach, E., Peled, A., 2012. Nicotinamide, a SIRT1 inhibitor, inhibits differentiation and facilitates expansion of hematopoietic progenitor cells with enhanced bone marrow homing and engraftment. Exp. Hematol. 40, 342-355.e1. https://doi.org/10.1016/j.exphem.2011.12.005

Pelletier, A.J., van der Laan, L.J., Hildbrand, P., Siani, M.A., Thompson, D.A., Dawson, P.E., Torbett, B.E., Salomon, D.R., 2000. Presentation of chemokine SDF-1 alpha by fibronectin mediates directed migration of T cells. Blood 96, 2682–90.

Petrie, T.A., Capadona, J.R., Reyes, C.D., Garcia, A.J., 2006. Integrin specificity and enhanced cellular activities associated with surfaces presenting a recombinant fibronectin fragment compared to RGD supports. Biomaterials 27, 5459–5470. https://doi.org/10.1016/j.biomaterials.2006.06.027

Phimphilai, M., Zhao, Z., Boules, H., Roca, H., Franceschi, R.T., 2006. BMP signaling is required for RUNX2-dependent induction of the osteoblast phenotype. J. Bone

Miner. Res. 21, 637–646. https://doi.org/10.1359/jbmr.060109

Pierschbacher, M.D., Ruoslahti, E., 1984. Cell attachment activity of fibronectin can be duplicated by small synthetic fragments of the molecule. Nature 309, 30–33. https://doi.org/10.1038/309030a0

Pinho, S., Frenette, P.S., 2019. Haematopoietic stem cell activity and interactions with the niche. Nat. Rev. Mol. Cell Biol. https://doi.org/10.1038/s41580-019-0103-9

Pinho, S., Lacombe, J., Hanoun, M., Mizoguchi, T., Bruns, I., Kunisaki, Y., Frenette, P.S., 2013. PDGFR A and CD51 mark human stem cells capable of hematopoietic progenitor cell expansion. J. Exp. Med. 210, 1351–1367. https://doi.org/10.1084/jem.20122252

Pollard, P.J., Kranc, K.R., 2010. Hypoxia Signaling in Hematopoietic Stem Cells : A Double-Edged Sword. Stem Cell 7, 276–278. https://doi.org/10.1016/j.stem.2010.08.006

Porazinski, S., Wang, H., Asaoka, Y., Behrndt, M., Miyamoto, T., Morita, H., Hata, S., Sasaki, T., Krens, S.F.G., Osada, Y., Asaka, S., Momoi, A., Linton, S., Miesfeld, J.B., Link, B.A., Senga, T., Castillo-Morales, A., Urrutia, A.O., Shimizu, N., Nagase, H., Matsuura, S., Bagby, S., Kondoh, H., Nishina, H., Heisenberg, C.P., Furutani-Seiki, M., 2015. YAP is essential for tissue tension to ensure vertebrate 3D body shape. Nature 521, 217–221. https://doi.org/10.1038/nature14215

Qian, H., Buza-Vidas, N., Hyland, C.D., Jensen, C.T., Antonchuk, J., Månsson, R., Thoren, L.A., Ekblom, M., Alexander, W.S., Jacobsen, S.E.W., 2007. Critical Role of Thrombopoietin in Maintaining Adult Quiescent Hematopoietic Stem Cells. Cell Stem Cell 1, 671–684. https://doi.org/10.1016/j.stem.2007.10.008

Qin, Z., Kreplak, L., Buehler, M.J., 2009. Hierarchical structure controls nanomechanical properties of vimentin intermediate filaments. PLoS One 4. https://doi.org/10.1371/journal.pone.0007294

Radaelli, M., Merlini, A., Greco, R., Sangalli, F., Comi, G., Ciceri, F., Martino, G., 2014. Autologous Bone Marrow Transplantation for the Treatment of Multiple Sclerosis. Curr. Neurol. Neurosci. Rep. 14, 478. https://doi.org/10.1007/s11910-014-0478-0

Raheja, L.F., Genetos, D.C., Yellowley, C.E., 2008. Hypoxic osteocytes recruit human MSCs through an OPN/CD44-mediated pathway. Biochem. Biophys. Res. Commun. 366, 1061–1066. https://doi.org/10.1016/j.bbrc.2007.12.076

Rashid, B., Destrade, M., Gilchrist, M.D., 2013. Influence of preservation temperature on the measured mechanical properties of brain tissue. J. Biomech. 46, 1276–1281. https://doi.org/10.1016/j.jbiomech.2013.02.014

Reid, S.E., Kay, E.J., Neilson, L.J., Henze, A., Serneels, J., McGhee, E.J., Dhayade, S., Nixon, C., Mackey, J.B., Santi, A., Swaminathan, K., Athineos, D., Papalazarou, V., Patella, F., Román-Fernández, Á., ElMaghloob, Y., Hernandez-Fernaud, J.R., Adams, R.H., Ismail, S., Bryant, D.M., Salmeron-Sanchez, M., Machesky, L.M., Carlin, L.M., Blyth, K., Mazzone, M., Zanivan, S., 2017. Tumor matrix stiffness promotes metastatic cancer cell interaction with the endothelium. EMBO J. 36, e201694912. https://doi.org/10.15252/embj.201694912

Rico, P., Rodríguez Hernández, J.C., Moratal, D., Altankov, G., Monleón Pradas, M., Salmerón-Sánchez, M., 2009. Substrate-induced assembly of fibronectin into networks: influence of surface chemistry and effect on osteoblast adhesion. Tissue Eng. Part A 15, 3271–3281. https://doi.org/10.1089/ten.tea.2009.0141

Riu, F., Slater, S.C., Garcia, E.J., Rodriguez-Arabaolaza, I., Alvino, V., Avolio, E., Mangialardi, G., Cordaro, A., Satchell, S., Zebele, C., Caporali, A., Angelini, G., Madeddu, P., 2017. The adipokine leptin modulates adventitial pericyte functions by autocrine and paracrine signalling. Sci. Rep. 7, 1–13. https://doi.org/10.1038/s41598-017-05868-y

Roberts, J.N., Sahoo, J.K., McNamara, L.E., Burgess, K. V., Yang, J., Alakpa, E. V., Anderson, H.J., Hay, J., Turner, L.A., Yarwood, S.J., Zelzer, M., Oreffo, R.O.C., Ulijn, R. V., Dalby, M.J., 2016. Dynamic Surfaces for the Study of Mesenchymal Stem Cell Growth through Adhesion Regulation. ACS Nano 10, 6667–6679. https://doi.org/10.1021/acsnano.6b01765

Roch, A., Giger, S., Girotra, M., Campos, V., Vannini, N., Naveiras, O., Gobaa, S., Lutolf, M.P., 2017. Single-cell analyses identify bioengineered niches for enhanced maintenance of hematopoietic stem cells. Nat. Commun. 8, 221. https://doi.org/10.1038/s41467-017-00291-3

Rödling, L., Schwedhelm, I., Kraus, S., Bieback, K., Hansmann, J., Lee-thedieck, C., 2017. 3D models of the hematopoietic stem cell niche under steady-state and active conditions. Sci. Rep. 1–15. https://doi.org/10.1038/s41598-017-04808-0

Rojewski, M.T., Weber, B.M., Schrezenmeier, H., 2008. Phenotypic characterization of mesenchymal stem cells from various tissues. Transfus. Med. Hemotherapy 35, 168–184. https://doi.org/10.1159/000129013

Ronaldson-Bouchard, K., Vunjak-Novakovic, G., 2018. Organs-on-a-Chip: A Fast Track for Engineered Human Tissues in Drug Development. Cell Stem Cell 22, 310–324. https://doi.org/10.1016/j.stem.2018.02.011

Ross, E.A., Turner, L., Saeed, A., Burgess, K. V, Blackburn, G., Wells, J.A., Mountford, J., Gadegaard, N., Salmeron-, M., Oreffo, R.O.C., Dalby, M.J., 2019. Nanotopography reveals metabolites that maintain the immunosuppressive phenotype of mesenchymal stem cells. BioRxiv.

Roy, S., Tripathy, M., Mathur, N., Jain, A., Mukhopadhyay, A., 2012. Hypoxia improves expansion potential of human cord blood-derived hematopoietic stem cells and marrow repopulation efficiency. Eur. J. Haematol. 88, 396–405. https://doi.org/10.1111/j.1600-0609.2012.01759.x

Sá da Bandeira, D., Casamitjana, J., Crisan, M., 2016. Pericytes, integral components of adult hematopoietic stem cell niches. Pharmacol. Ther. 171, 104–113. https://doi.org/10.1016/j.pharmthera.2016.11.006

Sacchetti, B., Funari, A., Michienzi, S., Di Cesare, S., Piersanti, S., Saggio, I., Tagliafico, E., Ferrari, S., Robey, P.G., Riminucci, M., Bianco, P., 2007. Self-Renewing Osteoprogenitors in Bone Marrow Sinusoids Can Organize a Hematopoietic Microenvironment. Cell 131, 324–336. https://doi.org/10.1016/j.cell.2007.08.025

Sahlgren, C.M., Mikhailov, A., Vaittinen, S., Pallari, H.-M., Kalimo, H., Pant, H.C., Eriksson, J.E., 2003. Cdk5 regulates the organization of Nestin and its association with p35. Mol. Cell. Biol. 23, 5090–5106. https://doi.org/10.1128/MCB.23.14.5090-5106.2003

Sahlgren, C.M., Pallari, H.M., He, T., Chou, Y.H., Goldman, R.D., Eriksson, J.E., 2006. A nestin scaffold links Cdk5/p35 signaling to oxidant-induced cell death. EMBO J. 25, 4808–4819. https://doi.org/10.1038/sj.emboj.7601366

Salceda, S., Caro, J., 1997. Hypoxia-inducible Factor 1α (HIF-1α) Protein Is Rapidly Degraded by the Ubiquitin-Proteasome System under Normoxic Conditions. J. Biol. Chem. 272, 22642–22647. https://doi.org/10.1074/jbc.272.36.22642

Salmerón-Sánchez, M., Dalby, M.J., 2016. Synergistic growth factor microenvironments. Chem. Commun. 52, 13327–13336. https://doi.org/10.1039/C6CC06888J

Salmerón-Sánchez, M., Rico, P., Moratal, D., Lee, T.T., Schwarzbauer, J.E., García, A.J., 2011. Role of material-driven fibronectin fibrillogenesis in cell differentiation. Biomaterials 32, 2099–2105. https://doi.org/10.1016/j.biomaterials.2010.11.057

Saraiva, L.R., Bocian, C., Jank, A.-M., Schulz, T.J., Ambrosi, T.H., Fan, H., Scialdone, A., Gohlke, S., Woelk, L., Logan, D.W., Schürmann, A., Graja, A., 2017. Adipocyte Accumulation in the Bone Marrow during Obesity and Aging Impairs Stem Cell-Based Hematopoietic and Bone Regeneration. Cell Stem Cell 20, 771-784.e6. https://doi.org/10.1016/j.stem.2017.02.009

Sayama, C., Willsey, M., Chintagumpala, M., Brayton, A., Briceño, V., Ryan, S.L., Luerssen, T.G., Hwang, S.W., Jea, A., 2015. Routine use of recombinant human bone morphogenetic protein-2 in posterior fusions of the pediatric spine and incidence of cancer. J. Neurosurg. Pediatr. 16, 4–13. https://doi.org/10.3171/2014.10.peds14199

Schneider, S., Unger, M., Van Griensven, M., Balmayor, E.R., 2017. Adipose-derived mesenchymal stem cells from liposuction and resected fat are feasible sources for regenerative medicine. Eur. J. Med. Res. 22, 1–11. https://doi.org/10.1186/s40001-017-0258-9

Schofield, R., 1978. The relationship between the spleen colony-forming cell and the haemopoietic stem cell. Blood Cells 4, 7—25.

Schvartzman, M., Palma, M., Sable, J., Abramson, J., Hu, X., Sheetz, M.P., Wind, S.J., 2011. Nanolithographic control of the spatial organization of cellular adhesion receptors at the single-molecule level. Nano Lett. 11, 1306–1312. https://doi.org/10.1021/nl104378f

Schwab, E.H., Pohl, T.L.M., Haraszti, T., Schwaerzer, G.K., Hiepen, C., Spatz, J.P., Knaus, P., Cavalcanti-Adam, E.A., 2015. Nanoscale control of surface immobilized BMP-2: Toward a quantitative assessment of BMP-mediated signaling events. Nano Lett. 15, 1526–1534. https://doi.org/10.1021/acs.nanolett.5b00315

Seita, J., Weissman, I.L., 2010. Hematopoietic stem cell: Self-renewal versus differentiation. Wiley Interdiscip. Rev. Syst. Biol. Med. 2, 640–653.

https://doi.org/10.1002/wsbm.86

Semenza, G.L., Agani, F., Booth, G., Forsythe, J., Iyer, N., Jiang, B.H., Leung, S., Roe, R., Wiener, C., Yu, A., 1997. Structural and functional analysis of hypoxia-inducible factor 1. Kidney Int. 51, 553–555. https://doi.org/10.1038/ki.1997.77

Shah, S.H., Sun, J.L., Stevens, R.D., Bain, J.R., Muehlbauer, M.J., Pieper, K.S., Haynes, C., Hauser, E.R., Kraus, W.E., Granger, C.B., Newgard, C.B., Califf, R.M., Newby, L.K., 2012. Baseline metabolomic profiles predict cardiovascular events in patients at risk for coronary artery disease. Am. Heart J. 163, 844-850.e1. https://doi.org/10.1016/j.ahj.2012.02.005

Sharma, M.B., Limaye, L.S., Kale, V.P., 2012. Mimicking the functional hematopoietic stem cell niche in vitro: Recapitulation of marrow physiology by hydrogel-based three-dimensional cultures of mesenchymal stromal cells. Haematologica 97, 651–660. https://doi.org/10.3324/haematol.2011.050500

Shima, H., Takubo, K., Iwasaki, H., Yoshihara, H., Gomei, Y., Hosokawa, K., Arai, F., Takahashi, T., Suda, T., 2009. Reconstitution activity of hypoxic cultured human cord blood CD34-positive cells in NOG mice. Biochem. Biophys. Res. Commun. 378, 467–472. https://doi.org/10.1016/j.bbrc.2008.11.056

Shin, J., Spinler, K.R., Swift, J., Chasis, J. a, Mohandas, N., Discher, D.E., 2013. Lamins regulate cell trafficking and lineage maturation of adult human hematopoietic cells. Proc. Natl. Acad. Sci. U. S. A. 110, 18892–18897. https://doi.org/10.1073/pnas.1304996110/-/DCSupplemental.www.pnas.org/cgi/doi/10.1073/pnas.1304996110

Shin, J.W., Buxboim, A., Spinler, K.R., Swift, J., Christian, D.A., Hunter, C.A., Léon, C., Gachet, C., Dingal, P.C.D.P., Ivanovska, I.L., Rehfeldt, F., Chasis, J.A., Discher, D.E., 2014. Contractile forces sustain and polarize hematopoiesis from stem and progenitor cells. Cell Stem Cell 14, 81–93. https://doi.org/10.1016/j.stem.2013.10.009

Simsek, T., Kocabas, F., Zheng, J., Deberardinis, R.J., Mahmoud, A.I., Olson, E.N., Schneider, J.W., Zhang, C.C., Sadek, H.A., 2010. The Distinct Metabolic Profile of Hematopoietic Stem Cells Reflects Their Location in a Hypoxic Niche. Stem Cell 7, 380–390. https://doi.org/10.1016/j.stem.2010.07.011

Singh, P., Carraher, C., Schwarzbauer, J.E., 2010. Assembly of fibronectin extracellular matrix. Annu Rev Cell Dev Biol 26, 397–419. https://doi.org/10.1146/annurev-cellbio-100109-104020

Sjöström, T., Mcnamara, L.E., Meek, R.M.D., Dalby, M.J., Su, B., 2013. 2D and 3D nanopatterning of titanium for enhancing osteoinduction of stem cells at implant surfaces. Adv. Healthc. Mater. 2, 1285–1293. https://doi.org/10.1002/adhm.201200353

Spangrude, G.J., Heimfeld, S., Weissman, I.L., 1988. Purification and characterization of mouse hematopoietic stem cells. Science (80-.). 241, 58–62.

Spencer, J.A., Ferraro, F., Roussakis, E., Klein, A., Wu, J., Runnels, J.M., Zaher, W., Mortensen, L.J., Alt, C., Turcotte, R., Yusuf, R., Côté, D., Vinogradov, S.A.,

Scadden, D.T., Lin, C.P., 2014. Direct measurement of local oxygen concentration in the bone marrow of live animals. Nature 508, 269–273. https://doi.org/10.1038/nature13034

Squillaro, T., Peluso, G., Galderisi, U., 2016. Clinical Trials With Mesenchymal Stem Cells: An Update. Cell Transplant. 25, 829–48. https://doi.org/10.3727/096368915X689622

Staller, P., Sulitkova, J., Lisztwan, J., Moch, H., 2003. Chemokine receptor CXCR4 downregulated by von Hippel – Lindau tumour suppressor pVHL 307–311.

Stier, S., Ko, Y., Forkert, R., Lutz, C., Neuhaus, T., Grünewald, E., Cheng, T., Dombkowski, D., Calvi, L.M., Rittling, S.R., Scadden, D.T., 2005. Osteopontin is a hematopoietic stem cell niche component that negatively regulates stem cell pool size. J. Exp. Med. 201, 1781–1791. https://doi.org/10.1084/jem.20041992

Suda, T., Takubo, K., Semenza, G.L., 2011. Metabolic Regulation of Hematopoietic Stem Cells in the Hypoxic Niche. Stem Cell 9, 298–310. https://doi.org/10.1016/j.stem.2011.09.010

Sugiyama, T., Kohara, H., Noda, M., Nagasawa, T., 2006. Maintenance of the Hematopoietic Stem Cell Pool by CXCL12-CXCR4 Chemokine Signaling in Bone Marrow Stromal Cell Niches. Immunity 25, 977–988. https://doi.org/10.1016/j.immuni.2006.10.016

Sunyer, R., Conte, V., Escribano, J., Elosegui-Artola, A., Labernadie, A., Valon, L., Navajas, D., Garcia-Aznar, J.M., Munoz, J.J., Roca-Cusachs, P., Trepat, X., 2016. Collective cell durotaxis emerges from long-range intercellular force transmission. Science (80-.). 353, 1157–1161. https://doi.org/10.5061/dryad.r8h3n

Sutherland, H.J., Lansdorp, P.M., Henkelman, D.H., Eaves, A.C., Eaves, C.J., 1990. Functional characterization of individual human hematopoietic stem cells cultured at limiting dilution on supportive marrow stromal layers. Proc. Natl. Acad. Sci. 87, 3584–3588. https://doi.org/10.1073/pnas.87.9.3584

Sweeney, E., Roberts, D., Jacenko, O., 2011. Altered matrix at the chondro-osseous junction leads to defects in lymphopoiesis. Ann. N. Y. Acad. Sci. 1237, 79–87. https://doi.org/10.1111/j.1749-6632.2011.06227.x

Sweeten, P., 2019. Modelling an in vitro haematopoietic stem cell niche using poly (ethyl acrylate) surfaces.

Taichman, R., Reilly, M.J., Emerson, S.G., 1996. Human osteoblasts support human hematopoietic progenitor cells in vitro bone marrow cultures. Blood 87, 518–524.

Takubo, K., Goda, N., Yamada, W., Iriuchishima, H., Ikeda, E., Kubota, Y., Shima, H., Johnson, R.S., Hirao, A., Suematsu, M., Suda, T., 2010. Regulation of the HIF-1 a Level Is Essential for Hematopoietic Stem Cells. Cell Stem Cell 7, 391–402. https://doi.org/10.1016/j.stem.2010.06.020

Takubo, K., Nagamatsu, G., Kobayashi, C.I., Nakamura-Ishizu, A., Kobayashi, H., Ikeda, E., Goda, N., Rahimi, Y., Johnson, R.S., Soga, T., Hirao, A., Suematsu, M., Suda, T., 2013. Regulation of glycolysis by Pdk functions as a metabolic checkpoint for

cell cycle quiescence in hematopoietic stem cells. Cell Stem Cell 12, 49–61. https://doi.org/10.1016/j.stem.2012.10.011

Thomas, J.W., Cooley, M.A., Broome, J.M., Salgia, R., Griffin, J.D., Lombardo, C.R., Schaller, M.D., 1999. The role of focal adhesion kinase binding in the regulation of tyrosine phosphorylation of paxillin. J. Biol. Chem. 274, 36684–36692. https://doi.org/10.1074/jbc.274.51.36684

Tian, H., McKnight, S.L., Russell, D.W., 1997. Endothelial PAS domain protein 1 (EPAS1), a transcription factor selectively expressed in endothelial cells. Genes Dev. 11, 72–82. https://doi.org/10.1101/gad.11.1.72

Tomita, M., Asada, M., Asada, N., Nakamura, J., Oguchi, A., Higashi, A.Y., Endo, S., Robertson, E., Kimura, T., Kita, T., Economides, A.N., Kreidberg, J., Yanagita, M., 2013. Bmp7 Maintains Undifferentiated Kidney Progenitor Population and Determines Nephron Numbers at Birth. PLoS One 8, e73554. https://doi.org/10.1371/journal.pone.0073554

Torisawa, Y.S., Spina, C.S., Mammoto, T., Mammoto, A., Weaver, J.C., Tat, T., Collins, J.J., Ingber, D.E., 2014. Bone marrow-on-a-chip replicates hematopoietic niche physiology in vitro. Nat. Methods 11, 663–669. https://doi.org/10.1038/nmeth.2938

Tormin, A., Li, O., Brune, J.C., Walsh, S., Schütz, B., Ehinger, M., Ditzel, N., Kassem, M., Scheding, S., 2011. CD146 expression on primary nonhematopoietic bone marrow stem cells is correlated with in situ localization. Blood 117, 5067–5077. https://doi.org/10.1182/blood-2010-08-304287

Totaro, A., Panciera, T., Piccolo, S., 2018. YAP/TAZ upstream signals and downstream responses. Nat. Cell Biol. 20, 888–899. https://doi.org/10.1038/s41556-018-0142-z

Traub, S., Morgner, J., Martino, M.M., Höning, S., Swartz, M.A., Wickström, S.A., Hubbell, J.A., Eming, S.A., 2013. The promotion of endothelial cell attachment and spreading using FNIII10 fused to VEGF-A165. Biomaterials 34, 5958–5968. https://doi.org/10.1016/j.biomaterials.2013.04.050

Trujillo, S., Dobre, O., Dalby, M.J., Salmeron-Sanchez, M., 2019a. Mechanotransduction and Growth Factor Signaling in Hydrogel-Based Microenvironments, in: Reference Module in Biomedical Sciences. Academic Press, pp. 87–101. https://doi.org/10.1016/b978-0-12-801238-3.11141-9

Trujillo, S., Gonzalez-garcia, C., Rico, P., Reid, A., Windmill, J., 2019b. Engineered full-length Fibronectin-based hydrogels sequester and present growth factors to promote regenerative responses in vitro and in vivo. BioRxiv.

Tsai, C.C., Chen, Y.J., Yew, T.L., Chen, L.L., Wang, J.Y., Chiu, C.H., Hung, S.C., 2011. Hypoxia inhibits senescence and maintains mesenchymal stem cell properties through down-regulation of E2A-p21 by HIF-TWIST. Blood 117, 459–469. https://doi.org/10.1182/blood-2010-05-287508

Tse, J.R., Engler, A.J., 2011. Stiffness gradients mimicking in vivo tissue variation regulate mesenchymal stem cell fate. PLoS One 6. https://doi.org/10.1371/journal.pone.0015978

Tsimbouri, P., Gadegaard, N., Burgess, K., White, K., Reynolds, P., Herzyk, P., Oreffo, R., Dalby, M.J., 2014. Nanotopographical effects on mesenchymal stem cell morphology and phenotype. J. Cell. Biochem. 115, 380–390. https://doi.org/10.1002/jcb.24673

Tsimbouri, P.M., Childs, P.G., Pemberton, G.D., Yang, J., Jayawarna, V., Orapiriyakul, W., Burgess, K., González-García, C., Blackburn, G., Thomas, D., Vallejo-Giraldo, C., Biggs, M.J.P., Curtis, A.S.G., Salmerón-Sánchez, M., Reid, S., Dalby, M.J., 2017. Stimulation of 3D osteogenesis by mesenchymal stem cells using a nanovibrational bioreactor. Nat. Biomed. Eng. 1, 758–770. https://doi.org/10.1038/s41551-017-0127-4

Tsimbouri, P.M., McMurray, R.J., Burgess, K. V, Alakpa, E. V, Reynolds, P.M., Murawski, K., Kingham, E., Oreffo, R.O.C., Gadegaard, N., Dalby, M.J., 2012. Using nanotopography and metabolomics to identify biochemical effectors of multipotency. ACS Nano 6, 10239–49. https://doi.org/10.1021/nn304046m

Tsimbouri, P.M., Murawski, K., Hamilton, G., Herzyk, P., Oreffo, R.O.C., Gadegaard, N., Dalby, M.J., 2013. A genomics approach in determining nanotopographical effects on MSC phenotype. Biomaterials 34, 2177–2184. https://doi.org/10.1016/j.biomaterials.2012.12.019

Tumbar, T., Guasch, G., Greco, V., Blanpain, C., Lowry, W.E., Rendl, M., Fuchs, E., 2004. Defining the Epithelial Stem Cell 303, 359–364. https://doi.org/10.1126/science.1092436

Uccelli, A., Moretta, L., Pistoia, V., 2008. Mesenchymal stem cells in health and disease. Nat. Rev. Immunol. 8, 726–736. https://doi.org/10.1038/nri2395

Vander Heiden, M.G., Cantley, L.C., Thompson, C.., 2009. Understanding the Warburg Effect: the metabolic requirements of cell proliferation. Science (80-.). 324, 1029–1033. https://doi.org/10.1126/science.1160809.Understanding

Vanterpool, F.A., Cantini, M., Seib, F.P., Salmerón-Sánchez, M., 2014. A Material-Based Platform to Modulate Fibronectin Activity and Focal Adhesion Assembly. Biores. Open Access 3, 286–296. https://doi.org/10.1089/biores.2014.0033

Veevers-Lowe, J., Ball, S.G., Shuttleworth, A., Kielty, C.M., 2011. Mesenchymal stem cell migration is regulated by fibronectin through 5 1-integrin-mediated activation of PDGFR- and potentiation of growth factor signals. J. Cell Sci. 124, 1288–1300. https://doi.org/10.1242/jcs.076935

Vicente-Manzanares, M., Horwitz, A.R., 2011. Adhesion dynamics at a glance. J. Cell Sci. 124, 3923–3927. https://doi.org/10.1242/jcs.095653

Vincent, L.G., Choi, Y.S., Alonso-Latorre, B., Del Álamo, J.C., Engler, A.J., 2013. Mesenchymal stem cell durotaxis depends on substrate stiffness gradient strength. Biotechnol. J. 8, 472–484. https://doi.org/10.1002/biot.201200205

Vining, K.H., Mooney, D.J., 2017. Mechanical forces direct stem cell behaviour in development and regeneration. Nat. Rev. Mol. Cell Biol. https://doi.org/10.1038/nrm.2017.108

von Erlach, T.C., Bertazzo, S., Wozniak, M.A., Horejs, C.-M., Maynard, S.A., Attwood, S., Robinson, B.K., Autefage, H., Kallepitis, C., del Río Hernández, A., Chen, C.S., Goldoni, S., Stevens, M.M., 2018. Cell-geometry-dependent changes in plasma membrane order direct stem cell signalling and fate. Nat. Mater. https://doi.org/10.1038/s41563-017-0014-0

Wagegg, M., Gaber, T., Lohanatha, F.L., Hahne, M., Strehl, C., Fangradt, M., Tran, C.L., Schönbeck, K., Hoff, P., Ode, A., Perka, C., Duda, G.N., Buttgereit, F., 2012. Hypoxia Promotes Osteogenesis but Suppresses Adipogenesis of Human Mesenchymal Stromal Cells in a Hypoxia-Inducible Factor-1 Dependent Manner. PLoS One 7, 1–11. https://doi.org/10.1371/journal.pone.0046483

Wagers, A.J., Weissman, I.L., 2004. Plasticity of adult stem cells. Cell 116, 639–648. https://doi.org/10.1016/S0092-8674(04)00208-9

Wagner, J.E., Brunstein, C.G., Boitano, A.E., Defor, T.E., McKenna, D., Sumstad, D., Blazar, B.R., Tolar, J., Le, C., Jones, J., Cooke, M.P., Bleul, C.C., 2016. Phase I/II Trial of StemRegenin-1 Expanded Umbilical Cord Blood Hematopoietic Stem Cells Supports Testing as a Stand-Alone Graft. Cell Stem Cell 18, 144–155. https://doi.org/10.1016/j.stem.2015.10.004

Wang, G.., Semenza, G.., 1995. Purification and Characterization of Hypoxia-inducible Factor 1. J. Biol. Chem. 270, 1230–1237.

Wang, N., Tytell, J.D., Ingber, D.E., 2009. Mechanotransduction at a distance: Mechanically coupling the extracellular matrix with the nucleus. Nat. Rev. Mol. Cell Biol. 10, 75–82. https://doi.org/10.1038/nrm2594

Wang, R.N., Green, J., Wang, Z., Deng, Y., Qiao, M., Peabody, M., Zhang, Q., Ye, J., Yan, Z., Denduluri, S., Idowu, O., Li, M., Shen, C., Hu, A., Haydon, R.C., Kang, R., Mok, J., Lee, M.J., Luu, H.L., Shi, L.L., 2014. Bone Morphogenetic Protein (BMP) signaling in development and human diseases. Genes Dis. 1, 87–105. https://doi.org/10.1016/j.gendis.2014.07.005

Wang, T.Y., Brennan, J.K., Wu, J.H., 1995. Multilineal hematopoiesis in a three-dimensional murine long-term bone marrow culture. Exp. Hematol. 23, 26—32.

Wang, X., Rivière, I., 2017. Genetic Engineering and Manufacturing of Hematopoietic Stem Cells. Mol. Ther. - Methods Clin. Dev. 5, 96–105. https://doi.org/10.1016/j.omtm.2017.03.003

Warburg, O., 1925. The metabolism of carcinoma cells. J. Cancer Res. 139–163. https://doi.org/10.1158/jcr.1925.148

Watari, S., Hayashi, K., Wood, J.A., Russel, P., Nealey, P.F., Murphy, C.J., Genetos, D.C., 2012. Modulation of osteogenic differentiation in hMSCs cells by submicron topographically-patterned ridges and grooves. Biomaterials 33, 265–275. https://doi.org/10.1007/s10955-011-0269-9.Quantifying

Weidemann, A., Johnson, R.S., 2008. Biology of HIF-1 a 621–627. https://doi.org/10.1038/cdd.2008.12

Wenger, R., Kurtcuoglu, V., Scholz, C., Marti, H., Hoogewijs, D., 2015. Frequently asked

questions in hypoxia research. Hypoxia 35. https://doi.org/10.2147/HP.S92198

Westrop, G.D., Wang, L., Blackburn, G.J., Zhang, T., Zheng, L., Watson, D.G., Coombs, G.H., 2017. Metabolomic profiling and stable isotope labelling of Trichomonas vaginalis and Tritrichomonas foetus reveal major differences in amino acid metabolism including the production of 2-hydroxyisocaproic acid, cystathionine and S-methylcysteine, PLoS ONE. https://doi.org/10.1371/journal.pone.0189072

Wiesener, M.S., Jürgensen, J.S., Rosenberger, C., Scholze, C.K., Hörstrup, J.A.N.H., Warnecke, C., Mandriota, S., Bechmann, I., Frei, U.A., Pugh, C.W., Ratcliffe, P.J., Bachmann, S., Maxwell, P.H., Eckardt, K.-U., 2002. Widespread hypoxia-inducible expression of HIF-2α in distinct cell populations of different organs. FASEB J. 17, 271–273. https://doi.org/10.1096/fj.02-0445fje

Woo, E.J., 2012. Recombinant human bone morphogenetic protein-2: Adverse events reported to the Manufacturer and User Facility Device Experience database. Spine J. 12, 894–899. https://doi.org/10.1016/j.spinee.2012.09.052

Wood, F.M., Kolybaba, M.L., Allen, P., 2006. The use of cultured epithelial autograft in the treatment of major burn injuries: A critical review of the literature. Burns 32, 395–401. https://doi.org/10.1016/j.burns.2006.01.008

Wood, M.A., Bagnaninchi, P., Dalby, M.J., 2008. The ß integrins and cytoskeletal nanoimprinting. Exp. Cell Res. 314, 927–935. https://doi.org/10.1016/j.yexcr.2007.10.003

Xie, J., Bao, M., Bruekers, S.M.C., Huck, W.T.S., 2017. Collagen Gels with Different Fibrillar Microarchitectures Elicit Different Cellular Responses. ACS Appl. Mater. Interfaces 9, 19630–19637. https://doi.org/10.1021/acsami.7b03883

Xie, Y., Yin, T., Wiegraebe, W., He, X.C., Miller, D., Stark, D., Perko, K., Alexander, R., Schwartz, J., Grindley, J.C., Park, J., Haug, J.S., Wunderlich, J.P., Li, H., Zhang, S., Johnson, T., Feldman, R.A., Li, L., 2009. Detection of functional haematopoietic stem cell niche using real-time imaging. Nature 457, 97–101. https://doi.org/10.1038/nature07639

Xu, C., Gao, X., Wei, Q., Nakahara, F., Zimmerman, S.E., Mar, J., Frenette, P.S., 2018. Stem cell factor is selectively secreted by arterial endothelial cells in bone marrow. Nat. Commun. 9, 1–13. https://doi.org/10.1038/s41467-018-04726-3

Yamamoto, R., Morita, Y., Ooehara, J., Hamanaka, S., Onodera, M., Rudolph, K.L., Ema, H., Nakauchi, H., 2013. Clonal analysis unveils self-renewing lineage-restricted progenitors generated directly from hematopoietic stem cells. Cell 154, 1112–1126. https://doi.org/10.1016/j.cell.2013.08.007

Yamazaki, S., Ema, H., Karlsson, G., Yamaguchi, T., Miyoshi, H., Shioda, S., Taketo, M.M., Karlsson, S., Iwama, A., Nakauchi, H., 2011. Nonmyelinating schwann cells maintain hematopoietic stem cell hibernation in the bone marrow niche. Cell 147, 1146–1158. https://doi.org/10.1016/j.cell.2011.09.053

Yang, C., Tibbitt, M.W., Basta, L., Anseth, K.S., 2014. Mechanical memory and dosing influence stem cell fate. Nat. Mater. 13, 645–652. https://doi.org/10.1038/nmat3889

Yang, J., McNamara, L.E., Gadegaard, N., Alakpa, E. V, Burgess, K. V, Meek, R.M.D., Dalby, M.J., 2014. Nanotopographical Induction of Osteogenesis through Adhesion, Bone Morphogenic Protein Cosignaling, and Regulation of MicroRNAs. ACS Nano 8, 9941–9953. https://doi.org/10.1021/nn504767g

Yang, Z.X., Han, Z.B., Ji, Y.R., Wang, Y.W., Liang, L., Chi, Y., Yang, S.G., Li, L.N., Luo, W.F., Li, J.P., Da Chen, D., Du, W.J., Cao, X.C., Zhuo, G.S., Wang, T., Han, Z.C., 2013. CD106 Identifies a Subpopulation of Mesenchymal Stem Cells with Unique Immunomodulatory Properties. PLoS One 8, 1–12. https://doi.org/10.1371/journal.pone.0059354

Yen, T.-H., Wright, N. a, 2006. The gastrointestinal tract stem cell niche. Stem Cell Rev. 2, 203–212. https://doi.org/10.1007/s12015-006-0048-1

Yilmaz, Ö.H., Kiel, M.J., Morrison, S.J., 2006. SLAM family markers are conserved among hematopoietic stem cells from old and reconstituted mice and markedly increase their purity. Blood 107, 924–930. https://doi.org/10.1182/blood-2005-05-2140

Yokota, T., Oritani, K., Takahashi, I., Ishikawa, J., Matsuyama, A., Ouchi, N., Kihara, S., Funahashi, T., Tenner, A.J., Tomiyama, Y., Matsuzawa, Y., 2000. Adiponectin, a new member of the family of soluble defense collagens, negatively regulates the growth of myelomonocytic progenitors and the functions of macrophages. Blood 96, 1723–32.

Yoon-Young, J., Sharkis, S.J., 2007. A low level of reactive oxygen species selects for primitive hematopoietic stem cells that may reside in the low-oxygenic niche. Blood 110, 3056–3063. https://doi.org/10.1182/blood-2007-05-087759

Yoshihara, H., Arai, F., Hosokawa, K., Hagiwara, T., Takubo, K., Nakamura, Y., Gomei, Y., Iwasaki, H., Matsuoka, S., Miyamoto, K., Miyazaki, H., Takahashi, T., Suda, T., 2007. Thrombopoietin/MPL Signaling Regulates Hematopoietic Stem Cell Quiescence and Interaction with the Osteoblastic Niche. Cell Stem Cell 1, 685–697. https://doi.org/10.1016/j.stem.2007.10.020

Yu, J., Smuga-Otto, K., Stewart, R., Frane, J.L., Tian, S., Slukvin, I.I., Nie, J., Antosiewicz-Bourget, J., Ruotti, V., Vodyanik, M.A., Jonsdottir, G.A., Thomson, J.A., 2007. Induced Pluripotent Stem Cell Lines Derived from Human Somatic Cells. Science (80-.). 318, 1917–1920. https://doi.org/10.1126/science.1151526

Yu, W.-M., Liu, X., Shen, J., Jovanovic, O., Pohl, E.E., Gerson, S.L., Finkel, T., Broxmeyer, H.E., Qu, C.-K., 2013. Metabolic regulation by the mitochondrial phosphatase PTPMT1 is required for hematopoietic stem cell differentiation. Cell Stem Cell 12, 62–74. https://doi.org/10.1016/j.stem.2012.11.022

Yue, R., Zhou, B.O., Shimada, I.S., Zhao, Z., Morrison, S.J., 2016. Leptin Receptor Promotes Adipogenesis and Reduces Osteogenesis by Regulating Mesenchymal Stromal Cells in Adult Bone Marrow. Cell Stem Cell 1–15. https://doi.org/10.1016/j.stem.2016.02.015

Zaim, M., Karaman, S., Cetin, G., Isik, S., 2012. Donor age and long-term culture affect differentiation and proliferation of human bone marrow mesenchymal stem cells. Ann. Hematol. 91, 1175–1186. https://doi.org/10.1007/s00277-012-1438-x

Zhang, J., Niu, C., Ye, L., Huang, H., He, X., Tong, W.-G., Ross, J., Haug, J., Johnson, T., Feng, J.Q., Harris, S., Wiedemann, L.M., Mishina, Y., Linheng, L., 2003. Identification of the haematopoietic stem cell niche and control of the niche size. Nature 425, 836–841. https://doi.org/10.1038/nature02064.1.

Zhang, J.Z., Behrooz, A., Ismail-Beigi, F., 1999. Regulation of glucose transport by hypoxia. Am. J. Kidney Dis. 34, 189–202. https://doi.org/10.1016/S0272-6386(99)70131-9

Zhang, Y., Gao, S., Xia, J., Liu, F., 2018. Hematopoietic Hierarchy – An Updated Roadmap. Trends Cell Biol. 28, 976–986. https://doi.org/10.1016/j.tcb.2018.06.001

Zhao Li, L., Lei, Q. and Guan, K. L., B., 2010. The Hippo-YAP pathway in organ size control and tumorgenesis: an updated version. Genes Dev. 24, 862–874. https://doi.org/10.1101/gad.1909210.The

Zhou, B.O., Ding, L., Morrison, S.J., 2015. Hematopoietic stem and progenitor cells regulate the regeneration of their niche by secreting Angiopoietin-1. Elife 2015, 1–25. https://doi.org/10.7554/eLife.05521

Zhou, B.O., Yue, R., Murphy, M.M.M., Peyer, J.G., Morrison, S.J.J., 2014. Leptin Receptor-expressing mesenchymal stromal cells represent the main source of bone formed by adult bone marrow. Cell Stem Cell 15, 156–168. https://doi.org/10.1016/j.micinf.2011.07.011.Innate

Zon, L.I., 2008. Intrinsic and extrinsic control of haematopoietic stem-cell self-renewal. Nature 453, 306–313. https://doi.org/10.1038/nature07038

Zonari, E., Desantis, G., Petrillo, C., Boccalatte, F.E., Lidonnici, M.R., Kajaste-Rudnitski, A., Aiuti, A., Ferrari, G., Naldini, L., Gentner, B., 2017. Efficient Ex Vivo Engineering and Expansion of Highly Purified Human Hematopoietic Stem and Progenitor Cell Populations for Gene Therapy. Stem Cell Reports 8, 977–990. https://doi.org/10.1016/j.stemcr.2017.02.010